frontiers | Research Topics

The Complex phenotype of diabetic cardiomyopathy: clinical indicators and novel treatment targets, volume II

Edited by
Ramoji Kosuru and Yin Cai

Coordinated by
Priyanka Choudhury

Published in
Frontiers in Endocrinology

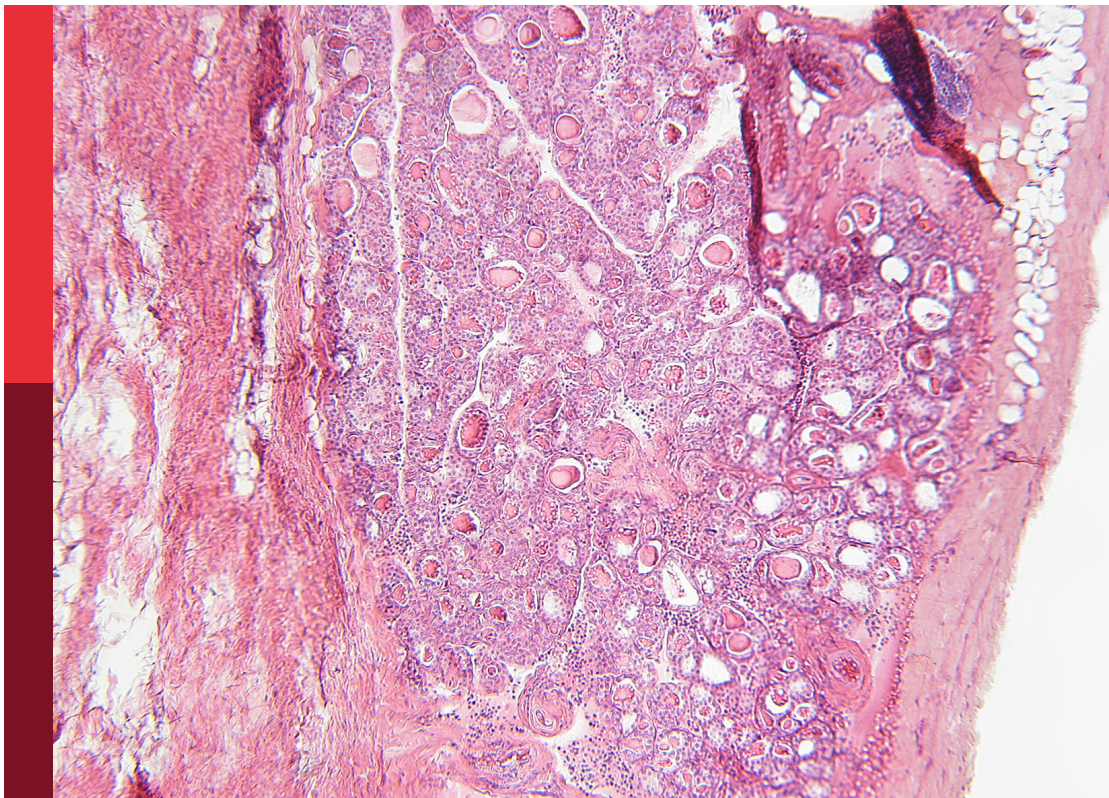

ISSN 1664-8714
ISBN 978-2-8325-7314-3
DOI 10.3389/978-2-8325-7314-3

Generative AI statement
Any alternative text (Alt text) provided alongside figures in the articles in this ebook has been generated by Frontiers with the support of artificial intelligence and reasonable efforts have been made to ensure accuracy, including review by the authors wherever possible. If you identify any issues, please contact us.

About Frontiers

Frontiers is more than just an open access publisher of scholarly articles: it is a pioneering approach to the world of academia, radically improving the way scholarly research is managed. The grand vision of Frontiers is a world where all people have an equal opportunity to seek, share and generate knowledge. Frontiers provides immediate and permanent online open access to all its publications, but this alone is not enough to realize our grand goals.

Frontiers journal series

The Frontiers journal series is a multi-tier and interdisciplinary set of open-access, online journals, promising a paradigm shift from the current review, selection and dissemination processes in academic publishing. All Frontiers journals are driven by researchers for researchers; therefore, they constitute a service to the scholarly community. At the same time, the *Frontiers journal series* operates on a revolutionary invention, the tiered publishing system, initially addressing specific communities of scholars, and gradually climbing up to broader public understanding, thus serving the interests of the lay society, too.

Dedication to quality

Each Frontiers article is a landmark of the highest quality, thanks to genuinely collaborative interactions between authors and review editors, who include some of the world's best academicians. Research must be certified by peers before entering a stream of knowledge that may eventually reach the public - and shape society; therefore, Frontiers only applies the most rigorous and unbiased reviews. Frontiers revolutionizes research publishing by freely delivering the most outstanding research, evaluated with no bias from both the academic and social point of view. By applying the most advanced information technologies, Frontiers is catapulting scholarly publishing into a new generation.

What are Frontiers Research Topics?

Frontiers Research Topics are very popular trademarks of the *Frontiers journals series*: they are collections of at least ten articles, all centered on a particular subject. With their unique mix of varied contributions from Original Research to Review Articles, Frontiers Research Topics unify the most influential researchers, the latest key findings and historical advances in a hot research area.

Find out more on how to host your own Frontiers Research Topic or contribute to one as an author by contacting the Frontiers editorial office: frontiersin.org/about/contact

The complex phenotype of diabetic cardiomyopathy: clinical indicators and novel treatment targets, volume II

Topic editors

Ramoji Kosuru — Versiti Blood Research Institute, United States

Yin Cai — Hong Kong Polytechnic University, Hong Kong, SAR China

Topic coordinator

Priyanka Choudhury — Medical College of Wisconsin, United States

Citation

Kosuru, R., Cai, Y., Choudhury, P., eds. (2026). *The complex phenotype of diabetic cardiomyopathy: clinical indicators and novel treatment targets, volume II*. Lausanne: Frontiers Media SA. doi: 10.3389/978-2-8325-7314-3

Table of contents

frontiers | Frontiers in Endocrinology

TYPE Editorial
PUBLISHED 11 December 2025
DOI 10.3389/fendo.2025.1752170

OPEN ACCESS

EDITED AND REVIEWED BY
Gaetano Santulli,
Albert Einstein College of Medicine,
United States

*CORRESPONDENCE
Priyanka Choudhury
priyanka.choudhury@hotmail.com

RECEIVED 22 November 2025
ACCEPTED 26 November 2025
PUBLISHED 11 December 2025

CITATION
Choudhury P and Cai Y (2025)
Editorial: The complex phenotype
of diabetic cardiomyopathy: clinical indicators
and novel treatment targets, volume II.
Front. Endocrinol. 16:1752170.
doi: 10.3389/fendo.2025.1752170

Editorial: The complex phenotype of diabetic cardiomyopathy: clinical indicators and novel treatment targets, volume II

Priyanka Choudhury[1]* and Yin Cai[2]

[1]Department of Pediatrics, Medical College of Wisconsin, Milwaukee, WI, United States, [2]Department of Health Technology and Informatics, The Hong Kong Polytechnic University, Hong Kong, Hong Kong SAR, China

KEYWORDS

diabetic cardiomyopathy, multimodality imaging, biomarker, lipid metabolism, angiogenesis

Editorial on the Research Topic
The complex phenotype of diabetic cardiomyopathy: clinical indicators and novel treatment targets, volume II

Diabetic cardiomyopathy (DCM) is a complex cardiovascular complication of diabetes mellitus, characterized by metabolic, structural, and functional abnormalities of the myocardium that occur independently of coronary artery disease or hypertension 1, 2). As global rates of type 2 diabetes mellitus (T2DM) continue to rise, the incidence of DCM is expected to increase substantially, underscoring the urgent need for deeper mechanistic insights, earlier diagnostic approaches, and targeted therapeutic strategies. This second volume of our Research Topic brings together diverse studies that collectively advance our understanding of DCM pathogenesis and clinical management, integrating perspectives from innovative preclinical models, advanced imaging, molecular investigations, and precision risk stratification tools.

One of the major contributions in this volume is the development of a combined nicotinamide/streptozotocin-induced T2DM and carotid vascular balloon injury (VBI) model in Sprague–Dawley rats (Wang et al.). Through percutaneous transluminal coronary angioplasty balloon catheterization, this model successfully induces rapid hyperglycemia, marked neointimal proliferation, and diminished plaque stability, overcoming key limitations of traditional DCM models that rely on genetic manipulation or longer induction periods. Importantly, rats exposed to both T2DM and VBI displayed vascular pathology at two weeks comparable to six-week outcomes in VBI-only controls, providing a valuable accelerated disease system for evaluating therapeutic interventions (Wang et al.).

Complementing these preclinical developments, several clinical studies included in this volume reinforce the interaction between metabolic disturbances and cardiac pathology in diabetes. CT-derived visceral fat area (VFA) was independently associated with cardiovascular disease in T2DM patients, emphasizing the role of abdominal adiposity in cardiovascular risk (Wu et al.). Multiparametric cardiac magnetic resonance imaging

(CMR) further demonstrated that impaired glucose metabolism is linked to increased myocardial fibrosis and subclinical inflammation in patients with hypertrophic cardiomyopathy (HCM) (Peng et al.). Prediabetic and diabetic cohorts showed progressively elevated myocardial T1 values and extracellular volume fractions (ECV), with strong positive correlations between ECV and HbA1c levels. Raised T2 values supported the presence of underlying inflammation. These effects were most pronounced in hypertrophied myocardial regions, highlighting the detrimental influence of even mild hyperglycemia on myocardial remodeling and supporting the early incorporation of metabolic control and CMR-based tissue characterization into HCM management (Peng et al.).

Sex-specific considerations also emerge in the analysis of insulin resistance and hypertension risk. A retrospective cohort study examining the triglyceride–glucose (TyG) index found that while the association between TyG and incident hypertension in men weakened after adjusting for confounders, spline analyses revealed stronger risk relationships in men than women (Sun et al.). Sensitivity analyses partially validated these findings, suggesting that biological sex may modulate hypertension risk associated with insulin resistance and pointing to a need for larger studies to guide personalized prevention strategies.

This volume also highlights the use of predictive modeling and bioinformatics to assess DCM risk. A nomogram developed by Luo et al., integrating age, duration of diabetes, systolic blood pressure, urinary albumin-to-creatinine ratio, left atrial diameter, and left ventricular posterior wall thickness, demonstrated excellent discrimination and calibration for predicting DCM. By leveraging routine clinical and echocardiographic parameters, the model provides an accessible tool for individualized risk stratification and early cardioprotective intervention.

At the molecular level, studies in this volume identify key regulators of angiogenesis and lipid metabolism as contributors to DCM pathogenesis. High-glucose stimulation significantly upregulated ephrinB2 (Efnb2), which sequencing analyses suggest may mediate angiogenic impairment in diabetic conditions (Hu et al.). Integrative bioinformatics identified two hub genes, Acsbg1 and Etnppl, out of intersecting lipid metabolism–related and DCM-associated gene sets (Huang et al.). Acyl-CoA Synthetase Bubblegum Family Member 1 (Acsbg1) was strongly upregulated in disease models, while ethanolamine-phosphate phospho-lyase (Etnppl) expression was reduced but recoverable with therapeutic intervention. Both genes localized to UCAGG motifs in RNA secondary structures and appeared to exert their effects through lysosomal pathways. These findings link dysregulated lipid metabolism to DCM progression and position Acsbg1 and Etnppl as promising diagnostic and therapeutic targets (Huang et al.).

Imaging and biomarker advancements further enhance precision in early DCM detection. Multimodality imaging techniques, including echocardiography, CMR, and nuclear imaging, continue to refine the evaluation of diastolic dysfunction, early hypertrophy, and myocardial fibrosis (Adel and Chen). Circulating biomarkers such as soluble suppression of tumorigenicity 2 (sST2), cardiotrophin-1 (CT-1), galectin-3, lysyl oxidase-like 2 (LOXL2), and electron transfer flavoprotein β (ETFβ) demonstrated strong associations with DCM severity and improved diagnostic accuracy when integrated with conventional indices such as ultrasound E/E′ ratio and NT-proBNP (Su et al.). Noninvasive techniques like skin autofluorescence also show emerging potential in risk assessment.

A unifying mechanistic perspective across several contributions is the central role of mitochondrial calcium dysregulation in DCM (Deng et al.). Impaired mitochondrial calcium uptake, excessive release, and reduced buffering capacity lead to bioenergetic collapse, oxidative stress, and cardiomyocyte injury. By linking metabolic stress and mitochondrial dysfunction, this framework highlights a key mechanistic hub in DCM development. Deng et al. further evaluate therapeutic strategies targeting the mitochondrial calcium uniporter (MCU), mitochondrial $Na^+/Ca^{2+}/Li^+$ exchanger (NCLX), and mitochondrial permeability transition pore (mPTP), offering critical insights into their translational viability.

Collectively, the studies in this volume highlight diabetic cardiomyopathy as a complex disorder shaped by interacting metabolic, vascular, inflammatory, and mitochondrial disturbances. By integrating accelerated animal models, advanced imaging, molecular analyses, and predictive tools, these contributions deepen our mechanistic understanding and strengthen the translational framework for improving early diagnosis and treatment.

Looking ahead, advancing diabetic cardiomyopathy research will require refined, physiologically relevant disease models to probe early pathogenesis and test therapies, alongside longitudinally validated multimodality imaging and circulating biomarkers for subclinical detection. Molecular targets, including regulators of lipid metabolism, angiogenesis, and mitochondrial calcium handling, merit further investigation, while predictive algorithms based on clinical and imaging measures should be expanded to support personalized risk assessment.

In parallel, nanoparticle-based therapeutics offer promising opportunities for organelle-specific drug delivery, enhanced stability, and modulation of key pathways in inflammation, angiogenesis, mitochondrial function, and fibrosis (3, 4). Future work should define molecular mechanisms of regeneration, mitochondrial homeostasis, immune activation, and extracellular matrix remodeling in diabetes, while rigorously evaluating nanoparticle biodistribution, immune responses, clearance, and toxicity. Integrating nanotechnology with mechanistic insights from metabolism, vascular biology, and mitochondrial signaling may enable precision therapies that prevent or reverse remodeling, ultimately shifting the trajectory of DCM rather than merely mitigating its consequences.

Author contributions

PC: Conceptualization, Investigation, Writing – review & editing, Data curation, Writing – original draft, Supervision, Validation, Project administration, Formal analysis. YC:

Supervision, Validation, Writing – review & editing, Writing – original draft, Formal analysis.

Acknowledgments

We appreciate all the authors for their dedication to contributing quality manuscripts and all reviewers for their insightful comments on manuscripts on this Research Topic. Lastly, we extend our sincere gratitude to the Editorial Office of Frontiers in Endocrinology for their valuable contributions to this Research Topic.

Conflict of interest

The authors declare that the research was conducted in the absence of any commercial or financial relationships that could be construed as a potential conflict of interest.

Generative AI statement

The author(s) declare that no Generative AI was used in the creation of this manuscript.

Any alternative text (alt text) provided alongside figures in this article has been generated by Frontiers with the support of artificial intelligence and reasonable efforts have been made to ensure accuracy, including review by the authors wherever possible. If you identify any issues, please contact us.

Publisher's note

References

1. Choudhury P, Kandula N, Kosuru R, Adena SKR. Nanomedicine: A great boon for cardiac regenerative medicine. *Eur J Pharmacol.* (2024) 982:176969. doi: 10.1016/j.ejphar.2024.176969

2. Prakash S, Choudhury P, Bisht S. Diabetic cardiomyopathy and COVID-19: intersecting pathways and amplified cardiovascular risk [Review. *Front Pharmacol.* (2025) 16:1683159. doi: 10.3389/fphar.2025.1683159

3. Choudhury P, Kosuru R, Cai Y. Editorial: The complex phenotype of diabetic cardiomyopathy: clinical indicators and novel treatment targets [Editorial. *Front Endocrinol.* (2024) 15:1497352. doi: 10.3389/fendo.2024.1497352

4. Liu M, Wang R, Hoi MPM, Wang Y, Wang S, Li G, et al. Nano-based drug delivery systems for managing diabetes: recent advances and future prospects. *Int J Nanomedicine.* (2025) 20:6221–52. doi: 10.2147/ijn.S508875

frontiers | Frontiers in Endocrinology

TYPE Mini Review
PUBLISHED 23 December 2024
DOI 10.3389/fendo.2024.1405031

OPEN ACCESS

EDITED BY
Rajesh Katare,
University of Otago, New Zealand

REVIEWED BY
Mengnan Liu,
Southwest Medical University, China

*CORRESPONDENCE
Horng H. Chen
Chen.Horng@mayo.edu

RECEIVED 22 March 2024
ACCEPTED 10 December 2024
PUBLISHED 23 December 2024

CITATION
Adel FW and Chen HH (2024) The role of multimodality imaging in diabetic cardiomyopathy: a brief review.
Front. Endocrinol. 15:1405031.
doi: 10.3389/fendo.2024.1405031

The role of multimodality imaging in diabetic cardiomyopathy: a brief review

Fadi W. Adel and Horng H. Chen*

Department of Cardiovascular Medicine, Mayo Clinic, Rochester, MN, United States

Diabetic cardiomyopathy (DMCM), defined as left ventricular dysfunction in the setting of diabetes mellitus without hypertension, coronary artery disease or valvular heart disease, is a well-recognized entity whose prevalence is certainly predicted to increase alongside the rising incidence and prevalence of diabetes mellitus. The pathophysiology of DMCM stems from hyperglycemia and insulin resistance, resulting in oxidative stress, inflammation, cardiomyocyte death, and fibrosis. These perturbations lead to left ventricular hypertrophy with associated impaired relaxation early in the course of the disease, and eventually culminating in combined systolic and diastolic heart failure. Echocardiography, cardiac nuclear imaging, and cardiac magnetic resonance imaging are crucial in the diagnosis and management of the structural and functional changes associated with DMCM. There appears to be a U-shaped relationship between glycemic control and mortality. Exogenous insulin therapy, while crucial, has been identified as an independent risk factor for worsening cardiovascular outcomes. On the other hand, Glucagon-like Peptide-1 Receptor Agonists and Sodium–Glucose Cotransporter 2 Inhibitors appear to potentially offer glycemic control and cardiovascular protection. In this review, we briefly discuss the pathophysiology, staging, role of multimodality imaging, and therapeutics in DMCM.

KEYWORDS

diabetic cardiomyopathy, heart failure, diabetes mellitus, multi-modality imaging, echocardiography, cardiac MRI, cardiac nuclear imaging, diabetes therapeutics

Introduction

In 2023, foremost societies, including the American Heart Association (AHA), the American College of Cardiology (ACC), and the European Society of Cardiology (ESC) endorsed its formal definition (1). Diabetic cardiomyopathy (DMCM) is defined as left ventricle (LV) dysfunction in the presence of diabetes mellitus (DM), whether it is type 1 (DM1) or type 2 (DM2), and in the absence of hypertension (HTN), obstructive epicardial coronary artery disease (CAD), and valvular heart disease (VHD) (2, 3).

Worldwide, the prevalence of DM increased from 151 million in 2000 to 537 million in 2021, and it is projected to increase to 643 million by 2030 (4). Among diabetic patients, the prevalence of DMCM ranges from 16.9% (5) to about 67% (6), depending on the criteria used for definition.

In this review, we will briefly discuss the pathophysiology, staging, and therapeutics, with a dedicated focus on the role of multi-modality imaging.

Pathophysiology & staging

The pathophysiology of DMCM involves a complex interplay of insulin resistance mediating hyperglycemia and lipotoxicity (Figure 1). In that milieu, oxidative stress ensues, with accompanying inflammation, resulting in cardiomyocyte calcium dyshomeostasis (7, 8), cardiomyocyte death (9, 10) and, later, hypertrophy (11), along with endothelial damage (12, 13) and interstitial fibrosis (14–16).

Early, patients usually experience impaired myocardial relaxation, which manifests as mild diastolic dysfunction (10, 17). As the disease progresses, patients develop left ventricular hypertrophy (LVH) in the setting of cardiomyocyte hypertrophy, interstitial fibrosis, and maladaptive inflammatory response. Clinically, this manifests as more advanced diastolic dysfunction and possibly early systolic dysfunction (10). In the late stages of the disease, severe neurohormonal disturbances, such as activation of both the Angiotensin-II and sympathetic nervous systems (17), lead to significant increases in LV thickness, mass, and size, with an accompanying impairment in both systolic and diastolic function (10, 17, 18).

Role of multimodality imaging

From a clinical perspective, the diagnosis of DMCM requires the utilization of at least one imaging modality to confirm LV

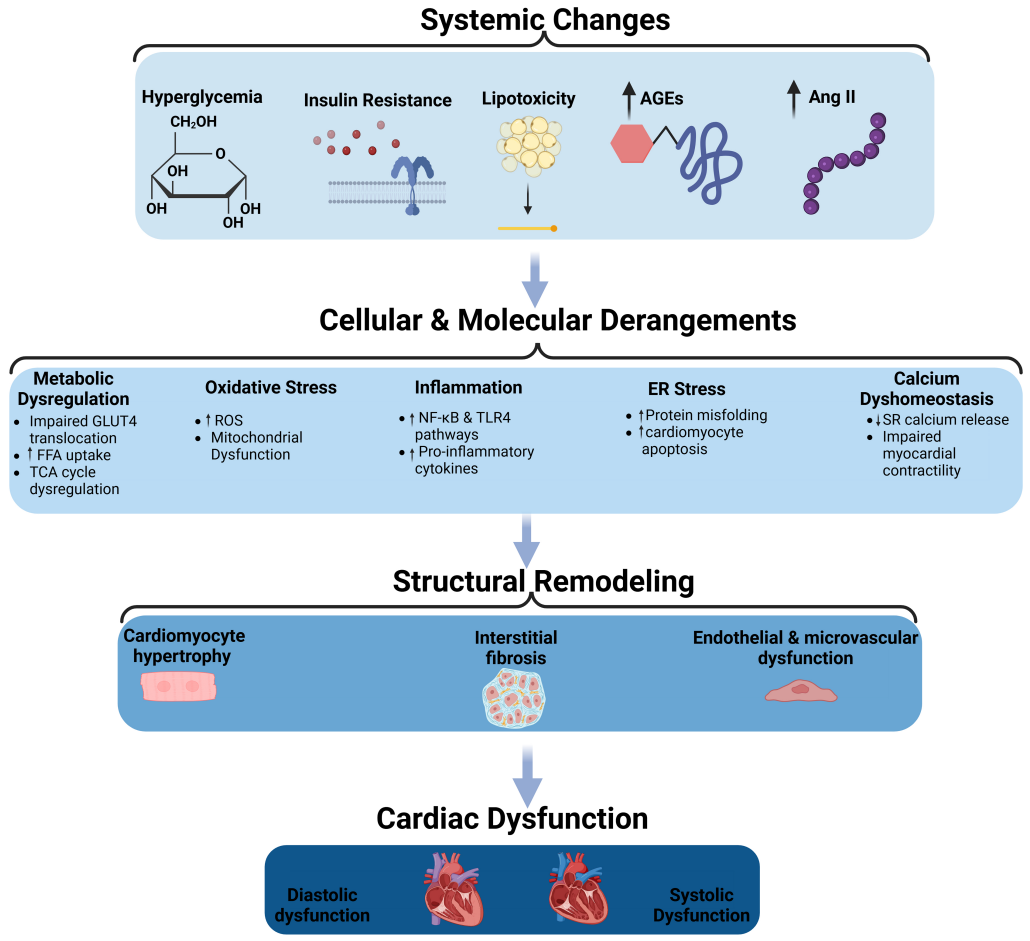

FIGURE 1
The pathophysiological mechanisms of diabetic cardiomyopathy. Schematic representation of the systemic, cellular, and molecular changes leading to structural remodeling and cardiac dysfunction in diabetic cardiomyopathy. Systemic changes such as hyperglycemia, insulin resistance, lipotoxicity, advanced glycation end-products (AGEs), and increased angiotensin II (Ang II) contribute to cellular and molecular derangements, including metabolic dysregulation, oxidative stress, inflammation, endoplasmic reticulum (ER) stress, and calcium dysregulation. These changes promote structural remodeling characterized by cardiomyocyte hypertrophy, interstitial fibrosis, and endothelial/microvascular dysfunction, ultimately leading to diastolic and systolic cardiac dysfunction. AGEs, Advanced Glycation End-products; Ang II, Angiotensin II; FFA, Free Fatty Acids; GLUT4, Glucose Transporter Type 4; TCA cycle, Tricarboxylic Acid Cycle; ROS, Reactive Oxygen Species; NF-κB, Nuclear Factor Kappa-Light-Chain-Enhancer of Activated B Cells; TLR4, Toll-like Receptor 4; ER, Endoplasmic Reticulum; SR, Sarcoplasmic Reticulum.

structural and functional impairments. Imaging also aids in monitoring the course of the disease and assess the impact of treatment. Furthermore, different imaging modalities allow the assessment of different mechanisms contributing to the development and progression of DMCM (3, 19, 20).

Echocardiography

Echocardiography is the gold standard in diagnosing DMCM, owing to its high temporal and spatial resolutions, accessibility, affordability, and harmlessness (19, 21). One of the earliest features of DMCM is the impairment of diastolic function (19). In a case-control study among patients with DM2 with a median duration of > 5 years, systolic function was preserved among all patients. However, 54% of the diabetic patients had diastolic dysfunction, compared to 11% among non-diabetic controls, with more incident diastolic dysfunction correlating with duration of diabetes (22).

Further, Somaratane et al. inspected the prevalence of LVH in a cohort of DM2, and found that 56% of the diabetic population exhibited this structural abnormality. Interestingly, electrocardiograms (EKG) only detected 5% of LVH cases, and while NT-proBNP was superior to EKG, it remained inadequate; this study underscores the significant utility of echocardiography in detecting LVH (23).

Additionally, in patients with DM1 and average HbA1c of 8%, the lateral mitral annular early diastolic velocity was lower compared to non-diabetic controls, which is a marker of diastolic dysfunction (24). Moreover, in DM2 patients with a mean diabetes duration of 6.3 years, 45% demonstrated abnormal global longitudinal strain, which conferred a higher risk for the development of all-cause mortality or hospitalization (25).

Impaired diastolic parameters among diabetic patients are evidently associated with worse clinical outcomes. Rorth et al. showed that, among DM1 patients, higher filling pressures, as measured by early mitral inflow velocity and mitral annular early diastolic velocity ratio (e/e'), was associated with a higher risk of non-fatal myocardial infarction, cerebrovascular accidents, and death (26). Similarly, From et al. demonstrated that, among DM2 patients, the cumulative probability of both the incidence of heart failure and death more than doubled among diabetics with higher filling pressures as measured by e/e' ratios (27).

In summary, echocardiography remains indispensable in the early detection and monitoring of DMCM, providing critical prognostic information that guides clinical decision-making and management. Its ability to identify subtle changes in cardiac structure and function underscores its role as the gold standard imaging modality in this patient population.

However, this technique is not without its challenges; the diagnostic accuracy can be operator-dependent, and image quality may be compromised in patients with poor acoustic windows, such as those with obesity or chronic lung disease (28). Additionally, while echocardiography is excellent for structural assessment, it provides limited information on myocardial tissue characterization and metabolism, which are crucial for understanding the pathophysiology of DMCM (3).

Cardiac magnetic resonance imaging

Cardiac magnetic resonance imaging (CMR) possesses higher spatial and temporal resolution than echocardiography, in addition to allowing the assessment of myocardial fibrosis and altered metabolism, which are hallmarks of DMCM (3, 19, 21).

Among DM1 patients, average HbA1c levels were inversely associated with stroke volume and positively correlated with the presence of myocardial scar tissue (29). Additionally, myocardial perfusion reserve and diastolic strain rate were abnormal in diabetic patients when compared to controls; further, increased myocardial triglyceride content, but not impaired myocardial flow reserve, was associated with abnormal diastolic function, suggesting that steatosis, but not necessarily small vessel disease, may be responsible for early diastolic dysfunction in DMCM (30). In a cohort derived from the general population, CMR revealed that pre-DM and DM were associated with LV remodeling compared to non-diabetic controls (31). Fibrotic tissue, as determined by late gadolinium enhancement, can be easily assessed using CMR and it has been associated with worse major adverse cardiovascular events (MACE) in diabetic patients (32).

However, CMR remains underutilized, largely owing to its perceived expense burden, patient comfort issues, and longer examination times (33). Additionally, traditional, older generation Gadolinium-based contrast media (CGBM) were associated with a low but serious risk of nephrogenic systemic fibrosis. Thankfully, with group II CGMB, this risk is significantly diminished (34). With further advancements in imaging and technology, it may be feasible in the future to incorporate CMR as a cornerstone in DMCM management.

Nuclear imaging

Nuclear imaging allows the detection of low-density processes, making it possible to measure myocardial metabolism and to assess molecular imaging (20). Gated SPECT possesses the capability to assess myocardial perfusion and LV function; however, limited data exist on its widespread clinical utility in DMCM (3).

Positron emission tomography (PET) allows flexibility in radiotracer design radiolabeled with a variety of radionuclides, and radiotracers administered at low doses do not alter metabolic processes (20). In order to circumvent the low spatial resolution observed in PET, it is usually combined with computer tomography or CMR to allow for accurate radiotracer localization (3, 20).

PET imaging has been utilized to study a multitude of metabolic parameters in DMCM. Using PET-CMR in DM2 patients with average HbA1c of 7.1% and mean diabetes duration of 4 years, Rijzewijk et al. demonstrated impaired diastolic parameters among diabetics; more importantly, they revealed increased myocardial fatty acid uptake and oxidation compared to controls, indicating myocardial metabolic remodeling (35). Similarly, in DM1 patients, PET imaging revealed increased free fatty acid utilization and decreased myocardial glucose uptake (36). Further, phase analysis of gated SPECT MPI revealed that asymptomatic DM2 patients with normal perfusion scans exhibited significant left ventricular mechanical dyssynchrony, particularly in those with a diabetes

duration of more than 15 years (37). In a study investigating the association between diabetes mellitus and myocardial glucose uptake using 18F-FDG PET/CT, it was demonstrated that DM is significantly associated with decreased myocardial glucose metabolism, with up to 84% of diabetic patients showing poor FDG uptake. Furthermore, multivariate logistic regression analysis revealed that gender (male), Homeostatic Model Assessment of Insulin Resistance, and metabolic dysfunction-associated steatotic liver disease were independent risk factors for poor myocardial FDG uptake in diabetic patients (38).

In summary, nuclear imaging techniques like PET and gated SPECT are valuable in assessing myocardial metabolism and function in DMCM, revealing significant alterations such as impaired diastolic parameters, increased myocardial fatty acid uptake and oxidation, decreased myocardial glucose uptake, and left ventricular mechanical dyssynchrony, particularly in patients with prolonged diabetes duration.

The main challenges associated with nuclear imaging include its high cost and limited availability (20). Additionally, the relatively low spatial resolution of PET compared to CMR can limit its ability to detect small areas of myocardial scar or fibrosis (19). The use of ionizing radiation in both PET and SPECT raises concerns about radiation exposure, particularly in younger patients and those requiring repeated imaging studies (20). Furthermore, the interpretation of nuclear imaging studies requires specialized expertise, which may not be readily available in all clinical settings (3).

In conclusion, while each imaging modality offers unique benefits in the assessment of DMCM, they also come with specific challenges (Table 1). A multimodality approach, leveraging the strengths of each technique, can provide a comprehensive evaluation of diabetic cardiomyopathy, improving diagnostic accuracy and informing therapeutic strategies. Future advancements in imaging technology and reductions in cost may further enhance the integration of these modalities into routine clinical practice.

TABLE 1 Strengths and limitations of multimodality imaging techniques in diabetic cardiomyopathy.

Modality	Strength	Limitation
Echocardiography	• High temporal and spatial resolutions, accessibility, affordability, harmlessness • Effective in detecting early diastolic dysfunction • Critical for early detection and monitoring of DMCM	• Operator-dependent diagnostic accuracy • Compromised image quality in patients with poor acoustic windows • Limited information on myocardial tissue characterization and metabolism
Cardiac MRI	• Higher spatial and temporal resolution, assesses myocardial fibrosis and altered metabolism • Can identify myocardial scar tissue and abnormal diastolic function • Comprehensive tissue characterization, high-resolution imaging	• Perceived expense burden, patient comfort issues, longer examination times • Risk of nephrogenic systemic fibrosis with older generation Gadolinium-based contrast media
Nuclear Imaging	• Detects low-density processes, measures myocardial metabolism, assesses molecular imaging • Flexible radiotracer design, accurate radiotracer localization with combined techniques • Reveals significant metabolic alterations in DMCM	• High cost and limited availability • Low spatial resolution compared to CMR, concerns about radiation exposure • Requires specialized expertise for interpretation

Therapeutics

In the UK Prospective Diabetes Study (UKPDS), a 1% decrease in HbA1c was associated with a 16% decrease in risk of myocardial infarction (39). Yet, it has become apparent that there is a U-curve relationship between HbA1c and mortality in diabetic patients with heart failure (40). Indeed, intensive glycemic control did not reduce cardiovascular events, and it was associated with a 47% increase in incident heart failure (41). Exogenous insulin therapy, which is utilized by all DM1 patients and 1/3rd of DM2 with heart failure patients (42), has been shown to be a risk factor for incident heart failure (43). Similarly, exogenous insulin use is associated with a higher risk of all-cause mortality, and HF rehospitalization (44). In a preclinical rodent model of experimental DM, insulin use was associated with increased interstitial fibrosis and cardiomyocyte apoptosis compared to both non-diabetic and untreated diabetic controls, further supporting the hypothesis that long-term exogenous insulin may adversely affect the myocardium (45).

Metformin use has yielded inconsistent results. In a metanalysis including 13,110 DM patients, metformin use did not bestow any HF benefit (46). On the other hand, in the UKPDS, metformin use was associated with a 39% reduction in the risk of myocardial infarction (47).

Sulfonylureas and thiazolidinediones have been associated with an increase in all-cause mortality and/or HF hospitalization among DM2 patients (48, 49). Dipeptidyl Peptidase 4 Inhibitors (DPP-4i) have not been associated with any cardiovascular benefit. In fact, saxagliptin has been associated with an increased risk of heart failure hospitalization (50). In the American Diabetes Association (ADA) Consensus Report in 2022, DPP-4i should be avoided in DM patients with ACC/AHA stage B and C (51). Glucagon-like Peptide-1 Receptor Agonists (GLP-1 RAs) use has been associated with a decreased risk of MACE in DM2 patients with established cardiovascular disease (52). While randomized clinical trials for GLP-1 RAs have shown no benefit when it comes to heart failure (53–56), the HARMONY Outcomes trial suggested a 29% reduction in heart failure hospitalization as a secondary outcome (57); further, in one meta-analysis, there was a 9% reduction in heart failure hospitalization (58). In STEP-HFpEF, heart failure hospitalization, as an exploratory end-point, seemed to be lower in the semaglutide group compared to placebo (59).

Sodium–Glucose Cotransporter 2 Inhibitors (SGLT2i) have been shown to decrease the risk of MACE and heart failure hospitalization among diabetics (60, 61). In fact, the ADA recommends SGLT2i use among DM patients with heart disease (62).

Conclusion

In conclusion, DMCM is a major and increasing health concern, fueled by the global rise in DM incidence (4–6). The complex pathophysiology of DMCM, characterized by insulin resistance, hyperglycemia, and lipotoxicity (18), leads to oxidative stress, inflammation, cardiomyocyte death, and fibrosis. These processes result in LVH and dysfunction (7–14). Multimodality imaging, encompassing echocardiography, CMR, and nuclear imaging, is crucial for the diagnosis, staging, and management of DMCM. Each imaging modality provides distinct insights into cardiac structure and function, metabolic changes, and tissue characterization, thus enhancing our comprehension and management of this intricate condition.

Author contributions

FA: Writing – original draft, Writing – review & editing. HC: Writing – review & editing.

Funding

The author(s) declare that no financial support was received for the research, authorship, and/or publication of this article.

Acknowledgments

We acknowledge the use of ChatGPT-4o for assistance with grammar and language refinement during the preparation of this manuscript. The authors also acknowledge that Figure 1 was created in BioRender. Adel, F. (2024) https://BioRender.com/f43t492.

Conflict of interest

HC reports being a co-Founder of Zumbro Discovery, receiving grants from Scios Inc, and receiving royalties from UpToDate, and that his institution has patents for designer natriuretic peptides.

The remaining author declares that the research was conducted in the absence of any commercial or financial relationships that could be construed as a potential conflict of interest.

Publisher's note

References

1. Authors/Task Force Members, Rydén L, Grant PJ, Anker SD, Berne C, Cosentino F, Danchin N, et al. ESC Guidelines on diabetes, pre-diabetes, and cardiovascular diseases developed in collaboration with the EASD: the Task Force on diabetes, pre-diabetes, and cardiovascular diseases of the European Society of Cardiology (ESC) and developed in collaboration with the European Association for the Study of Diabetes (EASD). *Eur Heart J*. (2013) 34:3035–87. doi: 10.1093/eurheartj/eht108

2. Jia G, Hill MA, Sowers JR. Diabetic cardiomyopathy: an update of mechanisms contributing to this clinical entity. *Circ Res*. (2018) 122:624–38. doi: 10.1161/CIRCRESAHA.117.311586

3. Lorenzo-Almorós A, Tuñón J, Orejas M, Cortés M, Egido J, Lorenzo Ó. Diagnostic approaches for diabetic cardiomyopathy. *Cardiovasc Diabetol*. (2017) 16:28. doi: 10.1186/s12933-017-0506-x

4. International Diabetes Federation. *IDF Diabetes Atlas. 10th edn*. Brussels, Belgium: IDF (2021). Available online at: https://www.diabetesatlas.org.

5. Dandamudi S, Slusser J, Mahoney DW, Redfield MM, Rodeheffer RJ, Chen HH. The prevalence of diabetic cardiomyopathy: A population-based study in Olmsted County, Minnesota. *J Cardiac Failure*. (2014) 20:304–9. doi: 10.1016/j.cardfail.2014.02.007

6. Segar MW, Khan MS, Patel KV, Butler J, Tang Wilson WH, Vaduganathan M, et al. Prevalence and prognostic implications of diabetes with cardiomyopathy in community-dwelling adults. *J Am Coll Cardiol*. (2021) 78:1587–98. doi: 10.1016/j.jacc.2021.08.020

7. Lebeche D, Davidoff AJ, Hajjar RJ. Interplay between impaired calcium regulation and insulin signaling abnormalities in diabetic cardiomyopathy. *Nat Clin Pract Cardiovasc Med*. (2008) 5:715–24. doi: 10.1038/ncpcardio1347

8. Al Kury L, Smail M, Qureshi MA, Sydorenko V, Shmygol A, Oz M, et al. Calcium signaling in the ventricular myocardium of the Goto-Kakizaki type 2 diabetic rat. *J Diabetes Res*. (2018) 2018:2974304. doi: 10.1155/2018/2974304

9. Cai L, Wang Y, Zhou G, Chen T, Song Y, Li X. Attenuation by metallothionein of early cardiac cell death via suppression of mitochondrial oxidative stress results in a prevention of diabetic cardiomyopathy. *J Am Coll Cardiol*. (2006) 48:1688–97. doi: 10.1016/j.jacc.2006.07.022

10. Jia G, DeMarco VG, Sowers JR. Insulin resistance and hyperinsulinaemia in diabetic cardiomyopathy. *Nat Rev Endocrinol*. (2016) 12:144–53. doi: 10.1038/nrendo.2015.216

11. Nakamura M, Sadoshima J. Mechanisms of physiological and pathological cardiac hypertrophy. *Nat Rev Cardiol*. (2018) 15:387–407. doi: 10.1038/s41569-018-0007-y

12. Wan A, Rodrigues B. Endothelial cell-cardiomyocyte crosstalk in diabetic cardiomyopathy. *Cardiovasc Res*. (2016) 111:172–83. doi: 10.1093/cvr/cvw159

13. Vulesevic B, McNeill B, Giacco F, Maeda K, Blackburn NJR, Brownlee M, et al. Methylglyoxal-induced endothelial cell loss and inflammation contribute to the development of diabetic cardiomyopathy. *Diabetes*. (2016) 65:1699–713. doi: 10.2337/db15-0568

14. Van Linthout S, Seeland U, Riad A, Eckhardt O, Hohl M, Dhayat N, et al. Reduced MMP-2 activity contributes to cardiac fibrosis in experimental diabetic cardiomyopathy. *Basic Res Cardiol*. (2008) 103:319–27. doi: 10.1007/s00395-008-0715-2

15. Biernacka A, Cavalera M, Wang J, Russo I, Shinde A, Kong P, et al. Smad3 signaling promotes fibrosis while preserving cardiac and aortic geometry in obese diabetic mice. *Circ Heart Fail*. (2015) 8:788–98. doi: 10.1161/CIRCHEARTFAILURE.114.001963

16. Zhang Y, Wang JH, Zhang YY, Wang YZ, Wang J, Zhao Y, et al. Deletion of interleukin-6 alleviated interstitial fibrosis in streptozotocin-induced diabetic cardiomyopathy of mice through affecting TGFβ1 and miR-29 pathways. *Sci Rep*. (2016) 6:23010. doi: 10.1038/srep23010

17. Paolillo S, Marsico F, Prastaro M, Renga F, Esposito L, Martino De F, et al. Diabetic cardiomyopathy. *Heart Failure Clinics*. (2019) 15:341–7. doi: 10.1016/j.hfc.2019.02.003

18. Tan Y, Zhang Z, Zheng C, Wintergerst KA, Keller BB, Cai L. Mechanisms of diabetic cardiomyopathy and potential therapeutic strategies: preclinical and clinical evidence. *Nat Rev Cardiol*. (2020) 17:585–607. doi: 10.1038/s41569-020-0339-2

19. Wamil M, Goncalves M, Rutherford A, Borlotti A, Pellikka PA. Multi-modality cardiac imaging in the management of diabetic heart disease. *Front Cardiovasc Med*. (2022) 9:1043711. doi: 10.3389/fcvm.2022.1043711

20. Peterson LR, Gropler RJ. Metabolic and molecular imaging of the diabetic cardiomyopathy. *Circ Res*. (2020) 126:1628–45. doi: 10.1161/CIRCRESAHA.120.315899

21. Cosentino F, Grant PJ, Aboyans V, Bailey CJ, Ceriello A, Delgado V, et al. 2019 ESC Guidelines on diabetes, pre-diabetes, and cardiovascular diseases developed in collaboration with the EASD. *Eur Heart J*. (2020) 41:255–323. doi: 10.1093/eurheartj/ehz486

22. Patil VC, Shah KB, Vasani JD, Shetty P, Patil HV. Diastolic dysfunction in asymptomatic type 2 diabetes mellitus with normal systolic function. *J Cardiovasc Dis Res*. (2011) 2:213–22. doi: 10.4103/0975-3583.89805

23. Somaratne JB, Whalley GA, Poppe KK, ter Bals MM, Wadams G, Pearl A, et al. Screening for left ventricular hypertrophy in patients with type 2 diabetes mellitus in the community. *Cardiovasc Diabetol*. (2011) 10:29. doi: 10.1186/1475-2840-10-29

24. Weber TR, Silva RLD, Cossul S, Lofrano Alves MS, Lee SVDS, Brum Marques JL. Echocardiographic evaluation in type 1 diabetes mellitus. *Rev Portuguesa Cardiologia (English Edition)*. (2021) 40:757–65. doi: 10.1016/j.repce.2021.08.003

25. Holland DJ, Marwick TH, Haluska BA, Leano R, Hordern MD, Hare JL, et al. Subclinical LV dysfunction and 10-year outcomes in type 2 diabetes mellitus. *Heart*. (2015) 101:1061–6. doi: 10.1136/heartjnl-2014-307391

26. Rørth R, Jørgensen PG, Andersen HU, Christoffersen C, Gøtze JP, Køber L, et al. Cardiovascular prognostic value of echocardiography and N terminal pro B-type natriuretic peptide in type 1 diabetes: the Thousand & 1 Study. *Eur J Endocrinol*. (2020) 182:481–8. doi: 10.1530/EJE-19-1015

27. From AM, Scott CG, Chen HH. The development of heart failure in patients with diabetes mellitus and pre-clinical diastolic dysfunction. *J Am Coll Cardiol*. (2010) 55:300–5. doi: 10.1016/j.jacc.2009.12.003

28. Powell-Wiley TM, Poirier P, Burke LE, Després JP, Gordon-Larsen P, Lavie CJ, et al. Obesity and cardiovascular disease: A scientific statement from the American heart association. *Circulation*. (2021) 143:e990–991. doi: 10.1161/CIR.0000000000000973

29. Turkbey EB, Backlund JYC, Genuth S, Jain AJ, Miao CM, Cleary PA, et al. Myocardial structure, function, and scar in patients with type 1 diabetes mellitus. *Circulation*. (2011) 124:1737–46. doi: 10.1161/CIRCULATIONAHA.111.022327

30. Korosoglou G, Humpert PM, Ahrens J, Oikonomou D, Osman NF, Gitsioudis G, et al. Left ventricular diastolic function in type 2 diabetes mellitus is associated with myocardial triglyceride content but not with impaired myocardial perfusion reserve. *J Magn Reson Imaging*. (2012) 35:804–11. doi: 10.1002/jmri.22879

31. Storz C, Hetterich H, Lorbeer R, Heber SD, Schafnitzel A, Patscheider H, et al. Myocardial tissue characterization by contrast-enhanced cardiac magnetic resonance imaging in subjects with prediabetes, diabetes, and normal controls with preserved ejection fraction from the general population. *Eur Heart J Cardiovasc Imaging*. (2018) 19:701–8. doi: 10.1093/ehjci/jex190

32. Kwong RY, Sattar H, Wu H, Vorobiof G, Gandla V, Steel K, et al. Incidence and prognostic implication of unrecognized myocardial scar characterized by cardiac magnetic resonance in diabetic patients without clinical evidence of myocardial infarction. *Circulation*. (2008) 118:1011–20. doi: 10.1161/CIRCULATIONAHA.107.727826

33. Siddiqui TA, Chamarti KS, Tou LC, Demirjian GA, Noorani S, Zink S, et al. The merits, limitations, and future directions of cost-effectiveness analysis in cardiac MRI with a focus on coronary artery disease: A literature review. *J Cardiovasc Dev Dis*. (2022) 9:357. doi: 10.3390/jcdd9100357

34. Weinreb JC, Rodby RA, Yee J, Wang CL, Fine D, McDonald RJ, et al. Use of intravenous gadolinium-based contrast media in patients with kidney disease: consensus statements from the American college of radiology and the national kidney foundation. *Radiology*. (2021) 298:28–35. doi: 10.1148/radiol.2020202903

35. Rijzewijk LJ, van der Meer RW, Lamb HJ, Jong HWAM, Lubberink M, Romijn JA, et al. Altered myocardial substrate metabolism and decreased diastolic function in nonischemic human diabetic cardiomyopathy: studies with cardiac positron emission tomography and magnetic resonance imaging. *J Am Coll Cardiol*. (2009) 54:1524–32. doi: 10.1016/j.jacc.2009.04.074

36. Herrero P, Peterson LR, McGill JB, Matthew S, Lesniak D, Dence C, et al. Increased myocardial fatty acid metabolism in patients with type 1 diabetes mellitus. *J Am Coll Cardiol*. (2006) 47:598–604. doi: 10.1016/j.jacc.2005.09.030

37. Hosseinzadeh E, Ghodsirad MA, Alirezaei T, Arfenia M, Pirayesh, Amoiee M, et al. Comparing left ventricular mechanical dyssynchrony between diabetic and non-diabetic patients with normal gated SPECT MPI. *Int J Cardiovasc Imaging*. (2022) 38:249–56. doi: 10.1007/s10554-021-02358-1

38. Hu L, Qiu C, Wang X, Xu M, Shao X, Wang Y. The association between diabetes mellitus and reduction in myocardial glucose uptake: a population-based 18F-FDG PET/CT study. *BMC Cardiovasc Disord*. (2018) 18:203. doi: 10.1186/s12872-018-0943-9

39. Klonoff DC. United Kingdom prospective diabetes study follow-up studies establish a legacy effect of therapy for hyperglycemia but not hypertension. *J Diabetes Sci Technol*. (2008) 2:922–4. doi: 10.1177/193229680800200601

40. Aguilar D, Bozkurt B, Ramasubbu K, Deswal A. Relationship of hemoglobin A1C and mortality in heart failure patients with diabetes. *J Am Coll Cardiol*. (2009) 54:422–8. doi: 10.1016/j.jacc.2009.04.049

41. Boussageon R, Bejan-Angoulvant T, Saadatian-Elahi M, Lafont S, Bergeonneau C, Kassaï B, et al. Effect of intensive glucose lowering treatment on all cause mortality, cardiovascular death, and microvascular events in type 2 diabetes: meta-analysis of randomised controlled trials. *BMJ*. (2011) 343:d4169. doi: 10.1136/bmj.d4169

42. American Diabetes Association. 2. Classification and diagnosis of diabetes: standards of medical care in diabetes-2020. *Diabetes Care*. (2020) 43:S14–31. doi: 10.2337/dc20-S002

43. Wang Y, Negishi T, Negishi K, Marwick TH. Prediction of heart failure in patients with type 2 diabetes mellitus- a systematic review and meta-analysis. *Diabetes Res Clin Pract*. (2015) 108:55–66. doi: 10.1016/j.diabres.2015.01.011

44. Cosmi F, Shen L, Magnoli M, Abraham WT, Anand IS, Cleland JG, et al. Treatment with insulin is associated with worse outcome in patients with chronic heart failure and diabetes. *Eur J Heart Fail*. (2018) 20:888–95. doi: 10.1002/ejhf.1146

45. Adel FW, Zheng Y, Wan SH, Christie G, Shuchong P, Syed A, et al. Insulin therapy is associated with increased myocardial interstitial fibrosis and cardiomyocyte apoptosis in a rodent model of experimental diabetes. *Front Physiol*. (2022) 13:890907. doi: 10.3389/fphys.2022.890907

46. Boussageon R, Supper I, Bejan-Angoulvant T, Kellou N, Cucherat M, Boissel JP, et al. Reappraisal of metformin efficacy in the treatment of type 2 diabetes: a meta-analysis of randomised controlled trials. *PloS Med*. (2012) 9:e1001204. doi: 10.1371/journal.pmed.1001204

47. Turner RC, Holman RR, Stratton IM, Cull CA, Matthews DR, Manley SE, et al. Effect of intensive blood-glucose control with metformin on complications in overweight patients with type 2 diabetes (UKPDS 34). UK Prospective Diabetes Study (UKPDS) Group. *Lancet*. (1998) 352:854–65. doi: 10.1016/S0140-6736(98)07037-8

48. Tzoulaki I, Molokhia M, Curcin V, Little MP, Millett CJ, Ng A, et al. Risk of cardiovascular disease and all cause mortality among patients with type 2 diabetes prescribed oral antidiabetes drugs: retrospective cohort study using UK general practice research database. *BMJ*. (2009) 339:b4731. doi: 10.1136/bmj.b4731

49. Lago RM, Singh PP, Nesto RW. Congestive heart failure and cardiovascular death in patients with prediabetes and type 2 diabetes given thiazolidinediones: a meta-analysis of randomised clinical trials. *Lancet*. (2007) 370:1129–36. doi: 10.1016/S0140-6736(07)61514-1

50. Scirica BM, Braunwald E, Raz I, Cavender MA, Morrow DA, Jarolim P, et al. Heart failure, saxagliptin, and diabetes mellitus: observations from the SAVOR-TIMI 53 randomized trial. *Circulation*. (2014) 130:1579–88. doi: 10.1161/CIRCULATIONAHA.114.010389

51. Pop-Busui R, Januzzi JL, Bruemmer D, Butalia S, Green JB, Horton WB, et al. Heart failure: an underappreciated complication of diabetes. A consensus report of the American diabetes association. *Diabetes Care*. (2022) 45:1670–90. doi: 10.2337/dci22-0014

52. Nauck MA, Quast DR, Wefers J, Meier JJ. GLP-1 receptor agonists in the treatment of type 2 diabetes - state-of-the-art. *Mol Metab*. (2021) 46:101102. doi: 10.1016/j.molmet.2020.101102

53. Marso SP, Daniels GH, Brown-Frandsen K, Kristensen P, Mann JF, Nauck MA, et al. Liraglutide and cardiovascular outcomes in type 2 diabetes. *N Engl J Med*. (2016) 375:311–22. doi: 10.1056/NEJMoa1603827

54. Marso SP, Bain SC, Consoli A, Eliaschewitz FG, Jódar E, Leiter LA, et al. Semaglutide and cardiovascular outcomes in patients with type 2 diabetes. *N Engl J Med*. (2016) 375:1834–44. doi: 10.1056/NEJMoa1607141

55. McGuire DK, Alexander JH, Johansen OE, Perkovic V, Rosenstock J, Cooper ME, et al. Linagliptin effects on heart failure and related outcomes in individuals with type 2 diabetes mellitus at high cardiovascular and renal risk in CARMELINA. *Circulation*. (2019) 139:351–61. doi: 10.1161/CIRCULATIONAHA.118.038352

56. Pfeffer MA, Claggett B, Diaz R, Dickstein K, Gerstein HC, Køber LV, et al. Lixisenatide in patients with type 2 diabetes and acute coronary syndrome. *N Engl J Med*. (2015) 373:2247–57. doi: 10.1056/NEJMoa1509225

57. Hernandez AF, Green JB, Janmohamed S, D'Agostino RB Sr, Granger CB, Jones NP, et al. Albiglutide and cardiovascular outcomes in patients with type 2 diabetes and cardiovascular disease (Harmony Outcomes): a double-blind, randomised placebo-controlled trial. *Lancet*. (2018) 392:1519–29. doi: 10.1016/S0140-6736(18)32261-X

58. Kristensen SL, Rørth R, Jhund PS. Cardiovascular, mortality, and kidney outcomes with GLP-1 receptor agonists in patients with type 2 diabetes: a systematic review and meta-analysis of cardiovascular outcome trials. *Lancet Diabetes Endocrinol*. (2019) 7:776–85. doi: 10.1016/S2213-8587(19)30249-9

59. Kosiborod MN, Abildstrøm SZ, Borlaug BA, Butler J, Rasmussen S, Davies M, et al. Semaglutide in patients with heart failure with preserved ejection fraction and obesity. *New Engl J Med*. (2023) 389:1069–84. doi: 10.1056/NEJMoa2306963

60. Wiviott SD, Raz I, Bonaca MP, Mosenzon O, Kato ET, Cahn A, et al. Dapagliflozin and cardiovascular outcomes in type 2 diabetes. *New Engl J Med*. (2019) 380:347–57. doi: 10.1056/NEJMoa1812389

61. Zinman B, Wanner C, Lachin JM, Fitchett D, Bluhmki E, Hantel S, et al. Empagliflozin, cardiovascular outcomes, and mortality in type 2 diabetes. *N Engl J Med*. (2015) 373:2117–28. doi: 10.1056/NEJMoa1504720

62. ElSayed NA, Aleppo G, Aroda VR, Bannuru RR, Brown FM, Bruemmer D, et al. 9. Pharmacologic approaches to glycemic treatment: standards of care in diabetes-2023. *Diabetes Care*. (2023) 46:S140–57. doi: 10.2337/dc23-S009

frontiers | Frontiers in Endocrinology

TYPE Original Research
PUBLISHED 20 March 2025
DOI 10.3389/fendo.2025.1525831

OPEN ACCESS

EDITED BY
Ramoji Kosuru,
Versiti Blood Research Institute, United States

REVIEWED BY
Priyanka Choudhury,
Medical College of Wisconsin, United States
Radha Vaddavalli,
The Ohio State University, United States

*CORRESPONDENCE
Lin Huang
hl16832@aliyun.com

RECEIVED 10 November 2024
ACCEPTED 04 March 2025
PUBLISHED 20 March 2025

CITATION
Huang X, Wang Y, Wan R, You Z and Huang L (2025) Identification of lipid metabolism-related genes in dapagliflozin treated rats with diabetic cardiomyopathy by bioinformatics. *Front. Endocrinol.* 16:1525831. doi: 10.3389/fendo.2025.1525831

Identification of lipid metabolism-related genes in dapagliflozin treated rats with diabetic cardiomyopathy by bioinformatics

Xun Huang[1], Yunhong Wang[2], Rong Wan[3], Zhigang You[1] and Lin Huang[1]*

[1]Department of Cardiovascular Medicine, The Second Affiliated Hospital of Nanchang University, Nanchang, Jiangxi, China, [2]Department of Cardiology, Ningdu County People's Hospital, Ganzhou, Jiangxi, China, [3]Jiangxi Key Laboratory of Molecular Medicine, The Second Affiliated Hospital, Jiangxi Medical College, Nanchang University, Nanchang, Jiangxi, China

Background: Diabetic cardiomyopathy (DCM) is a heart disease caused by the metabolic disorders of glucose and lipids associated with diabetes, leading to heart failure and death in diabetic patients. Dapagliflozin (DAPA) serves as a treatment for managing blood glucose levels in individuals with type 2 diabetes mellitus (DM). However, the specific mechanisms by which DAPA treats DCM are not yet fully understood.

Methods: Sprague-Dawley (SD) rats (n = 5/group) were randomly divided into control, model, and intervention groups. Lipid metabolism-related genes (LMRGs) were gotten from publicly available database. Differential expression analysis of model *vs.* control and intervention *vs.* model samples was performed to obtain differentially expressed genes (DEGs), and the result was recorded as DEGs-Model and DEGs-Intervention. The intersection of genes with opposing expression trends between DEGs-Model and DEGs-Intervention were considered as candidate genes. Subsequently, candidate genes and LMRGs were intersected to acquire hub genes, and the expression of hub genes was analyzed in each group of samples. Then, the mechanism of action of these hub genes were investigated through functional enrichment analysis, gene set enrichment analysis (GSEA), and predictive of m6A binding sites.

Results: Ultimately, 68 candidate genes and 590 LMRGs were intersected to derive 2 hub genes (Acsbg1 and Etnppl). Acsbg1 was significantly increase in model group compared with control group. RT-qPCR results confirmed Acsbg1 was obviously higher expression in model group, while Etnppl was significantly lower expression in model group compare to control groups and intervention group. While the expression of Etnppl was significantly increase in intervention group compared with model group. Functional enrichment analyses indicated

that Acsbg1 and Etnppl were associated with fatty acid metabolism. The findings of GSEA indicated that Acsbg1 and Etnppl might affect the occurrence and progression of DCM through lysosome. And the Acsbg1 and Etnppl were located at UCAGG in the RNA secondary structure.

Conclusion: This study identified 2 hub genes (Acsbg1 and Etnppl) as potential new focal points for diagnosing and treating DCM.

KEYWORDS

diabetic cardiomyopathy, dapagliflozin, lipid metabolism, hub gene, bioinformatics analysis

1 Introduction

Diabetic cardiomyopathy (DCM) is a distinct form of heart disease that occurs in patients with diabetes mellitus (DM), independent of traditional cardiovascular risk factors like hypertension, coronary artery disease, and valvular diseases (1), the prevalence of heart failure among diabetic patients globally ranges from 19% to 26%, DCM is the leading cause of heart failure in diabetic patients (2). DCM primarily arises from chronic hyperglycemia and insulin resistance, leading to a maladaptive shift in cardiomyocyte energy metabolism from glucose oxidation to excessive reliance on fatty acid (FA) oxidation. This metabolic shift, coupled with lipotoxicity-induced cellular damage, inflammatory responses, activation of the advanced glycation end products receptor for advanced glycation end products pathway, myocardial fibrosis, and impaired calcium homeostasis, culminates in structural and functional myocardial alterations, ultimately causing DCM (3, 4). Due to the incomplete understanding of the complex molecular mechanisms underlying DCM, developing reliable therapeutic targets and effective pharmacological interventions remains challenging (5). Therefore, exploring hub genes in DCM is crucial for understanding its exact mechanisms and developing new strategies to reduce the risk of DCM patients.

Lipid metabolism dysregulation plays a fundamental role in the pathogenesis of DCM (6). Lipid metabolism disorders lead to an increase in lipid peroxidation products, which further exacerbate oxidative stress and inflammatory responses (7). The involvement of peroxisome proliferator-activated receptor (PPAR) in diabetes-related metabolic disturbances and lysosomal abnormalities can impair lipophagy, the autophagic process that utilizes lipids as substrates, leading to intracellular lipid accumulation (1, 8). This is believed to significantly contribute to the development of DCM. Consequently, a more in-depth investigation into how lipid metabolism disorders contribute to DCM could offer new theoretical insights and identify potential targets for effective treatment of this condition.

Sodium-glucose cotransporter-2 (SGLT2) inhibitors, a novel class of glucose-lowering medications, reduce plasma glucose PG by producing glycosuria. significantly reduce hospitalization and mortality rates in patients with heart failure (9). SGLT2 inhibitors not only help lower blood sugar but also assist patients with type 2 diabetes in losing weight, reducing blood pressure, and decreasing the risk of cardiovascular events. SGLT2 inhibitors may promote FA oxidation and reduce fat accumulation in tissues by activating AMP-activated protein kinase (AMPK) and increasing the expression of fibroblast growth factor 21 (FGF21) (10). Dapagliflozin (DAPA) is one of the earliest SGLT2 inhibitors used for glycemic control in patients with type 2 diabetes mellitus (11). In obesity-related cardiomyopathy (HFD), DAPA can significantly reduce body weight and improve lipid levels (12). Besides its lipid-lowering effects, DAPA provides direct protective effects against myocardial cell damage induced by saturated FA However, the specific biological mechanisms of DAPA treatment in DCM are currently unclear.

To investigate the hub genes involved in lipid metabolism during DAPA treatment for DCM, this study used DCM rats as a model. Bioinformatics analysis was employed to examine the biological pathways these hub genes participate in, and the molecular regulatory network was explored. The aim is to provide new reference points for clinical treatment research of DCM.

2 Materials and methods

2.1 Establishment of DAPA-intervened DCM model

The 15 male Sprague-Dawley (SD) rats (180 g-220 g, 6-8 weeks old) were obtained from the Beijing Huafukang Bio-technology Co. (Production License No.: SCXK (Beijing) 2019-0010; Use License No.: SYXK (Dian) K2020-0006). The Ethics Committee of the Second Affiliated Hospital of Nanchang University granted ethical approval (Approval No. NCULAE-20221031151). The rats were randomly assigned to one of three groups: the control group (n = 5), the DCM model group (n = 5), and the DCM + DAPA intervention group (n = 5). Rats in the control group were fed a normal diet, while rats in the model and intervention groups were fed a high-fat, high-sugar diet for 4 weeks. After this feeding period, insulin resistance was assessed using the peritoneal glucose tolerance test

(IPGTT) and insulin tolerance test (IPITT). To induce DM in the model and intervention groups, rats were given a single intravenous injection of streptozotocin (STZ, 35 mg/kg). Control rats received an intraperitoneal injection of citrate buffer at the same time. Fasting blood glucose levels were measured from the tail vein 3 and 7 days after the STZ injection. Rats with fasting blood glucose levels ≥ 11.1 mmol/L were considered successfully induced DM. Following successful DM induction, rats in the DCM and DCM + DAPA groups continued to receive the high-fat, high-sugar diet, while the control group was maintained on a normal diet. After 8 weeks, echocardiography was performed, confirming the presence of left ventricular diastolic dysfunction in both the model and intervention groups, indicating successful induction of DCM. After DCM model was confirmed, rats in the DCM + DAPA group were administered dapagliflozin (DAPA) at a dose of 1 mg/kg/day in their drinking water, while rats in the DCM group received no treatment. Following 6 weeks of drug intervention, all rats were euthanized under anesthesia according to ethical guidelines, and myocardial tissue samples were collected from the left ventricle for further analysis.

2.2 Hematoxylin and eosin staining

HE staining is a fundamental technique in histology and pathology for visualizing tissue samples under a microscope. Tissue sections (5 μm thick) were prepared from paraffin-embedded specimens that had been fixed in 4% paraformaldehyde (PFA). After baking at 64°C for 1 h, the tissue sections were deparaffinized in xylene and then rehydrated through a graded ethanol series (100%, 95%, 80%, and 70%) to remove the xylene and gradually restore the tissue's water content. After rehydration, the sections were stained with hematoxylin for 5 min, followed by a wash in running tap water to differentiate the stain. The sections were then stained with eosin for 10-15 s to highlight cytoplasmic components. Finally, the slides were dehydrated through a graded ethanol series (95% and 100%), cleared in xylene, and mounted with a coverslip using a mounting medium for microscopic examination. Finally, the stained tissue sections were examined under a light microscope for histological analysis.

2.3 Masson staining

Masson's staining effectively highlights collagen fiber changes, enabling assessment of collagen proliferation and the progression of DCM. First, prepare Weigert's iron hematoxylin solution by mixing Reagents A1 and A2 in a 1:1 ratio just before use. Apply the solution to tissue sections for 5-10 min, then rinse with distilled water. Differentiate with acid ethanol for 5-15 s, followed by a 30 s wash in distilled water. Next, applying Masson's blueing solution for 3-5 min, then rinse with distilled water (30 s). After, Biebrich Scarlet-Acid Fuchsin was utilizing to stain for 5-10 min. During staining, prepare the weak acid solution by mixing distilled water and weak acid in a 2:1 ratio. Following this, apply the weak acid solution to the sections and wash for 30 s. Drain excess liquid and apply phosphomolybdic acid for 1-2 min, followed by a 30 s wash with the weak acid solution. Clear the sections in xylene twice, for 1-2 min each, then mount with neutral balsam. Finally, the proliferation of collagen fibers in the tissues was observed and captured in images.

2.4 Source of data

Lipid metabolism-related genes (LMRGs) were gotten from Molecular Signatures Database (MSigDB, https://www.gsea-msigdb.org/gsea/msigdb): Using "lipid metabolism" as the keyword, gene-ID was converted to rat gene, and then 590 LMRGs were obtained by removing duplicate genes (Supplementary Table S1) (13).

2.5 Transcriptome sequencing and data preprocessing

Total RNA was isolated and purified from tissue samples using TRIzol (Invitrogen, CA, USA). Next, the quantity and integrity of the total RNA were assessed using a NanoDrop ND-1000 spectrophotometer (NanoDrop, Wilmington, DE, USA) and a Bioanalyzer 2100 system (Agilent, CA, USA), respectively. Samples with concentrations > 50 ng/μL, RIN values > 7.0, OD 260/280 > 1.8, and total RNA > 1 μg were considered suitable for downstream experiments. Then, Poly(A) RNA was purified from 1 μg of total RNA using Dynabeads Oligo (dT)25-61005 (Thermo Fisher, CA, USA) through two rounds of purification. Subsequently, the poly(A) RNA was fragmented into small pieces using the Magnesium RNA Fragmentation Module (NEB, cat. e6150, USA) at 94°C for 5-7 minutes. The cleaved RNA fragments were then reverse-transcribed to create cDNA using SuperScript™ II Reverse Transcriptase (Invitrogen, cat. 1896649, USA). What's more, Polymerase Chain Reaction (PCR) amplification was performed under the following conditions: initial denaturation at 95°C for 3 minutes; 8 cycles of denaturation at 98°C for 15 seconds, annealing at 60°C for 15 seconds, and extension at 72°C for 30 seconds; followed by a final extension at 72°C for 5 minutes. The average insert size for the final cDNA library was 300 ± 50 bp. Sequencing was carried out on the Illumina NovaSeq 6000 platform using the paired-end 150 bp (PE150) sequencing mode.

Afterwards, data quality was assess using FastQC (v 0.11.9), and low-quality data were filtered using Trimmomatic (v 0.39). For mRNA sequencing reads alignment, clean data was mapped to the reference genome (Rat Rnor 6.0 genome) using the alignment tool hisat2 (v2.2.1) with default parameters. Finally, a gene expression matrix was generated for subsequent analysis.

2.6 Base mass value and content distribution of sequencing data

Phred scaled quality value (Q value) was used to assess the base error probability. The Q value was inversely proportional to the

probability of error, and when the Q value reached 30, the probability of a base being in error was only 0.001, meaning that only about 1 out of every 1,000 bases was likely to be in error. In addition, the distribution of base types in the sequencing data was analyzed, particularly with regard to the proportion of guanine (G) as well as cytosine (C) in the DNA sequences. In general, a uniform distribution of GC content means that the data have not been affected by exogenous DNA contamination or other technical factors.

2.7 Comparison of transcriptome data with reference genome sequences

To understand more deeply the comparison of the transcriptome data with the reference genome sequence, the study utilized a designated reference genome for alignment analysis. Firstly, the sequences in the transcriptome data were aligned with the reference genome sequences to determine their positions in the genome. Then, the successfully aligned sequences were assembled and quantitatively analyzed using StringTie software (v 2.1.6) to probe gene expression and gene structure. The analysis focused on the distribution of the sequences in different regions of the genome (e.g. exons, introns, and intergenic regions) (14).

2.8 Gene expression analysis

Next, the fragments per kilobase transcript model per million mapped fragments (FPKM) was calculated to measure the expression level of transcript or gene by the StringTie software (v 2.1.6). The FPKM standardization method takes into account differences in sequencing depth and gene length to make gene expression comparable across samples. The number of sequences mapped to the genome and the length of transcripts in each sample were normalized to calculate FPKM values for each gene. Then these FPKM values were log10 transformed to better demonstrate the distribution of gene expression.

2.9 Identification of differentially expressed genes

In order to assess the variability in the expression of the transcriptome data of the 3 groups of samples, the transcriptome sequencing data was analyzed via principal component analysis (PCA). Differential expression analysis of model *vs.* control and intervention *vs.* model samples was performed to obtain DEGs-Model and DEGs-Intervention by the "DESeq2" R package (v 1.34.0) (15) ($|\log_2$Fold Change (FC)$| > 0.5$ as well as p.value < 0.05). Volcano maps as well as heat maps of the DEGs-Model and DEGs-Intervention were visualized via "ggplot2" R package (v 3.4.3) (16) and "ComplexHeatmap" R package (v 2.14.0) (17).

2.10 Identification and functional enrichment analysis of candidate genes

The intersection of up-regulated genes in DEGs-Model with the down-regulated genes in DEGs-Intervention and down-regulated genes in DEGs-Model with the up-regulated genes in DEGs-Intervention were recorded as candidate genes via "ggvenn" R package (v 0.1.9) (18). To elucidate the potential biological functions and related pathways, Gene ontology (GO) enrichment analysis was performed on candidate genes (p.value < 0.05). The GO enriched results were sorted by P.value from smallest to largest, and the top 10 significant pathways were shown via "GOplot" R package (v 1.0.2) (19). Kyoto Encyclopedia of Genes and Genomes (KEGG) was performed on candidate genes (p.value < 0.05). The KEGG enriched results were sorted by count from smallest to largest, and the top 10 significant pathways were shown by "clusterProfiler" R package (v 4.7.1.003) (17).

2.11 Identification and functional enrichment analysis of hub genes

Candidate genes and LMRGs were intersected to acquire hub genes, while the expression of hub genes was analysed in each group of samples via "ggvenn" R package (v 0.1.9). Then, GO enrichment analysis was performed on hub genes (p.value < 0.05). The GO enriched results were sorted by p.value from smallest to largest, and the top 10 significant pathways were shown by "GOplot" R package (v 1.0.2). And KEGG was performed on hub genes (p.value < 0.05). The KEGG enriched results were sorted by count from smallest to largest, and the pathways were shown by "clusterProfiler" R package (v 4.7.1.003). Gene-gene interaction (GGI) network was constructed by GeneMANIA (http://www.genemania.org/), and the network interactions of hub genes and the biological functions involved were explored at the protein level.

2.12 Gene set enrichment analysis

The background gene set ("c2.cp.kegg_medicus.v2023.2.Hs.symbols.gmt") was downloaded from the MSigDB. The Spearman correlation coefficients between the expression levels of hub genes and other genes were ranked by "psych" R package (v 2.1.6) (20), and then the GSEA was performed through "clusterProfiler" R package (v 4.7.1.3) (21) ($|$normalized enrichment score (NES)$| > 1$ as well as adj. $p < 0.05$), and the pathways ranked in the top 5 in the |NES| were selected for presentation.

2.13 Predictive analysis of m6A binding sites

To investigate whether m6A affects the translational stability of hub genes, the m6A binding sites of hub genes were predicted. Sequence

files of the hub genes were acquired from National Center for Biotechnology Information (NCBI, https://www.ncbi.nlm.nih.gov/gene/). The m6A modification sites of the hub genes and their locations in the RNA secondary structure were predicted by the sequence-based RNA adenosine modification site predictor (SRAMP, http://www.cuilab.cn/sramp/) database, with set the parameter to "Analyze RNA secondary structure" and the tissue parameter to "General (default)".

2.14 Regulation network construction

The microRNAs (miRNAs) of biomarkers were predicted by miRWalk (http://mirwalk.umm.uni-heidelberg.de/) and TargetScan (http://www.targetscan.org/vert_72/) databases, and the intersection of the results predicted by 2 databases was taken as the key miRNA, and the key miRNA-mRNA network was visualized via Cytoscape software (v 3.10.2) (22). Transcription factors (TFs) for the hub genes were acquired from the Encyclopedia of DNA Elements (ENCODE, https://www.encodeproject.org/) database via NetworkAnalyst (http://www.networkanalyst.ca), and the hub genes-TF network was visualized via Cytoscape software (v 3.10.2).

2.15 Evaluation hub genes expression levels

A total of 15 tissue samples (5 control samples, 5 model samples, and 5 intervention samples) were acquired from the DCM model. Total RNA from the 15 samples were extracted with the TRIzol reagent (Ambion, USA) according to the manufacturer's protocol. Then the RNA concentration was tested using NanoPhotometer N50. The cDNA was synthetized by reverse-transcribed using the SureScript-First-strand-cDNA-synthesis-kit, and the reverse-transcribed was performed with S1000^{TM} Thermal Cycler (Bio-Rad, USA). The sequences of all primers can be found in Supplementary Table S2. The qPCR assay was performed with CFX Connect Real-time Quantitative Fluorescence PCR Instrument (Bio-Rad, USA) (pre-denaturation at 95℃ for 1 min, denaturation at 95℃ for 20s, annealing at 55℃ for 20s, extension at 72℃ for 30s, a total of 40 cycles). The relative quantification of mRNAs was calculated using the $2^{-\Delta\Delta CT}$ method. The results from the RT-qPCR were exported to Excel, and then imported into Graphpad Prism 5 for statistical analysis and visualization.

2.16 Statistical analysis

Bioinformatics analyses were performed by R programming language (v 4.2.2). The statistical difference between two groups was assessed using a Wilcoxon test. The $p < 0.05$ was considered statistically significant.

3 Results

3.1 Effect of DAPA treatment on myocardial injury and fibrosis

HE staining results showed that in the control group, cardiac muscle fibers were well-organized, with no evidence of myocardial fiber damage and normal cellular spacing. In contrast, myocardial tissue in the model group exhibited significant damage, with some myofibrils dissolved, cardiac muscle fibers broken, and cellular spaces markedly widened. After DAPA treatment, rat cardiac muscle fibers appeared relatively well-aligned, with no fiber damage and normal cellular spacing, suggesting that DAPA played an important role in regulating myocardial injury and associated pathological processes (Figures 1A–C). Additionally, Masson staining revealed that in the model group, the degree of fibrosis in myocardial tissue was severe, with abundant collagen deposition. However, after DAPA treatment, the amount of collagen fibers in the myocardial tissue was significantly reduced, indicating that DAPA treatment effectively alleviated myocardial tissue fibrosis (Figures 1D–F).

3.2 Quality control analysis of sequencing data

The quality of the sequencing data was above Q30, and the GC content was uniformly distributed and concentrated in 40%-60%, with no GC offset, which indicated that the sequencing data had high accuracy and stable quality (Figure 2A). The probability of sequence matching to the exons region was above 89%, which indicated the high availability and reliability of the data, and laid the foundation for the subsequent gene expression analysis (Figure 2B). The range and pattern of distribution of $\log_{10}$ (FPKM) in different samples and the mean line on a straight line were shown by box plots, which indicated there was good comparability in gene expression among the different samples. And the $\log_{10}$(FPKM) density distribution plot was showed that $\log_{10}$(FPKM) formed a centrally distributed peak for all samples, which indicated that gene expression was not biased on the whole (Figure 2C).

3.3 Identification and functional enrichment analysis of 68 candidate genes

PCA result was showed significant differences between all 3 groups (Figure 3A). A total of 1,311 DEGs-Model were screened in model *vs.* control samples, comprising 734 genes (Angptl4, Tekt4, and Vnn3, etc.) with increased expression and 577 genes (Ffar4, Krt86, and Olr649, etc.) with decreased expression (Figures 3B, C). A total of 466 DEGs_Intervention were screened in intervention *vs.* model samples, comprising 91 genes (AABR07021430.1,

10.3389/fendo.2025.1525831

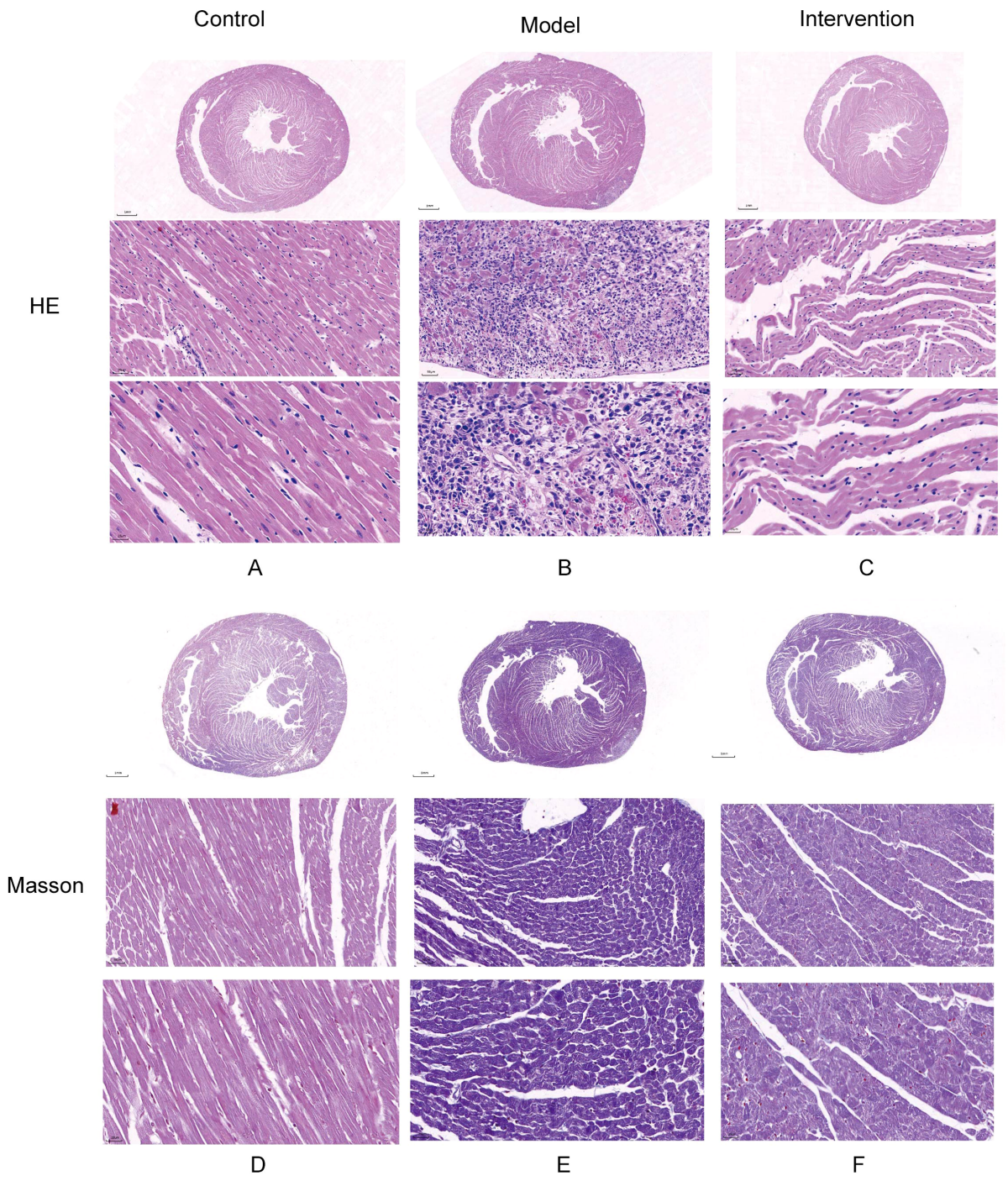

FIGURE 1
Histological analysis of myocardial injury and fibrosis in DCM rats. HE and Masson's trichrome staining were used to assess the effects of DAPA on myocardial injury and fibrosis in DCM rats. **(A)** The control group shows normal cardiac structure, while **(B)** the model group exhibits disrupted muscle fibers and widened spaces. DAPA treatment **(C)** improves these changes with better-organized cardiac structure. Masson's staining reveals normal collagen in controls **(D)**, increased fibrosis in the model group **(E)**, and reduced collagen deposition with DAPA treatment **(F)**. These results demonstrate that DAPA effectively alleviates myocardial injury and fibrosis in DCM rats.

AABR07028795.1, and RT1–S2, etc.) with increased expression and 375 genes (Pnoc, AABR07069371.1, and Thrsp, etc.) with decreased expression (Figures 3D, E). Subsequently, the 734 up-regulated genes in DEGs-Model with the 375 down-regulated genes in DEGs-Intervention and 577 down-regulated genes in DEGs-Model with the 91 up-regulated genes in DEGs-Intervention were intersected, resulting in the identification of 68 candidate genes (Figure 3F) (Supplementary Table S3). Furthermore, candidate genes were enriched and presented in 346 GO pathways, including 324 in biological

10.3389/fendo.2025.1525831

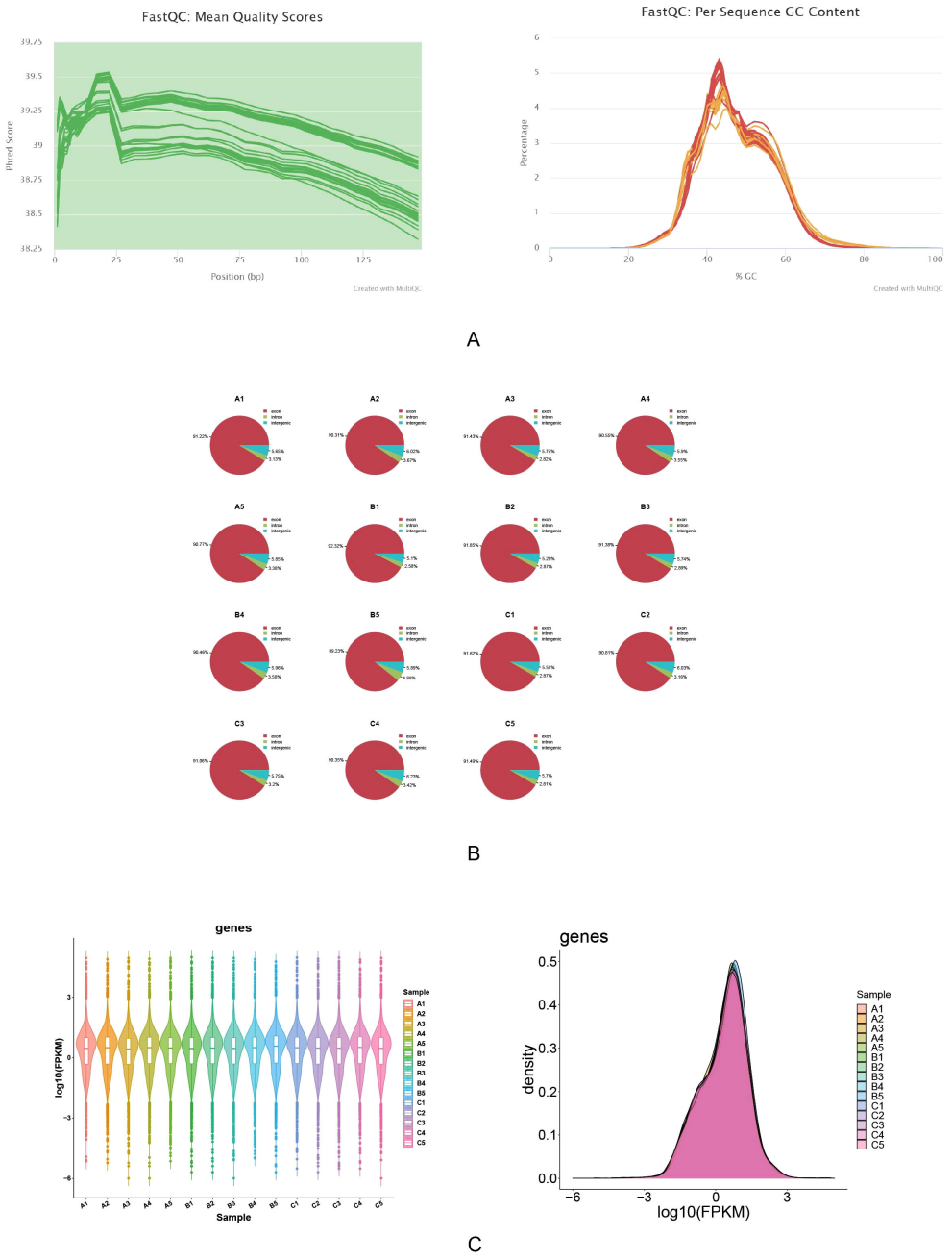

FIGURE 2
Quality assessment and gene expression analysis of RNA sequencing data. The quality of RNA sequencing data was evaluated using FastQC. **(A)** The mean quality scores across all bases remained high (>38), demonstrating excellent sequencing quality. **(B)** The per sequence GC content showed consistent distribution, with over 90% of sequences in each sample meeting quality standards. **(C)** Gene expression analysis indicated consistent distribution patterns across samples, with log10(FPKM) values primarily ranging from -3 to 3. These results confirm the high quality and reliability of the sequencing data.

process (BP), 12 in cellular component (CC), and 10 in molecular function (MF) (Figure 3G). For example, positive regulation of protein tyrosine kinase activity was enriched in BP; collagen-containing extracellular matrix was enriched in CC; FAD binding was enriched in MF. And the candidate genes were enriched and presented in 23 KEGG pathways (such as cAMP signaling pathway) (Figure 3H).

3.4 Identification and functional enrichment analysis of 2 hub genes

The 68 candidate genes and 590 LMRGs were intersected, resulting in the identification of 2 hub genes (Acsbg1 and Etnppl) (Figure 4A). In which, compared with control group, Acsbg1 was significantly increase in model group ($p < 0.05$). In transcriptome

10.3389/fendo.2025.1525831

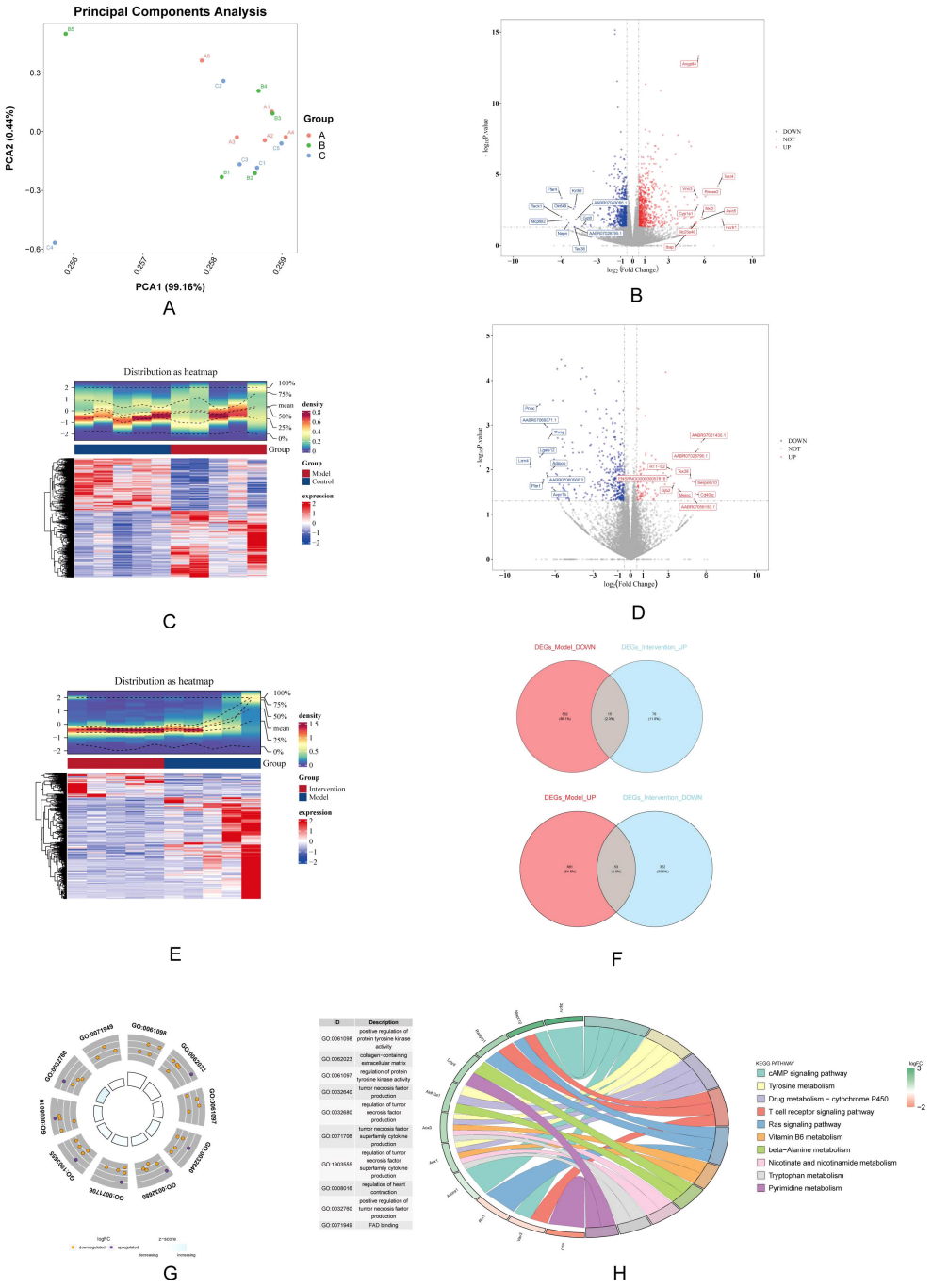

FIGURE 3
Differential gene expression analysis and functional enrichment. **(A)** PCA shows distinct clustering among the control, model, and DAPA groups, indicating clear separation of gene expression profiles. **(B)** Volcano plot displays significantly DEGs between model and control groups, highlighting upregulated (red) and downregulated (blue) genes. **(C)** Heatmap visualization illustrates the expression patterns of DEGs, with clear separation of groups. **(D)** A second volcano plot shows DEGs between the DAPA treatment and model groups. **(E)** The accompanying heatmap represents the distribution of DEGs, emphasizing the changes induced by DAPA. **(F)** Venn diagrams summarize the overlap of upregulated and downregulated genes across different comparisons. **(G)** GO analysis reveals significantly enriched biological processes. **(H)** KEGG enrichment analysis highlights pathways significantly associated with DEGs, detailing gene counts and statistical significance. These analyses underscore the molecular alterations and potential therapeutic targets in DCM treated with DAPA.

sequencing data, the expression of Etnppl was significantly increase in intervention group compared with model group ($p < 0.05$) (Figure 4B). Likewise, RT-qPCR results showed Acsbg1 was obviously higher expression in model group compare to control groups and intervention group, while Etnppl was significantly lower expression in model group compare to control groups and intervention group ($P < 0.05$) (Figure 4C). Furthermore, the Acsbg1 and Etnppl were enriched and presented in 31 GO

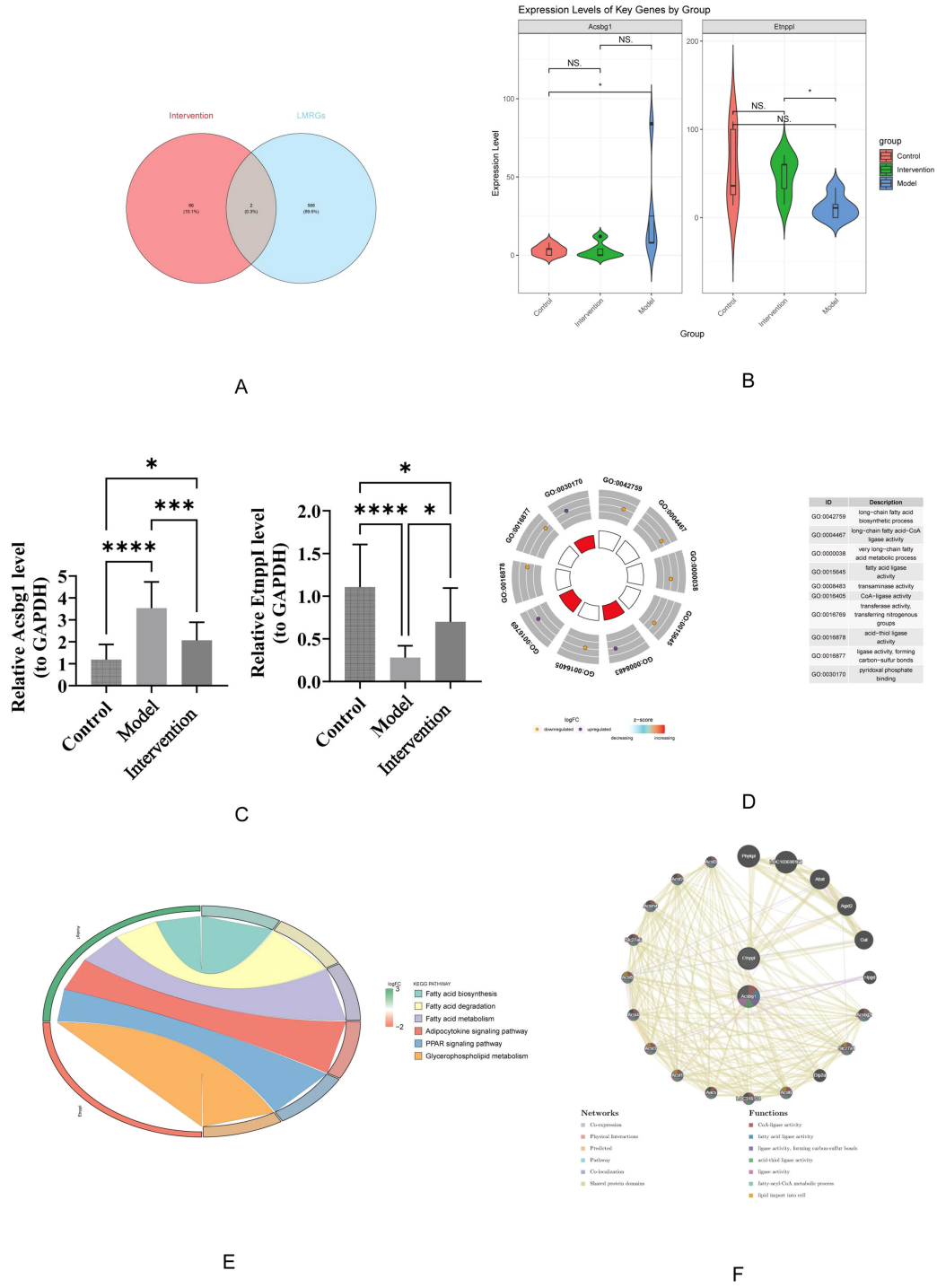

FIGURE 4
Key gene expression and functional enrichment analysis. **(A)** Venn diagram illustrating the overlap between intervention-related genes and LMRGs. **(B)** Violin plots show expression levels of key genes, Acsbg1 and Etnppl, across the control, model, and intervention groups, highlighting significant differences among the groups (p-values indicated). **(C)** Quantitative analysis confirms significant changes in gene expression levels between groups, with statistical significance denoted. **(D)** Gene Ontology (GO) enrichment analysis reveals that these key genes are primarily involved in fatty acid metabolism and regulation. **(E)** Further pathway analysis indicates significant enrichment in the fatty acid degradation, adipocytokine signaling, and PPAR signaling pathways. **(F)** Gene function network analysis illustrates complex interactions among these pathways. These results highlight the critical role of these key genes in mediating the effects of DAPA treatment in DCM.

pathways, including 18 in BP (such as long-chain FA biosynthetic process) and 13 in MF (such as transaminase activity) (Figure 4D). And the Acsbg1 and Etnppl were enriched and presented in 6 KEGG pathways (such as FA biosynthesis) (Figure 4E). The GGI network results showed that the hub genes were functionally associated with 18 genes (Abat, Agxt2,and Oat, etc.) and predicted 7 functions (such as CoA-ligase activity) (Figure 4F).

3.5 GSEA of Acsbg1 and Etnppl

The GSEA results showed that Acsbg1 was enriched to 13 KEGG pathways (lysosome, oxidative phosphorylation, and Parkinsons disease, etc.), and the Etnppl was enriched to 14 pathways (lysosome, proteasome, and ribosome, etc.) (Figures 5A, B). Among them, both Acsbg1 and Etnppl were significantly enriched for 14 pathways including spliceosome, lysosome, ribosome, proteasome, valine leucine and isoleucine degradation, N glycan biosynthesis, and DNA replication (Supplementary Table S4).

3.6 Predictive analysis of m6A binding sites for Acsbg1 and Etnppl

The m6A binding sites for Acsbg1 and Etnppl were located at UCAGG in the RNA secondary structure. The m6A modification sites of Acsbg1 were predominantly located in regions of low confidence, while the m6A modification sites of Etnppl were mostly concentrated in regions of moderate confidence, with 2 located in high confidence regions (Figures 6A, B).

3.7 Regulation network of Acsbg1 and Etnppl

A total of 292 miRNAs were predicted by TargetScan and 1,011 miRNAs were predicted by miRWalk were predicted by miRDB. The 200 key miRNA were taken from the intersection of the 2 database (Figure 7A). The key miRNA-mRNA regulatory network showed that the 184 key miRNAs were predicted by Acsbg1, and the 16 key miRNAs were predicted by Etnppl (Figure 7B). In which, rno-mir-153-5p, rno-mir-6316, rno-mir-500-5p, rno-mir-3594-5p, rno-mir-501-5p, and rno-mir-362-5p were co-predicted by Acsbg1 and Etnppl. Predicting the TFs of hub genes were important for probing the expression regulation mechanism of hub genes. In this study, 44 TFs were associated with Acsbg1 and Etnppl with potential regulatory relationships. Among them, FOXC1, ESR1, NF-κB1, TP63, SOX2, SRY, and POU2F2 were co-predicted by Acsbg1 and Etnppl. (Figure 7C).

4 Discussion

Lipid accumulation in the heart is an independent pathogenic event in the progression of DM, unrelated to other pathogenic factors such as ischemic, infectious, and rheumatic causes (23). Previous studies have shown that DAPA regulates blood lipids in diabetic patients to improve symptoms (24). Therefore, this study explores the therapeutic effects of DAPA on rats with DCM, identifying Acsbg1 and Etnppl as hub genes in the treatment process, and providing new reference points for subsequent clinical treatment research.

In this study, we established a DCM rat model and obtained myocardial tissue samples after DAPA intervention for sequencing, yielding stable and high-quality data. 1,311 genes were identified in the model group compared to the control group, and subsequently screened 68 candidate genes by intersecting DEG-model and DEG-control. Furthermore, we employed bioinformatics methods and intersected our findings with 590 LMRGs obtained from public databases, ultimately identifying Acsbg1 and Etnppl.

Etnppl is a gene that encodes the Etnppl protein, primarily expressed in the brain and liver, and is crucial for maintaining phospholipid homeostasis (25). In the Etnppl gene knockout mouse model constructed by Elmihi (26), increases in free glucose, total cholesterol, and very low-density lipoprotein (VLDL) were observed. This suggests that deletion of the Etnppl gene may lead to reduced expression of the LRP-1 gene in the liver, thereby decreasing VLDL uptake. Since the VLDL receptor is also expressed in heart tissue (27), which is consistent with our findings that in DCM rats treated with DAPA, increased expression of the Etnppl gene might improve myocardial lipid metabolism and alleviating the structural and functional disorders of DCM. Besides, research conducted by Wang et al. revealed that in a palmitic acid-induced diabetic mouse model, Etnppl suppresses autophagic flux through the activation of the ARG2/ROS signaling pathway, thereby mediating palmitic acid-induced hepatic insulin resistance (28). It is noteworthy that Xu et al. constructed a logistic regression model based on Etnppl to assess its clinical significance. Their findings indicated that the area under the AUC value was greater than 0.8, suggesting the model's efficacy in differentiating between DCM and healthy control samples. This observation underscores the potential of Etnppl as a target for DCM research (29). Therefore, targeting Etnppl may offer a potential therapeutic strategy for DCM.

The Acsbg1 gene is located on chromosome 15 at q25.1 and encodes the Acsbg1 protein. Acsbg1 is a member of the long-chain acyl-CoA synthetase family (30). Studies have shown that Acsbg1 affects FA β-oxidation and disrupts energy metabolism, leading to cardiac metabolic disorders and increased risk of cardiovascular diseases (31). Furthermore, Acsbg1 may be involved in chronic inflammation, immune responses, and vascular abnormalities, which are crucial factors in disease progression (32). Acsbg1 is predominantly expressed in regulatory T (Treg) cells, particularly showing high levels in pulmonary ST2+ Treg cells. Its expression is regulated by TGF-β through the Smad2/3 signaling pathway. Through lipid metabolism regulation, Acsbg1 maintains immune tolerance and homeostasis, thereby suppressing inflammation. This anti-inflammatory function may potentially influence inflammation levels in cardiomyocytes affected by DCM (33).The present study constitutes the initial discovery of an association between Acsbg1

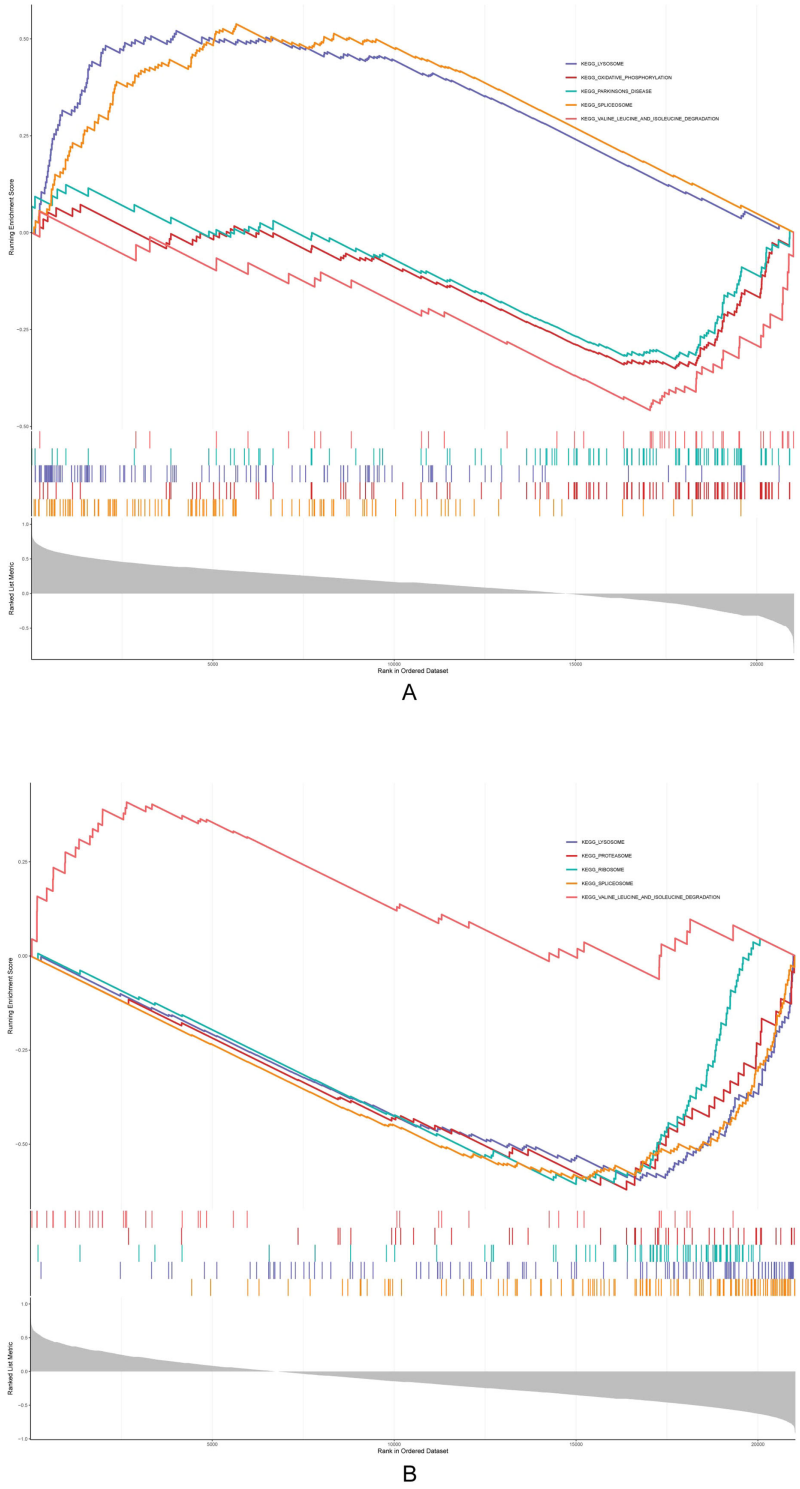

FIGURE 5
Gene set enrichment analysis (GSEA) of metabolic pathways. GSEA revealed significant enrichment of multiple metabolic pathways in the context of DAPA treatment. **(A)** Pathways related to lipid and glucose metabolism showed notable enhancement in the control group compared to the model group, particularly in fatty acid oxidation and glucose utilization processes. **(B)** Post-DAPA treatment, metabolic pathways demonstrated significant restoration, with marked enrichment in energy metabolism and fatty acid degradation pathways. These findings suggest that DAPA effectively modulates metabolic dysregulation in DCM, particularly impacting lipid and glucose metabolism.

10.3389/fendo.2025.1525831

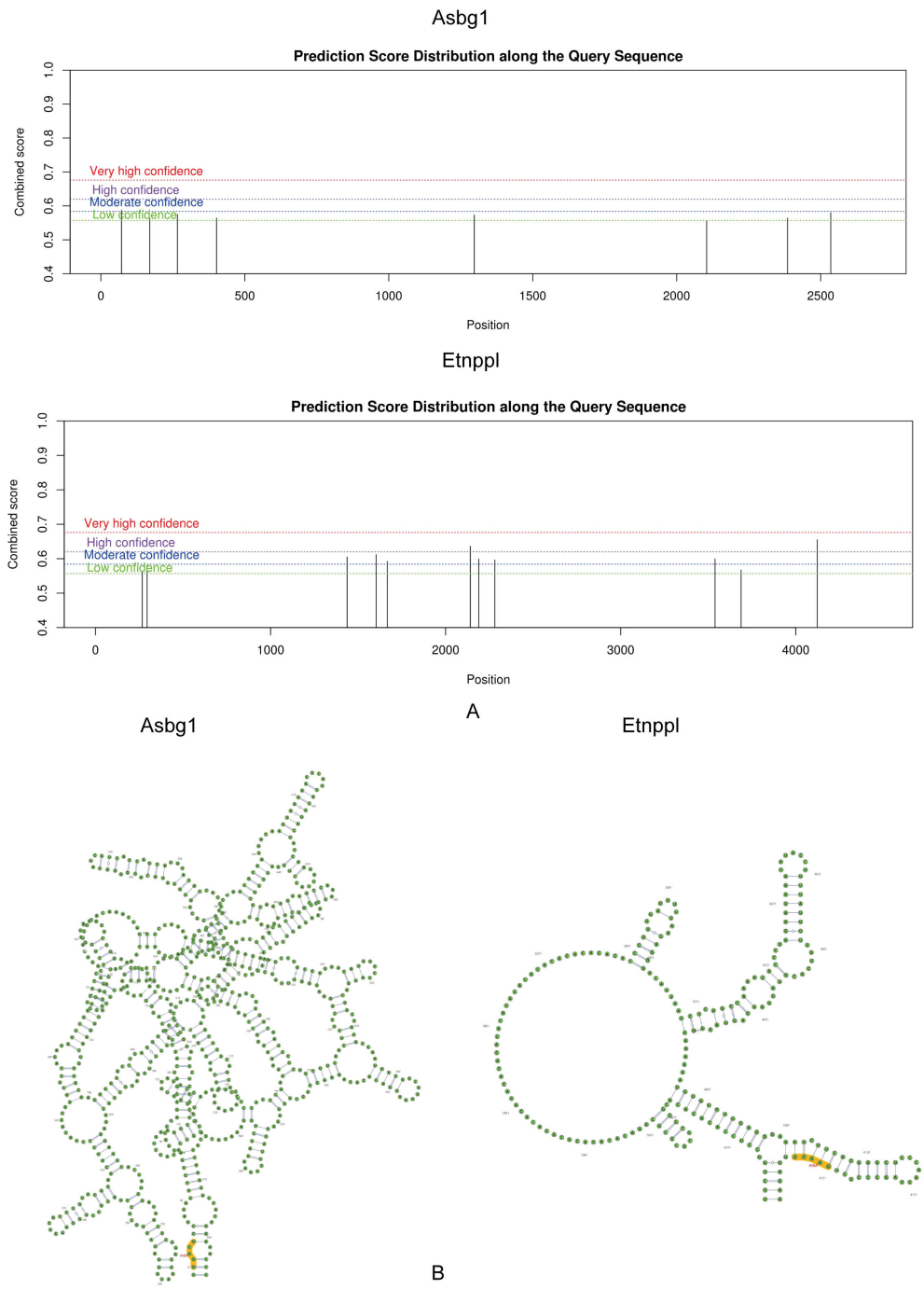

FIGURE 6
Prediction score distribution and secondary structure analysis of Acsbg1 and Etnppl. The prediction score distribution along the query sequences for Acsbg1 and Etnppl is depicted. **(A)** The score distribution for Acsbg1 reveals several high-confidence regions, indicating potential functional domains. **(B)** Etnppl also shows high-confidence predictions but with a distinct circular arrangement. The secondary structure analysis indicates that Acsbg1 exhibits a complex branching structure, while Etnppl is characterized by multiple protruding branches. Both proteins are noted for their conserved functional domains (highlighted in yellow), suggesting their important regulatory roles in metabolic processes.

and DCM as a novel therapeutic target. Subsequent research will focus on the role of Acsbg1 in diseases such as DCM, with the objective of elucidating its underlying mechanisms. Furthermore, future studies will explore whether Acsbg1 exhibits a specific expression pattern in DCM and whether it correlates with the severity or progression of the disease.

Our study indicated a significant increase in the expression of the Etnppl protein in the intervention group, while the expression of Acsbg1 was markedly elevated in the model group. These up-regulated and down-regulated genes suggest that the expression of genes in the DCM heart undergoes substantial changes under the conditions of DAPA intervention. In summary, Acsbg1 and Etnppl

10.3389/fendo.2025.1525831

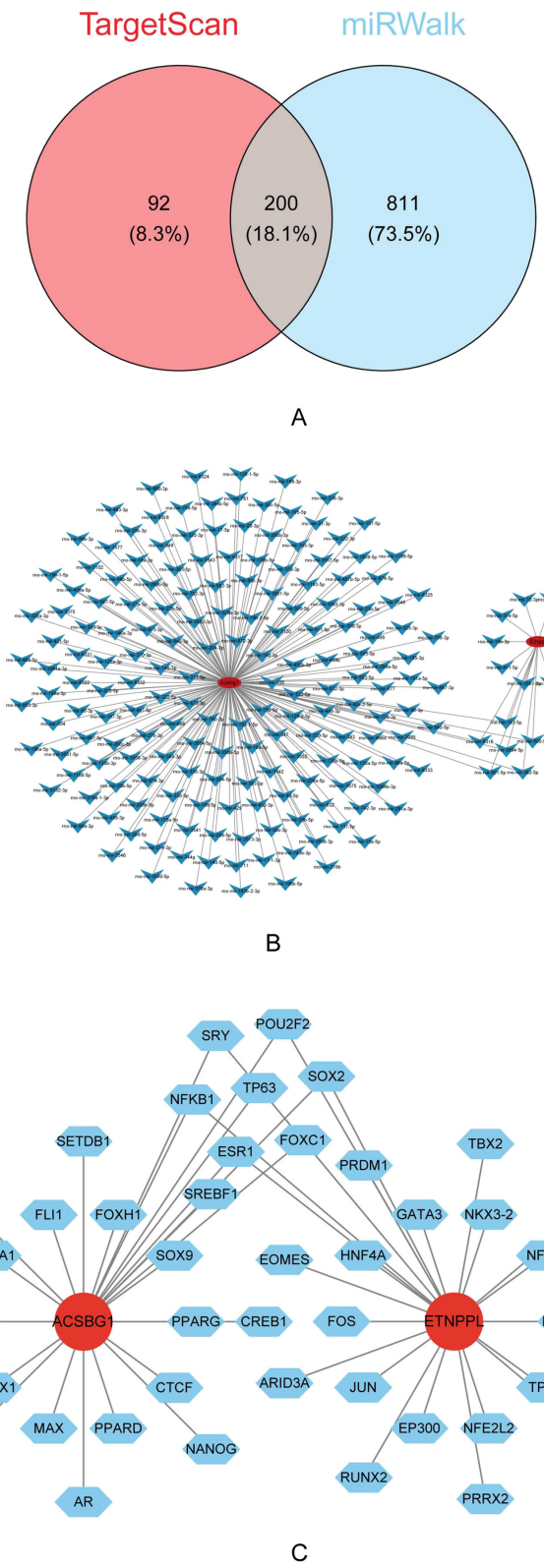

FIGURE 7
Regulatory mechanisms of key genes identified via bioinformatics analysis. **(A)** Venn diagram illustrating the overlap of predicted target genes between the TargetScan and miRWalk databases, revealing 200 shared genes (18.1%). **(B)** Interaction network analysis highlights extensive regulatory relationships among the predicted target genes. **(C)** Further transcription factor analysis identifies Acsbg1 and Etnppl as central regulatory nodes interacting with multiple transcription factors, including SOX2, GATA3, and PPARG. These findings suggest complex regulatory networks that underlie the therapeutic effects of DAPA in DCM.

are key regulators of lipid metabolism, which is closely linked to DCM. Therefore, targeting Acsbg1 and Etnppl could serve as a potential strategy for DAPA treatment of DCM.

The GO and KEGG enrichment analysis results of hub genes indicate their association with signaling pathways such as FA biosynthesis, FA degradation, and FA metabolism. One of the key characteristics of DCM is a disorder of energy metabolism, where toxic lipid metabolites accumulate in the diabetic heart a condition known as cardiac lipotoxicity (1). This may be related to increased uptake of FA by cardiomyocytes and/or reduced allosteric regulation of mitochondrial FA uptake, leading to incomplete FA oxidation. Excessive FA and FA-derived metabolites are the main pathogenic factors contributing to cardiac lipotoxicity in DCM (23, 34).

GSEA analysis revealed seven shared pathways between Acsbg1 and Etnppl, particularly the lysosomal pathway. Since excess saturated FA disrupt lysosomal function and increase protein toxicity in cardiomyocytes, we propose these hub genes may reduce lipid accumulation in DCM through enhanced lysosomal-mediated lipophagy, thereby improving FA metabolism (35, 36). Leucine accumulation, resulting from impaired BCAA metabolism, triggers both mTOR-mediated cell death and PPARα-enhanced FA oxidation, leading to increased cardiac lipid toxicity and vulnerability to ischemia-reperfusion injury (37). Another noteworthy pathway involves the proteasome, which plays a crucial role in cardiac function by clearing damaged proteins. In DCM, impaired proteasome activity leads to the accumulation of damaged proteins, resulting in proteotoxic stress and subsequent cardiac dysfunction (38). Related studies have shown that proteasome inhibition protects cardiac function by enhancing antioxidant gene expression and reducing oxidative damage and pathological remodeling (39). We hypothesized that Acsbg1 and Etnppl modulate these pathways in DCM pathogenesis. DAPA treatment appears to normalize both leucine metabolism and proteasome activity, potentially offering therapeutic benefits for DCM patients.

Subsequently, the hub genes-TFs regulatory networks for Acsbg1 and Etnppl were constructed to identify key TFs with potential regulatory roles. The cardioprotective effects of estrogen are well-established. The analysis of co-predicted TFs associated with hub genes, ESR1 emerged as a significant regulator of glucose homeostasis. ESR1 exerts its effects through dual regulation of solute carrier family 2 member 4 (Slc2a4), it enhances transcription through cooperative action with SP1 and CEBPA TF while inhibiting NF-κB activity, and promotes glucose transporter type 4 (GLUT4) translocation to the cell membrane. These mechanisms collectively contribute to improved insulin sensitivity (40). NF-κB is another crucial TF involved in DCM pathogenesis. It promotes disease development through two main mechanisms: inducing ferroptosis and mediating lipotoxicity-induced damage. These roles make NF-κB an important potential target for DCM therapeutic interventions (41). In summary, TFs such as ESR1 and NF-κB may influence DCM by regulating the transcription of Acsbg1 and Etnppl.

Studies have identified a strong involvement of pyroptosis in the progression of DCM (42), while m6A methylation acts as a crucial RNA epigenetic regulation mechanism (43). Meng et al. (44) discovered that METTL14 can suppress NLRP3-related pyroptosis in DCM by increasing the m6A methylation level of the TINCR gene, thereby reducing the mRNA stability of NLRP3. Previous research has also linked altered m6A modification patterns to myocardial fibrosis and myocyte hypertrophy in DCM (45). In the current study, the dysregulation of lipid and obesity-associated mRNAs in the DCM model might be related to altered m6A modifications of key genes (46). M6A sites were located at the UCAGG motifs in the RNA secondary structure, and suggest that DAPA might improve these differentially methylated sites directly or indirectly. However, further research is needed to confirm these findings. In this study, we employed bioinformatics approaches to analyze sequencing data and lipid metabolism-related genes, identifying two DCM-associated hub genes: Acsbg1 and Etnppl. Through comprehensive analyses including GSEA, m6A methylation profiling, and GGI network analysis, we further elucidated the molecular regulatory mechanisms of DAPA in DCM, providing a theoretical foundation for future investigations into the disease pathogenesis.

Despite the promising findings, our study has several limitations that warrant consideration. Due to limitations in terms of time, resources and other objective conditions, this study was unable to investigate the reversibility of the expression changes of Acsbg1 and Etnppl after the cessation of DAPA treatment. The significance of the reversibility of gene expression changes after DAPA treatment will be explored in future studies. To further validate and expand upon the current research results, it is planned that the relevant experiments will be repeated in a variety of different animal models in order to compare the intervention effect of DAPA on DCM in different animal models. At the same time, opportunities to collaborate with clinics will be actively sought in order to collect human tissue samples to investigate the mechanism and effect of DAPA on DCM from the human level. The small sample size of this study will be addressed by conducting large-scale sample analysis and introducing multi-sample validation experiments to enhance the extrapolation of results. Furthermore, the roles of other pathways in DCM will be explored to achieve a more comprehensive understanding of the pathogenesis of DCM. At the level of gene function research, the latest gene editing technology will be employed in combination with gene knockout experiments to provide a comprehensive analysis of the function of core genes in the pathogenesis of DCM. The development of DCM involves the abnormalities of many genes, and through gene knockdown, we can identify the specific roles of specific genes in the pathogenesis of DCM, which is of great significance.

5 Conclusion

In conclusion, this study successfully established a DAPA-treated DCM model and identified novel hub genes specifically associated with lipid metabolism in DCM pathogenesis. Through comprehensive functional prediction and systematic analysis of these genes, we have not only unveiled potential therapeutic

targets for DAPA treatment but also provided valuable insights into the molecular mechanisms underlying DCM. These findings contribute significantly to our understanding of DCM pathophysiology and may pave the way for developing more effective therapeutic strategies for DCM patients.

Data availability statement

The datasets presented in this study can be found in online repositories. The names of the repository/repositories and accession number(s) can be found below: https://www.gsea-msigdb.org/gsea/msigdb/human/collections.jsp, MsigDB.

Ethics statement

The animal study was approved by The Ethics Committee of the Second Affiliated Hospital of Nanchang University. The study was conducted in accordance with the local legislation and institutional requirements.

Author contributions

XH: Data curation, Formal Analysis, Writing – original draft, Writing – review & editing. YW: Methodology, Writing – original draft. RW: Methodology, Supervision, Writing – review & editing. ZY: Investigation, Project administration, Writing – review & editing. LH: Funding acquisition, Project administration, Supervision, Validation, Writing – review & editing.

Funding

The author(s) declare that financial support was received for the research and/or publication of this article. This research was supported by the Jiangxi Province Natural Science Foundation Project, grant number 20212BAB206042, the Jiangxi Province Traditional Chinese Medicine Science and Technology Plan Project, grant number 2020A0154, and the National Natural Science Foundation, grant number 82360081.

Acknowledgments

We thank all colleagues from the Department of Cardiology at the Second Affiliated Hospital of Nanchang University who supported this research.

Conflict of interest

The authors declare that the research was conducted in the absence of any commercial or financial relationships that could be construed as a potential conflict of interest.

Generative AI statement

The author(s) declare that no Generative AI was used in the creation of this manuscript.

Publisher's note

Supplementary material

The Supplementary Material for this article can be found online at: https://www.frontiersin.org/articles/10.3389/fendo.2025.1525831/full#supplementary-material

References

1. Ke J, Pan J, Lin H, Gu J. Diabetic cardiomyopathy: a brief summary on lipid toxicity. *ESC Heart failure*. (2023) 10:776–90. doi: 10.1002/ehf2.14224

2. Lorenzo-Almorós A, Tuñón J, Orejas M, Cortés M, Egido J, Lorenzo Ó. Diagnostic approaches for diabetic cardiomyopathy. *Cardiovasc diabetology*. (2017) 16:28. doi: 10.1186/s12933-017-0506-x

3. Murtaza G, Virk HUH, Khalid M, Lavie CJ, Ventura H, Mukherjee D, et al. Diabetic cardiomyopathy - A comprehensive updated review. *Prog Cardiovasc Diseases*. (2019) 62:315–26. doi: 10.1016/j.pcad.2019.03.003

4. Chen M-Y, Meng X-F, Han Y-P, Yan J-L, Xiao C, Qian L-B. Profile of crosstalk between glucose and lipid metabolic disturbance and diabetic cardiomyopathy: Inflammation and oxidative stress. *Front Endocrinol*. (2022) 13. doi: 10.3389/fendo.2022.983713

5. Wang W, Liu R, Zhu Y, Wang L, Tang Y, Dou B, et al. YuNü-Jian attenuates diabetes-induced cardiomyopathy: integrating network pharmacology and experimental validation. *Front Endocrinol (Lausanne)*. (2023) 14:1195149. doi: 10.3389/fendo.2023.1195149

6. Tan Y, Zhang Z, Zheng C, Wintergerst KA, Keller BB, Cai L. Mechanisms of diabetic cardiomyopathy and potential therapeutic strategies: preclinical and clinical evidence. *Nat Rev Cardiol*. (2020) 17:585–607. doi: 10.1038/s41569-020-0339-2

7. Wang M, Mo D, Zhang N, Yu H. Ferroptosis in diabetic cardiomyopathy: Advances in cardiac fibroblast-cardiomyocyte interactions. *Heliyon*. (2024) 10: e35219. doi: 10.1016/j.heliyon.2024.e35219

8. Zhang X, Mao M, Zuo Z. Palmitate induces mitochondrial energy metabolism disorder and cellular damage via the PPAR signaling pathway in diabetic cardiomyopathy. *Diabetes Metab syndrome obesity: Targets Ther*. (2022) 15:2287–99. doi: 10.2147/DMSO.S360931

9. Giugliano D, Longo M, Scappaticcio L, Bellastella G, Maiorino MI, Esposito K. SGLT-2 inhibitors and cardiorenal outcomes in patients with or without type 2

diabetes: a meta-analysis of 11 CVOTs. *Cardiovasc diabetology*. (2021) 20:236. doi: 10.1186/s12933-021-01430-3

10. Yaribeygi H, Maleki M, Reiner Z, Jamialahmadi T, Sahebkar A. Mechanistic view on the effects of SGLT2 inhibitors on lipid metabolism in diabetic milieu. *J Clin Med*. (2022) 11:6544. doi: 10.3390/jcm11216544

11. Arow M, Waldman M, Yadin D, Nudelman V, Shainberg A, Abraham NG, et al. Sodium-glucose cotransporter 2 inhibitor Dapagliflozin attenuates diabetic cardiomyopathy. *Cardiovasc Diabetol*. (2020) 19:7. doi: 10.1186/s12933-019-0980-4

12. Lin K, Yang N, Luo W, Qian JF, Zhu WW, Ye SJ, et al. Direct cardio-protection of Dapagliflozin against obesity-related cardiomyopathy via NHE1/MAPK signaling. *Acta Pharmacologica Sinica*. (2022) 43:2624–35. doi: 10.1038/s41401-022-00885-8

13. Zhu L, Ma M, Zhang L, Wang S, Guo Y, Ling X, et al. System analysis based on lipid-metabolism-related genes identifies AGT as a novel therapy target for gastric cancer with neoadjuvant chemotherapy. *Pharmaceutics*. (2023) 15:810. doi: 10.3390/pharmaceutics15030810

14. Pertea M, Pertea GM, Antonescu CM, Chang TC, Mendell JT, Salzberg SL. StringTie enables improved reconstruction of a transcriptome from RNA-seq reads. *Nat Biotechnol*. (2015) 33:290–5. doi: 10.1038/nbt.3122

15. Love MI, Huber W, Anders S. Moderated estimation of fold change and dispersion for RNA-seq data with DESeq2. *Genome Biol*. (2014) 15:550. doi: 10.1186/s13059-014-0550-8

16. Gustavsson EK, Zhang D, Reynolds RH, Garcia-Ruiz S, Ryten M. ggtranscript: an R package for the visualization and interpretation of transcript isoforms using ggplot2. *Bioinf (Oxford England)*. (2022) 38:3844–6. doi: 10.1101/2022.03.28.486050

17. Gu Z, Eils R, Schlesner M. Complex heatmaps reveal patterns and correlations in multidimensional genomic data. *Bioinf (Oxford England)*. (2016) 32:2847–9. doi: 10.1093/bioinformatics/btw313

18. Mao W, Ding J, Li Y, Huang R, Wang B. Inhibition of cell survival and invasion by Tanshinone IIA via FTH1: A key therapeutic target and biomarker in head and neck squamous cell carcinoma. *Exp Ther Med*. (2022) 24:521. doi: 10.3892/etm.2022.11449

19. Walter W, Sánchez-Cabo F, Ricote M. GOplot: an R package for visually combining expression data with functional analysis. *Bioinf (Oxford England)*. (2015) 31:2912–4. doi: 10.1093/bioinformatics/btv300

20. Robles-Jimenez LE, Aranda-Aguirre E, Castelan-Ortega OA, Shettino-Bermudez BS, Ortiz-Salinas R, Miranda M, et al. Worldwide traceability of antibiotic residues from livestock in wastewater and soil: A systematic review. *Animals: an Open Access J MDPI*. (2021) 12:60. doi: 10.3390/ani12010060

21. Wu T, Hu E, Xu S, Chen M, Guo P, Dai Z, et al. clusterProfiler 4.0: A universal enrichment tool for interpreting omics data. *Innovation (Cambridge (Mass))*. (2021) 2:100141. doi: 10.1016/j.xinn.2021.100141

22. Shannon P, Markiel A, Ozier O, Baliga NS, Wang JT, Ramage D, et al. Cytoscape: a software environment for integrated models of biomolecular interaction networks. *Genome Res*. (2003) 13:2498–504. doi: 10.1101/gr.1239303

23. Marfella R, Amarelli C, Cacciatore F, Balestrieri ML, Mansueto G, D'Onofrio N, et al. Lipid accumulation in hearts transplanted from nondiabetic donors to diabetic recipients. *J Am Coll Cardiol*. (2020) 75:1249–62. doi: 10.1016/j.jacc.2020.01.018

24. Tu J, Liu Q, Sun H, Gan L. Farrerol alleviates diabetic cardiomyopathy by regulating AMPK-mediated cardiac lipid metabolic pathways in type 2 diabetic rats. *Cell Biochem biophysics*. (2024) 82:2427–37. doi: 10.1007/s12013-024-01353-2

25. White CJ, Ellis JM, Wolfgang MJ. The role of ethanolamine phosphate phospholyase in regulation of astrocyte lipid homeostasis. *J Biol Chem*. (2021) 297:100830. doi: 10.1016/j.jbc.2021.100830

26. Elmihi KA, Leonard KA, Nelson R, Thiesen A, Clugston RD, Jacobs RL. The emerging role of ethanolamine phosphate phospholyase in regulating hepatic phosphatidylethanolamine and plasma lipoprotein metabolism in mice. *FASEB journal: Off Publ Fed Am Societies Exp Biol*. (2024) 38:e70063. doi: 10.1096/fj.202401321R

27. Oshio Y, Hattori Y, Kamata H, Ozaki-Masuzawa Y, Seki A, Tsuruta Y, et al. Very low-density lipoprotein receptor increases in a liver-specific manner due to protein deficiency but does not affect fatty liver in mice. *Sci Rep*. (2021) 11:8003. doi: 10.1038/s41598-021-87568-2

28. Wang C, Li X, Zhang W, Liu W, Lv Z, Gui R, et al. ETNPPL impairs autophagy through regulation of the ARG2-ROS signaling axis, contributing to palmitic acid-induced hepatic insulin resistance. *Free Radical Biol Med*. (2023) 199:126–40. doi: 10.1016/j.freeradbiomed.2023.02.017

29. Xu M, Guo YY, Li D, Cen XF, Qiu HL, Ma YL, et al. Screening of lipid metabolism-related gene diagnostic signature for patients with dilated cardiomyopathy. *Front Cardiovasc Med*. (2022) 9:853468. doi: 10.3389/fcvm.2022.853468

30. Mashek DG, Li LO, Coleman RA. Long-chain acyl-CoA synthetases and fatty acid channeling. *Future lipidology*. (2007) 2:465–76. doi: 10.2217/17460875.2.4.465

31. Gholipour A, Shakerian F, Zahedmehr A, Irani S, Malakootian M, Mowla SJ. Bioinformatics analysis to find novel biomarkers for coronary heart disease. *Iranian J Public Health*. (2022) 51:1152–60. doi: 10.18502/ijph.v51i5.9430

32. Gudjonsson JE, Ding J, Li X, Nair RP, Tejasvi T, Qin ZS, et al. Global gene expression analysis reveals evidence for decreased lipid biosynthesis and increased innate immunity in uninvolved psoriatic skin. *J Invest Dermatol*. (2009) 129:2795–804. doi: 10.1038/jid.2009.173

33. Kanno T, Nakajima T, Kawashima Y, Yokoyama S, Asou HK, Sasamoto S, et al. Acsbg1-dependent mitochondrial fitness is a metabolic checkpoint for tissue T(reg) cell homeostasis. *Cell Rep*. (2021) 37:109921. doi: 10.1016/j.celrep.2021.109921

34. Jia G, Hill MA, Sowers JR. Diabetic cardiomyopathy: an update of mechanisms contributing to this clinical entity. *Circ Res*. (2018) 122:624–38. doi: 10.1161/CIRCRESAHA.117.311586

35. Xing R, Liu D, Cheng X, Tian X, Yan C, Han Y. MiR-207 inhibits autophagy and promotes apoptosis of cardiomyocytes by directly targeting LAMP2 in type 2 diabetic cardiomyopathy. *Biochem Biophys Res Commun*. (2019) 520:27–34. doi: 10.1016/j.bbrc.2019.09.092

36. Trivedi PC, Bartlett JJ, Perez LJ, Brunt KR, Legare JF, Hassan A, et al. Glucolipotoxicity diminishes cardiomyocyte TFEB and inhibits lysosomal autophagy during obesity and diabetes. *Biochim Biophys Acta*. (2016) 1861:1893–910. doi: 10.1016/j.bbalip.2016.09.004

37. Xiong Y, Jiang L, Li T. Aberrant branched-chain amino acid catabolism in cardiovascular diseases. *Front Cardiovasc Med*. (2022) 9:965899. doi: 10.3389/fcvm.2022.965899

38. Zhang X, Hu C, Yuan XP, Yuan YP, Song P, Kong CY, et al. Osteocrin, a novel myokine, prevents diabetic cardiomyopathy via restoring proteasomal activity. *Cell Death disease*. (2021) 12:624. doi: 10.1038/s41419-021-03922-2

39. Wang Y, Sun W, Du B, Miao X, Bai Y, Xin Y, et al. Therapeutic effect of MG-132 on diabetic cardiomyopathy is associated with its suppression of proteasomal activities: roles of Nrf2 and NF-κB. *Am J Physiol Heart Circulatory Physiol*. (2013) 304:H567–78. doi: 10.1152/ajpheart.00650.2012

40. Gregorio KCR, Laurindo CP, MaChado UF. Estrogen and glycemic homeostasis: the fundamental role of nuclear estrogen receptors ESR1/ESR2 in glucose transporter GLUT4 regulation. *Cells*. (2021) 10:99. doi: 10.3390/cells10010099

41. Wu S, Zhou Y, Liang J, Ying P, Situ Q, Tan X, et al. Upregulation of NF-κB by USP24 aggravates ferroptosis in diabetic cardiomyopathy. *Free Radical Biol Med*. (2024) 210:352–66. doi: 10.1016/j.freeradbiomed.2023.11.032

42. Xie Y, Huang Y, Ling X, Qin H, Wang M, Luo B. Chemerin/CMKLR1 axis promotes inflammation and pyroptosis by activating NLRP3 inflammasome in diabetic cardiomyopathy rat. *Front Physiol*. (2020) 11:381. doi: 10.3389/fphys.2020.00381

43. Zhang BY, Han L, Tang YF, Zhang GX, Fan XL, Zhang JJ, et al. METTL14 regulates M6A methylation-modified primary miR-19a to promote cardiovascular endothelial cell proliferation and invasion. *Eur Rev Med Pharmacol Sci*. (2020) 24:7015–23. doi: 10.26355/eurrev_202006_21694

44. Meng L, Lin H, Huang X, Weng J, Peng F, Wu S. METTL14 suppresses pyroptosis and diabetic cardiomyopathy by downregulating TINCR lncRNA. *Cell Death disease*. (2022) 13:38. doi: 10.1038/s41419-021-04484-z

45. Liu K, Gao Y, Gan K, Wu Y, Xu B, Zhang L, et al. Prognostic roles of N6-methyladenosine METTL3 in different cancers: A system review and meta-analysis. *Cancer control: J Moffitt Cancer Center*. (2021) 28:1073274821997455. doi: 10.1177/1073274821997455

46. Ju W, Liu K, Ouyang S, Liu Z, He F, Wu J. Changes in N6-methyladenosine modification modulate diabetic cardiomyopathy by reducing myocardial fibrosis and myocyte hypertrophy. *Front Cell Dev Biol*. (2021) 9:702579. doi: 10.3389/fcell.2021.702579

frontiers | Frontiers in Endocrinology

TYPE Original Research
PUBLISHED 17 April 2025
DOI 10.3389/fendo.2025.1561142

OPEN ACCESS

EDITED BY
Ramoji Kosuru,
Versiti Blood Research Institute, United States

REVIEWED BY
Priyanka Choudhury,
Medical College of Wisconsin, United States
Haskly Mokoena,
University of Limpopo, South Africa

*CORRESPONDENCE
Ling Xue
27500318@hebmu.edu.cn

RECEIVED 15 January 2025
ACCEPTED 27 March 2025
PUBLISHED 17 April 2025

CITATION
Hu F, Guo R, Zhi Y, Hu H, Tang T, Wang P and Xue L (2025) Exploring the key target molecules of angiogenesis in diabetic cardiomyopathy based on bioinformatics analysis. *Front. Endocrinol.* 16:1561142. doi: 10.3389/fendo.2025.1561142

Exploring the key target molecules of angiogenesis in diabetic cardiomyopathy based on bioinformatics analysis

Fengli Hu[1,2], Ruixue Guo[1,2], Yaxin Zhi[1,2], Haijuan Hu[1], Ting Tang[1,2], Pengfei Wang[1,2] and Ling Xue[1*]

[1]Department of Cardiology, Second Hospital of Hebei Medical University, Shijiazhuang, China, [2]Department of Internal Medicine, Hebei Medical University, Shijiazhuang, China

Backgrounds: Diabetic cardiomyopathy has a very high incidence and serious clinical consequences, making it an urgent clinical problem to be solved. Angiogenesis is a significant phenotype in the occurrence and development of diabetic cardiomyopathy, especially the damage to angiogenesis of cardiac microvessels, which is inextricably linked to the cardiac risk of diabetic patients. In the current basic and clinical research, there is still a lack of treatment methods that directly target the angiogenesis of diabetic cardiomyopathy. This study hopes to discover the key molecules related to diabetic cardiomyopathy and angiogenesis damage, to provide ideas for possible interventions.

Methods: Sequencing data of animals and cells were obtained from the GEO database, and differentially expressed genes were analyzed. Subsequently, the angiogenesis-related genes were clustered for functional and pathway analysis. Then, the microangiogenesis of the diabetic mice and the angiogenesis changes of high glucose-stimulated HUVECs were verified, and the top three genes related to diabetic cardiomyopathy and angiogenesis were verified using western blot.

Results: 24 differentially expressed genes associated with angiogenesis were found in GSE241565(human) and GSE215979(mice). Among them, 11 genes showed the same trend in the two databases. Then CD31 staining of diabetic mice hearts showed that microvascular angiogenesis was impaired, high glucose-stimulated HUVECs decreased tube formation, and wound healing migration was weakened. Finally, the top 3 genes most associated with diabetic cardiomyopathy were verified, and there was no significant difference between the changes of Edn1 and Lepr. At the same time, Efnb2 was significantly increased under high glucose stimulation.

Conclusion: Combined with the sequencing data of animal and cell models of diabetic cardiomyopathy, the differential genes associated with angiogenesis were screened. These findings not only elucidate a novel molecular axis linking angiogenesis damage to diabetic cardiomyopathy but also highlight Efnb2 as a potential therapeutic target.

KEYWORDS

diabeticcardiomyopathy, angiogenesis, bioinformatics, therapeutictargets, EFNB2

1 Introduction

In 2019, 463 million adults were reported to have diabetes, and this number is expected to reach 700 million by 2045 (1). Cardiovascular disease is a common complication in diabetics and is thought to be the leading cause of death and disability in diabetic patients thus the continued surge in the prevalence of diabetes has increased the burden of diabetic cardiomyopathy (DCM) and has become a key issue in the diabetes field (2–4). Unlike other cardiovascular complications, DCM is usually absent in the absence of coronary artery disease or hypertension but is often associated with left ventricular diastolic dysfunction, ventricular hypertrophy, and myocardial fibrosis (3, 5). Currently, there are many mechanisms involved in the development of DCM, and many studies have focused on myocardial inflammation (6, 7), pyroptosis (7), ferroptosis (8–11), and so on. Whereas We are very interested in vascular injury, especially angiogenesis.

As we all know, the effect of diabetes on angiogenesis may not be consistent in different organs (12, 13). On the one hand, the increase in pathological angiogenesis is associated with diabetic retinopathy and nephropathy; On the other hand, in diabetes, angiogenesis in the coronary and peripheral arteries of the heart is weakened (14, 15). Studies have found that microvascular angiogenesis is affected in diabetes or metabolic disorders (16, 17). Endothelial cell damage is thought to be the origin of microvascular dysfunction in early type 2 diabetes (18), and as many researchers have assumed, impaired angiogenesis in diabetic cardiomyopathy is a key factor in the development of serious adverse cardiovascular events in many patients with diabetes (19). Angiogenesis is significantly affected in DCM, and key genes in DCM are enriched in the angiogenesis process (20), but there is still a lack of specific interventions targeting angiogenesis in DCM, and no key molecules affecting angiogenesis in DCM have been identified.

With the development of a variety of biological science and technology, many researchers are concerned about the molecular changes associated with diabetic cardiomyopathy. Identifying these specific molecules, can not only help to enhance the possibility of diagnosis and treatment (21–23) but also predict the risk of heart failure (24), which can help to identify high-risk patients. Thus based on the tissue and cell sequencing data of diabetic cardiomyopathy, combined with relevant databases, we screened out genes that are significantly associated with angiogenesis when diabetic cardiomyopathy occurs. Subsequently, similar animal and cell models were constructed to verify the differential gene expression, suggest the existence of key molecules, and provide the possibility for the next targeted intervention.

2 Materials and methods

2.1 Data preparation

By searching the NCBI GEO database(https://www.ncbi.nlm.nih.gov/geo) for diabetic cardiomyopathy and diabetes-related vascular injury, two datasets piqued our interest. Among them, GSE241565 (25) was experimented with human umbilical vein endothelial cells (HUVEC), and high-throughput sequencing was performed after 8 days of stimulation with different sugar concentrations (5.5 mM *vs.* 30 mM). Another dataset GSE215979 (26) contains information on hearts of STZ-induced diabetic mice. The list of genes associated with human angiogenesis was obtained from the GeneCards database (https://www.genecards.org/), while the list of genes associated with angiogenesis in MICE was downloaded from the Mouse Genome Informatics(https://www.informatics.jax.org/). Otherwise, genes associated with human diabetic cardiomyopathy were obtained from the Comparative Toxicogenomics Database (CTD, https://ctdbase.org/).

2.2 Differential expressed genes screening

GSE241565 differentially expressed genes were analyzed by online GEO2R, in which all genes of Padj<0.05 were included in the preliminary analysis set. P value adjustment is calculated by Benjamini & Hochberg (False discovery rate), and online analysis is based on R 4.2.2 and limma 3.54.0. In GSE215979, we performed differentially expressed gene analysis using the R package “limma”, and P<0.05 was set as the identification threshold. In order not to miss potentially differentially expressed genes, we did not limit fold

change values. Subsequently, genes associated with angiogenesis in the two datasets were merged by homologous gene conversion of different species. Heatmap was plotted by https://www.bioinformatics.com.cn (last accessed on 10 Nov 2023), an online platform for data analysis and visualization.

2.3 Protein-protein interaction and functional enrichment analysis

The selected differentially expressed genes were analyzed using the STRING database(https://cn.string-db.org/) for protein-protein interaction network analysis and interaction network diagram. In the next step, the functional and pathway enrichment analysis of differentially expressed genes was performed by DAVID Bioinformatics (https://davidbioinformatics.nih.gov/). The visualization of the pathway analysis was performed using the WeBio website (27). Among them, the most relevant molecular pathway analysis of the KEGG pathway was performed using KEGG online analysis (https://www.genome.jp/kegg/). And the subcellular localization and the membrane type of proteins were predicted in DeepLoc-2.1 (https://services.healthtech.dtu.dk/services/DeepLoc-2.1/).

2.4 Animal model

All C57BL/4N mice (male, 7 weeks, 21–25g) were purchased from Vital River and randomly divided into diabetes mellitus group (DM) and negative control group(NC) after adaptive feeding. All mice live in a quiet environment, with 12 hours of alternating light and dark and regular disinfection and sterilization. Mice have free access to food and clean drinking water. Diabetic model mice are fed with a High-fat diet (HFD) and injected intraperitoneally with STZ (30 mg/kg) dissolved in sodium citrate buffer(pH4.5, sterile, Solaibio, C1013). The control mice were intraperitoneally injected with sodium citrate buffer solution at the same time and in the same body weight ratio.

2.5 Immunofluorescence staining

For immunofluorescence staining of cardiac tissue, OCT-embedded fresh cardiac tissue is sectioned using a cryostat (thickness of 5 microns), and the tissue sections are spread flat on a glass slide. Equilibrate for 10 minutes at room temperature followed by 3 washes in PBS, followed by blocking with 5% goat serum for 30 minutes at room temperature, followed by CD31 (1:50, mouse primary antibody from GeneTex. GTX20218) at 4°C overnight. On the second day, the fluorescent secondary antibody (1:100) was incubated for 1 hour at room temperature in the dark, and the mounting was performed with DAPI containing quenching inhibitor after washing. Finally, the images were observed and photographed under a confocal microscope (Olympus).

2.6 Cell culture

Human Umbilical Vein Endothelial Cells(HUVECs) were routinely cultured with Dulbecco's modified Eagle medium (DMEM) (containing 25 mM glucose) containing 10% fetal bovine serum and 1% penicillin/streptomycin, 30 mM glucose were used as high-glucose stimulation conditions, and the cells were collected for follow-up experiments after 48 hours of normal culture and high-glucose stimulation. The incubator is set at 37°C, 5% carbon dioxide, and 95% humidity.

2.7 Wound healing assay

To test the angiogenesis ability of endothelial cells, a wound-healing assay was performed. HUVECs were planted in 6-well plates. After LG or HG stimulation for 48 hours, a 200-μl pipette tip was used to vertically and straightly scratch. Then, sterile PBS was gently rinsed 3 times to remove the cell debris produced by the scratch. Finally, the DMEM medium without FBS was changed to continue the culture, and pictures were taken under a light microscope at 0h, 12h, and 24h. After collecting the pictures, the scratch migration length was measured by ImageJ analysis software, and the scratch in the same well was measured at least 3 times, and the average value was taken to calculate the migration rate.

2.8 Tube formation assay

Matrigel (Corning, USA) at 4°C overnight in advance, and pre-cool the 24-well plate and pipette tip in the refrigerator. The next day, evenly apply the melted matrix gel to the 24-well plate (20 μl per well) and then incubate in a cell culture incubator for 30 minutes. Digest and resuspend HUVECs for 72 hours, inoculate 15×104 per well on the coated plate, continue to culture with DMEM medium without FBS, and observe the tube formation phenomenon with an inverted optical microscope and take pictures. Finally, use the Image J software plug-in "Angiogenesis Analyzer" for quantitative analysis of tube formation.

2.9 Western blot

HUVECs were lysed for 30 minutes to one hour using RIPA lysis buffer containing 1% PMSF, and the supernatant was collected after centrifugation at 12,000 rpm for 10 minutes at 4°C. The protein was then quantified using a BCA protein assay kit (Solaibio, China). After determining the appropriate concentration, 5× loading buffer was added and the sample was boiled at 95-100°C for 5-10 minutes. Proteins were separated by protein electrophoresis using 10% SDS-PAGE gel and then transferred to a PVDF membrane (Millipore, Burlington, MA, USA). The membrane was blocked with 5% milk at room temperature for one hour and then incubated with the primary antibodies against EDN1 (1:500, Wanleibio, WL02780, China), LEPR

(1:1000, Wanleibio, WL0162a China), EFNB2 (1:1000, Abways, CY7104, China) and GAPDH (1:1000, Huabio, R1210-1, China) at 4°C overnight. The next day, the HRP secondary antibody was incubated at room temperature for 1 hour and then developed using a bio-rad gel imager. GAPDH was used as an internal reference protein for standardization and quantitative analysis was performed using ImageJ software.

2.10 Statistical analysis

All data were presented as mean ± standard error of the mean (SEM), and the statistical analysis was conducted by GraphPad Prism 8.0 (GraphPad Software, Inc., San Diego, CA, USA). Statistical differences between the two groups were analyzed using an unpaired t-test. In addition, $P<0.05$ was considered statistically significant.

3 Results

3.1 Screening of differential DCM genes associated with angiogenesis in human-derived sequencing information

First, we performed a differentially expressed gene analysis on the GSE241565 dataset using an online GEO2R analysis tool. The data available for analysis in this dataset include sequencing data for HUVECs stimulated by HGs: GSEM7731057, GSEM7731058, and GSEM7731059. The LG group as a control group contains 2 samples: GSEM7731060, and GSEM7731062 (where the GSEM7731061 dataset does not upload raw data). After analysis, it was found that there were 1833 differential genes between groups, including 462 up-regulated genes and 1371 down-regulated genes (Figure 1A). Subsequently, we searched the human gene database (Genecards) for all genes associated with "angiogenesis", for a total of 6144. Finally, 591 differentially expressed genes related to human angiogenesis were obtained (Figure 1B). Then, these 591 genes were heatmapped (Figure 1C), and the exact differences between groups were found.

3.2 Screening of differential DCM genes associated with angiogenesis in mouse-derived sequencing information

For differential gene screening in animal models of DCM, we performed a "limma" differential analysis of GSE215979, which included sequencing results of diabetic and negative control mouse hearts with 3 samples each. As a result, 4562 differential genes were obtained, of which 2859 were up-regulated and 1703 were down-regulated (Figure 2A). Next, 601 genes associated with mouse angiogenesis were extracted from the mouse genome informatics database (MGI). Similarly to the previous one, it was found that there were 174 differential genes for DCM associated with angiogenesis in mice (Figure 2B). These differential genes were also heat-mapped to visualize the differences between groups (Figure 2C).

3.3 Analysis of gene interactions associated with DCM angiogenesis

Considering that the genes of humans and mice do not correspond completely, we homologous converted 591 differential genes related to angiogenesis in HUVECs to obtain 539 corresponding mouse genes. Subsequently, it was integrated with 174 differential genes related to angiogenesis in mice, and finally, 24 angiogenesis-related genes were obtained that were differentiated in both humans and mice (Figure 3A). To clarify the correlation between these differential genes, we mapped the protein-protein interactions using the STRING online analysis tool (Figure 3B). We not only focus on the interactions between differential genes but also explore pathways that are significantly associated with angiogenesis impairment in DCM. Next, GO(Gene Ontology) analysis found that all differential genes involved BP(biological process) included angiogenesis, cell adhesion, positive regulation of angiogenesis, positive regulation of cell population proliferation, negative regulation of gene expression, CC (cellular component) included extracellular region, focal adhesion, collagen-containing extracellular matrix, and finally MF(molecular function) included extracellular matrix structural, constituent, heparin-binding, integrin binding, fibroblast growth factor binding, ephrin receptor binding (Figure 3C).

3.4 Analysis of gene pathway enrichment associated with DCM angiogenesis

Pathway enrichment analysis was performed for angiogenesis-related differential genes, including KEGG and REACTOME pathway analysis, respectively (Figure 4A). It is associated with PI3K-Akt signaling pathway, Human papillomavirus infection, Pathways in cancer, ECM-receptor interaction, Focal adhesion, Cytoskeleton in muscle cells, Hypertrophic cardiomyopathy, Signaling pathways regulating pluripotency of stem cells, Rap1 signaling pathway in the KEGG pathway. And in the REACTOME pathway, includes Signal Transduction, Developmental Biology, Axon guidance, Nervous system development, Integrin cell surface interactions, Extracellular matrix organization, Signaling by Receptor Tyrosine Kinases, and Signaling by PDGF.

Of all the KEGG pathways involved, the PI3K (Phosphatidylinositol 3-Kinase)-AKT signaling pathway is the first and significantly related pathway. We then performed a further pathway map analysis, in which the up-regulated genes were labeled in red, down-regulated in blue, and the background color was pink by default (Figure 4B). The results showed that GF (Growth Factor), RTK(receptor tyrosine kinase), ECM (Extracellular Matrix), ITGB(Integrin Beta), and JAK(Janus Kinase) in the upstream of the signaling pathway were associated with impaired angiogenesis in DCM, in which GF was up-regulated and JAK was down-regulated.

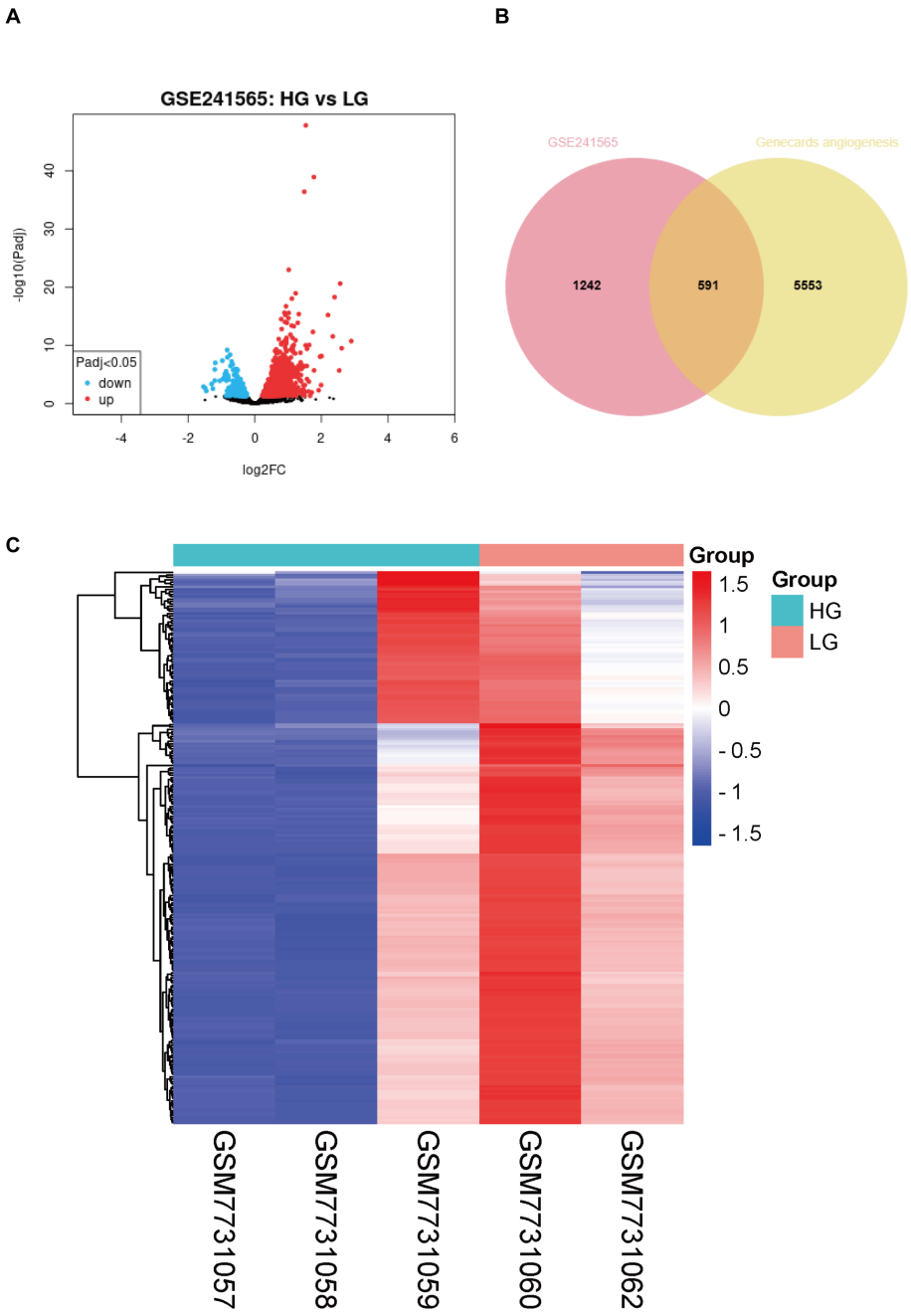

FIGURE 1
Analysis of differentially expressed genes associated with angiogenesis in high-glucose-stimulated HUVECs. **(A)** Volcano plot of differentially expressed genes from the GSE241565 dataset. **(B)** Venn diagram of GSE241565 differentially expressed genes and angiogenesis related genes in Genecards. **(C)** Heat map of differentially expressed genes associated with angiogenesis in HG-stimulated HUVECs. LG, low glucose; HG, high glucose; HUVECs, Human umbilical vein endothelial cells.

3.5 Verification of angiogenesis in diabetic cardiomyopathy

To assess cardiac angiogenesis in diabetic cardiomyopathy mice, we performed immunofluorescence staining on frozen sections of heart tissue (Figure 5A). Among them, CD31(red) represents an indicator of angiogenesis, and the CD31 staining of microvessels in the heart of DM mice is attenuated overall. Subsequently, HG was used in cells as an adverse stimulus in diabetes mellitus, and angiogenesis-related experiments were evaluated. Among them, the tube formation function of HUVECs is weakened at HG, and the associated tube length is significantly reduced (P= 0.0253) (Figure 5B). In addition, the results of the scratch-healing assay showed that high glucose stimulation impaired the migration ability of HUVECs, and the mobility rate was significantly reduced at 12 h and 24 h (Figure 5C). There was a

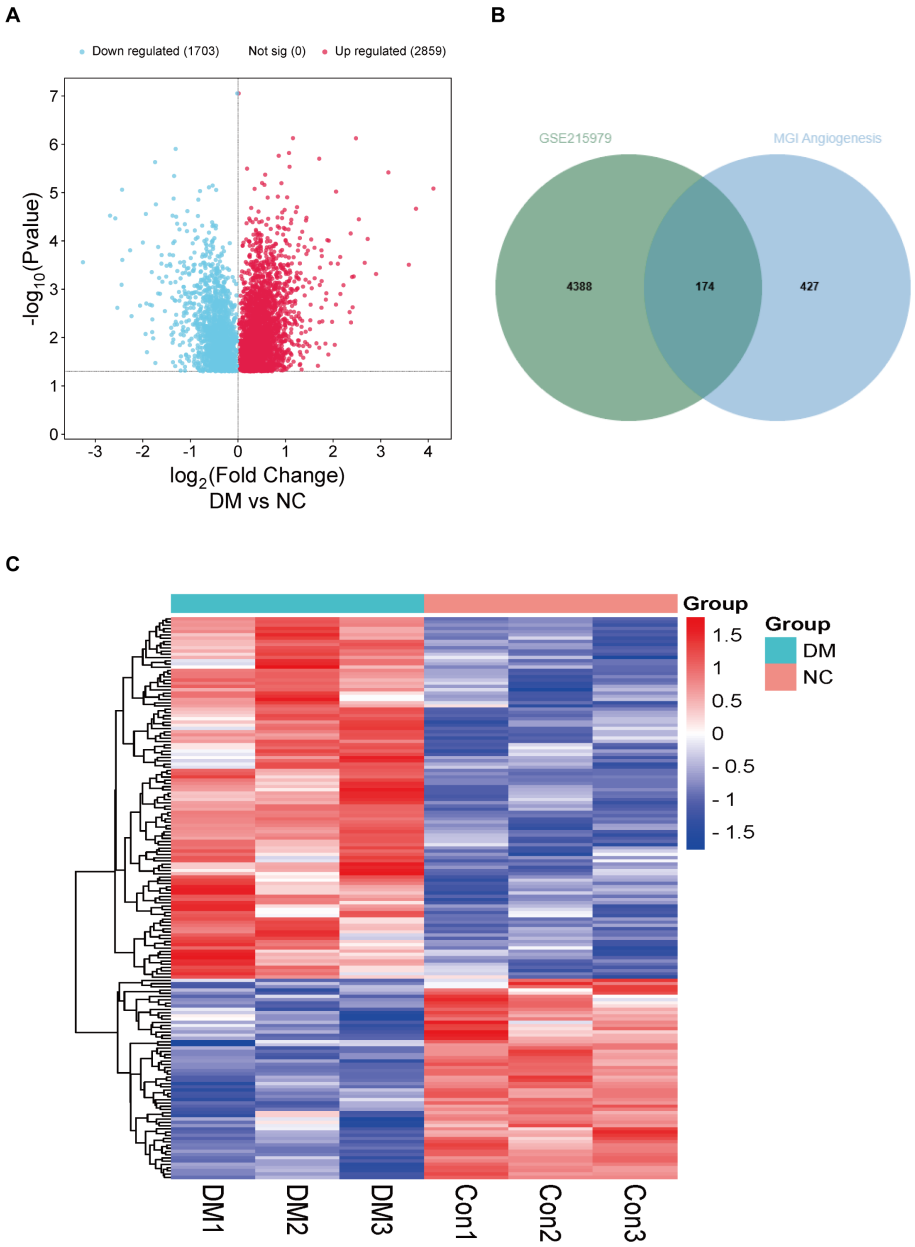

FIGURE 2
Analysis of differentially expressed genes associated with angiogenesis in hearts of DM mice. **(A)** Volcano plot of differentially expressed genes from the GSE215979 dataset. **(B)** Venn diagram of GSE215979 differentially expressed genes and angiogenesis related genes in MGI. **(C)** Heat map of differentially expressed genes associated with angiogenesis in DM mice.NC, negative control; DM, diabetes mellitus.

significant difference between 12 and 24 hours(P = 0.041720, 0.007644 respectively).

3.6 Western blotting were carried out to verify differentially expressed genes

Integrating all sequencing data, there are 11 genes with the same change trend: EDN1, LEPR, EFNB2, JAK1, RHOB, CFH, APLN, EFNA1, SMAD1, ARHGAP24, ARHGAP22. Among them, 7 (EDN1, LEPR, EFNB2, RHOB, CFH, EFNA1, SMAD1) were upregulated and 4(Jak1, Apln, Arhgap24, Arhgap22) were downregulated. To gain a better understanding of the genes involved, the subcellular localization and the membrane type of proteins were predicted in DeepLoc-2.1 (Table 1). These genes were then searched in the CTD (Comparative Toxicogenomics Database) for genes/proteins related to diabetic cardiomyopathy, and reference scores for all genes were obtained (Table 1). Firstly, the expression of each gene was standardized in the control group, and a box plot was drawn (Figure 6A). Finally, the top 3 proteins with the CTD reference scores were evaluated by western blotting. There was no significant difference between the groups in EDN1 and

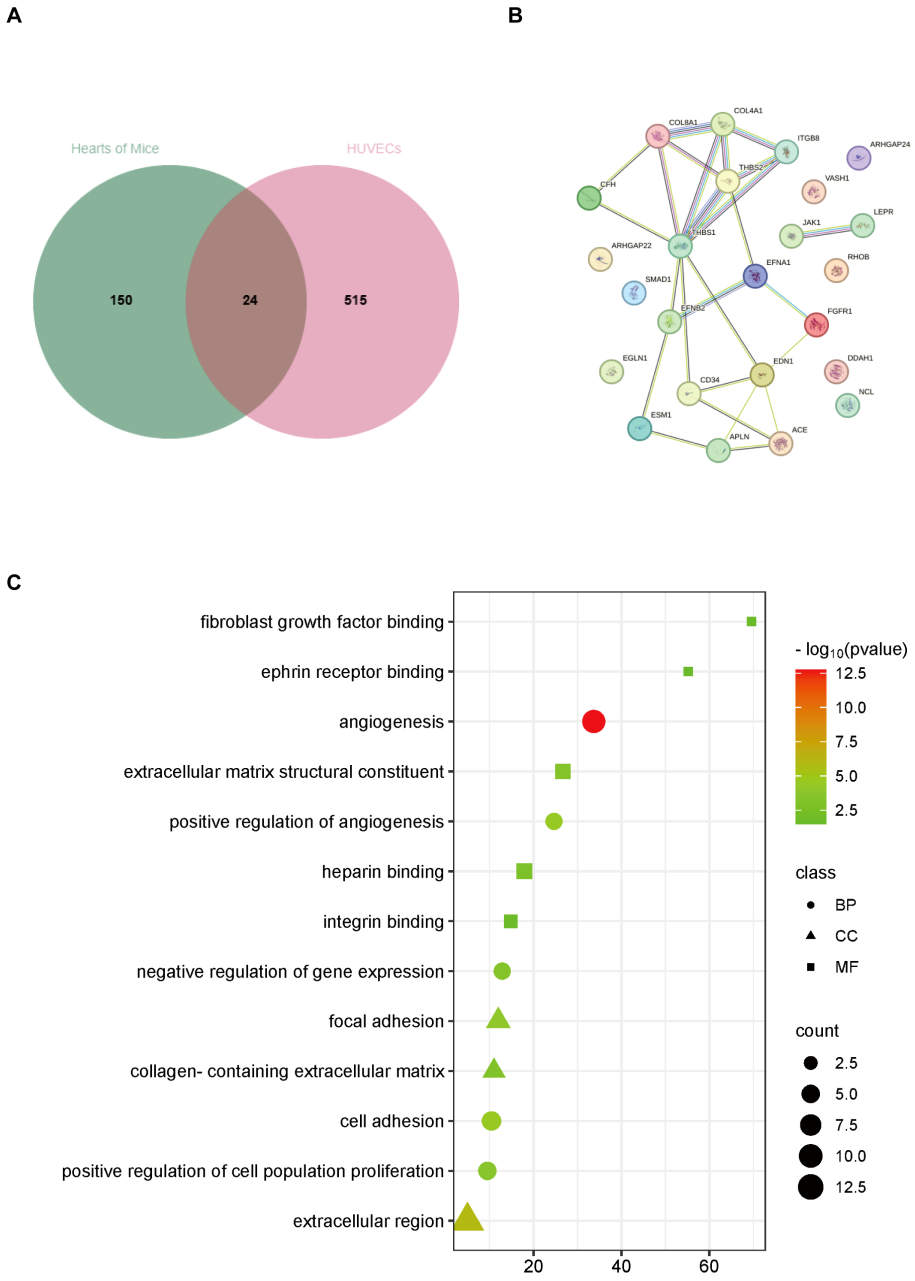

FIGURE 3
Analysis of differentially expressed genes associated with angiogenesis both in hearts of DM mice and HG-stimulated HUVECs. **(A)** Venn diagram of differentially expressed genes. **(B)** Protein-protein interaction network analysis of differentially expressed genes. **(C)** GO analysis of differentially expressed genes. BP, biological process; CC, cellular component; MF, molecular function.

LEPR (P = 0.4082, 0.9896 respectively) (Figures 6B, C), while EFNB2 was significantly increased when stimulated by high glucose (P = 0.0094) (Figure 6D).

4 Discussion

Diabetic cardiomyopathy increases significantly with the rapid increase in the prevalence of diabetes, and the pathological processes involved are very complex, including diastolic dysfunction, myocardial fibrosis, and microvascular dysfunction. As many researchers hypothesize, impaired microvascular angiogenesis in diabetic cardiomyopathy may be the culprit behind the occurrence of serious adverse cardiovascular events in many patients with diabetes. Although many drugs and biological therapies are currently dedicated to improving diabetic cardiomyopathy-related lesions, there is still a lack of interventions targeting diabetic cardiomyopathy angiogenesis. We hope to combine sequencing databases and experimental studies to screen for differential molecules and signaling pathways associated

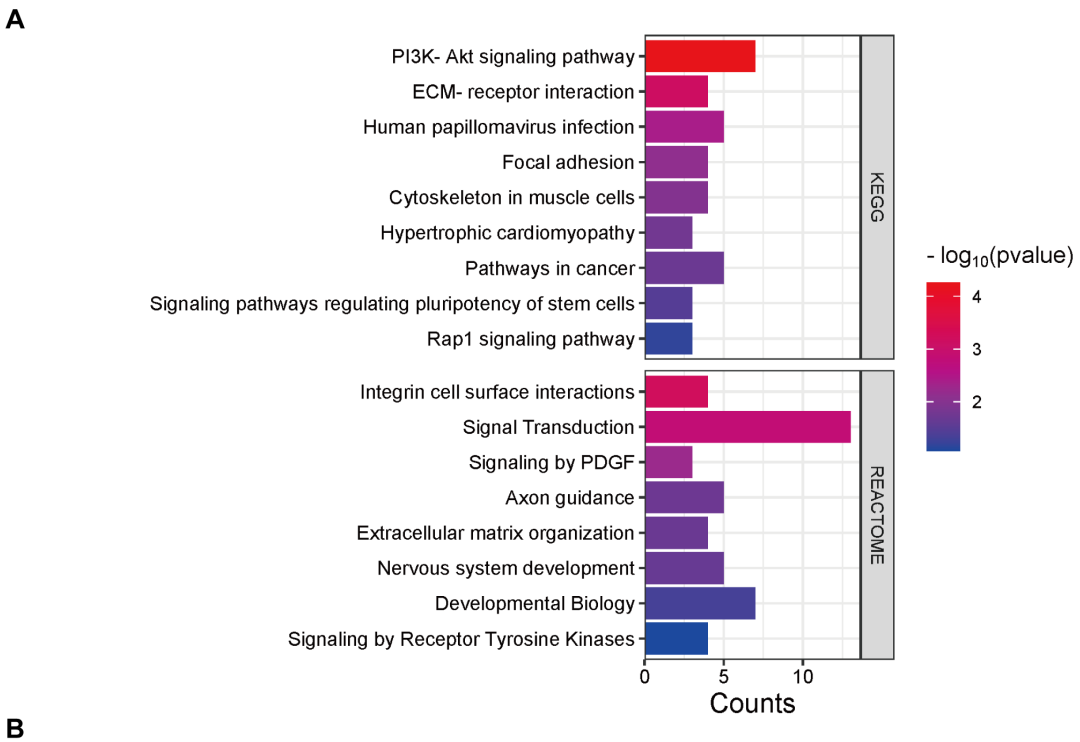

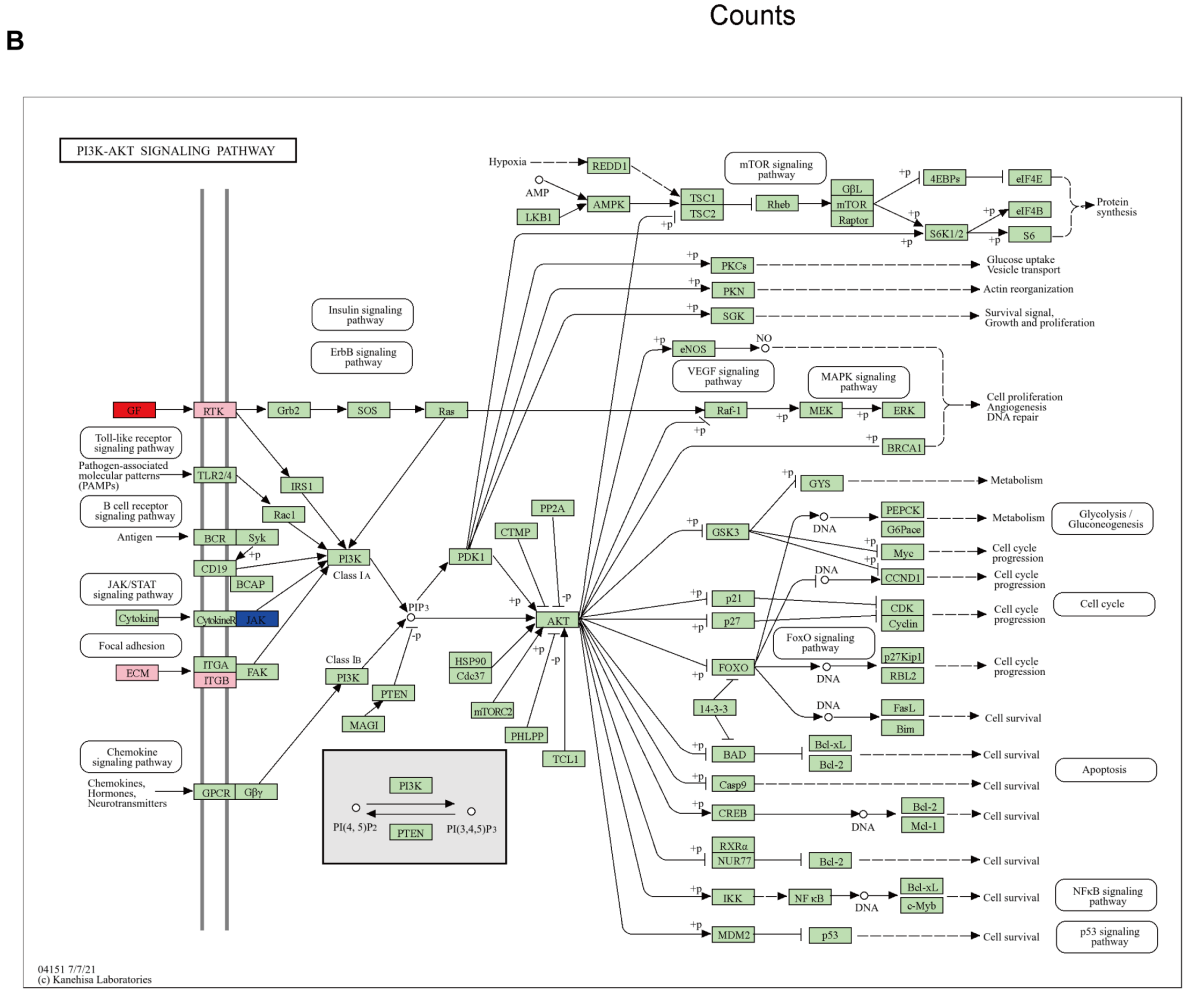

FIGURE 4
Analysis of relevant pathways about differentially expressed genes associated with angiogenesis. **(A)** KEGG and REACTOME analysis of differentially expressed genes. **(B)** KEGG pathway analysis of PI3K-AKT signaling pathway. Pink is chosen as the background color, where the up-regulated genes are labeled red and down-regulated are blue.

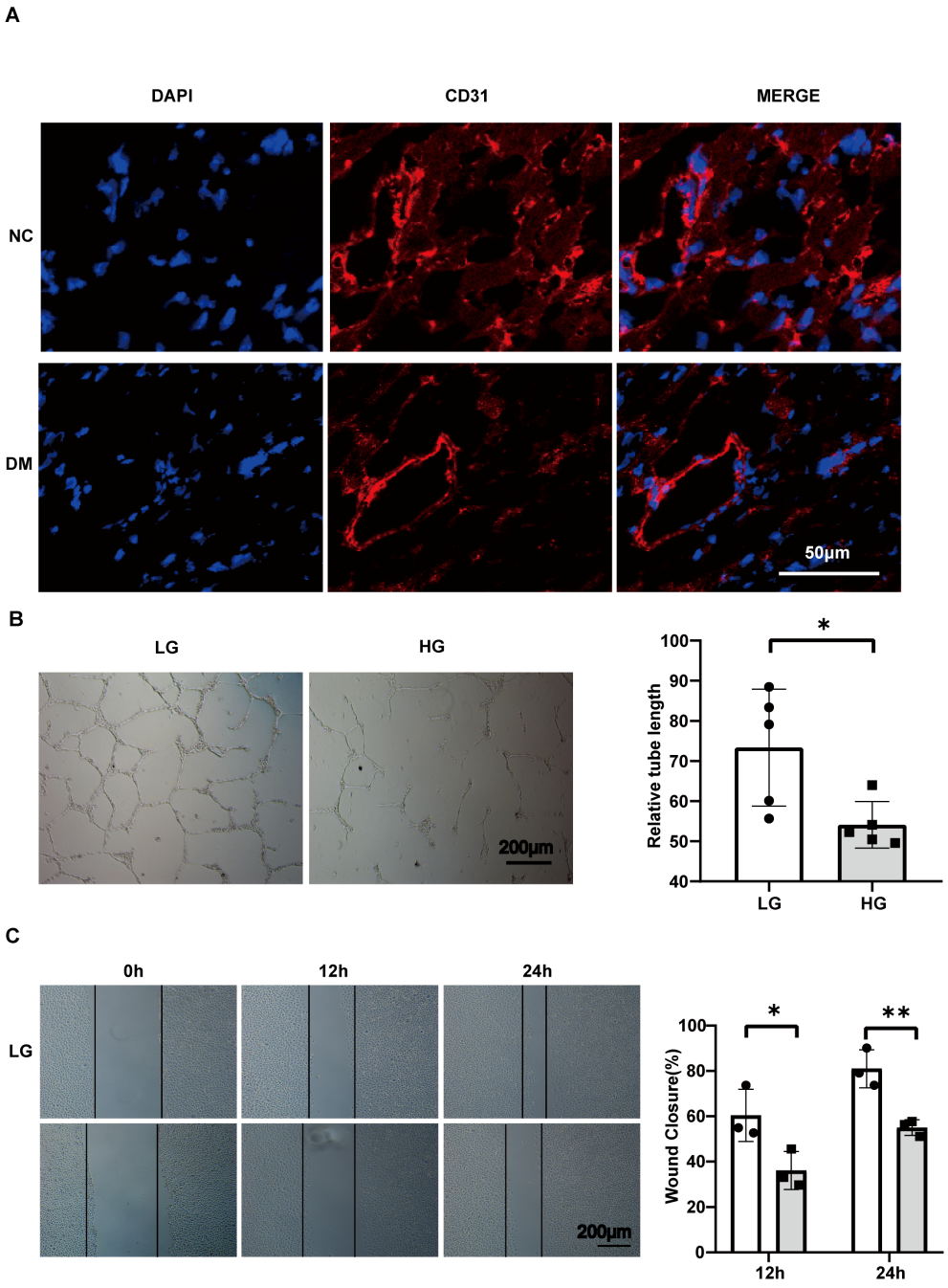

FIGURE 5
Angiogenesis impairment occurs in the hearts of DM mice and in HG-stimulated HUVECs. **(A)** Confocal image of cardiac microangiogenesis (CD31, red) in mouse heart tissue, scale bar, 50 μm. **(B)** Tube formation assay and related analysis of HUVECs, scale bar, 200 μm. n=5. **(C)** Wound healing assay and related analysis of HUVECs, scale bar, 200 μm. n=3. Data represent the mean ± SEM. *P<0.05, **P<0.01. NC, negative control; DM, diabetes mellitus; LG, low glucose; HG, high glucose; HUVECs, Human umbilical vein endothelial cells.

with angiogenesis in diabetic cardiomyopathy, thereby providing the possibility of specific targeted interventions in the future.

Our transcriptomic analysis revealed significant enrichment of differentially expressed genes in the PI3K-AKT signaling pathway, and the PI3K-AKT pathway is an important intracellular signal transduction pathway, which is involved in the regulation of cell survival, proliferation, metabolism, and apoptosis. Emerging evidence further highlights the central role of PI3K-AKT signaling as a regulatory hub for diverse interventions in DCM (28–30). For instance, NLRP3 inflammasome knockout in endothelial progenitor cells (EPCs) was reported to rescue angiogenesis in diabetic mice with myocardial infarction, suggesting that the PI3K/AKT/mTOR cascade acts as a downstream effector of NLRP3-mediated inflammatory responses (31). Additionally, innovative approaches such as ultrasound-mediated microbubble cavitation have demonstrated dose-dependent pro-angiogenic effects in diabetic models,

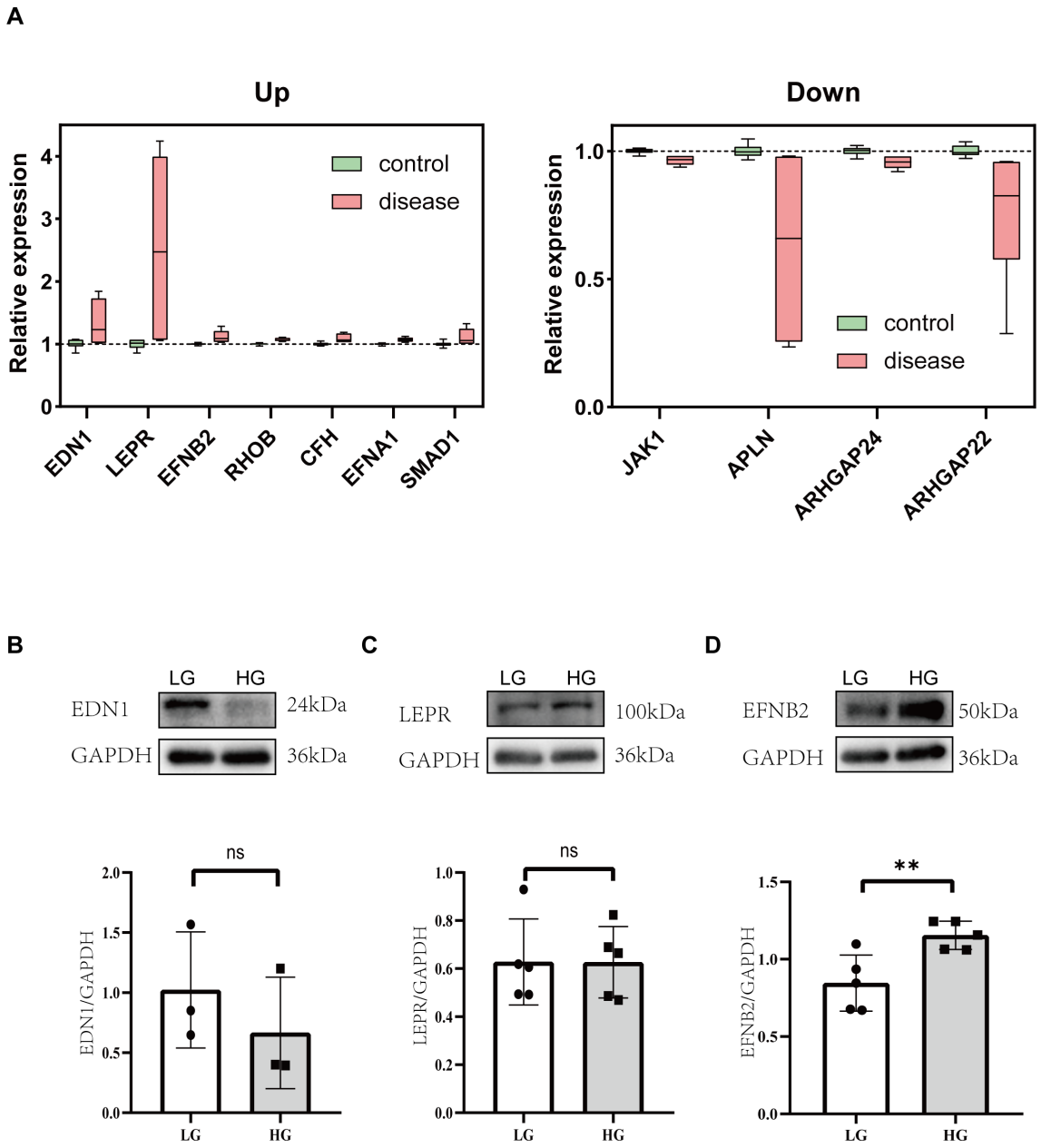

FIGURE 6
Analysis of proteins associated with impaired angiogenesis in diabetic cardiomyopathy. **(A)** Box plots of the relative changes in differentially expressed genes with consistent trends. **(B)** Representative western blot images and relative analysis of EDN1 on HG-stimulated HUVECs. n=3. **(C)** Representative western blot images and relative analysis of LEPR on HG-stimulated HUVECs. n=5. **(D)** Representative western blot images and relative analysis of EFNB2 on HG-stimulated HUVECs. n=5. Data represent the mean ± SEM. *P<0.05, **P<0.01.LG, low glucose; HG, high glucose; HUVECs, Human umbilical vein endothelial cells; EDN1, endothelin 1; LEPR, leptin receptor; EFNB2, ephrin B2.

mechanistically attributed to PI3K-AKT-eNOS pathway activation and subsequent improvement in cardiac function (32). These data collectively position PI3K-AKT signaling as a critical mediator of both metabolic adaptation and vascular remodeling in diabetic hearts.

The differences between EDN1 and LEPR in our experimental validation did not show a statistical difference, but previous studies have identified EDN1 as a potential biomarker for DCM (33, 34). A DCM dataset (GSE62203) has been used to find that PGK1, LDHA, and EDN1 may promote M1 macrophage polarization in DCM (33). LEPR, on the other hand, is a leptin receptor that has been found to play an important role in cardiac hypertrophy, heart failure, and diabetes mellitus (35, 36). Therefore, these molecules may have different changes at different stages of DCM, and further research is needed to clarify their specific roles.

Further We found a significant increase in EFNB2 (EphrinB2) expression in HG-stimulated HUVECs, consistent with sequencing data. Previous studies have demonstrated that EphrinB2 plays a key role in angiogenesis and lymphangiogenesis (37, 38). In heart-

TABLE 1 Protein localization and membrane type analysis corresponding to differentially expressed genes with consistent trends.

Gene	Protein	CTD Inference Score	Protein_ID	Localizations	Membrane types
EDN1	endothelin 1	40.2	AAA52339.1	Extracellular	Soluble
LEPR	leptin receptor	24.85	AAB09673.1	Cell membrane	Transmembrane
EFNB2	ephrin B2	22.77	URS64290.1	Extracellular	Transmembrane|Soluble
JAK1	Janus kinase 1	20.31	BAE02826.1	Cytoplasm Cell membrane	Peripheral|Soluble
RHOB	ras homolog family member B	19.72	KAI4033686.1	Cell membrane	Lipid anchor
CFH	complement factor H	17.31	CAA30403.1	Extracellular	Soluble
APLN	apelin	14.14	AAF25815.1	Extracellular	Soluble
EFNA1	ephrin A1	12.48	AAH95432.1	Cell membrane	Lipid anchor
SMAD1	SMAD family member 1	9.76	KAI4027178.1	Nucleus	Soluble
ARHGAP24	Rho GTPase activating protein 24	6.38	KAI4026049.1	Cytoplasm	Peripheral|Soluble
ARHGAP22	Rho GTPase activating protein 22	6.31	KAI4075927.1	Cytoplasm	Peripheral|Soluble

related studies, researchers have high hopes for its ability to promote angiogenesis (39), but some studies have found that it plays a profibrotic role in cardiac fibrosis (40). However, recent studies have found that EphrinB2 prevents ischemic cardiac remodeling and dysfunction after myocardial infarction by activating the cardiac lymphatic vessels to produce signaling pathways (41). In addition, diabetes has been found to increase the expression of Ephrin-B2 in cerebral blood vessels and pericytes and increase cerebral neovascularization, which may be related to impaired cognitive function in diabetic patients (42). EphrinB2 elevation in diabetic cardiomyopathy may be a compensatory protective mechanism, or it may also play a multiple role in angiogenesis. More studies are still needed to uncover the role of EphrinB2 in angiogenesis in diabetic cardiomyopathy. However, screening of sequencing data can quickly and cost-effectively focus on key possible targets in many regulatory molecules.

Similar to relative studies, we also found that angiogenesis is suppressed in diabetic cardiomyopathy. Some studies have found that interventions such as apelin (17, 43), adipsin (44), cilostazol (45), and salvianolic acid B (46) can help improve angiogenesis in DCM. In addition, genetically engineered cell therapies (47) and stem cell transplantation (48) have also shown therapeutic potential. The emerging intervention regimens have shown certain therapeutic potential, but more efforts are still needed for targeted interventions based on key molecules and further clinical translation.

But inevitably, this study also has some limitations. First, we identified 11 genes associated with angiogenesis, but only the first 3 were immunoblotted. It is possible that other molecules also played an important role, but further validation is still needed. Second, we focused on angiogenesis in diabetic cardiomyopathy but did not link clinical information, and included patients with diabetic cardiomyopathy for clinical sample validation. Finally, focusing only on molecular changes cannot fully and accurately explain the changes in angiogenesis, and more experiments are still needed to discover the related regulatory pathways and regulatory patterns. These limitations require more time and experimental validation and are the next step we need to consider for further study.

5 Conclusion

In summary, this study systematically investigated angiogenesis impairment in DCM through integrated bioinformatics analysis, preclinical models, and molecular validation. By combining transcriptomic profiling of human and murine datasets with functional experiments in diabetic mice and high glucose-stimulated endothelial cells, we identified Efnb2 as a central regulator of microvascular dysfunction in DCM. These findings not only elucidate a novel molecular axis linking angiogenesis damage to DCM but also highlight Efnb2 as a potential therapeutic target.

Data availability statement

The original contributions presented in the study are included in the article material. Further inquiries can be directed to the corresponding author.

Ethics statement

The animal study was approved by Experimental Animal Ethics and Welfare Committee of Hebei Medical University. The study was conducted in accordance with the local legislation and institutional requirements.

Author contributions

FH: Writing – original draft, Formal Analysis, Visualization, Writing – review & editing. RG: Writing – review & editing,

Software. YZ: Writing – review & editing. HH: Writing – review & editing. TT: Data curation, Methodology, Writing – review & editing. PW: Writing – review & editing. XL: Investigation, Project administration, Writing – original draft, Writing – review & editing.

Funding

The author(s) declare that no financial support was received for the research, authorship, and/or publication of this article.

Conflict of interest

The authors declare that the research was conducted in the absence of any commercial or financial relationships that could be construed as a potential conflict of interest.

Generative AI statement

The author(s) declare that no Generative AI was used in the creation of this manuscript.

Publisher's note

Supplementary material

The Supplementary Material for this article can be found online at: https://www.frontiersin.org/articles/10.3389/fendo.2025.1561142/full#supplementary-material

References

1. Demir S, Nawroth PP, Herzig S, Ekim Üstünel B. Emerging targets in type 2. Diabetes and diabetic complications. *Adv Sci (Weinh)*. (2021) 8:e2100275. doi: 10.1002/advs.202100275

2. Sun HJ, Ni ZR, Liu Y, Fu X, Liu SY, Hu JY, et al. Deficiency of neutral cholesterol ester hydrolase 1 (NCEH1) impairs endothelial function in diet-induced diabetic mice. *Cardiovasc Diabetol*. (2024) 23:138. doi: 10.1186/s12933-024-02239-6

3. Luo J, Hu S, Liu J, Shi L, Luo L, Li W, et al. Cardiac-specific PFKFB3 overexpression prevents diabetic cardiomyopathy via enhancing OPA1 stabilization mediated by K6-linked ubiquitination. *Cell Mol Life Sci*. (2024) 81:228. doi: 10.1007/s00018-024-05257-5

4. Hou J, Liang WY, Xiong S, Long P, Yue T, Wen X, et al. Identification of hub genes and potential ceRNA networks of diabetic cardiomyopathy. *Sci Rep*. (2023) 13:10258. doi: 10.1038/s41598-023-37378-5

5. Elia E, Ministrini S, Carbone F, Montecucco F. Diabetic cardiomyopathy and inflammation: development of hostile microenvironment resulting in cardiac damage. *Minerva Cardiol Angiol*. (2022) 70:357–69. doi: 10.23736/S2724-5683.20.05454-7

6. Zhao X, Shang L, Shen C. Daphnetin ameliorates diabetic cardiomyopathy by regulating inflammation and endoplasmic reticulum stress-induced apoptosis. *Exp Anim*. (2024) 74:49–57. doi: 10.1538/expanim.24-0027

7. Yang Q, Chen Q, Li S, Luo J. Mesenchymal stem cells ameliorate inflammation and pyroptosis in diabetic cardiomyopathy via the miRNA-223-3p/NLRP3 pathway. *Diabetol Metab Syndr*. (2024) 16:146. doi: 10.1186/s13098-024-01389-7

8. Zhao M, Shen Z, Zheng Z, Xu Y, Zhang J, Liu J, et al. Cardiomyocyte LGR6 alleviates ferroptosis in diabetic cardiomyopathy via regulating mitochondrial biogenesis. *Metabolism*. (2024) 159:155979. doi: 10.1016/j.metabol.2024.155979

9. Wang R, Zhang X, Ye H, Yang X, Zhao Y, Wu L, et al. Fibroblast growth factor 21 improves diabetic cardiomyopathy by inhibiting ferroptosis via ferritin pathway. *Cardiovasc Diabetol*. (2024) 23:394. doi: 10.1186/s12933-024-02469-8

10. Zhen J, Sheng X, Chen T, Yu H. Histone acetyltransferase Kat2a regulates ferroptosis via enhancing Tfrc and Hmox1 expression in diabetic cardiomyopathy. *Cell Death Dis*. (2024) 15:406. doi: 10.1038/s41419-024-06771-x

11. Xiang H, Lyu Q, Chen S, Ouyang J, Xiao D, Liu Q, et al. PACS2/CPT1A/DHODH signaling promotes cardiomyocyte ferroptosis in diabetic cardiomyopathy. *Cardiovasc Diabetol*. (2024) 23:432. doi: 10.1186/s12933-024-02514-6

12. Tan S, Zang G, Wang Y, Sun Z, Li Y, Lu C, et al. Differences of angiogenesis factors in tumor and diabetes mellitus. *Diabetes Metab Syndr Obes*. (2021) 14:3375–88. doi: 10.2147/DMSO.S315362

13. Akbarian M, Bertassoni LE, Tayebi L. Biological aspects in controlling angiogenesis: current progress. *Cell Mol Life Sci*. (2022) 79:349. doi: 10.1007/s00018-022-04348-5

14. Abaci A, Oğuzhan A, Kahraman S, Eryol NK, Unal S, Arinç H, et al. Effect of diabetes mellitus on the formation of coronary collateral vessels. *Circulation*. (1999) 99:2239–42. doi: 10.1161/01.cir.99.17.2239

15. Werner GS, Ferrari M, Betge S, Gastmann O, Richartz BM, Figulla HR. Collateral function in chronic total coronary occlusions is related to regional myocardial function and duration of occlusion. *Circulation*. (2001) 104:2784–90. doi: 10.1161/hc4801.100352

16. Kaur N, Gare SR, Ruiz-Velasco A, Miller JM, Abouleisa R, Ou Q, et al. FGF21/FGFR1-β-KL cascade in cardiomyocytes modulates angiogenesis and inflammation under metabolic stress. *Heliyon*. (2023) 9:e14952. doi: 10.1016/j.heliyon.2023.e14952

17. Li B, Yin J, Chang J, Zhang J, Wang Y, Huang H, et al. Apelin/APJ relieve diabetic cardiomyopathy by reducing microvascular dysfunction. *J Endocrinol*. (2021) 249:1–18. doi: 10.1530/JOE-20-0398

18. Hahad O, Wild PS, Prochaska JH, Schulz A, Hermanns I, Lackner KJ, et al. Endothelial function assessed by digital volume plethysmography predicts the development and progression of type 2 diabetes mellitus. *J Am Heart Assoc*. (2019) 8:e012509. doi: 10.1161/JAHA.119.012509

19. Wang X, Gu H, Huang W, Peng J, Li Y, Yang L, et al. Hsp20-mediated activation of exosome biogenesis in cardiomyocytes improves cardiac function and angiogenesis in diabetic mice. *Diabetes*. (2016) 65:3111–28. doi: 10.2337/db15-1563

20. Zhong Z, Zhang H, Xu T, Hao J, Chen X, Sun S, et al. Identification and verification of immune-related biomarkers and immune infiltration in diabetic heart failure. *Front Cardiovasc Med*. (2022) 9:931066. doi: 10.3389/fcvm.2022.931066

21. Cui M, Wu H, An Y, Liu Y, Wei L, Qi X. Identification of important modules and biomarkers in diabetic cardiomyopathy based on WGCNA and LASSO analysis. *Front Endocrinol (Lausanne)*. (2024) 15:1185062. doi: 10.3389/fendo.2024.1185062

22. Zheng ZQ, Cai DH, Song YF. Identification of immune feature genes and intercellular profiles in diabetic cardiomyopathy. *World J Diabetes*. (2024) 15:2093–110. doi: 10.4239/wjd.v15.i10.2093

23. Rooney MR, Chen J, Echouffo-Tcheugui JB, Walker KA, Schlosser P, Surapaneni A, et al. Proteomic predictors of incident diabetes: results from the atherosclerosis risk in communities (ARIC) study. *Diabetes Care*. (2023) 46:733–41. doi: 10.2337/dc22-1830

24. Conning-Rowland MS, Giannoudi M, Drozd M, Brown OI, Yuldasheva NY, Cheng CW, et al. The diabetic myocardial transcriptome reveals Erbb3 and Hspa2 as a novel biomarkers of incident heart failure. *Cardiovasc Res*. (2024) 120:1898–906. doi: 10.1093/cvr/cvae181

25. Wilson-Verdugo M, Bustos-García B, Adame-Guerrero O, Hersch-González J, Cano-Domínguez N, Soto-Nava M, et al. Reversal of high-glucose-induced transcriptional and epigenetic memories through NRF2 pathway activation. *Life Sci Alliance*. (2024) 7:e202302382. doi: 10.26508/lsa.202302382

26. Li H, Zhu X, Cao X, Lu Y, Zhou J, Zhang X. Single-cell analysis reveals lysyl oxidase (Lox)(+) fibroblast subset involved in cardiac fibrosis of diabetic mice. *J Adv Res*. (2023) 54:223–37. doi: 10.1016/j.jare.2023.01.018

27. Tang D, Chen M, Huang X, Zhang G, Zeng L, Zhang G, et al. SRplot: A free online platform for data visualization and graphing. *PloS One*. (2023) 18:e0294236. doi: 10.1371/journal.pone.0294236

28. Li W, Liu X, Liu Z, Xing Q, Liu R, Wu Q, et al. The signaling pathways of selected traditional Chinese medicine prescriptions and their metabolites in the treatment of diabetic cardiomyopathy: a review. *Front Pharmacol*. (2024) 15:1416403. doi: 10.3389/fphar.2024.1416403

29. Boshchenko AA, Maslov LN, Mukhomedzyanov AV, Zhuravleva OA, Slidnevskaya AS, Naryzhnaya NV, et al. Peptides are cardioprotective drugs of the future: the receptor and signaling mechanisms of the cardioprotective effect of glucagon-like peptide-1 receptor agonists. *Int J Mol Sci*. (2024) 25:4900. doi: 10.3390/ijms25094900

30. Cai L, Tan Y, Watson S, Wintergerst K. Diabetic cardiomyopathy - Zinc preventive and therapeutic potentials by its anti-oxidative stress and sensitizing insulin signaling pathways. *Toxicol Appl Pharmacol*. (2023) 477:116694. doi: 10.1016/j.taap.2023.116694

31. Li JP, Qiu S, Tai GJ, Liu YM, Wei W, Fu MM, et al. NLRP3 inflammasome-modulated angiogenic function of EPC via PI3K/Akt/mTOR pathway in diabetic myocardial infarction. *Cardiovasc Diabetol*. (2025) 24:6. doi: 10.1186/s12933-024-02541-3

32. Zhou NQ, Song YT, Liu WZ, Yue RZ, Tian XQ, Yang SC, et al. Diagnostic ultrasound-mediated microbubble cavitation dose-dependently improves diabetic cardiomyopathy through angiogenesis. *Cell Biol Int*. (2023) 47:178–87. doi: 10.1002/cbin.11918

33. Liu Y, Zhang J, Han Q, Li Y, Xue Y, Liu X. Identification of biomarkers associated with macrophage polarization in diabetic cardiomyopathy based on bioinformatics and machine learning approaches. *Life Sci*. (2025) 364:123443. doi: 10.1016/j.lfs.2025.123443

34. Guo Q, Zhu Q, Zhang T, Qu Q, Cheang I, Liao S, et al. Integrated bioinformatic analysis reveals immune molecular markers and potential drugs for diabetic cardiomyopathy. *Front Endocrinol (Lausanne)*. (2022) 13:933635. doi: 10.3389/fendo.2022.933635

35. Karmazyn M, Gan XT. Molecular and cellular mechanisms underlying the cardiac hypertrophic and pro-remodelling effects of leptin. *Int J Mol Sci*. (2024) 25:1137. doi: 10.3390/ijms25021137

36. Olczyk P, Koprowski R, Komosinska-Vassev K, Jura-Półtorak A, Winsz-Szczotka K, Kuźnik-Trocha K, et al. Adiponectin, leptin, and leptin receptor in obese patients with type 2 diabetes treated with insulin detemir. *Molecules*. (2017) 22:1274. doi: 10.3390/molecules22081274

37. Wang Y, Nakayama M, Pitulescu ME, Schmidt TS, Bochenek ML, Sakakibara A, et al. Ephrin-B2 controls VEGF-induced angiogenesis and lymphangiogenesis. *Nature*. (2010) 465:483–6. doi: 10.1038/nature09002

38. Sawamiphak S, Seidel S, Essmann CL, Wilkinson GA, Pitulescu ME, Acker T, et al. Ephrin-B2 regulates VEGFR2 function in developmental and tumour angiogenesis. *Nature*. (2010) 465:487–91. doi: 10.1038/nature08995

39. Yang D, Jin C, Ma H, Huang M, Shi GP, Wang J, et al. EphrinB2/EphB4 pathway in postnatal angiogenesis: a potential therapeutic target for ischemic cardiovascular disease. *Angiogenesis*. (2016) 19:297–309. doi: 10.1007/s10456-016-9514-9

40. Su SA, Yang D, Wu Y, Xie Y, Zhu W, Cai Z, et al. EphrinB2 regulates cardiac fibrosis through modulating the interaction of stat3 and TGF-β/smad3 signaling. *Circ Res*. (2017) 121:617–27. doi: 10.1161/CIRCRESAHA.117.311045

41. Bai Y, Chen L, Guo F, Zhang J, Hu J, Tao X, et al. EphrinB2-mediated CDK5/ISL1 pathway enhances cardiac lymphangiogenesis and alleviates ischemic injury by resolving post-MI inflammation. *Signal Transduct Target Ther*. (2024) 9:326. doi: 10.1038/s41392-024-02019-4

42. Coucha M, Barrett AC, Elgebaly M, Ergul A, Abdelsaid M. Inhibition of Ephrin-B2 in brain pericytes decreases cerebral pathological neovascularization in diabetic rats. *PloS One*. (2019) 14:e0210523. doi: 10.1371/journal.pone.0210523

43. Zeng H, He X, Hou X, Li L, Chen JX. Apelin gene therapy increases myocardial vascular density and ameliorates diabetic cardiomyopathy via upregulation of sirtuin 3. *Am J Physiol Heart Circ Physiol*. (2014) 306:H585–97. doi: 10.1152/ajpheart.00821.2013

44. Zhang X, Duan Y, Zhang X, Jiang M, Man W, Zhang Y, et al. Adipsin alleviates cardiac microvascular injury in diabetic cardiomyopathy through Csk-dependent signaling mechanism. *BMC Med*. (2023) 21:197. doi: 10.1186/s12916-023-02887-7

45. Tseng SY, Chang HY, Li YH, Chao TH. Effects of cilostazol on angiogenesis in diabetes through adiponectin/adiponectin receptors/sirtuin1 signaling pathway. *Int J Mol Sci*. (2022) 23:14839. doi: 10.3390/ijms232314839

46. Li CL, Liu B, Wang ZY, Xie F, Qiao W, Cheng J, et al. Salvianolic acid B improves myocardial function in diabetic cardiomyopathy by suppressing IGFBP3. *J Mol Cell Cardiol*. (2020) 139:98–112. doi: 10.1016/j.yjmcc.2020.01.009

47. Gatina DZ, Gazizov IM, Zhuravleva MN, Arkhipova SS, Golubenko MA, Gomzikova MO, et al. Induction of angiogenesis by genetically modified human umbilical cord blood mononuclear cells. *Int J Mol Sci*. (2023) 24:4396. doi: 10.3390/ijms24054396

48. Wang Y, Zhang Y, Chen K, Liu J, Wu D, Cheng Y, et al. Insufficient S-adenosylhomocysteine hydrolase compromises the beneficial effect of diabetic BMSCs on diabetic cardiomyopathy. *Stem Cell Res Ther*. (2022) 13:418. doi: 10.1186/s13287-022-03099-1

frontiers | Frontiers in Endocrinology

TYPE Original Research
PUBLISHED 08 August 2025
DOI 10.3389/fendo.2025.1641114

OPEN ACCESS

EDITED BY
Ramoji Kosuru,
Versiti Blood Research Institute, United States

REVIEWED BY
Qinan Wu,
Dazu Hospital of Chongqing Medical University, China
İnci Tuğçe Çöllüoğlu,
Karabuk Universitesi, Türkiye

*CORRESPONDENCE
Feng Qiu
923189400@qq.com
Jiadan Yang
202632@hospital.cqmu.edu.cn

†These authors have contributed equally to this work

RECEIVED 04 June 2025
ACCEPTED 22 July 2025
PUBLISHED 08 August 2025

CITATION
Luo Z, Pi D, Xi T, Jiang W, Qiu F and Yang J (2025) Predicting diabetic cardiomyopathy in type 2 diabetes: development and validation of a nomogram based on clinical and echocardiographic parameters.
Front. Endocrinol. 16:1641114.
doi: 10.3389/fendo.2025.1641114

Predicting diabetic cardiomyopathy in type 2 diabetes: development and validation of a nomogram based on clinical and echocardiographic parameters

Zilang Luo[1,2†], Damao Pi[1†], Tianlan Xi[2†], Wenli Jiang[1,2], Feng Qiu[1*] and Jiadan Yang[1*]

[1]Department of Pharmacy, The First Affiliated Hospital of Chongqing Medical University, Chongqing, China, [2]College of Pharmacy, Chongqing Medical University, Chongqing, China

Objective: Diabetic cardiomyopathy (DCM) is a myocardial dysfunction disorder driven by diabetes-associated metabolic disorders, significantly elevating the risk of heart failure in patients with type 2 diabetes mellitus (T2DM). We aimed to develop and validate a nomogram for individualized DCM risk prediction in T2DM populations.

Methods: This retrospective study enrolled 525 consecutive T2DM patients admitted to our hospital (June 2022-June 2024). Participants were randomly allocated to training (70%) or validation (30%) cohorts. Baseline clinical characteristics, laboratory profiles, and echocardiographic parameters were collected. Predictors were identified via univariate then multivariate logistic regression, followed by nomogram construction. Model validation included: (1) internal validation via 1000 bootstrap resamples; (2) discrimination assessed by the area under the receiver operating characteristic curve (AUC-ROC); (3) calibration evaluated using calibration plots and the Hosmer-Lemeshow goodness-of-fit test; (4) clinical utility determined by decision curve analysis (DCA) and clinical impact curves (CIC).

Results: Six independent predictors—age, duration of type 2 diabetes mellitus (T2DM Duration), systolic blood pressure (SBP), urinary albumin-to-creatinine ratio (UACR), left atrial diameter (LAD), and left ventricular posterior wall thickness at end-diastole (LVPWd)—were incorporated. The model showed excellent discrimination: AUC 0.947 (95% CI: 0.916-0.967) in training and 0.922 (95% CI: 0.870-0.956) in validation cohorts. Calibration indicated strong agreement (Hosmer-Lemeshow χ^2 = 9.2119, P = 0.3247). DCA and CIC confirmed clinical utility.

Conclusions: This nomogram integrates routine clinical/echocardiographic parameters to predict DCM risk in T2DM patients, facilitating individualized risk stratification and guiding early cardioprotective interventions in high-risk populations.

Clinical Trial Registration: https://www.chictr.org.cn/index.html, identifier ChiCTR2400093755.

KEYWORDS

diabetic cardiomyopathy, type 2 diabetes mellitus, nomogram, risk prediction model, echocardiographic

Introduction

Type 2 diabetes mellitus (T2DM) represents a global health crisis, with its prevalence and incidence exhibiting persistent upward trends. According to projections by the International Diabetes Federation (IDF), the global population with T2DM is anticipated to reach 700 million by 2045 (1). Beyond conventional micro- and macrovascular complications, T2DM directly contributes to myocardial pathology through diabetic cardiomyopathy (DCM)—a distinct entity characterized by diabetes-associated metabolic derangements that induce structural and functional cardiac alterations independent of coronary artery disease, valvular abnormalities, congenital heart defects, or other established etiologies of heart failure (HF) (2, 3). Epidemiological studies have demonstrated that cardiovascular mortality quadruples in diabetic populations compared to non-diabetic individuals (4), with DCM prevalence ranging from 10% to 21% among individuals with diabetes and associated mortality rates reaching 31% (5).

The pathogenesis of DCM is principally driven by metabolic dysregulation of carbohydrate and lipid homeostasis, triggering a cascade of pathophysiological events including oxidative stress generation, chronic inflammatory responses, endothelial dysfunction, and mitochondrial impairment (6, 7). These interconnected mechanisms collectively promote key pathological processes: cardiomyocyte hypertrophy, interstitial fibrosis, programmed cell death, coronary endothelial injury, and microvascular dysfunction (8, 9). Clinically, DCM manifests initially as elevated left ventricular filling pressures and diastolic dysfunction (10), progressing through stages of worsening diastolic impairment and eventual systolic failure, culminating in overt HF (11). Notably, asymptomatic left ventricular diastolic dysfunction frequently precedes symptomatic HF in T2DM patients, representing the earliest detectable functional manifestation of DCM (12). This insidious progression underscores the critical need for early detection and intervention to alleviate the escalating global burden of HF (13, 14).

Current diagnostic challenges persist due to the lack of disease-specific biomarkers, while advanced imaging modalities such as cardiac magnetic resonance imaging (CMR) remain cost-prohibitive for routine clinical implementation (15). Although prior studies have attempted to develop predictive models for DCM in T2DM patients, Existing tools exhibit certain limitations. First, certain models were derived from limited cohorts (e.g., one nomogram study with n = 84 cases), potentially compromising statistical power and increasing risks of overfitting or reduced generalizability (16). Second, some prediction frameworks rely exclusively on basic clinical characteristics (e.g., age, body mass index) and laboratory parameters (e.g., lipids, electrolytes), omitting cardiac structural/functional metrics essential for capturing DCM pathophysiology (17). To address these gaps, we developed and validated a clinical nomogram integrating routinely accessible clinical and echocardiographic parameters for DCM risk prediction in T2DM patients. This tool aims to enable early risk stratification, facilitating timely preventive strategies and targeted interventions to mitigate DCM-associated morbidity in high-risk populations.

Methods

Study design and participants

This study utilized electronic medical records from the Endocrinology Department of the First Affiliated Hospital of Chongqing Medical University (Chongqing, China). We consecutively screened patients admitted between June 2022 and June 2024, ultimately enrolling 525 eligible individuals with T2DM. Eligible participants were randomly allocated (7:3 ratio) to training (n = 367) and validation (n = 158) cohorts using computer-generated random numbers.

Inclusion and exclusion criteria

The inclusion criteria included (1): Age ≥18 years (2); Diagnosis of T2DM is established based on the American Diabetes Association (ADA) criteria (18): Hemoglobin A1c (HbA1c) ≥6.5% or fasting plasma glucose ≥7.0 mmol/L or 2-Hour plasma glucose during oral glucose tolerance test (OGTT) ≥11.1 mmol/L or random plasma glucose ≥11.1 mmol/L; (3) Complete echocardiographic evaluation.

The exclusion criteria included: (1) Established cardiovascular pathology: (a) HF, established diagnosis or typical heart failure symptoms and signs (NYHA class II-IV symptoms) who were on long-term anti-HF medications; (b) hypertensive heart disease, documented history or uncontrolled severe hypertension; (c) coronary artery disease, known history of coronary artery disease, myocardial infarction, or coronary angiography demonstrating ≥50% luminal stenosis; (d) significant valvular disease, moderate-to-severe valvular stenosis/regurgitation confirmed by echocardiography; (e) congenital heart defects, clinically significant congenital heart disease verified by medical history or echocardiography. (2) Comorbid conditions: active malignancies, systemic infections (CRP >10 mg/L), hepatic insufficiency (Child-Pugh B/C), renal dysfunction (eGFR <30 mL/min/1.73m^2); (3) Diabetes subtypes: Type 1 diabetes, gestational diabetes, secondary diabetes; (4) Incomplete core clinical parameters.

Diagnosis of DCM

In accordance with the 2024 ESC Position Paper on DCM (endorsed by the Heart Failure Association and Working Group on Myocardial and Pericardial Diseases), DCM is defined as systolic and/or diastolic myocardial dysfunction occurring in patients with diabetes mellitus (19). Given this study's focus on early-stage DCM risk prediction, we targeted the initial disease continuum: Diastolic dysfunction represents the earliest detectable phenotype of diabetic myocardial injury. Systolic dysfunction (LVEF <50%) typically indicates advanced disease incompatible with early warning objectives (2).

Therefore, through strict application of pre-specified inclusion/exclusion criteria, study participants were confirmed as DCM cases upon meeting the criteria for left ventricular diastolic dysfunction. Diastolic dysfunction was defined per the 2016 ASE/EACVI Recommendations for the Evaluation of Left Ventricular Diastolic Function, requiring ≥3 of the following echocardiographic criteria (20): (1) Septal e' velocity <7 cm/s or Lateral e' velocity <10 cm/s; (2) Peak tricuspid regurgitation velocity >2.8 m/s; (3) Early diastolic mitral inflow velocity to tissue Doppler mitral annular early diastolic velocity ratio (E/e') >14; (4) Left atrial volume index (LAVI) >34 mL/m^2.

Baseline data collection

Clinical characteristics and laboratory parameters were systematically collected through standardized protocols. Demographic and clinical variables included: age, sex, body mass index (BMI), duration of type 2 diabetes mellitus (T2DM Duration) (calculated from initial diagnosis to current hospitalization), heart rate, systolic blood pressure (SBP), diastolic blood pressure (DBP), smoking status, and alcohol consumption history. We obtained fasting venous blood samples were obtained within 24 hours of admission using standardized phlebotomy procedures. Complete blood counts - including white blood cells (WBC), neutrophils (NEU), lymphocytes (LYM), and platelets (PLT) - were analyzed using an automated hematology analyzer, with derived platelet-to-lymphocyte ratio (PLR) and neutrophil-to-lymphocyte ratio (NLR). Glycated hemoglobin (HbA1c) was measured by high-performance liquid chromatography, while biochemical profiles (triglycerides [TG], total cholesterol [TC], high-density lipoprotein cholesterol [HDL-C], low-density lipoprotein cholesterol [LDL-C], and serum creatinine [Scr]) were assessed using a clinical chemistry analyzer. First-morning midstream urine specimens were collected for urinary albumin-to-creatinine ratio (UACR) measurement via immunoturbidimetry. Estimated glomerular filtration rate (eGFR) was calculated applying the Chronic Kidney Disease Epidemiology Collaboration (CKD-EPI) equation (21). All data underwent dual-entry verification by independent investigators to ensure completeness and validity.

Standardized transthoracic echocardiography was performed by certified sonographers using a GE Vivid E95 ultrasound system (GE Healthcare) equipped with M5S transducers (1.5-4.6 MHz). Measured parameters included: left atrial diameter (LAD), left ventricular end-diastolic diameter (LVEDD), interventricular septal thickness at end-diastole (IVSd), left ventricular posterior wall thickness at end-diastole (LVPWd), relative wall thickness (RWT; 2×LVPWd/LVEDD), left ventricular ejection fraction (LVEF; Simpson's biplane method). Left ventricular mass index (LVMI) was calculated using the Devereux formula (22). Measurement of diastolic function and tissue Doppler parameters: early diastolic mitral annular velocities (e') were acquired using pulsed-wave tissue Doppler imaging (TDI) at the basal septal and lateral segments in the apical four-chamber view. Mitral inflow E-wave velocity was subsequently measured by placing the pulsed-wave Doppler sample volume at the mitral valve leaflet tips in the standard apical four-chamber view. The E/e' ratiowas calculated as the ratio of mitral E-wave velocity to the average of septal and lateral e' velocities. The LAVI was quantified in apical four- and two-chamber views using the biplane area-length method and indexed to body surface area. Additionally, peak TRV was obtained via continuous-wave (CW) Doppler in either the apical four-chamber view or dedicated right ventricular inflow view.

Statistical analysis

All statistical analyses were conducted using R software (version 4.4.1; R Foundation) and IBM SPSS Statistics (version 25.0; IBM Corp). Continuous variables were assessed for normality through Shapiro-Wilk tests supplemented by histogram visualization. Normally distributed variables were expressed as mean ± standard deviation (SD) and compared using Student's t-test, while non-normally distributed variables were reported as median (interquartile range [IQR]) with Mann-Whitney U test comparisons. Categorical variables were presented as frequencies (percentages) and analyzed by χ^2 test or Fisher's exact test as appropriate. we performed univariate logistic regression analysis on the training cohort and the independent risk factors were further analyzed by multivariate logistic regression (Stepwise backward regression method). This model was visualized as a

nomogram using the rms package in R with proportional scaling. Internal validation employed 1000 bootstrap resamples to estimate optimism-corrected performance metrics and mitigate overfitting risks. Model discrimination was evaluated via receiver operating characteristic (ROC) curve analysis reporting area under the curve (AUC) with 95% confidence intervals. Calibration was assessed using Hosmer-Lemeshow goodness-of-fit tests and calibration plots comparing predicted versus observed probabilities. Clinical utility was assessed through decision curve analysis (DCA) and clinical impact curves (CIC), with DCA quantifying the net benefit across threshold probabilities and CIC estimating true-positive versus false-positive classification rates. The P value of <0.05 indicated statistical significance.

Results

Baseline characteristics

The study flowchart is presented in Figure 1. The study cohort comprised 525 patients with T2DM, among whom 174 (33.1%) met diagnostic criteria for DCM. Table 1 presents comparative analyses of clinical and echocardiographic parameters between the training (n = 367) and validation (n = 158) cohorts. The training cohort demonstrated a median age of 54.0 years (IQR 45.0-61.0) with male predominance (64.3%), while the validation cohort had comparable baseline characteristics: median age 54.0 years (IQR 45.0-63.0) and male proportion 67.1%. Intergroup comparisons revealed statistically significant differences only in smoking status (P = 0.047), with no clinically relevant disparities observed in T2DM duration, BMI, SBP, or other key variables. This baseline homogeneity supports the validity of the internal model validation procedures.

Univariate and multivariable logistic regression analysis

Univariate logistic regression analysis identified 17 variables significantly associated with DCM (P <0.05) in the training cohort. To mitigate overfitting and multicollinearity risks, we adhered to the events per variable (EPV) ≥10 principle (23), permitting inclusion of ≤12 variables given 125 DCM events. Variables were prioritized based on statistical significance (P <0.01), with 12 candidate variables retained for subsequent multivariate analysis. After performing multivariate logistic regression analysis (using backward stepwise regression), a variance inflation factor (VIF) less than 5 indicates acceptable multicollinearity, six independent predictors emerged (P *<0.05*): Age (OR = 1.046, 95% CI:1.008-1.088, P = 0.0198), T2DM Duration (OR = 1.254, 95% CI: 1.167-1.359, P <0.001), SBP (OR = 1.033, 95% CI:1.011-1.055, P = 0.0028), UACR (OR = 1.014, 95% CI:1.008-1.020, P <0.001), LAD (OR = 1.33, 95% CI:1.178-1.519, P <0.001), LVPWd (OR = 2.33, 95% CI:1.542-3.636, P <0.001). Detailed results are presented in Tables 2 and 3.

Development of the nomogram prediction model

The nomogram (Figure 2) was constructed to visualize the final multivariable logistic regression model. Point values assigned to each predictor were automatically calculated based on their corresponding regression coefficients (β-coefficients) using the rms package in R software. This mathematical transformation process ensures that the point scale accurately preserves both the relative weights of variables within the model and the risk differences between categorical levels of individual predictors.

To apply the model, clinicians first assign individualized scores by mapping a patient's clinical parameters to the corresponding variable axes. These scores are then summed to calculate a total risk score, which is subsequently projected onto the probability axis to estimate the personalized likelihood of DCM. For instance, a 75-year-old patient with T2DM, a 20-year disease duration, SBP of 129 mmHg, UACR of 13.6 mg/g, LAD of 30 mm, and LVPWd of 9 mm would accumulate a total score of 127.5 points, corresponding to a 65% predicted probability of DCM (Figure 3). This integrative tool enables rapid risk stratification and supports clinical decision-making for early intervention in high-risk populations.

Model performance

Internal validation through 1000 bootstrap resamples demonstrated robust model discrimination, with a C-index of 0.9376 (95% CI: 0.9024-0.9728), indicating minimal overfitting risk. ROC analysis revealed excellent predictive accuracy in both training (AUC = 0.947, 95% CI: 0.916-0.967) and validation cohorts (AUC = 0.922, 95% CI: 0.870-0.956), surpassing the clinical utility threshold (AUC >0.75) (Figure 4). Calibration plots exhibited strong concordance between predicted probabilities and observed outcomes across risk strata (Figure 5). The Hosmer-Lemeshow test confirmed adequate model calibration (χ^2 = 9.2119, P = 0.3247), with non-significant deviation from ideal prediction (P >0.05).

Model clinical utility

The DCA of the nomogram demonstrated superior net clinical benefits compared to default strategies ("Treat All" or "Treat None") across low-to-medium risk thresholds (0.0-0.8), with both training and validation cohort curves exhibiting parallel trajectories and minimal divergence (Figure 6A). This consistency indicates robust generalizability without significant overfitting. CIC analysis further revealed high concordance between model-predicted high-risk cases and actual event occurrences at thresholds >0.6, highlighting its precision for resource-intensive interventions (Figure 6B). Integrating cost-benefit ratios, we recommend adopting flexible threshold selection (0.4-0.8) to optimize risk stratification and healthcare resource allocation based on clinical priorities and resource availability.

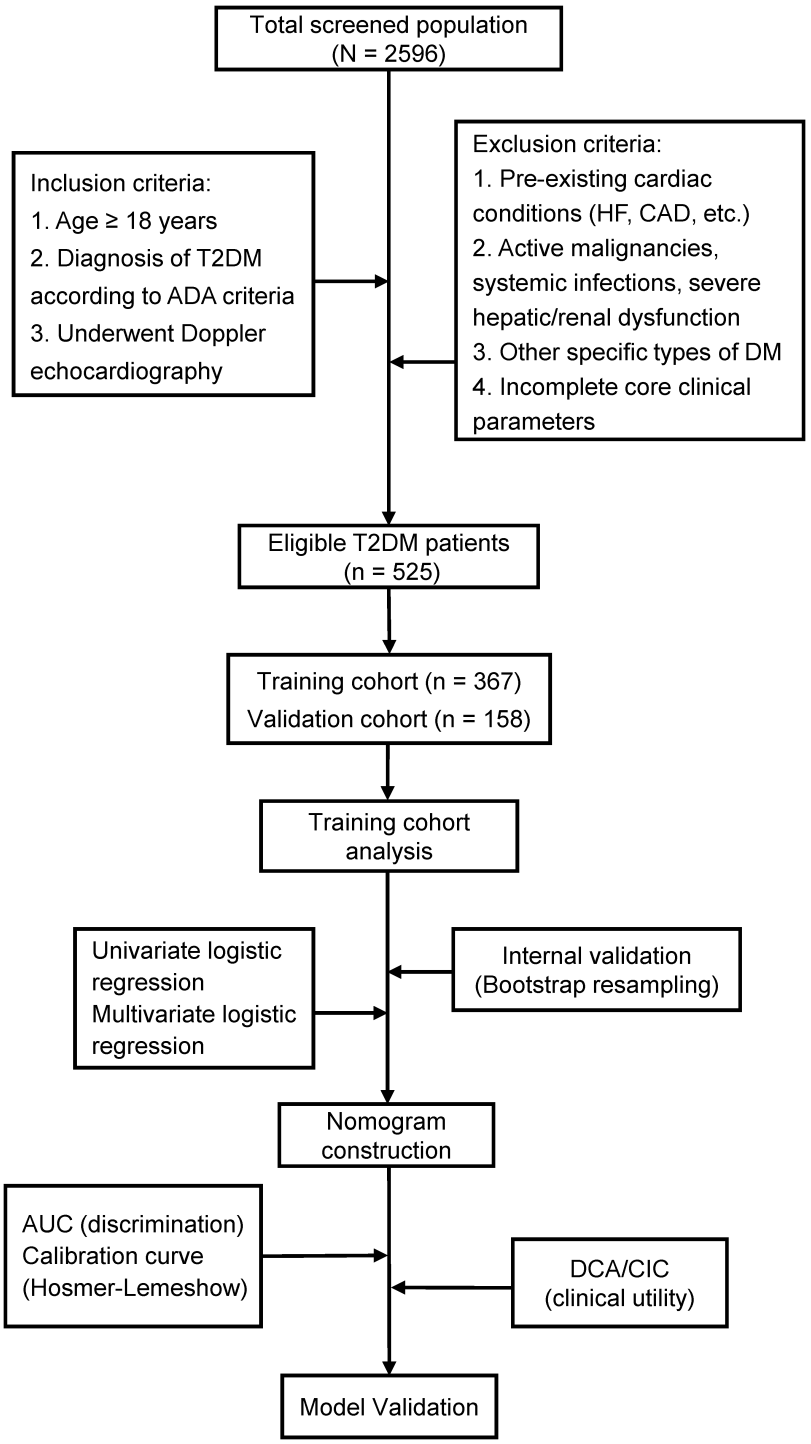

FIGURE 1
Flow diagram of study design.

Discussion

Summary and interpretation of key findings

HF secondary to DCM represents a major contributor to premature mortality in patients with T2DM. While prior studies have established associations between echocardiographic parameters, biomarkers, and HF risk in diabetes (14, 24, 25), limited research has focused on predicting DCM progression in T2DM populations. To address this gap, we conducted a retrospective analysis of hospital-based data, identifying conventional clinical indicators (age, T2DM Duration, SBP, UACR) and cardiac structural remodeling markers (LAD, LVPWd) as independent predictors of DCM. Leveraging these

10.3389/fendo.2025.1641114

TABLE 1 The baseline characteristics of patients in the training and validation cohort.

Parameter	Training cohort (n = 367)	Validation cohort (n = 158)	χ^2/z/t	*P*
Clinical information				
Age (years)	54.00 (45.00, 61.00)	54.00 (45.00, 63.00)	-0.388	0.698[a]
Gender (n, %)			0.377	0.539[c]
Female	131 (35.7)	52 (32.9)		
Male	236 (64.3)	106 (67.1)		
T2DM Duration (years)	8.00 (2.00, 14.00)	7.00 (2.00, 12.00)	-0.959	0.337[a]
BMI (kg/m^2)	23.73 (21.85, 25.97)	24.33 (21.88, 26.77)	-1.233	0.218[a]
Heart rate (bpm)	88.00 (81.00, 96.00)	89.00 (80.00, 99.00)	-0.661	0.508[a]
SBP (mmHg)	129.00 (118.00, 144.00)	130.00 (119.00, 142.00)	-0.661	0.508[a]
DBP (mmHg)	79.22 ± 11.99	79.91 ± 11.30	-0.615	0.539[b]
Smoking (n, %)			3.932	0.047[c]
Yes	129 (35.1)	70 (44.3)		
No	238 (64.9)	88 (55.7)		
Drinking (n, %)			0.560	0.454[c]
Yes	111 (30.2)	53 (33.5)		
No	256 (69.8)	105 (66.5)		
WBC (10^9/L)	6.53 (5.38, 7.78)	6.60 (5.26, 7.99)	-0.318	0.750[a]
PLR	129.32 (99.27, 157.95)	118.67 (94.02, 159.35)	-1.167	0.243[a]
NLR	2.39 (1.75, 3.29)	2.31 (1.74, 3.15)	-0.716	0.474[a]
SCr (μmol/L)	67.00 (55.00, 75.00)	67.00 (55.00, 78.25)	-0.129	0.898[a]
UACR (mg/g)	19.85 (11.30, 49.68)	17.00 (10.60, 47.23)	-0.400	0.689[a]
eGFR (mL/min/1.73m^2)	105.20 (91.65, 117.60)	105.56 (93.22, 117.92)	-0.500	0.617[a]
TC (mmol/L)	4.39 (3.67, 5.21)	4.51 (3.83, 5.31)	-1.241	0.214[a]
TG (mmol/L)	1.57 (1.07, 2.69)	1.74 (1.11, 3.10)	-0.779	0.436[a]
HDL (mmol/L)	1.01 (0.83, 1.24)	1.02 (0.86, 1.24)	-0.440	0.660[a]
LDL (mmol/L)	2.62 (1.20, 3.21)	2.72 (2.07, 3.34)	-1.034	0.301[a]
HbA1c (%)	9.65 (7.58, 11.53)	9.60 (8.08, 11.53)	-0.568	0.570[a]
Echocardiographic parameters				
LAD (mm)	31.00 (29.00, 33.00)	31.00 (29.00, 32.00)	-0.644	0.519[a]
LVEDD (mm)	45.00 (42.00, 48.00)	45.00 (41.00, 48.00)	-1.618	0.106[a]
IVSd (mm)	10.00 (10.00, 11.00)	10.00 (10.00, 11.00)	-0.179	0.858[a]
LVPWd (mm)	10.00 (10.00, 11.00)	10.00 (10.00, 11.00)	-0.520	0.603[a]
RWT	0.43 (0.40, 0.45)	0.44 (0.41, 0.46)	-1.840	0.66[a]
LVMI (g/m²)	91.59 (81.18, 103.30)	86.92 (78.99, 102.83)	-1.756	0.079[a]
LVEF (%)	64.00 (61.00, 67.00)	63.50 (61.00, 66.00)	-0.464	0.643[a]

BMI, body mass index; DBP, diastolic blood pressure; eGFR, Estimated glomerular filtration rate; HbA1c, glycated hemoglobin; HDL-C, high-density lipoprotein cholesterol; IVSd, Interventricular septal thickness at end-diastole; LAD, Left atrial diameter; LDL-C, low-density lipoprotein cholesterol; LVEDD, Left ventricular end-diastolic diameter; LVEF, Left ventricular ejection fraction; LVMI, Left ventricular mass index; LVPWd, Left ventricular posterior wall thickness at end-diastole; NLR, neutrophil-to-lymphocyte ratio; PLR, platelet-to-lymphocyte ratio; RWT, relative wall thickness; SBP, systolic blood pressure; Scr, serum creatinine; T2DM Duration, duration of type 2 diabetes mellitus; TC, total cholesterol; TG, triglycerides; UACR, urinary albumin-to-creatinine ratio; WBC, white blood cells. [a]Results shown as median and interquartile range and analyzed using Mann-Whitney U-test. [b]Results shown as mean ± standard and analyzed using Student's t-test. [c]Chi-square test was used for proportions comparison.

10.3389/fendo.2025.1641114

TABLE 2 Univariate logistic regression analysis of patients in the training cohort.

Parameter	OR (95% CI)	*P*
Clinical information		
Age (years)	1.087 (1.062-1.111)	< 0.001
Gender (n, %)	0.614 (0.393-0.958)	0.032
T2DM Duration (years)	1.244 (1.188-1.304)	< 0.001
BMI (kg/m^2)	1.031 (0.973-1.093)	0.305
Heart rate (bpm)	0.991 (0.974-1.009)	0.33
SBP (mmHg)	1.035 (1.022-1.049)	< 0.001
DBP (mmHg)	0.982 (0.964-1.000)	0.046
Smoking (n, %)	0.766 (0.484-1.213)	0.255
Drinking (n, %)	1.133 (0.711-1.807)	0.599
WBC (10^9/L)	1.029 (0.921-1.151)	0.613
PLR	1.005 (1.000-1.009)	0.031
NLR	1.539 (1.290-1.837)	< 0.001
SCr (μmol/L)	1.031 (1.020-1.042)	< 0.001
UACR (mg/g)	1.019 (1.013-1.025)	< 0.001
eGFR (mL/min/1.73m^2)	0.956 (0.944-0.967)	< 0.001
TC (mmol/L)	0.880 (0.746-1.039)	0.132
TG (mmol/L)	0.956 (0.860-1.063)	0.406
HDL-C (mmol/L)	1.195 (0.604-2.366)	0.608
LDL-C (mmol/L)	0.740 (0.590-0.928)	0.009
HbA1c (%)	1.001 (0.924-1.086)	0.976
Echocardiographic parameters		
LAD (mm)	1.358 (1.248-1.477)	< 0.001
LVEDD (mm)	1.075 (1.017-1.135)	0.01
IVSd (mm)	3.144 (2.345-4.213)	< 0.001
LVPWd (mm)	3.214 (2.373-4.354)	< 0.001
RWT	1.820 (1.110-2.984)	0.018
LVMI (g/m²)	1.063 (1.047-1.081)	< 0.001
LVEF (%)	0.982 (0.931-1.037)	0.518

BMI, body mass index; DBP, diastolic blood pressure; eGFR, Estimated glomerular filtration rate; HbA1c, glycated hemoglobin; HDL-C, high-density lipoprotein cholesterol; IVSd, Interventricular septal thickness at end-diastole; LAD, Left atrial diameter; LDL-C, low-density lipoprotein cholesterol; LVEDD, Left ventricular end-diastolic diameter; LVEF, Left ventricular ejection fraction; LVMI, Left ventricular mass index; LVPWd, Left ventricular posterior wall thickness at end-diastole; NLR, neutrophil-to-lymphocyte ratio; PLR, platelet-to-lymphocyte ratio; RWT, relative wall thickness; SBP, systolic blood pressure; Scr, serum creatinine; T2DM Duration, duration of type 2 diabetes mellitus; TC, total cholesterol; TG, triglycerides; UACR, urinary albumin-to-creatinine ratio; WBC, white blood cells.

TABLE 3 Multivariate logistic regression analysis of patients in the training cohort.

Variable	β	SE	Wald	OR (95% CI)	*P*
Intercept	-27.798	3.713	56.046	–	< 0.001
Age	0.045	0.019	5.425	1.046 (1.008-1.088)	0.0198
T2DM Duration	0.226	0.039	34.006	1.254 (1.167-1.359)	< 0.001
SBP	0.032	0.011	8.889	1.033 (1.011-1.055)	0.0028
NLR	0.010	0.167	0.003	1.010 (0.728-1.400)	0.954
Scr	-0.001	0.016	0.006	0.999 (0.968-1.030)	0.937
UACR	0.014	0.003	21.192	1.014 (1.008-1.02)	< 0.001
eGFR	-0.009	0.011	0.721	0.991 (0.969-1.012)	0.396
LDL-C	-0.032	0.194	0.027	0.968 (0.662-1.417)	0.868
LAD	0.285	0.065	19.452	1.33 (1.178-1.519)	< 0.001
IVSd	0.189	0.366	0.268	1.208 (0.590-2.474)	0.605
LVPWd	0.846	0.218	15.074	2.33 (1.542-3.636)	< 0.001
LVMI	0.016	0.013	1.705	1.017 (0.992-1.042)	0.192

eGFR, Estimated glomerular filtration rate; IVSd, Interventricular septal thickness at end-diastole; LAD, Left atrial diameter; LDL-C, low-density lipoprotein cholesterol; LVPWd, Left ventricular posterior wall thickness at end-diastole; LVMI, Left ventricular mass index; NLR, neutrophil-to-lymphocyte ratio; SBP, systolic blood pressure; Scr, serum creatinine; T2DM Duration, duration of type 2 diabetes mellitus; UACR, urinary albumin-to-creatinine ratio.

factors, we developed and validated a clinically practical nomogram model. These results advance early DCM risk stratification and provide a framework for targeted clinical interventions.

The progression of DCM in patients with T2DM is synergistically driven by aging and prolonged hyperglycemic exposure. Extensive evidence identifies age as a critical determinant of cardiac dysfunction in T2DM populations (26–28), primarily through age-related cardiovascular remodeling characterized by myocardial stiffening, atherosclerotic changes, and metabolic dysregulation. These alterations establish a pathological substrate that amplifies diabetes-induced cardiac injury, particularly in elderly individuals with compromised metabolic homeostasis (26). Furthermore, diabetes duration emerges as an independent predictor of cardiovascular morbidity (29–31), reflecting cumulative hyperglycemic damage mediated by chronic oxidative stress, endothelial dysfunction, and cardiomyocyte apoptosis (29). The interplay between aging and diabetic metabolic disturbances creates a vicious cycle: Age-dependent myocardial fibrosis and diastolic impairment are exacerbated by persistent hyperglycemia, which accelerates glycation end-product accumulation and reactive oxygen species generation (14). This synergy explains why elderly patients with extended T2DM duration exhibit more severe myocardial injury and earlier onset of diastolic dysfunction (32). Our findings highlight the clinical imperative to incorporate both aging and glycemic exposure duration into DCM risk stratification frameworks, enabling targeted monitoring of high-risk subgroups.

Elevated blood pressure is a well-established risk factor for T2DM (33, 34), with diabetic populations exhibiting higher average blood pressure levels. A cross-sectional study in high-altitude Chinese populations identified hypertension and hyperglycemia as critical contributors to increased LVDD risk (35). Further supporting this, a 2018 clinical comparative study demonstrated a direct association between SBP and diastolic dysfunction severity (36). While diabetes alone rarely causes isolated myocardial impairment, its synergistic interactions with hypertension, obesity, and chronic kidney disease often amplify cardiac damage (19). In our study, elevated SBP

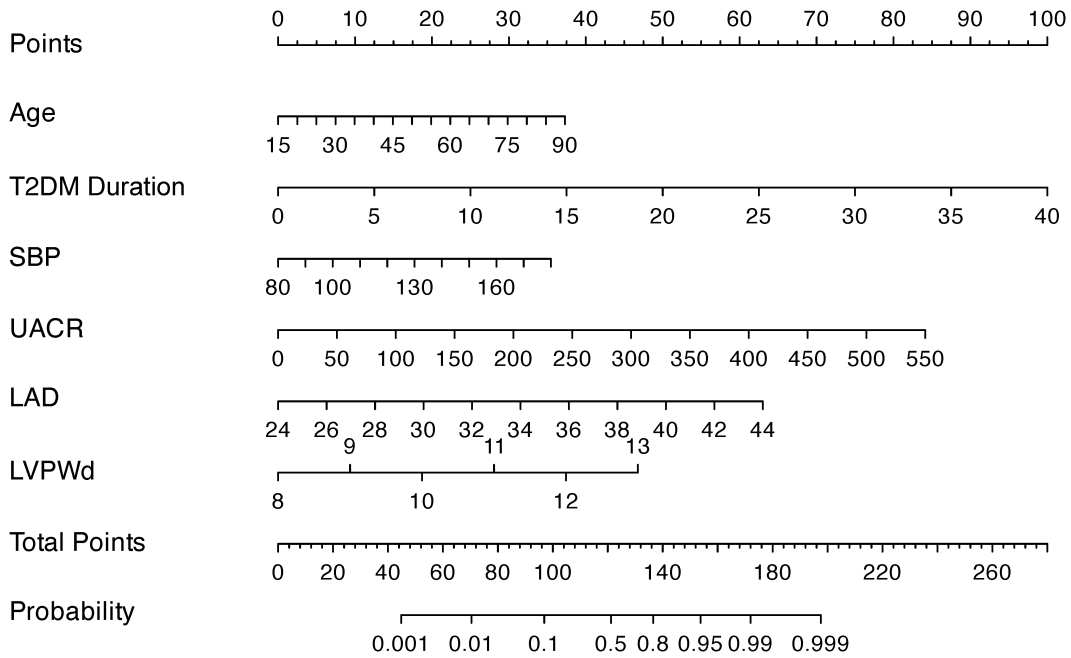

FIGURE 2
A nomogram integrating clinical indicators (age, T2DM Duration, SBP, UACR) and echocardiographic parameters (LAD, LVPWd) to predict DCM risk in T2DM patients.

emerged as a key driver of DCM progression. Mechanistically, prolonged hypertension induces myocardial hypertrophy and fibrosis, exacerbating cardiac workload and thereby aggravating LVDD in T2DM patients.

The UACR serves as a sensitive indicator of diabetic nephropathy, with renal impairment demonstrating strong cardiometabolic associations (37). Prevalent LVDD has been documented across stages of moderately increased (microalbuminuria) and severely increased albuminuria (macroalbuminuria), whereas left ventricular systolic dysfunction predominantly manifests in subgroups with advanced macroalbuminuria (38). Seminal investigations, including *The Strong Heart Study*, established associations between albuminuria,

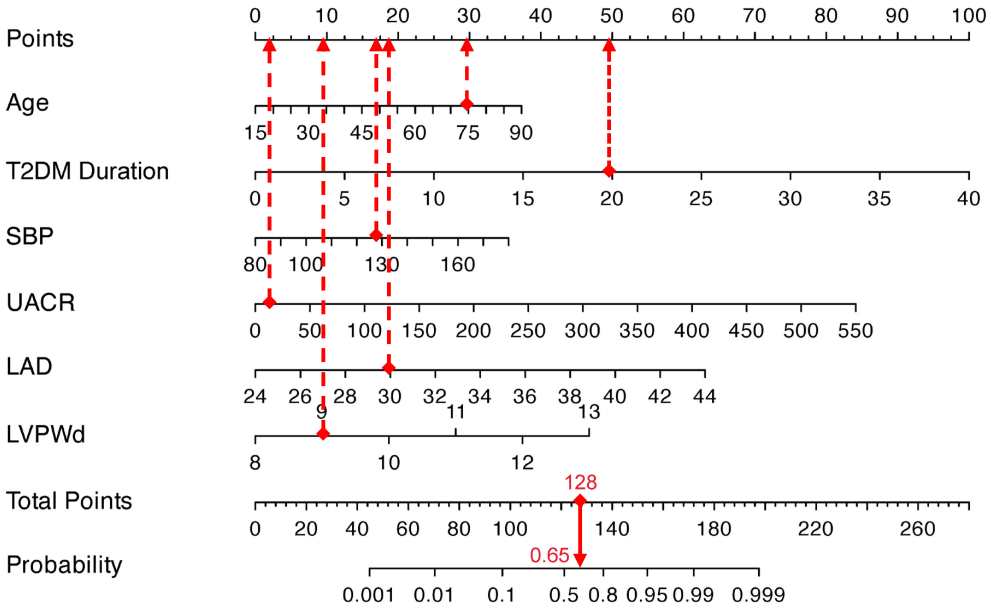

FIGURE 3
Visualization application of the nomogram prediction for the risk of DCM in patients with T2DM.

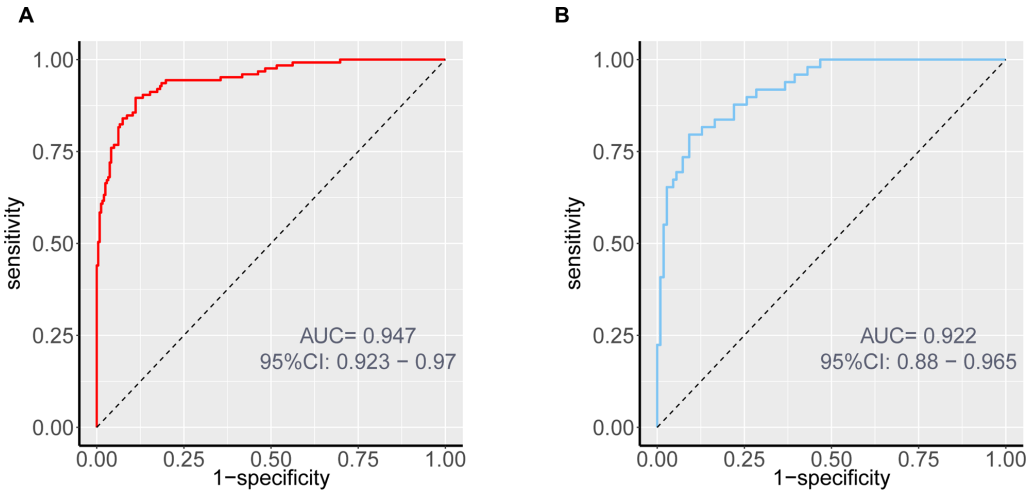

FIGURE 4
ROC curves of the nomogram prediction for the risk of DCM in patients with T2DM in the training cohort **(A)** and validation cohort **(B)**.

left ventricular mass index, and diastolic impairment. Notably, albuminuria independently correlates with multisystem damage irrespective of diabetes status, elevating risks of atherosclerotic cardiovascular events (myocardial infarction, ischemic stroke, cardiac mortality) and congestive heart failure (39). This aligns with our findings, reinforcing UACR's dual role as both an early diabetic nephropathy marker and an independent predictor of cardiovascular outcomes, underscoring the cardiorenal continuum in diabetes pathophysiology.

In this study, LAD and LVPWd were identified as predictive indices, highlighting the critical role of cardiac structural remodeling in early DCM diagnosis. Left atrial enlargement and increased LVPWd in diabetic populations reflect adaptive cardiac responses to chronic hemodynamic stress, particularly in hypertensive conditions, ultimately progressing to myocardial dysfunction and heart failure (10, 40). A pooled analysis of three U.S. cohort studies (n = 10,208 participants without baseline cardiovascular disease or heart failure) demonstrated significantly higher prevalence of echocardiographic structural abnormalities—including left atrial dilation and left ventricular hypertrophy—among patients with T2DM. These abnormalities independently predicted 5-year incident heart failure risk (41, 42). Machine learning-based models for early DCM risk stratification similarly prioritize left ventricular mass and chamber size as key predictors (43). Our findings reinforce the necessity of proactive echocardiographic screening in T2DM patients with suboptimal glycemic control to detect structural cardiac alterations, enabling timely intervention to mitigate adverse outcomes.

This study revealed a noteworthy phenomenon: HbA1c—traditionally recognized as a key metabolic control indicator for diabetic complications—failed to demonstrate independent predictive value in our model. We postulate three underlying mechanisms:

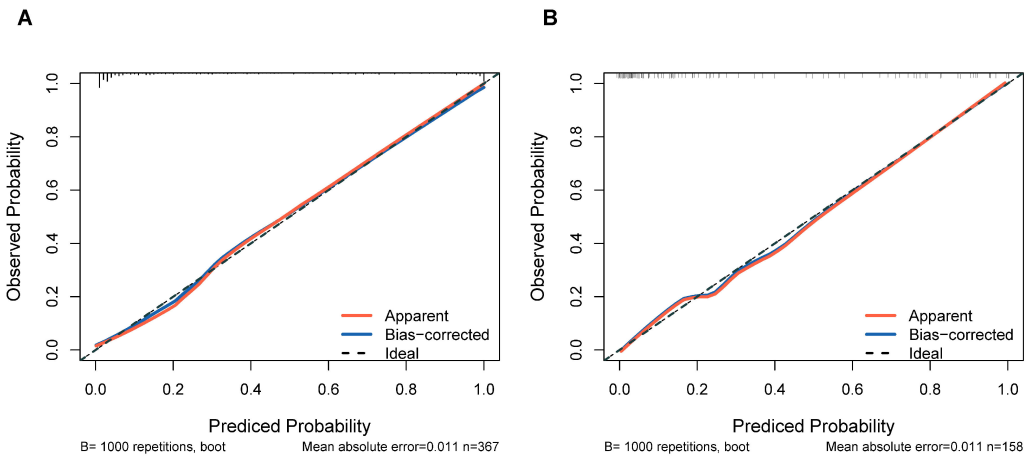

FIGURE 5
Calibration plots of the nomogram prediction for the risk of DCM in patients with T2DM in the training cohort **(A)** and validation cohort **(B)**.

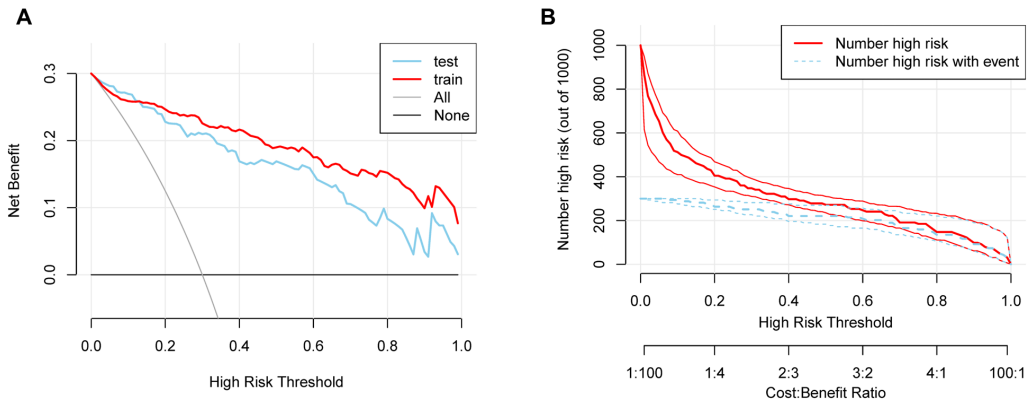

FIGURE 6
(A) DCA demonstrating the clinical utility of the nomogram across various risk thresholds. **(B)** CIC showing the relationship between predicted high-risk cases and actual event occurrences.

(1) Metabolic memory effect (44): Persistent myocardial alterations (e.g., fibrosis and advanced glycation end-product deposition) induced by chronic hyperglycemia endure beyond glycemic correction. Consequently, baseline HbA1c inadequately reflects cumulative damage, explaining the superior predictive capacity of T2DM Duration. (2) Hierarchical masking in modeling: As disease progresses to structural remodeling stages (e.g., left ventricular hypertrophy/left atrial enlargement), imaging biomarkers may supersede upstream metabolic indicators. Concurrently, the synergistic modulation of glycemic exposure by age and diabetes duration further diminishes HbA1c's contribution. (3) Temporal limitations of measurement: HbA1c captures only short-term (2-3-month) glycemic averages, failing to account for long-term cumulative myocardial injury from glycemic variability—a critical factor in chronic progressive disorders like DCM (45).

Clinical significance and practical applications

Given the elevated risk of HF in patients with T2DM, early detection and intervention of DCM are critical for HF prevention. Predictive models enable clinicians to stratify high-risk individuals during the asymptomatic phase, facilitating timely implementation of tailored interventions—such as lifestyle modifications, metabolic parameter optimization, and evidence-based pharmacotherapy—to reduce cardiovascular morbidity (46). Current preventive strategies for T2DM-associated cardiovascular disease include: 1. Lifestyle intensification: Structured dietary control, weight management, and physical activity regimens (47). The European Society of Preventive Cardiology guidelines advocate for individualized exercise regimens tailored to patient-specific characteristics to optimize cardiovascular adaptation and metabolic homeostasis (48); 2. Metabolic control: Tight regulation of glycemic, blood pressure, and lipid profiles; 3. Cardioprotective pharmacotherapy: Prioritization of glucose-lowering agents with proven cardiovascular benefits, notably sodium-glucose cotransporter 2 inhibitors (SGLT2i). Critically, the therapeutic value of SGLT2i extends beyond glycemic control and cardiovascular protection. Their efficacy aligns profoundly with the concept of the cardiorenal metabolic syndrome (CRMS), which recognizes the intricate interplay and share pathophysiological mechanisms linking T2DM, cardiovascular diseases, and chronic kidney disease (49). A multinational cohort study (N = 309,056) demonstrated that SGLT2i initiation significantly reduced HF hospitalization risk and all-cause mortality compared to alternative therapies (50). Importantly, landmark trials have consistently shown that SGLT2i also provide significant renoprotection, reducing the risk of worsening kidney function, end-stage kidney disease, and death from renal causes (51). This dual cardiorenal benefit uniquely positions SGLT2i as foundational therapy for patients with T2DM and DCM, who frequently exhibit features of CRMS.

The early initiation of SGLT2i in high-risk populations, particularly those identified with early-stage DCM within the spectrum of CRMS, remains a critical priority. Despite robust evidence supporting their cardioprotective efficacy, widespread clinical adoption of SGLT2i is hindered by cost-related barriers and limited accessibility in resource-constrained settings (52). To reconcile this disparity, risk stratification strategies leveraging predictive models offer a pragmatic solution: targeted prioritization of SGLT2i therapy for individuals identified with early-stage DCM and/or concomitant renal risk markers through validated risk algorithms. Furthermore, integrating predictive models into personalized medicine frameworks holds transformative potential. By synthesizing patient-specific clinical indicators (including those reflecting cardiorenal metabolic risk, such as albuminuria, eGFR trajectory, along with cardiac structural/functional parameters), these tools enable clinicians to formulate precision-guided management plans tailored to individual risk trajectories. This approach not only enhances therapeutic efficacy by addressing the multifaceted nature of CRMS but also optimizes healthcare resource utilization, ultimately improving patient-reported outcomes and quality of life.

Study limitations and future directions

Despite the insights provided, this study has several limitations. First, the single-center retrospective design resulted in a relatively limited sample size, potentially restricting the generalizability of the findings. Second, retrospective data collection introduces challenges in fully accounting for unmeasured confounders. To address these limitations, future research should validate the model's validity and reliability through large-scale, multicenter prospective studies. Additionally, investigations into novel biomarkers and advanced imaging parameters are warranted to enhance predictive precision and clinical utility.

Conclusion

We developed a validated nomogram integrating clinical indicators (age, T2DM Duration, SBP, UACR) and echocardiographic parameters (LAD, LVPWd) to predict DCM risk in T2DM patients. This tool enables early risk stratification, supporting timely interventions to reduce heart failure progression. Further multicenter validation and integration of novel biomarkers are warranted to enhance clinical utility and address global diabetes-related cardiovascular burdens.

Data availability statement

The raw data supporting the conclusions of this article will be made available by the authors, without undue reservation.

Ethics statement

The studies involving humans were approved by The First Affiliated Hospital of Chongqing Medical University. The studies were conducted in accordance with the local legislation and institutional requirements. Written informed consent for participation was not required from the participants or the participants' legal guardians/next of kin in accordance with the national legislation and institutional requirements. Written informed consent was obtained from the individual(s) for the publication of any potentially identifiable images or data included in this article.

Author contributions

ZL: Writing – review & editing, Methodology, Writing – original draft, Data curation, Validation. DP: Writing – review & editing, Methodology. TX: Data curation, Writing – original draft. WJ: Writing – review & editing, Software, Data curation. FQ: Writing – review & editing, Funding acquisition, Resources. JY: Funding acquisition, Resources, Writing – review & editing.

Funding

The author(s) declare financial support was received for the research and/or publication of this article. This work was supported by the Medical Scientific Research Project of Chongqing, China (No.2024GDRC012), the Natural Science Foundation of Chongqing, China (No.CSTB2023NSCQ-MSX0392), Chongqing Municipal Health Commission Project, China (No.2025cgjstg001).

Acknowledgments

We would like to express our gratitude to all participants for their involvement, as their contributions were essential to the successful completion of our research.

Conflict of interest

The authors declare that the research was conducted in the absence of any commercial or financial relationships that could be construed as a potential conflict of interest.

Generative AI statement

The author(s) declare that no Generative AI was used in the creation of this manuscript.

Publisher's note

References

1. Shah AD, Langenberg C, Rapsomaniki E, Denaxas S, Pujades-Rodriguez M, Gale CP, et al. Type 2 diabetes and incidence of cardiovascular diseases: A cohort study in 1·9 million people. *Lancet Diabetes Endocrinol.* (2015) 3:105–13. doi: 10.1016/s2213-8587(14)70219-0

2. Jia G, Hill MA, Sowers JR. Diabetic cardiomyopathy: an update of mechanisms contributing to this clinical entity. *Circ Res.* (2018) 122:624–38. doi: 10.1161/circresaha.117.311586

3. Nakamura K, Miyoshi T, Yoshida M, Akagi S, Saito Y, Ejiri K, et al. Pathophysiology and treatment of diabetic cardiomyopathy and heart failure in patients with diabetes mellitus. *Int J Mol Sci.* (2022) 23(7):3587. doi: 10.3390/ijms23073587

4. Kannel WB, McGee DL. Diabetes and cardiovascular disease. *Framingham Study JAMA.* (1979) 241:2035–8. doi: 10.1001/jama.241.19.2035

5. Dandamudi S, Slusser J, Mahoney DW, Redfield MM, Rodeheffer RJ, Chen HH. The prevalence of diabetic cardiomyopathy: A population-based study in olmsted county, minnesota. *J Card Fail*. (2014) 20:304–9. doi: 10.1016/j.cardfail.2014.02.007

6. Ritchie RH, Abel ED. Basic mechanisms of diabetic heart disease. *Circ Res*. (2020) 126:1501–25. doi: 10.1161/circresaha.120.315913

7. Wang M, Li Y, Li S, Lv J. Endothelial dysfunction and diabetic cardiomyopathy. *Front Endocrinol (Lausanne)*. (2022) 13:851941. doi: 10.3389/fendo.2022.851941

8. Jia G, DeMarco VG, Sowers JR. Insulin resistance and hyperinsulinaemia in diabetic cardiomyopathy. *Nat Rev Endocrinol*. (2016) 12:144–53. doi: 10.1038/nrendo.2015.216

9. Tan Y, Zhang Z, Zheng C, Wintergerst KA, Keller BB, Cai L. Mechanisms of diabetic cardiomyopathy and potential therapeutic strategies: preclinical and clinical evidence. *Nat Rev Cardiol*. (2020) 17:585–607. doi: 10.1038/s41569-020-0339-2

10. Boudina S, Abel ED. Diabetic cardiomyopathy revisited. *Circulation*. (2007) 115:3213–23. doi: 10.1161/circulationaha.106.679597

11. Dillmann WH. Diabetic cardiomyopathy. *Circ Res*. (2019) 124:1160–2. doi: 10.1161/circresaha.118.314665

12. From AM, Scott CG, Chen HH. The development of heart failure in patients with diabetes mellitus and pre-clinical diastolic dysfunction a population-based study. *J Am Coll Cardiol*. (2010) 55:300–5. doi: 10.1016/j.jacc.2009.12.003

13. Kane GC, Karon BL, Mahoney DW, Redfield MM, Roger VL, Burnett JCJr., et al. Progression of left ventricular diastolic dysfunction and risk of heart failure. *Jama*. (2011) 306:856–63. doi: 10.1001/jama.2011.1201

14. Seferović PM, Paulus WJ. Clinical diabetic cardiomyopathy: A two-faced disease with restrictive and dilated phenotypes. *Eur Heart J*. (2015) 36:1718–27. doi: 10.1093/eurheartj/ehv134

15. Adel FW, Chen HH. The role of multimodality imaging in diabetic cardiomyopathy: A brief review. *Front Endocrinol (Lausanne)*. (2024) 15:1405031. doi: 10.3389/fendo.2024.1405031

16. Chen Y, Yu M, Lan Y, Feng F, Jiang C. Development of a nomogram for predicting the risk of left ventricular diastolic function in subjects with type-2 diabetes mellitus. *Int J Cardiovasc Imaging*. (2022) 38:15–23. doi: 10.1007/s10554-021-02338-5

17. Hao M, Huang X, Liu X, Fang X, Li H, Lv L, et al. Novel model predicts diastolic cardiac dysfunction in type 2 diabetes. *Ann Med*. (2023) 55:766–77. doi: 10.1080/07853890.2023.2180154

18. ElSayed NA, Aleppo G, Aroda VR, Bannuru RR, Brown FM, Bruemmer D, et al. 2. Classification and diagnosis of diabetes: standards of care in diabetes-2023. *Diabetes Care*. (2023) 46(Suppl 1):S19–s40. doi: 10.2337/dc23-S002

19. Seferović PM, Paulus WJ, Rosano G, Polovina M, Petrie MC, Jhund PS, et al. Diabetic myocardial disorder. A clinical consensus statement of the heart failure association of the esc and the esc working group on myocardial & Pericardial diseases. *Eur J Heart Fail*. (2024) 26:1893–903. doi: 10.1002/ejhf.3347

20. Nagueh SF, Smiseth OA, Appleton CP, Byrd BF 3rd, Dokainish H, Edvardsen T, et al. Recommendations for the evaluation of left ventricular diastolic function by echocardiography: an update from the american society of echocardiography and the european association of cardiovascular imaging. *J Am Soc Echocardiogr*. (2016) 29:277–314. doi: 10.1016/j.echo.2016.01.011

21. Stevens LA, Claybon MA, Schmid CH, Chen J, Horio M, Imai E, et al. Evaluation of the chronic kidney disease epidemiology collaboration equation for estimating the glomerular filtration rate in multiple ethnicities. *Kidney Int*. (2011) 79:555–62. doi: 10.1038/ki.2010.462

22. Devereux RB, Alonso DR, Lutas EM, Gottlieb GJ, Campo E, Sachs I, et al. Echocardiographic assessment of left ventricular hypertrophy: comparison to necropsy findings. *Am J Cardiol*. (1986) 57:450–8. doi: 10.1016/0002-9149(86)90771-x

23. Peduzzi P, Concato J, Kemper E, Holford TR, Feinstein AR. A simulation study of the number of events per variable in logistic regression analysis. *J Clin Epidemiol*. (1996) 49:1373–9. doi: 10.1016/s0895-4356(96)00236-3

24. Marwick TH, Ritchie R, Shaw JE, Kaye D. Implications of underlying mechanisms for the recognition and management of diabetic cardiomyopathy. *J Am Coll Cardiol*. (2018) 71:339–51. doi: 10.1016/j.jacc.2017.11.019

25. Pandey A, Vaduganathan M, Patel KV, Ayers C, Ballantyne CM, Kosiborod MN, et al. Biomarker-Based Risk Prediction of Incident Heart failure in Pre-Diabetes And diabetes. *JACC Heart Fail*. (2021) 9:215–23. doi: 10.1016/j.jchf.2020.10.013

26. Lakatta EG, Levy D. Arterial and cardiac aging: major shareholders in cardiovascular disease enterprises: part ii: the aging heart in health: links to heart disease. *Circulation*. (2003) 107:346–54. doi: 10.1161/01.cir.0000048893.62841.f7

27. Segar MW, Vaduganathan M, Patel KV, McGuire DK, Butler J, Fonarow GC, et al. Machine learning to predict the risk of incident heart failure hospitalization among patients with diabetes: the watch-dm risk score. *Diabetes Care*. (2019) 42:2298–306. doi: 10.2337/dc19-0587

28. Yang X, Ma RC, So WY, Kong AP, Ko GT, Ho CS, et al. Development and validation of a risk score for hospitalization for heart failure in patients with type 2 diabetes mellitus. *Cardiovasc Diabetol*. (2008) 7:9. doi: 10.1186/1475-2840-7-9

29. de Jong M, Woodward M, Peters SAE. Duration of diabetes and the risk of major cardiovascular events in women and men: A prospective cohort study of uk biobank participants. *Diabetes Res Clin Pract*. (2022) 188:109899. doi: 10.1016/j.diabres.2022.109899

30. Fox CS, Sullivan L, D'Agostino RB Sr., Wilson PW. The significant effect of diabetes duration on coronary heart disease mortality: the framingham heart study. *Diabetes Care*. (2004) 27:704–8. doi: 10.2337/diacare.27.3.704

31. Zoungas S, Woodward M, Li Q, Cooper ME, Hamet P, Harrap S, et al. Impact of age, age at diagnosis and duration of diabetes on the risk of macrovascular and microvascular complications and death in type 2 diabetes. *Diabetologia*. (2014) 57:2465–74. doi: 10.1007/s00125-014-3369-7

32. Jia G, Whaley-Connell A, Sowers JR. Diabetic cardiomyopathy: A hyperglycaemia- and insulin-resistance-induced heart disease. *Diabetologia*. (2018) 61:21–8. doi: 10.1007/s00125-017-4390-4

33. Petrie JR, Guzik TJ, Touyz RM. Diabetes, hypertension, and cardiovascular disease: clinical insights and vascular mechanisms. *Can J Cardiol*. (2018) 34(5):575–84. doi: 10.1016/j.cjca.2017.12.005

34. Pechère-Bertschi A, Greminger P, Hess L, Philippe J, Ferrari P. Swiss hypertension and risk factor program (Sharp): cardiovascular risk factors management in patients with type 2 diabetes in Switzerland. *Blood Press*. (2005) 14:337–44. doi: 10.1080/08037050500340018

35. Zheng C, Chen Z, Zhang L, Wang X, Dong Y, Wang J, et al. Metabolic risk factors and left ventricular diastolic function in middle-aged chinese living in the tibetan plateau. *J Am Heart Assoc*. (2019) 8:e010454. doi: 10.1161/jaha.118.010454

36. Jørgensen PG, Jensen MT, Biering-Sørensen T, Mogelvang R, Fritz-Hansen T, Vilsbøll T, et al. Burden of uncontrolled metabolic risk factors and left ventricular structure and function in patients with type 2 diabetes mellitus. *J Am Heart Assoc*. (2018) 7:e008856. doi: 10.1161/jaha.118.008856

37. Gross JL, de Azevedo MJ, Silveiro SP, Canani LH, Caramori ML, Zelmanovitz T. Diabetic nephropathy: diagnosis, prevention, and treatment. *Diabetes Care*. (2005) 28:164–76. doi: 10.2337/diacare.28.1.164

38. Jørgensen PG, Biering-Sørensen T, Mogelvang R, Fritz-Hansen T, Vilsbøll T, Rossing P, et al. Presence of micro- and macroalbuminuria and the association with cardiac mechanics in patients with type 2 diabetes. *Eur Heart J Cardiovasc Imaging*. (2018) 19:1034–41. doi: 10.1093/ehjci/jex231

39. Kramer H, Jacobs DR Jr., Bild D, Post W, Saad MF, Detrano R, et al. Urine albumin excretion and subclinical cardiovascular disease. The multi-ethnic study of atherosclerosis. *Hypertension*. (2005) 46:38–43. doi: 10.1161/01.Hyp.0000171189.48911.18

40. Marwick TH, Gillebert TC, Aurigemma G, Chirinos J, Derumeaux G, Galderisi M, et al. Recommendations on the use of echocardiography in adult hypertension: A report from the european association of cardiovascular imaging (Eacvi) and the american society of echocardiography (Ase)†. *Eur Heart J Cardiovasc Imaging*. (2015) 16:577–605. doi: 10.1093/ehjci/jev076

41. Segar MW, Khan MS, Patel KV, Butler J, Tang WHW, Vaduganathan M, et al. Prevalence and prognostic implications of diabetes with cardiomyopathy in community-dwelling adults. *J Am Coll Cardiol*. (2021) 78:1587–98. doi: 10.1016/j.jacc.2021.08.020

42. Wang Y, Yang H, Huynh Q, Nolan M, Negishi K, Marwick TH. Diagnosis of nonischemic stage B heart failure in type 2 diabetes mellitus: optimal parameters for prediction of heart failure. *JACC Cardiovasc Imaging*. (2018) 11:1390–400. doi: 10.1016/j.jcmg.2018.03.015

43. Segar MW, Usman MS, Patel KV, Khan MS, Butler J, Manjunath L, et al. Development and validation of a machine learning-based approach to identify high-risk diabetic cardiomyopathy phenotype. *Eur J Heart Fail*. (2024) 26:2183–92. doi: 10.1002/ejhf.3443

44. Ding M, Shi R, Du Y, Chang P, Gao T, De D, et al. O-glcnacylation-mediated endothelial metabolic memory contributes to cardiac damage via small extracellular vesicles. *Cell Metab*. (2025) 37:1344–63.e6. doi: 10.1016/j.cmet.2025.03.006

45. Fang Q, Shi J, Zhang J, Peng Y, Liu C, Wei X, et al. Visit-to-visit hba1c variability is associated with aortic stiffness progression in participants with type 2 diabetes. *Cardiovasc Diabetol*. (2023) 22:167. doi: 10.1186/s12933-023-01884-7

46. Galis P, Bartosova L, Farkasova V, Bartekova M, Ferenczyova K, Rajtik T. Update on clinical and experimental management of diabetic cardiomyopathy: addressing current and future therapy. *Front Endocrinol (Lausanne)*. (2024) 15:1451100. doi: 10.3389/fendo.2024.1451100

47. Chen L, Pei JH, Kuang J, Chen HM, Chen Z, Li ZW, et al. Effect of lifestyle intervention in patients with type 2 diabetes: A meta-analysis. *Metabolism*. (2015) 64:338–47. doi: 10.1016/j.metabol.2014.10.018

48. Kemps H, Kränkel N, Dörr M, Moholdt T, Wilhelm M, Paneni F, et al. Exercise training for patients with type 2 diabetes and cardiovascular disease: what to pursue and how to do it. A position paper of the european association of preventive cardiology (Eapc). *Eur J Prev Cardiol*. (2019) 26:709–27. doi: 10.1177/2047487318820420

49. Giugliano D, Longo M, Scappaticcio L, Caruso P, Esposito K. Sodium-glucose transporter-2 inhibitors for prevention and treatment of cardiorenal complications of type 2 diabetes. *Cardiovasc Diabetol*. (2021) 20:17. doi: 10.1186/s12933-021-01213-w

50. Kosiborod M, Cavender MA, Fu AZ, Wilding JP, Khunti K, Holl RW, et al. Lower risk of heart failure and death in patients initiated on sodium-glucose cotransporter-2 inhibitors versus other glucose-lowering drugs: the cvd-real study (Comparative effectiveness of cardiovascular outcomes in new users of sodium-glucose cotransporter-2 inhibitors). *Circulation*. (2017) 136:249–59. doi: 10.1161/circulationaha.117.029190

51. Dharia A, Khan A, Sridhar VS, Cherney DZI. Sglt2 inhibitors: the sweet success for kidneys. *Annu Rev Med*. (2023) 74:369–84. doi: 10.1146/annurev-med-042921-102135

52. Zelniker TA, Wiviott SD, Raz I, Im K, Goodrich EL, Bonaca MP, et al. Sglt2 inhibitors for primary and secondary prevention of cardiovascular and renal outcomes in type 2 diabetes: A systematic review and meta-analysis of cardiovascular outcome trials. *Lancet*. (2019) 393:31–9. doi: 10.1016/s0140-6736(18)32590-x

frontiers | Frontiers in Endocrinology

TYPE Original Research
PUBLISHED 08 August 2025
DOI 10.3389/fendo.2025.1636890

OPEN ACCESS

EDITED BY
Ramoji Kosuru,
Versiti Blood Research Institute, United States

REVIEWED BY
Yuansong Zhuang,
Chinese Academy of Medical Sciences and Peking Union Medical College, China
Radha Vaddavalli,
The Ohio State University, United States
Moses Banyeh,
University for Development Studies, Ghana

*CORRESPONDENCE
Yuzhan Lin
1016099047@qq.com
Cheng Fu
fucheng9404@163.com

†These authors have contributed equally to this work

RECEIVED 28 May 2025
ACCEPTED 22 July 2025
PUBLISHED 08 August 2025

CITATION
Sun R, Cai J, Yan S, Qian J, Fu C and Lin Y (2025) Sex-specific associations between the triglyceride-glucose index and new-onset hypertension in a hospital employee cohort: evidence from longitudinal annual health examinations. *Front. Endocrinol.* 16:1636890. doi: 10.3389/fendo.2025.1636890

Sex-specific associations between the triglyceride-glucose index and new-onset hypertension in a hospital employee cohort: evidence from longitudinal annual health examinations

Ruixue Sun[1†], Jianze Cai[2†], Shaorong Yan[1], Jue Qian[3], Cheng Fu[4*] and Yuzhan Lin[1*]

[1]Department of Clinical Laboratory, The Third Affiliated Hospital of Wenzhou Medical University, Ruian, Zhejiang, China, [2]Hospital Infection Management Department (Public Health Department), The Third Affiliated Hospital of Wenzhou Medical University, Ruian, Zhejiang,, China, [3]Information Department, Ruian Traditional Chinese Medicine Hospital, Ruian, Zhejiang, China, [4]Department of Clinical Laboratory, Ruian Traditional Chinese Medicine Hospital, Ruian, Zhejiang, China

Background: The triglyceride-glucose (TyG) index is a surrogate marker of insulin resistance and has been associated with incident hypertension. However, evidence regarding sex-specific differences in this association remains limited. This study aimed to investigate whether sex modifies the association between the TyG index and incident hypertension in the general population.

Methods: We conducted a retrospective cohort study involving 3,465 employees who underwent annual health check-ups in 2021 at the Third Affiliated Hospital of Wenzhou Medical University, with follow-up until December 2024. Participants with hypertension at baseline were excluded. The TyG index was calculated as ln [fasting triglycerides (mg/dL) × fasting glucose (mg/dL)/2]. Cox proportional hazards models and restricted cubic spline (RCS) analyses were used to evaluate the association between TyG index and incident hypertension across sex-specific subgroups. Sensitivity analyses tested robustness.

Results: The incidence of hypertension increased across TyG quartiles in both sexes ($p < 0.01$). In women, the highest TyG quartile was associated with a significantly higher hypertension risk (HR = 1.82, 95% CI: 1.06–3.13). In men, the association was attenuated after adjustment. The results of the RCS analysis revealed that when TyG levels were high, the risk of hypertension was greater in men than in women. This conclusion was partially validated by the findings from the sensitivity analyses.

Conclusions: In this retrospective cohort study based on annual health check-up data from hospital employees, we found that the TyG index may be positively associated with the risk of new-onset hypertension, with differences observed between sexes. Further research is needed to validate these findings and address potential confounding and concerns about generalizability.

KEYWORDS

TyG index, new onset hypertension, sex differences, insulin resistance, cohort study

Introduction

Hypertension is one of the most widespread chronic conditions globally and remains a leading contributor to cardiovascular morbidity and mortality (1). According to the World Health Organization, approximately 1.28 billion adults aged 30 to 79 had hypertension in 2019, with fewer than one in five achieving adequate blood pressure control (2). In China, the prevalence of hypertension among community-dwelling adults aged 35 to 75 has reached 44.7% (age- and sex-standardized rate: 37.2%), affecting nearly half of the adult population, with a rising trend (3). More concerningly, recent epidemiological studies have reported an increasing trend in early-onset hypertension, with rising detection rates among young adults and the working population (4, 5). The rising incidence of hypertension among younger individuals highlights the importance of early detection and intervention during the prehypertensive or normotensive stages to prevent irreversible vascular damage and reduce long-term cardiovascular risk. Therefore, research on new-onset hypertension, particularly the early identification of high-risk individuals, is urgently needed.

Insulin resistance (IR) is considered both a pathogenic factor and an early predictor of hypertension (6). However, the clinical application of gold-standard methods, such as the hyperinsulinemic-euglycemic clamp test, is limited due to their complexity and invasiveness (7). The triglyceride-glucose (TyG) index, derived from fasting triglyceride and fasting glucose levels, has emerged as a simple and reliable surrogate marker of IR (8). Previous studies have shown that the TyG index is associated with elevated blood pressure and the development of hypertension. Individuals with higher TyG levels have a 1.51-fold increased risk of developing hypertension compared to those with lower levels (2). Additionally, longitudinal increases in TyG levels are also linked to elevated blood pressure and incident hypertension (9).

However, evidence regarding sex-specific differences in the association between the TyG index and new-onset hypertension remains limited, and findings across studies are inconsistent, with some reporting no sex differences (10–13) and one study suggesting the presence of differences (14). Moreover, these studies either conducted subgroup analyses using generalized linear models (10–13), or observed such differences only in populations aged over 40 years (14). Therefore, this study aims to examine sex-specific differences in the association between the TyG index and new-onset hypertension using longitudinal data from annual health check-ups of employees at the Health Examination Center of the Third Affiliated Hospital of Wenzhou Medical University.

Methods

Study population and ethics

Baseline was defined as the period from January 1 to December 31, 2021, during which all employees of the Third Affiliated Hospital of Wenzhou Medical University (Ruian People's Hospital) underwent annual health examinations. All participants completed baseline questionnaires, physical examinations, and blood tests. A total of 3,465 individuals participated in the annual health check-ups in 2021. Participants were followed longitudinally from baseline in 2021 through December 31, 2024.

The exclusion criteria were as follows (1): participants without blood test data at baseline (2); those with pre-existing hypertension at baseline; and (3) those with unclear hypertension status during follow-up.

This study was approved by the Ethics Committee of the Third Affiliated Hospital of Wenzhou Medical University. Because the study was retrospective and the data were anonymized, the ethics committee waived written informed consent (Ethics approval number, YJ2025062).

Definition of hypertension and new-onset hypertension

Hypertension was defined as meeting at least one of the following criteria (1): systolic blood pressure (SBP) ≥140 mmHg or diastolic blood pressure (DBP) ≥90 mmHg (2); use of antihypertensive medication; or (3) self-reported physician diagnosis of hypertension (15).

New-onset hypertension was defined as the development of hypertension during follow-up among participants who were normotensive at baseline. The occurrence of hypertension during follow-up was determined based on blood pressure measurements,

medication records, and self-reported diagnoses. At each follow-up visit, the diagnosis of hypertension was based on the same three criteria described above. The date of blood pressure measurement, medication initiation, or self-report was recorded and used to calculate follow-up time. For participants who did not develop hypertension during follow-up, the follow-up duration was calculated as the time between baseline and the last available follow-up visit (9).

Calculation of TyG index

The TyG index was calculated using the formula: TyG index = ln [fasting triglycerides (mg/dL) × fasting glucose (mg/dL)/2]

Collection and definition of covariates

Baseline data were collected through comprehensive health examinations and included the following components: Demographic information included age, sex, marital status, family history of hypertension or diabetes, and department affiliation. Physical examination data included height, weight, body mass index (BMI), waist circumference, systolic blood pressure (SBP), and diastolic blood pressure (DBP). Laboratory results included complete blood count and biochemical tests, such as fasting plasma glucose, triglycerides (TG), total cholesterol (TC), high-density lipoprotein cholesterol (HDL-C), and low-density lipoprotein cholesterol (LDL-C).

Blood pressure was measured using an automated electronic sphygmomanometer after participants had rested in a seated position for at least 5 minutes. Personal and family histories of hypertension and diabetes were obtained via standardized questionnaires. Medication history was obtained from the hospital's Health Information System (HIS); participants with records of antihypertensive drug use were considered to have received antihypertensive treatment. Marital status was self-reported and categorized as married or unmarried. Departments were classified according to their functional nature into clinical, medical technology, administrative, pharmacy, and retired groups. BMI was calculated as weight in kilograms divided by height in meters squared (kg/m^2). Biochemical measurements were performed using fasting venous blood samples collected in yellow-top vacuum tubes after an overnight fast of at least 8 hours. Whole blood samples were centrifuged within 2 hours at 4°C using a refrigerated centrifuge at 1000–1200 ×g for 10–15 minutes to separate the serum (16).

Statistical analysis

All analyses were conducted using R software (version 4.2.2; http://www.R-project.org, The R Foundation) and EmpowerStats (version 4.2; http://www.empowerstats.com, X&Y Solutions, Inc.).

Continuous variables were expressed as mean ± standard deviation (SD) or median with interquartile range (IQR), depending on their distribution. Categorical variables were presented as frequencies and percentages. For comparisons of continuous variables across four groups, one-way analysis of variance (ANOVA) was used if the data were normally distributed; otherwise, the Kruskal–Wallis test was applied. Categorical variables were compared using the chi-square test; if the expected cell count was less than 10, Fisher's exact test was used instead. Cox proportional hazards models were used to evaluate the association between the TyG index and the risk of new-onset hypertension. Covariates were selected based on previously published literature (9, 17), and multivariable models were constructed to adjust for potential confounding factors. Regression results were presented as unadjusted, partially adjusted, and fully adjusted models (18). Restricted cubic spline (RCS) curves were used to examine potential nonlinear associations between the TyG index and the risk of new-onset hypertension in the overall population as well as in sex-specific subgroups, with log (HR) plotted on the Y-axis (19). To verify the stability of the results, a sensitivity analysis was performed in which RCS curves were analyzed separately in people who were not retired, were of Han ethnicity, and were not diabetic at baseline.

Results

Baseline characteristics of participants

Figure 1 presents the flowchart of participant enrollment. Among the 3,465 employees who underwent annual health examinations in 2021, a total of 2,643 participants were included in the final analysis after applying exclusion criteria. Baseline characteristics stratified by TyG quartiles and sex are shown in Table 1. In both women and men, higher TyG levels were associated with older age, higher BMI, and elevated blood pressure ($p < 0.001$). Additionally, higher levels of glucose, triglycerides, uric acid, and liver enzymes were observed in participants with higher TyG levels ($p < 0.001$). The incidence of new-onset hypertension increased significantly across TyG quartiles, rising from 9.3% to 18.5% in women ($p < 0.001$) and from 11.8% to 29.2% in men ($p = 0.007$). As TyG levels increased, HDL-C levels decreased while LDL-C levels increased.

Association of TyG index with incident hypertension in sex-specific subgroups

Table 2 presents the results of the Cox regression analysis. In the unadjusted model, higher TyG index levels were associated with an increased risk of new-onset hypertension in both men and women. Among women, the highest TyG quartile (Q4) was significantly associated with an increased risk of hypertension compared to the lowest quartile (Q1) in the unadjusted model (HR = 2.16, 95% CI: 1.49–3.14, $P < 0.0001$), and the association remained significant after full adjustment (HR = 1.82, 95% CI: 1.06–3.13, $P = 0.0307$). In men, a significant association was also observed in the unadjusted

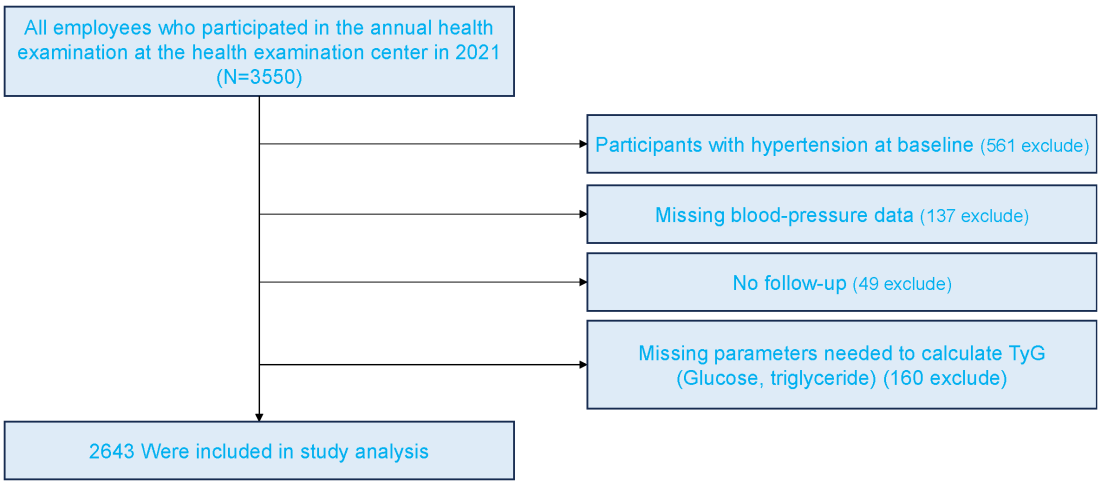

FIGURE 1
Flowchart of the study population.

model (Q4 vs. Q1: HR = 3.05, 95% CI: 1.33–7.01, P = 0.0085), but it was no longer significant after full adjustment. In the overall population, a significant positive association between the TyG index and hypertension was observed in the unadjusted model, but the association was not significant in the fully adjusted model.

Figure 2 illustrates the association between the TyG index and the risk of new-onset hypertension using a RCS model. In the overall population, a nonlinear positive relationship was observed between the TyG index and the risk of new-onset hypertension. In Figure 2B, stratified analyses by sex showed that the risk of new-onset hypertension increased with rising TyG levels in both men and women. However, the risk of hypertension differed between sexes at different TyG levels, with men exhibiting a greater risk than women when the TyG index reached higher levels.

Sensitivity analysis

Stratified analyses using the RCS model were performed in the non-retired population, Han Chinese participants, and individuals without diabetes at baseline (Figure 3). In all these subgroups, sex differences were observed in the association between TyG levels and new-onset hypertension. Among Han participants and those without baseline diabetes, women had a lower incidence of hypertension than men when TyG levels were high. However, this pattern was not observed in the non-retired population.

Discussion

In this retrospective cohort study based on annual health check-up data of hospital employees, we found that higher TyG index levels were significantly associated with an increased risk of new-onset hypertension, and this association differed by sex. To our knowledge, this is the first study to investigate sex-specific differences in the association between the TyG index and incident hypertension.

Previous studies have also confirmed a positive association between the TyG index and new-onset hypertension. For example, Wang et al. (9) reported that baseline TyG levels were positively associated with new-onset hypertension. Each one-unit increase in TyG was associated with a 21% higher risk of hypertension (HR = 1.21, 95% CI: 1.13–1.29). Similarly, a 9-year cohort study by Zheng et al. (20) reported consistent findings, with participants in the highest TyG quartile having a significantly higher risk of hypertension compared to those in the lowest quartile (Q4 vs. Q1: HR = 1.53, 95% CI: 1.07–2.19). In addition, Gao et al. (11) and Liu et al. (10) analyzed two large nationwide datasets with representative Chinese populations—the CHNS and CHARLS—and reported similar results. Similar associations were also observed in studies conducted among Singaporean (21) and Spanish (13) populations. In the two studies based on nationwide Chinese population data, generalized linear models were used for subgroup analyses by sex. No significant sex differences were observed (CHARLS: male HR = 1.17, female HR = 1.20; CHNS: male HR = 1.27, female HR = 1.35). In our study, Cox regression analysis showed that the HR for women (1.18) was slightly higher than that for men (1.01), which is consistent with previous findings. Using RCS, we found a sex difference in the association between TyG levels and new-onset hypertension. Among individuals with higher TyG levels, women had a lower risk of hypertension compared to men. Our study also collected information on participants' departments and adjusted for this variable in the analysis. This is a strength of our study, as in Chinese hospitals, different departments are often associated with distinct work patterns and lifestyle behaviors (22, 23). A recent meta-analysis concluded that the association between TyG and new-onset hypertension is not affected by sex (2). This conclusion is controversial compared to our findings. Since our data are derived from a single-center study, additional evidence is needed to further explore sex differences and support our observations.

TABLE 1 Baseline characteristics of participants (N =2643).

TyG quartile	Female				P-value	Male				P-value
	Q1	Q2	Q3	Q4		Q1	Q2	Q3	Q4	
N	702	611	461	259		51	105	190	264	
Age, years	31.83 ± 7.47	33.00 ± 8.43	35.04 ± 10.00	39.08 ± 12.94	<0.001	32.49 ± 8.22	35.06 ± 10.02	35.49 ± 9.16	40.70 ± 11.32	<0.001
Marital status, %					<0.001					<0.001
Married	481 (68.52)	439 (71.85)	369 (80.04)	224 (86.49)		30 (58.82%)	77 (73.33%)	147 (77.78%)	234 (88.64%)	
Unmarried	221 (31.48)	172 (28.15)	92 (19.96)	35 (13.51)		21 (41.18%)	28 (26.67%)	42 (22.22%)	30 (11.36%)	
Retired, %					<0.001					0.346
No	693 (98.72)	594 (97.22)	438 (95.01)	217 (83.78)		50 (98.04%)	103 (98.10%)	187 (98.42%)	253 (95.83%)	
Yes	9 (1.28)	17 (2.78)	23 (4.99)	42 (16.22)		1 (1.96%)	2 (1.90%)	3 (1.58%)	11 (4.17%)	
Department, %					<0.001					0.033
CD	540 (76.92)	438 (71.69)	319 (69.20)	161 (62.16)		29 (56.86%)	57 (54.29%)	116 (61.05%)	145 (54.92%)	
AD	79 (11.25)	78 (12.77)	55 (11.93)	31 (11.97)		16 (31.37%)	20 (19.05%)	46 (24.21%)	70 (26.52%)	
Retired	8 (1.14)	17 (2.78)	23 (4.99)	42 (16.22)		1 (1.96%)	2 (1.90%)	3 (1.58%)	12 (4.55%)	
MTD	46 (6.55)	46 (7.53)	47 (10.20)	13 (5.02)		3 (5.88%)	16 (15.24%)	23 (12.11%)	29 (10.98%)	
PSD	29 (4.13)	32 (5.24)	17 (3.69)	12 (4.63)		2 (3.92%)	10 (9.52%)	2 (1.05%)	7 (2.65%)	
Race, %					0.356					0.678
Han	591 (98.17)	529 (99.44)	394 (99.24)	225 (99.56)		44 (100.00%)	84 (100.00%)	154 (98.72%)	206 (99.52%)	
Non-han	11 (1.83)	3 (0.56)	3 (0.76)	1 (0.44)		0 (0.00%)	0 (0.00%)	2 (1.28%)	1 (0.48%)	
DBP, mmHg	65.51 ± 8.13	66.16 ± 8.21	66.75 ± 7.96	69.01 ± 8.23	<0.001	71.26 ± 7.23	69.38 ± 8.99	71.21 ± 7.18	73.39 ± 7.83	<0.001
SBP, mmHg	108.28 ± 10.57	108.65 ± 10.95	109.57 ± 10.59	114.21 ± 11.59	<0.001	119.89 ± 10.07	119.00 ± 10.19	118.80 ± 9.54	121.16 ± 10.91	0.076
Pulse rate, beats/min (bpm)	80.81 ± 11.02	83.40 ± 12.10	83.03 ± 12.03	83.95 ± 11.27	<0.001	78.19 ± 14.23	74.22 ± 10.94	77.38 ± 10.64	78.09 ± 11.02	0.022
Height, cm	159.81 ± 5.26	159.39 ± 5.27	159.02 ± 5.66	158.59 ± 5.46	0.008	172.04 ± 5.37	172.26 ± 7.01	172.45 ± 5.89	170.75 ± 6.34	0.026
Weight, kg	51.84 ± 6.34	53.18 ± 7.51	54.38 ± 7.59	57.09 ± 8.69	<0.001	64.06 ± 9.72	67.15 ± 10.57	68.80 ± 9.06	70.22 ± 9.41	<0.001
BMI, kg/m^2	20.29 ± 2.26	20.91 ± 2.61	21.51 ± 2.88	22.68 ± 3.09	<0.001	21.62 ± 2.98	22.58 ± 2.93	23.11 ± 2.62	24.06 ± 2.64	<0.001
WBC, 10^9/L	5.42 ± 1.31	5.66 ± 1.45	5.86 ± 1.61	6.29 ± 1.78	<0.001	5.41 ± 1.22	5.91 ± 1.30	5.99 ± 1.24	6.48 ± 1.55	<0.001
NE, %	55.95 ± 7.85	56.04 ± 8.36	57.30 ± 8.74	58.21 ± 8.65	<0.001	53.63 ± 7.28	54.10 ± 7.80	54.19 ± 7.38	55.02 ± 7.40	0.366

(Continued)

10.3389/fendo.2025.1636890

TABLE 1 Continued

TyG quartile	Female				P-value	Male				P-value
	Q1	Q2	Q3	Q4		Q1	Q2	Q3	Q4	
AST, U/L	18.00 (16.00-21.00)	19.00 (16.00-22.00)	19.00 (16.00-22.00)	20.00 (17.00-25.00)	<0.001	21.00 (18.50-24.00)	22.00 (19.00-25.00)	23.00 (19.00-27.00)	24.00 (20.00-31.00)	<0.001
ALT, U/L	12.00 (10.00-16.00)	13.00 (10.50-18.00)	14.00 (11.00-19.00)	18.00 (13.00-26.00)	<0.001	19.00 (13.00-26.00)	21.00 (15.00-30.00)	24.00 (16.25-33.00)	31.00 (22.00-47.00)	<0.001
ALB, g/L	44.96 ± 2.06	45.10 ± 2.02	44.98 ± 2.31	45.11 ± 2.49	0.181	46.75 ± 2.11	45.87 ± 2.23	46.28 ± 2.05	46.38 ± 2.03	0.065
HDLC	1.53 ± 0.30	1.43 ± 0.27	1.33 ± 0.29	1.24 ± 0.32	<0.001	1.28 ± 0.22	1.23 ± 0.26	1.17 ± 0.25	1.07 ± 0.21	<0.001
LDLC	2.55 ± 0.73	2.76 ± 0.71	3.02 ± 0.79	3.14 ± 0.95	<0.001	2.84 ± 0.76	2.95 ± 0.71	3.21 ± 0.77	3.35 ± 0.95	<0.001
Glu, mmol/L	4.36 ± 0.33	4.51 ± 0.35	4.58 ± 0.41	4.82 ± 0.81	<0.001	4.30 ± 0.44	4.47 ± 0.49	4.54 ± 0.47	4.91 ± 1.07	<0.001
TG, mmol/L	0.62 ± 0.10	0.87 ± 0.10	1.20 ± 0.16	2.15 ± 0.97	<0.001	0.68 ± 0.09	0.90 ± 0.11	1.26 ± 0.18	2.34 ± 0.96	<0.001
UA, μmol/L	280.64 ± 60.82	286.37 ± 58.14	294.08 ± 65.57	318.10 ± 78.35	<0.001	391.92 ± 64.96	396.72 ± 73.74	412.68 ± 80.13	439.34 ± 86.42	<0.001
History of diabetes, %					0.036					0.012
No	695 (99.00)	606 (99.18)	452 (98.05)	251 (96.91)		51 (100.00%)	102 (97.14%)	187 (98.42%)	246 (93.18%)	
Yes	7 (1.00)	5 (0.82)	9 (1.95)	8 (3.09)		0 (0.00%)	3 (2.86%)	3 (1.58%)	18 (6.82%)	
Family history of hypertension, %					0.092					0.908
No	323 (96.42)	284 (95.30)	232 (97.07)	109 (91.60)		32 (96.97%)	53 (98.15%)	95 (95.96%)	134 (96.40%)	
Yes	12 (3.58)	14 (4.70)	7 (2.93)	10 (8.40)		1 (3.03%)	1 (1.85%)	4 (4.04%)	5 (3.60%)	
New-onset hypertension, %					<0.001					0.007
No	637 (90.74)	540 (88.38)	415 (90.02)	211 (81.47)		45 (88.24%)	85 (80.95%)	154 (81.05%)	187 (70.83%)	
Yes	65 (9.26)	71 (11.62)	46 (9.98)	48 (18.53)		6 (11.76%)	20 (19.05%)	36 (18.95%)	77 (29.17%)	

Baseline characteristics are presented separately by sex. Within each sex, participants were categorized into four TyG quartiles, and comparisons across quartiles were conducted using one-way ANOVA for normally distributed continuous variables, Kruskal–Wallis test for skewed continuous variables, and chi-square or Fisher's exact test for categorical variables. *Post hoc* pairwise comparisons were not performed, as the purpose was descriptive comparison of baseline characteristics.

BMI, body mass index; WBC, white blood cell count; NE, neutrophil percentage; AST, aspartate aminotransferase; ALT, alanine aminotransferase; ALB, serum albumin; DBP, diastolic blood pressure; SBP, systolic blood pressure; Glu, fasting blood glucose; TG, triglycerides; UA, uric acid; TyG, triglyceride-glucose index; CD, clinical department; AD, administrative department; MTD, medical technology department; PSD, pharmaceutical sciences department; HDL-C, high density lipoprotein cholesterol; LDL-C, low-density lipoprotein cholesterol.

10.3389/fendo.2025.1636890

TABLE 2 Associations between TyG index and new-onset hypertension.

Exposure	Non-adjusted (HR, 95%CI, P)	Adjust I (HR, 95%CI, P)	Adjust II (HR,95%CI, P)
In female			
TyG continuous	1.44 (1.10, 1.87) 0.0070	1.16 (0.83, 1.62) 0.3738	1.15 (0.78, 1.69) 0.4920
TyG quartile			
Q1	1.0	1.0	1.0
Q2	1.28 (0.91, 1.79) 0.1494	1.17 (0.78, 1.77) 0.4443	1.26 (0.83, 1.90) 0.2788
Q3	1.11 (0.76, 1.62) 0.5975	0.88 (0.55, 1.42) 0.6092	0.91 (0.55, 1.50) 0.7040
Q4	2.16 (1.49, 3.14) <0.0001	1.71 (1.07, 2.74) 0.0263	1.82 (1.06, 3.13) 0.0307
P for trend	0.0011	0.1256	0.1347
In male			
TyG continuous	2.01 (1.51, 2.67) <0.0001	1.20 (0.78, 1.83) 0.4064	1.07 (0.60, 1.93) 0.8081
TyG quartile			
Q1	1.0	1.0	1.0
Q2	1.72 (0.69, 4.28) 0.2462	1.49 (0.54, 4.16) 0.4432	1.62 (0.56, 4.70) 0.3707
Q3	1.71 (0.72, 4.05) 0.2264	0.93 (0.34, 2.52) 0.8879	0.84 (0.30, 2.33) 0.7357
Q4	3.05 (1.33, 7.01) 0.0085	1.45 (0.55, 3.81) 0.4535	1.32 (0.46, 3.79) 0.6092
P for trend	0.0004	0.5969	0.9780
In total			
TyG continuous	1.67 (1.38, 2.03) <0.0001	1.15 (0.89, 1.48) 0.2731	1.08 (0.79, 1.48) 0.6133
TyG quartile			
Q1	1.0	1.0	1.0
Q2	1.32 (0.96, 1.80) 0.0837	1.25 (0.86, 1.81) 0.2394	1.30 (0.89, 1.90) 0.1713
Q3	1.20 (0.87, 1.67) 0.2652	0.91 (0.60, 1.36) 0.6386	0.90 (0.59, 1.39) 0.6366
Q4	2.27 (1.66, 3.10) <0.0001	1.53 (1.02, 2.28) 0.0377	1.52 (0.96, 2.41) 0.0776
P for trend	<0.0001	0.1213	0.2561

Non-adjusted model adjust for: None
Adjust I model adjust for: Age; Race; Department; BMI.
Adjust II model adjust for: Age; Race; Department; BMI; Marital status; History of diabetes; WBC; NE; AST; ALT; ALB; HDL-C; LDL-C; UA.
BMI, body mass index; WBC, white blood cell count; NE, neutrophil percentage; AST, aspartate aminotransferase; ALT, alanine aminotransferase; ALB, serum albumin; TyG, triglyceride-glucose index; HDL-C, high density lipoprotein cholesterol; LDL-C, low-density lipoprotein cholesterol; UA, uric acid.

In the sensitivity analyses, we found significant differences in the risk of new-onset hypertension between men and women as TyG levels increased across different subpopulations. Among Han participants and those without diabetes at baseline, women had a lower risk of developing hypertension than men at higher TyG levels. However, this pattern was not observed in the non-retired population. Considering that our study population consisted of hospital employees from various clinical and administrative departments, female healthcare workers may experience greater occupational stress, particularly nurses. Factors such as night shifts and heavy workloads may increase the risk of metabolic disorders and elevated blood pressure in this group (24). In addition, women often bear additional family responsibilities in society (25), which may partially explain our findings. However, further studies are needed to support this hypothesis.

Several potential pathophysiological mechanisms may explain the association between the TyG index and hypertension. The TyG index is widely recognized as a surrogate marker of insulin resistance (26), which influences blood pressure through multiple pathways. For example, IR can lead to endothelial dysfunction by reducing nitric oxide production, which impairs vasodilation and increases peripheral vascular resistance (27). Additionally, IR activates the sympathetic nervous system through both central and peripheral mechanisms, leading to increased heart rate and vasoconstriction (28). It also promotes renal sodium reabsorption, resulting in fluid retention and increased blood volume (29). Moreover, individuals with elevated TyG levels often exhibit chronic low-grade inflammation and sustained oxidative stress, which contribute to atherosclerosis and vascular remodeling (30), further increasing blood pressure.

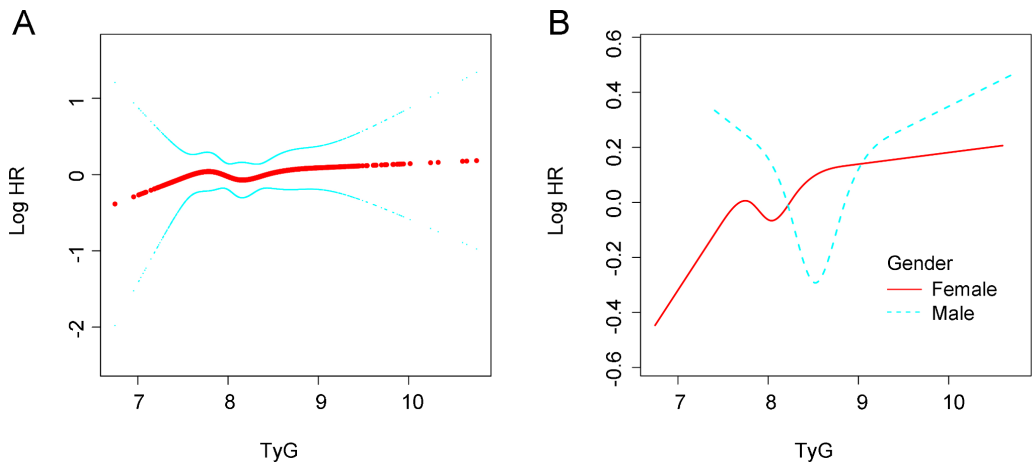

FIGURE 2
Association between TyG and new-onset hypertension. **(A)** in the general population. **(B)** In different gender groups. All analyses were adjusted for confounding factors including. Age; ARace; Department; BMI; Marital status; History of diabetes; WBC; NE; AST; ALT; ALB; HDL-C; LDL-C; UA. BMI, body mass index; WBC, white blood cell count; NE, neutrophil percentage; AST, aspartate aminotransferase; ALT, alane aminotransferase; ALB, serum neutrophil perecntage; AST, aspartate aminotransferase; ALT, alane aminotransferase; ALB, serum albumin; TyG, tryglyceride-fglucose index; HDL-C, High density liproprotein cholesterol; LDL-C, Low-density lipoprotein cholesterol; UA, uric acid.

In our study, the risk of new-onset hypertension tended to stabilize in women with higher TyG levels compared to men. We speculate that this phenomenon may be attributed to the protective effects of estrogen on lipid metabolism, insulin resistance, and cardiovascular as well as blood pressure regulation. Estrogen has been shown in multiple studies to enhance insulin sensitivity by promoting glucose uptake in peripheral tissues and suppressing hepatic gluconeogenesis, thereby lowering blood glucose levels (31). It also mobilizes systemic fat stores and reduces visceral fat accumulation (32). In addition, estrogen downregulates hepatic angiotensinogen synthesis, thereby inhibiting the renin–angiotensin–aldosterone system, reducing vasoconstriction and sodium retention (33). Estrogen also inhibits both central and peripheral sympathetic nervous system activity, leading to reduced norepinephrine release and vascular tone, which ultimately lowers blood pressure (34). Furthermore, estrogen enhances endothelial function and vasodilation by activating endothelial nitric oxide synthase and promoting nitric oxide production (35). Beyond blood pressure regulation, estrogen also exerts significant anti-inflammatory and antioxidant effects. Estrogen suppresses the expression of pro-inflammatory cytokines such as tumor necrosis factor-α, interleukin-6, and C-reactive protein (36), while upregulating anti-inflammatory cytokines like interleukin-10 (37), thereby modulating and reducing systemic inflammation.

This study also has several limitations. First, the data were obtained from a single center and included only hospital employees

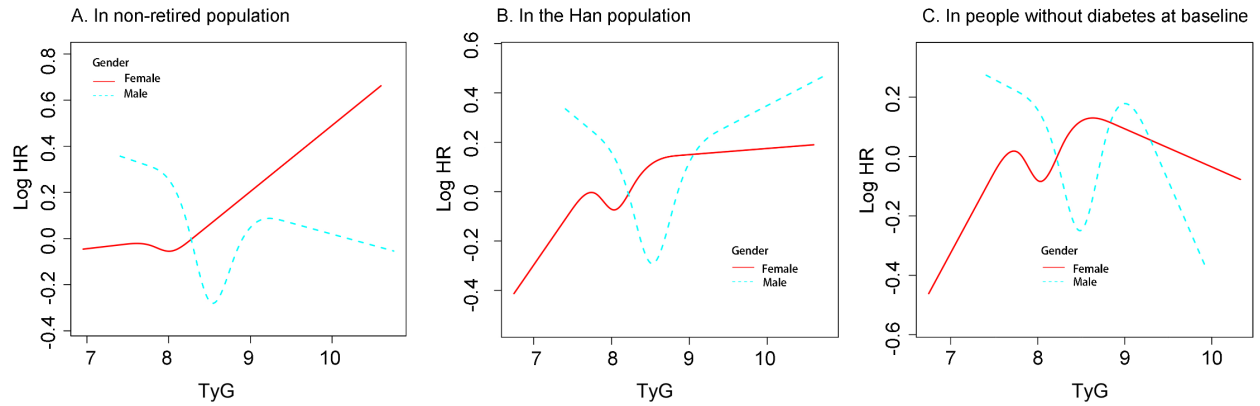

FIGURE 3
The associatioon between TyG and new-onset hypertension differed by gender in different population **(A)** In non-retired popultaion. **(B)** in the Han population. **(C)** In people without diabetes at baseline. Restricted cubic spline analysis was used to construct stratification curves, and all analyses were adjusted for confounding factors. Including: Age : Race; Department; BMI;Marital status; History of diabtes; WBC; NE; AST; ALT; ALB; HDL-C; LDL-C; UA (Excluding the variable of restricted poplulation) BMI, body mass index; WBC, white blood cell count; NE, Neutrophil percentage; AST, aspartate aminotransferase; ALT, alanine amonitransferase; ALB,serum albumin; TyG, triglyceride-glucose index; HDL-C, High density lipoprotein cholesterol; LDC-C, low density lipoprotein cholesterol; UA, Uric acid.

undergoing annual health examinations, which may limit the generalizability of our findings to other populations. Second, although we adjusted for multiple confounders as much as possible, unmeasured confounding remains due to the retrospective nature of this study. Variables such as smoking, alcohol consumption, sleep apnea, sleep quality, dietary habits, and physical activity were not collected. Therefore, we collected other variables to partially account for relevant confounding factors. For example, we collected information on participants' clinical department to serve as a proxy for occupational stress. However, residual confounding cannot be completely eliminated. Third, due to the observational nature of this study, we can only establish an association between the TyG index and new-onset hypertension, rather than causality. Fourth, we analyzed only baseline TyG levels and did not assess the potential impact of longitudinal changes in TyG on hypertension risk. Further studies are warranted to explore this issue.

Conclusions

In this retrospective cohort study based on annual health check-up data from hospital employees, we found that the TyG index may be positively associated with the risk of new-onset hypertension, and this association may be nonlinear. Moreover, our analysis suggested that at higher TyG levels, men had a greater risk of developing hypertension compared to women. Further studies are needed to address potential confounding and improve the generalizability of these findings.

Data availability statement

The raw data supporting the conclusions of this article will be made available by the authors, without undue reservation.

Ethics statement

The studies involving humans were approved by the Ethics Committee of the Third Affiliated Hospital of Wenzhou Medical University. The studies were conducted in accordance with the local legislation and institutional requirements. The ethics committee/institutional review board waived the requirement of written informed consent for participation from the participants or the participants' legal guardians/next of kin because the study was retrospective and the data were anonymized, the ethics committee waived written informed consent (Ethics approval number, YJ2025062).

Author contributions

RS: Writing – review & editing. JC: Writing – review & editing. SY: Writing – review & editing. JQ: Writing – original draft. CF: Writing – review & editing. YL: Writing – review & editing, Writing – original draft.

Funding

The author(s) declare that no financial support was received for the research and/or publication of this article.

Acknowledgments

The authors thank the field investigators for their contribution and the participants for their cooperation.

Conflict of interest

The authors declare that the research was conducted in the absence of any commercial or financial relationships that could be construed as a potential conflict of interest.

Generative AI statement

The author(s) declare that no Generative AI was used in the creation of this manuscript.

Publisher's note

References

1. Al-Makki A, DiPette D, Whelton PK, Murad MH, Mustafa RA, Acharya S, et al. Hypertension pharmacological treatment in adults: A world health organization guideline executive summary. *Hypertension.* (2022) 79:293–301. doi: 10.1161/HYPERTENSIONAHA.121.18192

2. Yang C, Song Y, Wang P. Relationship between triglyceride-glucose index and new-onset hypertension in general population-a systemic review and meta-analysis of cohort studies. *Clin Exp Hypertens.* (2024) 46:2341631. doi: 10.1080/10641963.2024.2341631

3. Lu J, Lu Y, Wang X, Li X, Linderman GC, Wu C, et al. Prevalence, awareness, treatment, and control of hypertension in China: data from 1·7 million adults in a population-based screening study (China PEACE Million Persons Project). *Lancet.* (2017) 390:2549–58. doi: 10.1016/S0140-6736(17)32478-9

4. Suvila K, Lima JAC, Cheng S, Niiranen TJ. Clinical correlates of early-onset hypertension. *Am J Hypertens*. (2021) 34:915–8. doi: 10.1093/ajh/hpab066

5. Fang Y, Xie H, Fan C. Association of hypertension with helicobacter pylori: A systematic review and meta–analysis. *PloS One*. (2022) 17:e0268686. doi: 10.1371/journal.pone.0268686

6. Tagi VM, Mainieri F, Chiarelli F. Hypertension in patients with insulin resistance: etiopathogenesis and management in children. *Int J Mol Sci*. (2022) 23:10. doi: 10.3390/ijms23105814

7. Muniyappa R, Lee S, Chen H, Quon MJ. Current approaches for assessing insulin sensitivity and resistance *in vivo*: advantages, limitations, and appropriate usage. *Am J Physiol Endocrinol Metab*. (2008) 294:E15–26. doi: 10.1152/ajpendo.00645.2007

8. Guo Y, Zhao J, Zhang Y, Wu L, Yu Z, He D, et al. Triglyceride glucose index influences platelet reactivity in acute ischemic stroke patients. *BMC Neurol*. (2021) 21:409. doi: 10.1186/s12883-021-02443-x

9. Wang D, Li W, Zhou M, Ma J, Guo Y, Yuan J, et al. Association of the triglyceride-glucose index variability with blood pressure and hypertension: a cohort study. *QJM*. (2024) 117:277–82. doi: 10.1093/qjmed/hcad252

10. Liu T, Xuan H, Yin J, Wang L, Wang C, Xu X, et al. Triglyceride glucose index increases significantly risk of hypertension development in chinese individuals aged ≥45 years old: analysis from the China health and retirement longitudinal study. *J Multidiscip Healthc*. (2023) 16:63–73. doi: 10.2147/JMDH.S391905

11. Gao Q, Lin Y, Xu R, Luo F, Chen R, Li P, et al. Positive association of triglyceride-glucose index with new-onset hypertension among adults: a national cohort study in China. *Cardiovasc Diabetol*. (2023) 22:58. doi: 10.1186/s12933-023-01795-7

12. Zhao Y, Yang X, Wu Y, Huang H, Hu F, Zhang M, et al. Association of triglyceride-glucose index and its 6-year change with risk of hypertension: A prospective cohort study. *Nutr Metab Cardiovasc Dis*. (2023) 33:568–76. doi: 10.1016/j.numecd.2022.12.001

13. Sánchez-Íñigo L, Navarro-González D, Pastrana-Delgado J, Fernández-Montero A, Martínez JA. Association of triglycerides and new lipid markers with the incidence of hypertension in a Spanish cohort. *J Hypertens*. (2016) 34:1257–65. doi: 10.1097/HJH.0000000000000941

14. Lee JH, Heo S-J, Kwon Y-J. Sex-specific comparison between triglyceride glucose index and modified triglyceride glucose indices to predict new-onset hypertension in middle-aged and older adults. *J Am Heart Assoc*. (2023) 12:e030022. doi: 10.1161/JAHA.123.030022

15. Zhang Y, Zhang W, Liu L. Comments on 2018 ESC/ESH hypertension guidelines: chinese perspective. *Circ Res*. (2019) 124:978–80. doi: 10.1161/CIRCRESAHA.119.314997

16. Xu M, Xu K, Lin W, Sun R, Yan S, Chen X, et al. Sex-specific differences in the relationship between fasting plasma glucose and carotid plaque in a cardiovascular high-risk population: a cross-sectional study. *Front Endocrinol (Lausanne)*. (2025) 16:1478640. doi: 10.3389/fendo.2025.1478640

17. Li W, Yi G, Chen Z, Wu J, Lu Z, Liang J, et al. Association of occupational noise exposure, bilateral hearing loss with hypertension among Chinese workers. *J Hypertens*. (2021) 39:643–50. doi: 10.1097/HJH.0000000000002696

18. Vandenbroucke JP, Ev E, DG A, PC G, CD M, SJ P, et al. Strengthening the reporting of observational studies in epidemiology (STROBE): explanation and elaboration. *Вопросы Современной Педиатрии*. (2022) 21:173–208. doi: 10.1371/journal.pmed.0040297

19. Garzotto M, Beer TM, Hudson RG, Peters L, Hsieh Y-C, Barrera E, et al. Improved detection of prostate cancer using classification and regression tree analysis. *J Clin Oncol*. (2005) 23:4322–9. doi: 10.1200/JCO.2005.11.136

20. Zheng R, Mao Y. Triglyceride and glucose (TyG) index as a predictor of incident hypertension: a 9-year longitudinal population-based study. *Lipids Health Dis*. (2017) 16:175. doi: 10.1186/s12944-017-0562-y

21. Khoo JK, Low S, Irwan B, Tang JI, Sum CF, Subramaniam T, et al. The role of triglyceride-glucose index in the prediction of the development of hypertension - findings from a community cohort in Singapore. *J ASEAN Fed Endocr Soc*. (2023) 38:62–7. doi: 10.15605/jafes.038.01.09

22. Gong Y, Han T, Chen W, Dib HH, Yang G, Zhuang R, et al. Prevalence of anxiety and depressive symptoms and related risk factors among physicians in China: a cross-sectional study. *PloS One*. (2014) 9:e103242. doi: 10.1371/journal.pone.0103242

23. Tsou M-T, Pai T-P, Chiang T-M, Huang W-H, Lin H-M, Lee S-C. Burnout and metabolic syndrome among different departments of medical center nurses in Taiwan-Cross-sectional study and biomarker research. *J Occup Health*. (2021) 63:e12188. doi: 10.1002/1348-9585.12188

24. Sooriyaarachchi P, Jayawardena R, Pavey T, King NA. Shift work and the risk for metabolic syndrome among healthcare workers: A systematic review and meta-analysis. *Obes Rev*. (2022) 23:e13489. doi: 10.1111/obr.13489

25. Artazcoz L, Borrell C, Cortès I, Escribà-Agüir V, Cascant L. Occupational epidemiology and work related inequalities in health: a gender perspective for two complementary approaches to work and health research. *J Epidemiol Community Health*. (2007) 61 Suppl 2::ii39–ii45. doi: 10.1136/jech.2007.059774

26. Nandhini ST. Association of triglyceride–glucose index (TyG index) with hbA1c and insulin resistance in type 2 diabetes mellitus. *Maedica – A J Clin Med*. (2021) 16:375–81. doi: 10.26574/maedica.2021.16.3.375

27. Karaca Ü, Schram MT, Houben AJHM, Muris DMJ, Stehouwer CDA. Microvascular dysfunction as a link between obesity, insulin resistance and hypertension. *Diabetes Res Clin Pract*. (2014) 103:382–7. doi: 10.1016/j.diabres.2013.12.012

28. MRd S, DM V, IS A, MJ O, Linhares D, Nevès N, et al. Interplay between sympathetic nervous system and inflammation in aseptic loosening of hip joint replacement. *Sci Rep*. (2018) 8:16044. doi: 10.1038/s41598-018-33360-8

29. Pöyhönen-Alho M, Viitasalo M, Nicholls MG, Lindström B, Väänänen H, Kaaja R. Imbalance of the autonomic nervous system at Night in women with gestational diabetes. *Diabetic Med*. (2010) 27:988–94. doi: 10.1111/j.1464-5491.2010.03062.x

30. Bonomini F, Rodella LF, Rezzani R. Metabolic syndrome, aging and involvement of oxidative stress. *Aging Disease*. (2015) 6:109. doi: 10.14336/AD.2014.0305

31. Barros RPA, Gustafsson J. Estrogen receptors and the metabolic network. *Cell Metab*. (2011) 14:289–99. doi: 10.1016/j.cmet.2011.08.005

32. Zhu L, Martinez MN, Emfinger CH, Palmisano BT, Stafford JM. Estrogen signaling prevents diet-induced hepatic insulin resistance in male mice with obesity. *Am J Physiol Endocrinol Metab*. (2014) 306:E1188–E97. doi: 10.1152/ajpendo.00579.2013

33. Colafella KMM, Denton KM. Sex-specific differences in hypertension and associated cardiovascular disease. *Nat Rev Nephrol*. (2018) 14:185–201. doi: 10.1038/nrneph.2017.189

34. Young BE, Kissell CE, Vranish JR, Stephens BY, Holwerda SW, Fadel PJ. Sex differences in sympathetic transduction in black and white adults: implications for racial disparities in hypertension and cardiovascular disease risk. *Am J Physiol Heart Circ Physiol*. (2024) 327:H672–H80. doi: 10.1152/ajpheart.00337.2024

35. Chambliss KL, Shaul PW. Estrogen modulation of endothelial nitric oxide synthase. *Endocr Rev*. (2002) 23:665–86. doi: 10.1210/er.2001-0045

36. Straub RH. The complex role of estrogens in inflammation. *Endocr Rev*. (2007) 28:521–74. doi: 10.1210/er.2007-0001

37. Vegeto E, Benedusi V, Maggi A. Estrogen anti-inflammatory activity in brain: a therapeutic opportunity for menopause and neurodegenerative diseases. *Front Neuroendocrinol*. (2008) 29:507–19. doi: 10.1016/j.yfrne.2008.04.001

frontiers | Frontiers in Endocrinology

TYPE Review
PUBLISHED 12 August 2025
DOI 10.3389/fendo.2025.1618230

OPEN ACCESS

EDITED BY
Ramoji Kosuru,
Versiti Blood Research Institute, United States

REVIEWED BY
Kulvinder Kochar Kaur,
Kulvinder Kaur Centre For Human Reproduction, India
Radha Vaddavalli,
The Ohio State University, United States

*CORRESPONDENCE
Mingfeng Cao
18653192961@163.com
Yan Wang
8482487@163.com

†These authors have contributed equally to this work and share first authorship

‡These authors have contributed equally to this work

RECEIVED 25 April 2025
ACCEPTED 23 July 2025
PUBLISHED 12 August 2025

CITATION
Su N, Zhao J, Zhang W, Zhang X, Lu K, Ma Y, Wang Y and Cao M (2025) Study of independent diagnostic efficacy and co-diagnostic strategies of molecular markers for diabetic cardiomyopathy. *Front. Endocrinol.* 16:1618230. doi: 10.3389/fendo.2025.1618230

Study of independent diagnostic efficacy and co-diagnostic strategies of molecular markers for diabetic cardiomyopathy

Na Su[1,2†], Jingxuan Zhao[1,2†], Weiyi Zhang[1,2†], Xinhuan Zhang[2], Kunna Lu[2], Yan Ma[2], Yan Wang[2*‡] and Mingfeng Cao[2*‡]

[1]Graduate School, Shandong First Medical University & Shandong Academy of Medical Sciences, Jinan, China, [2]Department of Endocrinology, Second Affiliated Hospital of Shandong First Medical University, Tai'an, China

Word count of the full article: 4834Diabetic cardiomyopathy (DCM) is defined as myocardial dysfunction in diabetes mellitus (DM) patients independent of coronary artery disease (CAD) or hypertension (HTN). With high morbidity and mortality, DCM poses a significant threat to patient health. Its underlying pathogenesis remains incompletely elucidated, and the prolonged subclinical phase renders early diagnosis and precise treatment clinically challenging. Thus, identifying viable biomarkers for early diagnosis and intervention has emerged as a research imperative, whereas a systematic DCM diagnostic and therapeutic strategy remains to be established. Our examination revealed that circulating soluble suppression of tumorigenicity 2 (sST2), Cardiotrophin-1 (CT-1), and galectin-3 levels correlate closely with DCM progression stages. Combining Lysyl Oxidase-Like 2 (LOXL2) and Electron Transfer Flavoprotein β Subunit (ETFβ) measurements with ultrasound E/E' ratio and NT-proBNP enhances diagnostic accuracy. Novel noninvasive markers (e.g., skin autofluorescence) show promise. This article comprehensively evaluates the clinical applications of these molecular markers within DCM's pathophysiological classification framework.

KEYWORDS

diabetic cardiomyopathy, molecular markers, oxidative stress, non-coding RNA, early diagnosis

1 Introduction

DM is a global public health problem, affecting 4%–17% of the population worldwide. The International Diabetes Federation (IDF) predicts that the number of DM patients will exceed 610 million by 2045 (1). Cardiovascular complications of DM, such as myocardial remodeling and heart failure (HF)—account for 80% of DM-related deaths. DM is an independent predictor of HF, even after excluding traditional risk factors like CAD and HTN. In 2017, Lorenzo-Almorós et al. (2) proposed the first diagnostic criteria for DCM, with core features including left ventricular diastolic dysfunction (LVDD), reduced ejection

fraction (EF), pathological myocardial hypertrophy, and interstitial fibrosis. Although recent studies have elucidated DCM's pathological mechanisms (e.g., abnormal myocardial metabolism, mitochondrial dysfunction, oxidative stress, and fibrotic cascade activation) (3), early diagnosis remains challenging due to nonspecific cardiac alterations and a prolonged subclinical phase. This review systematically integrates the latest research progress on novel molecular markers (e.g., soluble suppression of tumorigenicity 2 [sST2], adiponectin [APN], and develops strategies for "molecular marker combinations" and "integration of molecular markers with imaging technologies" to provide a theoretical basis for the early and accurate diagnosis of DCM.

2 Indicators associated with myocardial oxidative stress and inflammatory response

2.1 soluble suppression of tumorigenicity 2

Suppression of tumorigenicity 2 (ST2), a member of the interleukin-1 receptor family (IL-1R family), exists in two subtypes: transmembrane (ST2L) and soluble (sST2). As a decoy receptor for IL-33, sST2 competitively binds to IL-33, thereby interfering with the IL-33/ST2L signaling pathway and modulating pathological processes such as atherosclerosis and cardiac remodeling (4). Fousteris et al. (5) demonstrated that plasma sST2 levels were significantly elevated in patients with T2DM compared to healthy controls, with further increases observed in those with comorbid left ventricular diastolic dysfunction (LVDD). While existing studies have established the prognostic value of sST2 in heart failure with mid-range ejection fraction (HFmrEF) (6), its predictive efficacy in HFmrEF patients with comorbid T2DM remains unclear.

2.2 Nod-like receptor family pyrin domain containing 3 inflammasome (NLRP3 inflammasome)

The Nod-like Receptor Family Pyrin Domain Containing 3 Inflammasome (NLRP3 inflammasome) is a multimeric complex consisting of NLRP3 protein and apoptosis-associated speck-like protein (ASC). This multimeric complex, whose aberrant activation may be closely associated with the pathological processes of autoimmune and metabolic diseases. Luo et al. (7) found that high glucose-induced oxidative stress activates the NLRP3 inflammasome via thioredoxin-interacting proteins, thereby promoting cardiomyocyte apoptosis and myocardial fibrosis. A 2020 review (8) summarized the dual role of NLRP3 in DCM: short-term anti-inflammatory benefits, but long-term overactivation exacerbates myocardial injury. Kai et al. (9) demonstrated that NLRP3 activation leads to the release of IL-1β and IL-18, which exacerbate myocardial fibrosis, oxidative damage, and disturbed energy metabolism; thus, targeting the NLRP3 inflammasome may serve as a therapeutic strategy for DCM.

2.3 Growth differentiation factor-15

Growth differentiation factor-15 (GDF-15), a member of the transforming growth factor-β (TGF-β) superfamily, plays a key role in regulating inflammatory responses and promoting cell growth and differentiation. Notably, Dominguez-Rodriguez et al. (10) reported that serum GDF-15 levels were significantly upregulated in asymptomatic DCM patients. Additionally, a review highlighted that high glucose induces GDF-15 expression in endothelial cells via the p53 pathway, which subsequently attenuates endothelial cell apoptosis by activating the PI3K/Akt/eNOS pathway, thus suggesting GDF-15's potential role in DM-related vascular protection (11). However, due to the lack of specificity of GDF-15 in metabolic diseases (12), its clinical utility in predicting disease progression remains controversial.

2.4 High mobility group A1 and high-mobility group box 1

High mobility group A1 (HMGA1), a specific cofactor for gene activation, plays a critical role in key biological processes, including cell cycle regulation, embryonic development, tumor cell transformation and differentiation, apoptosis, and DNA repair. In cardiac muscle and fibroblasts of DM mice, HMGA1 expression is significantly elevated, and its overexpression promotes autophagy through the miR-222-mediated P27/CDK2/mTOR signaling pathway, which in turn exacerbates inflammatory responses and apoptosis in cardiomyocytes in a high-glucose environment, and participates in the process of cardiac remodeling in DCM (13).

High-mobility group box 1 (HMGB1) is a highly conserved nuclear protein commonly found in various tissues and cells of mammals, and plays an important role in the regulation of inflammatory responses. Tao et al. (14) found that cardiomyocyte-derived HMGB1 promoted DCM by inhibiting fibroblastic IL-33 expression via TLR4 and promoting collagen production. Both resveratrol and ustekinumab induced the downregulation of HMGB1 expression, demonstrating a protective effect against DCM: Resveratrol prevented oxidative damage, myocardial fibrosis, and inflammation by inhibiting the HMGB1/RAGE/TLR4/NF-κB signaling pathway (15), whereas ustekin exerted a protective effect against DCM by reducing inflammation and cardiomyocyte apoptosis through inhibition of the JNK and p38 signaling pathways (16).

2.5 Chitinase-3-like protein 1

Chitinase-3-like protein 1 (CHI3L1/YKL-40) belongs to the chitinase family and is involved in endothelial dysfunction and tissue remodeling. CHI3L1/YKL-40 is highly expressed in a variety of infectious and non-infectious inflammatory diseases and is considered a noninvasive prognostic biomarker of inflammation. Serum CHI3L1/YKL-40 levels in patients with DCM were positively correlated with left ventricular mass index (LVMI)and degree of LVDD (17). In a multicenter cohort study, it was observed that

CHI3L1/YKL-40 was significantly elevated in the serum of patients with DCM, and its levels correlated with markers of myocardial fibrosis (e.g., PIIINP) and myocardial scar area as detected via Cardiac Magnetic Resonance Imaging (CMR) (18).

2.6 Neutrophil-to-lymphocyte ratio

Neutrophil-to-lymphocyte ratio (NLR) is a simple and cost-effective index for assessing inflammatory status, which is widely used in clinical and scientific research. Huang et al. (19) found that serum NLR was significantly higher in the DCM group than in the T2DM-only group in a cross-sectional study of 507 T2DM patients, suggesting that NLR is associated with subclinical DCM.

2.7 C-reactive protein

C-reactive protein (CRP) is a plasma protein that participates in the systemic inflammatory response as an acute-phase reactant, and its plasma concentration is elevated in the inflammatory state. The high-sensitivity C-reactive protein (hsCRP) assay can accurately measure low concentrations of CRP in blood. A study by Mano et al. (20) found that elevated CRP levels exacerbated LVDD in patients with DCM, a finding that is closely related to myocardial inflammatory responses, angiotensinogen levels, and AT1 receptor expression.

2.8 Other pro-inflammatory cytokines

During the pathological process of DM, cardiomyocytes and fibroblasts release a variety of pro-inflammatory cytokines, including IL-1, IL-6, IL-12, IL-18, and TNF-α, which mediate the pathological damage induced by glycotoxicity and lipotoxicity by triggering mitochondrial dysfunction, oxidative stress, insulin resistance (IR), and β-cell apoptosis and other pathways. Epidemiologic studies conducted in areas with a high prevalence of DM (e.g., West Virginia, USA) (21) have shown that serum TNF-α, IL-6, and isoprostanes (IsoPs) levels are significantly elevated in patients with early-stage DCM, whereas bilirubin (Bil) concentrations are decreased. Although plasma concentrations of proinflammatory cytokines alone cannot distinguish DCM from other myocardial diseases, their dynamics have been shown to assist in assessing the pathologic progression of DCM.

3 Indicators of myocardial metabolic disorders

3.1 Adiponectin

Adiponectin (APN) is an adipokine composed of 244 amino acids and belongs to the collagen superfamily. It is involved in the regulation of glucolipid metabolism by binding to its cognate receptors, promoting fatty acid oxidation and glucose uptake, and enhancing insulin (INS) sensitivity. Shaver et al. (21) found that serum levels of APN were lower than those in normal controls in patients with DM and DCM, and this reduction was particularly significant and were particularly significant in patients with DCM. In a rat model of DCM (22), reduced myocardial and serum levels of APN were negatively correlated with IR index, triglyceride (TG) and total cholesterol levels, suggesting that APN may influence the progression of DCM through IR. In addition, Battiprolu et al. (23) demonstrated that APN antagonized the progression of DCM by reducing cardiomyocyte death by inhibiting cardiomyocyte hypertrophy and inflammatory responses.

3.2 Insulin-like growth factor binding protein-7

Insulin-like growth factor binding protein-7 (IGFBP-7), a member of the IGFBP superfamily, regulates the insulin (INS) receptor signaling pathway by binding to insulin-like growth factor-1. The results of Shaver et al. (21) showed that plasma levels of IGFBP-7 were significantly increased in patients with DCM. Ruan et al. (24) demonstrated that higher levels of IGFBP-7 were associated with worse clinical characteristics and increased risk of adverse clinical outcomes in patients with HFrEF. All of the above suggests that IGFBP-7 may be a biomarker for early diagnosis of DCM and cardiac fibrosis.

3.3 Activin A

Activin A, a member of the TGF-β superfamily, is secreted by epicardial adipose tissue. Greulich et al. (25) found that activin A signaling overactivation led to IR and cardiac systolic dysfunction in a guinea pig model induced by STZ/HFD. Further studies showed that plasma activin A levels were significantly elevated in T2DM patients with impaired myocardial glucose metabolism and left ventricular remodeling compared with those with T2DM alone (26). Molecular mechanism studies have shown that activin A exacerbates myocardial metabolic disturbances by inhibiting INS-mediated phosphorylation in the PI3K/Akt signaling pathway, which is a key regulatory pathway for myocardial glucose uptake, revealing its central role in the pathological process of DCM (27).

3.4 Other indicators of metabolic disorders

A prospective study in the United Kingdom (28) showed a significant positive correlation between the incidence of HF and the level of glycated hemoglobin (HbA1c) in patients with T2DM, highlighting the clinical value of HbA1c as an indicator of long-term glycemic control. Advanced glycation end products (AGEs) are heterogeneous macromolecules formed by cross-linking sugar molecules with proteins, lipids, and nucleic acids through non-enzymatic reactions. Accumulation of AGEs in a high-glycemic

environment induces cross-linking of myocardial collagen and other proteins, triggering interstitial fibrosis and ultimately leading to LVDD (29). Leptin, a circulating signaling molecule secreted by white adipocytes, mainly reflects TG storage status and is involved in the regulation of obesity and related metabolic disorders. Shaver et al. (21) found that serum leptin levels were significantly elevated in patients with DM combined with LVDD (especially in the high BMI group) and negatively correlated with APN levels, suggesting that leptin may become an early biomarker in DCM patients with high BMI. IsoPs are specific products of peroxidation of polyunsaturated fatty acids, and Luo et al. (30) found that hyperoxidative stress in myocardial tissues was accompanied by a significant increase in IsoPs levels in a T1DM rat model. Bilirubin (Bil), as a heme catabolic metabolite, has antioxidant properties since its antioxidant properties were first demonstrated by Ames et al. in 1987, and Chung et al. (31) found a negative correlation between serum total bilirubin levels and the incidence of cardiovascular autonomic neuropathy by analyzing data from 3015 T2DM patients.

4 Myocardial fibrosis-related indicators

4.1 Galectin-3

Galectin-3, a member of the lectin family, is involved in the regulation of fibrotic and inflammatory responses in cardiac, renal, and hepatic diseases. Flores-Ramírez et al. (32) demonstrated that the serum concentration of Galectin-3 was significantly elevated in patients with DM combined with reduced LVEF, suggesting that it may be a potential biomarker for identifying the early stages of LVDD in DM patients. In a 2022 review (33), Galectin-3 was described as a potential therapeutic target in DCM, where it may exacerbate cardiac dysfunction by promoting myocardial fibrosis and inflammatory responses.

4.2 Cardiotrophin-1

Cardiotrophin-1 (CT1), a member of the gp130 family, is a potent inducer of cardiomyocyte hypertrophy. Gamella-Pozuelo et al. (34) found that serum CT-1 levels were significantly elevated in patients with T2DM and HTN and were positively correlated with LV hypertrophy and arterial stiffness. Gamella-Pozuelo et al. (35) demonstrated a significant positive correlation between plasma CT-1 levels and basal blood glucose levels and the degree of left ventricular hypertrophy in patients with T2DM, and CT-1 concentrations were significantly higher in individuals with impaired glucose tolerance or newly diagnosed DM than in healthy controls.

4.3 Transforming growth factor-beta

Transforming Growth Factor-beta (TGF-β), as a member of the multifunctional cytokine superfamily, plays a central regulatory role in cell proliferation, differentiation, migration, and the dynamic homeostasis of the extracellular matrix (ECM).A 2017 review (36) indicated that TGF-β can promote myocardial fibroblast proliferation and collagen deposition through Smad-dependent and Smad-independent pathways and inhibit matrix metalloproteinase (MMP) activity, which in turn leads to myocardial fibrosis and ventricular remodeling; whereas TGF-β-neutralizing antibodies attenuates myocardial collagen deposition and improves diastolic dysfunction in DM mice.

4.4 N-terminal propeptide of procollagen type I and N-terminal propeptide of procollagen type III

Collagen Type I and Collagen Type III are the most abundant collagen types in the myocardium and other tissues, and serum N-terminal Propeptide of Procollagen Type I (PINP) and N-terminal Propeptide of Procollagen Type III (PIIINP) serve as specific biomarkers for their synthesis, respectively. Among them, PIIINP levels can also be used to assess the status of ECM renewal. Ihm et al. (37) showed that serum PINP was significantly elevated in patients with early-stage T2DM, which was significantly associated with myocardial fibrosis and LVDD. Quilliot et al. (38) found that PIIINP levels were significantly associated with early-stage LVDD in IR individuals in a normotensive, non-DM population.

4.5 Cellular communication network factor 2

Cellular communication network factor 2 (CCN2/CTGF) is a cysteine-rich stromal cell protein that plays an important role in connective tissue growth regulation and angiogenesis. Studies have shown that CCN2/CTGF induces cardiomyocyte hypertrophy and apoptosis during the pathological process of DCM, and CCN2/CTGF may serve as a sensitive biomarker for the early diagnosis of DCM and potentially play a protective role in myocardial injury (39).

5 Indicators related to myocardial steatosis and other injuries

5.1 Fatty acid binding proteins

Fatty Acid Binding Proteins (FABPs), as lipid chaperone proteins, are involved in multi-organ metabolic networks through the regulation of lipid flow, transport, and signaling. The STZ/HFD-induced T2DM mouse model showed that serum FABP4 levels were elevated in parallel with myocardial neutral lipid content, suggesting that it may be a novel biomarker for assessing myocardial lipid deposition (40). Human heart-type fatty acid binding protein (H-FABP), a myocardial-specific cytoplasmic protein responsible for transporting fatty acids to mitochondria for oxidative energy supply, is usually not detected in the serum of healthy individuals. Notably, Akbal et al. (41) found that serum H-

FABP levels were significantly elevated in patients with T2DM combined with early cardiac injury. Taken together, the FABP family (especially FABP4 and H-FABP) may serve as a potential biomarker combination for the early diagnosis of DCM.

5.2 Natriuretic peptide family

Atrial natriuretic peptide (ANP) and brain natriuretic peptide (BNP), as cardiac endocrine hormones, act through activating the guanylate cyclase (GC)/cGMP signaling pathway to exert vasodilatory, natriuretic (sodium-excretory), and kaliuretic (potassium-excretory) effects, while inhibiting the renin-angiotensin-aldosterone system (RAAS) and sympathetic activity. In the STZ-induced DM rat model, BNP was compensatorily elevated in plasma and atrial myocardial tissue, accompanied by a decrease in short-axis shortening of cardiomyocytes, suggesting that it may delay the deterioration of cardiac function through a negative feedback mechanism (42). Mid-range atrial natriuretic peptide precursor (MR-proANP) is a mid-range fragment of ANP, and Jensen et al. (43) found that MR-proANP was positively correlated with left atrial volume and LVMI in patients with T2DM complicated with Heart Failure with Preserved Ejection Fraction (HFpEF), this finding provides a new tool for accurate stratification of HFpEF.

N-terminal Pro-Brain Natriuretic Peptide (NT-proBNP), an inactive precursor fragment of BNP, has demonstrated clinical value in the diagnosis of HF superior to BNP because of its long plasma half-life and stability. Malachias et al. (44) found that elevated NT-proBNP levels were significantly and positively associated with all-cause mortality, cardiovascular mortality, and HF in patients with T2DM. The Portuguese Multi-Society Consensus (45) was the first to systematically standardize the clinical use of NT-proBNP in patients with DM, emphasizing routine testing in people over 50 years of age, initiating screening in younger patients based on risk factors, and recommending individualized adjustment of thresholds to provide a practical framework for the early identification of cardiac lesions and the development of therapeutic regimens.

5.3 Fibroblast growth factors

Fibroblast Growth Factors (FGFs), a superfamily of peptide growth factors, are involved in embryonic development, organogenesis, and maintenance of metabolic homeostasis by activating FGF receptor tyrosine kinase activity. FGF-21 is mainly secreted into the bloodstream by the liver, but cardiomyocytes can also synthesize it autocrinally. In the STZ/HFD-induced DM mouse model (46), FGF-21 knockout mice showed a significant increase in myocardial lipid uptake and deposition, and Yang et al. (47) found that FGF21 inhibited oxidative stress and lipid accumulation through the AMPK/AKT/Nrf2 pathway to improve cardiac function in T2DM mice, which provides a new target for DCM intervention. Sørensen et al. (48) analyzed 246 T2DM patients by CMR and found that FGF-23 levels were significantly associated with LVDD and reduced myocardial perfusion. In conclusion, FGF-21/FGF-23 may be a novel molecular marker for the diagnosis and prognosis of DCM.

5.4 Myocardial TG and their intermediate metabolites

In patients with DM, abnormal glucose uptake and hypermetabolism of fatty acids (FAs) lead to abnormal accumulation of myocardial TG and cholesterol. Rijzewijk et al. (49) found that myocardial TG deposition in patients with uncomplicated T2DM was significantly positively correlated with LVDD, and that this correlation was independent of age and BMI. Abnormal accumulation of cardiac TG can produce a toxic metabolic intermediate, ceramide (Cer). Cer protects cell membranes from damage by free FAs, but in excess it induces apoptosis and fibrosis. Studies have shown that Cer levels can independently predict the risk of T2DM and cardiovascular disease (50), but its clinical value as a diagnostic marker for DCM needs further validation.

5.5 G protein-coupled receptor kinase-2

G protein-coupled receptor kinase-2 (GRK2) belongs to the serine/threonine family of protein kinases and is involved in myocardial contraction, angiogenesis, inflammation, and metabolic homeostasis by phosphorylating and regulating the desensitization and internalization of G protein-coupled receptors (GPCRs). Lai et al. (51) observed significant upregulation of GRK2 expression in both myocardial tissue and peripheral blood mononuclear cells in a mouse model of DCM and in DM patients complicated with LVDD. These findings suggest that GRK2 may be a novel molecular marker for the early diagnosis of DCM.

5.6 3-Nitrotyrosine

3-Nitrotyrosine (3-NT), a nitration product of protein tyrosine residues, induces structural and functional changes in proteins and mediates myocardial mitochondrial impairment. STZ-induced T2DM rat model showed a positive correlation between the expression of 3-NT and the number of apoptotic myocytes in myocardial tissues, and treatment with valsartan significantly reversed 3-NT elevation and apoptotic cell death in the diabetic state, suggesting its potential as a diagnostic and therapeutic efficacy assessment marker (52). Jakubiak et al. (53) systematically reviewed the role of 3-NT in diabetic cardiovascular complications, emphasizing its association with myocardial nitrative stress, fibrosis, and diastolic dysfunction, and suggesting that future focus should be on the function of nitration-modified proteins.

6 Non-coding RNA

Non-coding RNA (ncRNA), as an important gene regulatory molecule, is involved in myocardial fibrosis, abnormal energy metabolism, and other pathological processes in DCM through epigenetic and post-transcriptional regulation. A review published by our team in 2024 (54) systematically summarized the research progress of ncRNA in the early diagnosis of DCM, revealing that it can be used as a biomarker reflecting myocardial remodeling and a therapeutic target for intervening in the fibrotic pathway. Future studies will further explore the potential of ncRNA as a molecular marker for DCM.

7 Novel molecular markers

7.1 Endothelin 1

Endothelin 1 (EDN1) is a vasoactive peptide encoded by the EDN1 gene, which exerts biological effects such as vasoconstriction, proliferation/migration-promoting activity, and inflammatory activation by binding to endothelin receptor A/B (ETA/ETB). Hyperglycemia and metabolic disorders are involved in the pathology of DCM through activation of the immune system. Widyantoro et al. (55) showed that knockdown of the EDN1 gene in a mouse model of DM could reverse myocardial fibrosis and improve cardiac function. Guo et al. (56) found that the expression of the EDN1 gene was significantly upregulated in the myocardial tissues of patients with DCM, and the expression level was positively correlated with the degree of macrophage infiltration. Mechanistic studies showed that EDN1 may promote myocardial inflammation by activating the NF-κB pathway, suggesting that EDN1 may serve as a potential biomarker of the immune microenvironment in DCM.

7.2 Skin autofluorescence

As previously mentioned, AGEs have been demonstrated to possess potential as biomarkers for DCM. Skin autofluorescence (SAF), as a non-invasive biomarker reflecting tissue deposition of AGEs, can be quantitatively measured via a dedicated SAF reader. By leveraging the inherent fluorescent properties of AGEs, SAF intensity correlates with their accumulation and facilitates the assessment of disease progression. A Dutch cohort study (57) showed that SAF values were independently associated with cardiovascular risk (CVD) and all-cause mortality in patients with T2DM, with a 2.59-fold increase in the risk of CVD events or death for every 1-unit increase in SAF. A Japanese cross-sectional study (58) found that SAF values were significantly and positively correlated with high-sensitivity cardiac troponin T (hs-cTnT) levels in DM patients. As a non-invasive test, SAF may become a novel tool to replace invasive tests for early identification of DCM.

8 Combined diagnosis

Currently, the combined application of molecular markers has become an important strategy to improve the accuracy of disease diagnosis. By integrating the combined detection of molecular markers and the combined analysis of molecular marker-imaging technique combinations, not only can the molecular pathological mechanisms of the disease be more comprehensively analyzed, but also the diagnostic sensitivity and specificity can be significantly improved, thus enabling early and accurate identification and typing of the disease. The following section describes the potential applications of several molecular markers and their combination with imaging techniques in the diagnosis of DCM, and their key roles in enhancing diagnostic efficacy (see Table 1 for details).

8.1 TNF-α, INS, AGEs and creatinine

Abdelrahman et al. (65) identified a set of biomarkers for detecting cardiac structural and functional changes in early-stage DCM. Among them, a combination of four biomarkers—TNF-α, INS, AGEs, and Creatinine (Cr)—could predict the occurrence of diastolic dysfunction (DD) in patients with T2DM, with a sensitivity of approximately 79% and specificity of 100%. Additionally, a two-biomarker combination (IL-6 and AGEs) differentiated between SD and DD in diabetic patients with a sensitivity of 90.6%. Meanwhile, a three-biomarker panel (TNF-α, IL-6, and AGEs) achieved approximately 85% sensitivity and specificity in distinguishing DCM patients from diabetic patients with normal cardiac function. These biomarkers may serve as predictors for early DCM diagnosis and could aid in developing strategies to prevent HF.

8.2 Lysyl oxidase-like 2 and electron transfer flavoprotein β subunit

Lysyl Oxidase-Like 2 (LOXL2), a key cross-linking enzyme of the LOX family, catalyzes the cross-linking of collagen to elastin in the ECM. LOXL2 activation via the TGF-β/Smad pathway in the diabetic state promotes myocardial fibroblast proliferation and collagen deposition. Zhao et al. (70) found that elevated serum LOXL2 levels promote cardiac fibrosis by enhancing collagen cross-linking, which in turn leads to cardiac contractile dysfunction and LVDD. Electron Transfer Flavoprotein β Subunit (ETFβ), as a key component of the electron transport chain, is involved in the oxidative energy supply of amino acids and fatty acids. Johnson et al. (59) found in a mouse model of DM that elevated serum LOXL2 levels accompanied by decreased levels of ETFβ were significantly correlated with a decrease in LVEF as detected by echocardiography, and that this alteration appeared earlier than the cardiac pathological structural changes.

TABLE 1 Relevant literature and efficacy analysis of biomarker combined diagnosis.

Type of study	Study group and subjects	Detection indicators	Results	Author, country, year.
Animal experimental study	T2DM group (db/db mice); N = 40; Age: 6–16 weeks Control group (db/+ mice); N = 40; Age: 6–16 weeks	LOXL2 and ETFβ	In db/db mice, the combined detection of elevated serum LOXL2 levels and decreased serum ETFβ levels demonstrated superior predictive efficacy (AUC = 0.813), outperforming single indicators alone.	Johnson et al. (59), South Africa, 2020
Review	None	ANGPTL4 and LPL	Maintaining the balance of LPL and ANGPTL4 levels is crucial for preventing DCM lesions, and their combined detection helps in early problem identification.	Puthanveetil et al. (60), Canada, 2015
Cross-sectional study	T2DM group; N = 78; age: 45–65 yr Control group; N = 12; age: 45–65 yr	miR-1, miR-133a	1. The levels of miR-1 and miR-133a were positively correlated with myocardial fat deposition (r = 0.68, p < 0.001). 2. The diagnostic efficacy (AUC = 0.89) of miR-1/miR-133a combined with HbA1c for myocardial fat deposition was significantly higher than that of the single-index.	De Gonzalo - Calvo et al. (61), Spain, 2016
Cross-sectional study	DCM group; N = 49; age: 56.33 ± 8.19 yr; T2DM group; N = 49; age: 53.35 ± 8.29 yr	miR-21, HbA1c, DM duration, and blood lipid levels	Combining miR-21, DM duration, HbA1c%, and blood lipid indices achieves the highest diagnostic efficiency (AUC = 0.939).	Tao et al. (62), China, 2000
Cross-sectional study	DCM group; N = 92; age: 60.18 ± 12.26 yr T2DM group; N = 105; age: 57.50 ± 15.02 yr	Butyric acid and the methylation status of 7 CpG sites in intron 1 of HIF3A	The AUC of combining butyric acid with CpG-6 methylation reached 0.737, which was superior to that of the single-index.	Guo et al. (63), China, 2021
Cross-sectional study	T2DM group; N = 60; age: 45–65 yr Control group; N = 40; age: 45–65 yr	MMPs and TIMPs	In patients with DM complicated with LVDD, the levels of MMP-9 and MMP-7 in plasma were elevated, and the ratio of TIMP-1 to MMP-9 was decreased.	Ban et al. (64), Australia, 2010
Cross-sectional study	DM-DD group; N = 47; age: 45–65 yr Simple DM group; N = 34; age: 45–65 yr	TNF-α, INS, AGEs, Cr	1.INS ≥22.7, TNF-α ≥3.9, AGEs ≥11.6, and Cr ≥1.1 are important predictive factors for distinguishing DM-DD from DM-N. 2.Combined markers (TNF-α + INS + AGEs + Cr) exhibit an AUC of 0.913 and a specificity of 100%.	Abdelrahman et al. (65), Egypt, 2021
Cross-sectional study	DM-DD group; N = 47; age: 45–65 yr DM-SD group; N = 32; age: 45–65 yr	IL-6, AGEs	1. AGEs ≥14.2 and IL-6 ≥6.4 are important predictive factors for distinguishing DM-SD from DM-DD. 2.Combined markers (IL-6 + AGEs) exhibit an AUC of 0.796 and a sensitivity of 90.6%.	Abdelrahman et al. (65), Egypt, 2021
Cross-sectional study	DCM (DM-DD + DM-SD) group; N = 79; age: 45–65 yr DM-N group; N = 34; age: 45–65 yr	TNF-α, IL-6, AGEs	1.TNF-α ≥1.7, AGEs ≥11.4, and IL-6 ≥3.5 are important predictive factors for distinguishing DCM from DM-N. 2. Combined markers (TNF-α + IL-6 + AGEs) exhibit an AUC of 0.924, a sensitivity of 84.8%, and a specificity of 88.2%.	Abdelrahman et al. (65), Egypt, 2021
Cohort study	DM-HF group; N = 385; age: 67.8 ± 10.3 yr Non-DM-HF group; N =	sST2 and hs-cTnT	Combined detection of sST2 and hs-cTnT in plasma improves the diagnostic efficacy of clinical outcomes in HF patients with and without DM (AUC = 0.811) and is significantly superior to single markers.	Alonso et al. (66), Spain, 2016

(Continued)

TABLE 1 Continued

Type of study	Study group and subjects	Detection indicators	Results	Author, country, year.
	684; age: 65.3 ± 14 yr			
Cohort study	DM group; N = 2266; age: average 57 yr Prediabetic group; N = 4533; age: average 57 yr	hs-cTnT, NT-proBNP, hs-CRP, LVH	Based on a simple integer score of hs-cTnT, NT-proBNP, hs-CRP, LVH, it can effectively stratify the heart failure risk in patients with diabetes and prediabetes.	Pandey et al. (67), USA, 2021
Cross-sectional study	DM-mdEF group; N = 14; age: 55.42 ± 8.51 yr DM-pEF group; N = 76; age: 55.25 ± 10.62 yr Control group; N = 31; age: 50.89 ± 9.66 yr	Gal-3 level, GLS	Galectin-3 > 2.71 ng/ml + GLS < -18%: The sensitivity for diagnosing LVDD is 85%, the specificity is 81%, and the negative predictive value (NPV) is 97%, suggesting that combined detection can effectively exclude low-risk populations.	Flores - Ramirez R et al. (68), Mexico, 2017
Cohort study	T1DM patients; N = 960; age: average 48 yr	NT-proBNP, echocardiographic index (E/e')	Patients with NT-proBNP > 300 pg/mL and E/e' > 12 have a cardiovascular risk incidence of 115 cases per 1000 person-years, which is 23 times that of the low-risk group (NT-proBNP < 150 pg/mL and E/e' < 8).	Rørth et al. (69), Denmark, 2020

8.3 Angiopoietin-like 4 and lipoprotein lipase

Angiopoietin-like 4 (ANGPTL4), a metabolic and vascular homeostasis regulatory protein, is involved in TG metabolism mainly through the inhibition of Lipoprotein Lipase (LPL) activity. In a DCM mouse model (71), ANGPTL4 gene expression was significantly upregulated and promoted cardiomyocyte apoptosis through the Focal Adhesion Kinase/Sirtuin 3/Reactive Oxygen Species signaling axis. In addition, the inhibitory effect of ANGPTL4 on LPL is closely associated with lipotoxicity and inflammatory responses in DCM (60), suggesting that maintaining the LPL-ANGPTL4 dynamic balance is critical for cardioprotection in DM.

8.4 MicroRNAs

De Gonzalo-Calvo et al. (61) found a dose-dependent positive correlation between myocardial fat deposition and serum miR-1/miR-133a levels in patients with T2DM and in a mouse model of IR. Tao et al. (62) demonstrated that blood miR-21 combined with HbA1c, the duration of DM and lipid parameters could significantly improve the early diagnosis of DCM by constructing a diagnostic model. These findings provide new evidence for the clinical translation of circulating microRNAs (miRNAs) as biomarkers for DCM.

8.5 Short-chain fatty acids and HIF3A mRNA

Short-chain fatty acids (SCFAs), which are metabolites of dietary fiber fermentation by colonic flora, mainly include acetic acid, propionic acid, and butyric acids. Guo et al. (63) first found that plasma levels of SCFAs were significantly lower in patients with DCM than in patients with T2DM alone, with the most significant difference in butyric acid (BA). The plasma BA level was negatively correlated with Cytosine-phosphate-Guanine-6 (CpG-6) methylation in a dose-dependent manner. This study suggests that the combination of plasma BA level and HIF3A intron 1 CpG-6 methylation status may be a novel combination of molecular markers to distinguish DCM from T2DM alone.

8.6 Matrix metalloproteinases and tissue inhibitors of metalloproteinases

Matrix Metalloproteinases (MMPs), a family of zinc-dependent endopeptidases, are involved in tissue remodeling by degrading ECM proteins. Cardiac fibroblasts maintain the dynamic homeostasis of the ECM through the secretion of MMPs and their inhibitors Tissue Inhibitors of Metalloproteinases (TIMPs). Ban et al. (64) observed an increase in plasma MMP-9/MMP-7 levels along with a decrease in the TIMP-1/MMP-9 ratio in patients with DM complicated with LVDD. These studies suggest that MMPs-TIMPs imbalance may serve as a novel combination of biomarkers for the assessment of diastolic dysfunction.

8.7 Cardiac troponin, NT-proBNP, hs-CRP, electrocardiogram

As a core regulator of myocardial contraction, the cTns consist of three subunits—cardiac troponin I (cTnI), cardiac troponin T (cTnT), and cardiac troponin C (cTnC)—among which cTnI and cTnT serve as highly sensitive markers of myocardial injury. hs-cTnT serves as a highly sensitive assay version of cTnT, enabling

precise identification of small myocardial injuries, and several of the other markers have been mentioned above. In a prospective cohort study, Pandey et al. noted that a combined integer score of hs-cTnT, NT-proBNP, hs-CRP, and electrocardiogram (ECG)-diagnosed left ventricular hypertrophy (LVH, diagnosed by the Sokolow-Lyon criterion) was effective in stratifying the risk of HF in patients with DM and antecedent cardiovascular disease. and identifying those at high risk (scores of ≥3) (67), and that this score is expected to become a clinical tool for identifying the occurrence of HF in DM.

8.8 hs-cTnT and sST2

In a cohort study (66) that included 1069 patients with HF, the investigators categorized them into the HF complicated with DM group and the HF without DM group. The results showed that hs-cTnT and sST2 were the only markers independently associated with both all-cause and cardiovascular death in the DM-HF group, and the combination of the two significantly improved the predictive accuracy.

8.9 Molecular markers combined with imaging markers

Global Longitudinal Strain (GLS) is a quantitative measure of longitudinal contractile function of the LV myocardium assessed by cardiac ultrasound strain imaging, reflecting the overall shortening capacity of the myocardium in the long-axis direction (apical to basal).Flores-Ramírez et al. (68) found that GLS in combination with serum Gal-3 testing could noninvasively screen for subclinical LVDD in patients with asymptomatic DM, with patients with preserved EF having significantly higher Gal-3 levels and lower GLS values compared with patients with DM alone. Rørth et al. (69) followed up 960 T1DM patients with normal EF for 6.3 years, and found that echocardiographic E/E' ratios in conjunction with serum NT-proBNP levels identified a population with very high cardiovascular risk (NT-proBNP >300 pg/mL and E/e'>12) and may provide a low-cost, easily accessible tool for accurate clinical stratification.

9 Conclusion and future perspectives

The European Society of Cardiology (ESC) HF guidelines (72) state that there is a significant evidence gap in the study of the pathogenesis of DM complicated with HF in the population, and there is currently no consensus in the academic community on the etiologic definition of DCM, resulting in a lack of specific clinical diagnostic criteria. Given the high morbidity and mortality of DCM, it is especially critical to establish an accurate early diagnosis system. Early identification can not only accurately assess the myocardial pathological status, but also delay the progression of heart failure through interventions. Recent studies have shown that circulating biomarkers (e.g., sST2, CT-1, galectin-3) correlate well with the pathologic stage of DCM, and their convenience and affordability make them potential diagnostic tools. It is worth noting that combined detection strategies (e.g., LOXL2 + ETFβ, LPL + ANGPTL4) can significantly improve diagnostic specificity, but face limitations such as long testing periods and high costs. Emerging markers such as EDN1 gene methylation and AF provide new ideas for non-invasive diagnosis, but their clinical translation still requires multi-center validation. The current core challenge in the field is: how to translate research results into clinical practice, focusing on when to implement, who will implement, and how to implement. In summary, the search for effective and implementable molecular markers has remained one of the key tasks in the field of DCM for decades.

Author contributions

NS: Writing – original draft. JZ: Writing – review & editing. WZ: Data curation, Writing – review & editing. XZ: Writing – review & editing. KL: Writing – review & editing. YM: Writing – review & editing. YW: Writing – review & editing. MC: Writing – review & editing

Funding

The author(s) declare financial support was received for the research and/or publication of this article. The authors gratefully acknowledge the grant support from the Tai'an Science and Technology Innovation Development Program (2022NS153; 2023NS156).

Conflict of interest

The authors declare that the research was conducted in the absence of any commercial or financial relationships that could be construed as a potential conflict of interest.

Generative AI statement

The author(s) declare that no Generative AI was used in the creation of this manuscript.

Publisher's note

References

1. Teo ZL, Tham YC, Yu M, Chee ML, Rim TH, Cheung N, et al. Global prevalence of diabetic retinopathy and projection of burden through 2045. *Ophthalmology*. (2021) 128:1580–91. doi: 10.1016/j.ophtha.2021.04.027

2. Lorenzo-Almorós A, Tuñón J, Orejas M, Cortés M, Egido J, Lorenzo Ó. Diagnostic approaches for diabetic cardiomyopathy. *Cardiovasc Diabetology*. (2017) 16:28. doi: 10.1186/s12933-017-0506-x

3. Peng C, Zhang Y, Lang X, Zhang Y. Role of mitochondrial metabolic disorder and immune infiltration in diabetic cardiomyopathy: new insights from bioinformatics analysis. *J Transl Med*. (2023) 21:66. doi: 10.1186/s12967-023-03928-8

4. Zhang J, Chen Z, Ma M, He Y. Soluble ST2 in coronary artery disease: clinical biomarkers and treatment guidance. *Front Cardiovasc Med*. (2022) 9:924461. doi: 10.3389/fcvm.2022.924461

5. Fousteris E, Melidonis A, Panoutsopoulos G, Tzirogiannis K, Foussas S, Theodosis-Georgilas A, et al. Toll/interleukin-1 receptor member ST2 exhibits higher soluble levels in type 2 diabetes, especially when accompanied with left ventricular diastolic dysfunction. *Cardiovasc Diabetol*. (2011) 10:101. doi: 10.1186/1475-2840-10-101

6. Song Y, Li F, Xu Y, Liu Y, Wang Y, Han X, et al. Prognostic value of sST2 in patients with heart failure with reduced, mid-range and preserved ejection fraction. *Int J Cardiol*. (2020) 304:95–100. doi: 10.1007/s11426-024-2381-0

7. Luo B, Huang F, Liu Y, Liang Y, Wei Z, Ke H, et al. NLRP3 inflammasome as a molecular marker in diabetic cardiomyopathy. *Front Physiol*. (2017) 8:519. doi: 10.3389/fphys.2017.00519

8. Zhao YK, Wu BW, Li J. Research progress on the mechanism of NLRP3 inflammasome in diabetic cardiomyopathy (DCM). *Fudan Univ J Med Sci*. (2020) 47:117–21 (in Chinese).

9. Ding K, Song C, Hu H, Yin K, Huang H, Tang H. The role of NLRP3 inflammasome in diabetic cardiomyopathy and its therapeutic implications. *Oxid Med Cell Longev*. (2022), 1–19. doi: 10.1155/2022/3790721

10. Dominguez-Rodriguez A, Abreu-Gonzalez P, Avanzas P. Usefulness of growth differentiation factor-15 levels to predict diabetic cardiomyopathy in asymptomatic patients with type 2 diabetes mellitus. *Am J Cardiol*. (2014) 114:890–4. doi: 10.1016/j.amjcard.2014.06.020

11. Eddy AC, Trask AJ. Growth differentiation factor-15 and its role in diabetes and cardiovascular disease. *Cytokine Growth Factor Rev*. (2021) 57:11–8. doi: 10.1016/j.cytogfr.2020.11.002

12. Tsygankova PG, Itkis YS, Krylova TD, Kurkina MV, Bychkov IO, Ilyushkina AA, et al. Plasma FGF-21 and GDF-15 are elevated in different inherited metabolic diseases and are not diagnostic for mitochondrial disorders. *J Inherit Metab Dis*. (2019) 42:918–33. doi: 10.1002/jimd.12142

13. Wu QQ, Liu C, Cai Z, Xie Q, Hu T, Duan M, et al. High-mobility group AT-hook 1 promotes cardiac dysfunction in diabetic cardiomyopathy via autophagy inhibition. *Cell Death Dis*. (2020) 11:160. doi: 10.1038/s41419-020-2316-4

14. Tao A, Song J, Lan T, Xu X, Kvietys P, Kao R, et al. Cardiomyocyte–fibroblast interaction contributes to diabetic cardiomyopathy in mice: role of HMGB1/TLR4/IL-33 axis. *Biochim Biophys Acta BBA - Mol Basis Dis*. (2015) 1852:2075–85. doi: 10.1016/j.bbadis.2015.07.015

15. Wu H, Sheng ZQ, Xie J, Li R, Chen L, Li GN, et al. Reduced HMGB 1-mediated pathway and oxidative stress in resveratrol-treated diabetic mice: a possible mechanism of cardioprotection of resveratrol in diabetes mellitus. *Oxid Med Cell Longev*. (2016) 1):9836860. doi: 10.1155/2016/9836860

16. Wang WK, Lu QH, Wang X, Wang B, Wang J, Gong HP, et al. Ulinastatin attenuates diabetes-induced cardiac dysfunction by the inhibition of inflammation and apoptosis. *Exp Ther Med*. (2017) 14:2497–504. doi: 10.3892/etm.2017.4824

17. Di Rosa M, Malaguarnera L. Chitinase 3 like-1: an emerging molecule involved in diabetes and diabetic complications. *Pathobiology*. (2016) 83:228–42. doi: 10.1159/000444855

18. Deng Y, Li G, Chang D, Su X. YKL-40 as a novel biomarker in cardio-metabolic disorders and inflammatory diseases. *Clin Chim Acta*. (2020) 511:40–6. doi: 10.1016/j.cca.2020.09.035

19. Huang X, Qin Z, Xu M, Zhang F, Jiang X, Hua F, et al. Neutrophil: lymphocyte ratio is positively associated with subclinical diabetic cardiomyopathy. *BMC Endocr Disord*. (2020) 20:99. doi: 10.1186/s12902-020-00571-y

20. Mano Y, Anzai T, Kaneko H, Nagatomo Y, Nagai T, Anzai A, et al. Overexpression of human C-reactive protein exacerbates left ventricular remodeling in diabetic cardiomyopathy. *Circ J*. (2011) 75:1717–27. doi: 10.1253/circj.CJ-10-1199

21. Shaver A, Nichols A, Thompson E, Mallick A, Payne K, Jones C. Role of serum biomarkers in early detection of diabetic cardiomyopathy in the west virginian population. *Int J Med Sci*. (2016) 13:1027–37. doi: 10.7150/ijms.14141

22. Li J, Su S, Zong X. Analysis of the association between adiponectin, adiponectin receptor 1 and diabetic cardiomyopathy. *Exp Ther Med*. (2024) 7:1023–7. doi: 10.3892/etm.2014.1539

23. Battiprolu PK, Lopez-Crisosto C, Wang ZV, Nemchenko A, Lavandero S, Hill JA. Diabetic cardiomyopathy and metabolic remodeling of the heart. *Life Sci*. (2013) 92:609–15. doi: 10.1016/j.lfs.2012.10.011

24. Ruan W, Lai M. Insulin-like growth factor binding protein: a possible marker for the metabolic syndrome? *Acta Diabetol*. (2010) 47:5–14. doi: 10.1007/s00592-009-0142-3

25. Greulich S, Maxhera B, Vandenplas G, de Wiza DH, Smiris K, Mueller H, et al. Secretory products from epicardial adipose tissue of patients with type 2 diabetes mellitus induce cardiomyocyte dysfunction. *Circulation*. (2012) 126:2324–34. doi: 10.1161/CIRCULATIONAHA.111.039586

26. Chen WJ, Greulich S, Smit JW, Romijn JA, Ruige JB, Lammertsma AA, et al. Activin a is associated with impaired myocardial glucose metabolism and left ventricular remodeling in patients with uncomplicated type 2 diabetes. *Cardiovasc Diabetol*. (2013) 12:150. doi: 10.1186/1475-2840-12-150

27. Blumensatt M, Greulich S, de Wiza DH, Mueller H, Maxhera B, Rabelink MJ, et al. Activin A impairs insulin action in cardiomyocytes via up-regulation of miR-143. *Cardiovasc Res*. (2013) 100:201–210. doi: 10.1093/cvr/cvt173

28. Stratton IM, Adler AI, Neil HAW, Matthews DR, Manley SE, Cull CA, et al. Association of glycaemia with macrovascular and microvascular complications of type 2 diabetes (UKPDS 35): prospective observational study. *BMJ (British Med Journal)*. (2000) 321:405–12. doi: 10.1136/bmj.321.7258.405

29. Hegab Z, Gibbons S, Neyses L, Mamas MA. Role of advanced glycation end products in cardiovascular disease. *World J Cardiol*. (2012) 4:90–102. doi: 10.4330/wjc.v4.i4.90

30. Luo J, Yan D, Li S, Liu S, Zeng F, Cheung CW, et al. Allopurinol reduces oxidative stress and activates Nrf2/p62 to attenuate diabetic cardiomyopathy in rats. *J Cell Mol Med*. (2020) 24:1760–73. doi: 10.1111/jcmm.14870

31. Chung JO, Cho DH, Chung DJ, Chung MY. Physiological serum bilirubin concentrations are inversely associated with the prevalence of cardiovascular autonomic neuropathy in patients with Type 2 diabetes. *Diabetes Med*. (2014) 31:185–91. doi: 10.1111/dme.12338

32. Flores-Ramírez R, Azpiri-López JR, González-González JG, Ordaz-Farías A, González-Carrillo LE, Carrizales-Sepúlveda EF, et al. Global longitudinal strain as a biomarker in diabetic cardiomyopathy: a comparative study with galectin-3 in patients with preserved ejection fraction. *Cardiovasc Med*. (2016) 7:189–96. doi: 10.1016/j.acmx.2016.06.002

33. Li Y, Li T, Zhou Z, Xiao Y. Emerging roles of galectin-3 in diabetes and diabetes complications: a snapshot. *Rev Endocr Metab Disord*. (2022) 23:569–77. doi: 10.1007/s11154-021-09704-7

34. Gamella-Pozuelo L, Fuentes-Calvo I, Gómez-Marcos MA, Recio-Rodriguez JI, Agudo-Conde C, Fernández-Martín JL, et al. Plasma cardiotrophin-1 as a marker of hypertension and diabetes-induced target organ damage and cardiovascular risk. *Med (Baltimore)*. (2015) 94:e1218. doi: 10.1097/MD.0000000000001218

35. Hung HC, Lu FH, Ou HY, Wu HT, Wu JS, Yang YC, et al. Increased cardiotrophin-1 in subjects with impaired glucose tolerance and newly diagnosed diabetes. *Int J Cardiol*. (2013) 169:e33–4. doi: 10.1016/j.ijcard.2013.08.112

36. Yue Y, Meng K, Pu Y, Zhang X. Transforming growth factor beta (TGF-β) mediates cardiac fibrosis and induces diabetic cardiomyopathy. *Diabetes Res Clin Pract*. (2017) 133:124–30. doi: 10.1016/j.diabres.2017.08.018

37. Ihm SH, Youn HJ, Shin DI, Jang SW, Park CS, Kim PJ, et al. Serum carboxy-terminal propeptide of type I procollagen (PIP) is a marker of diastolic dysfunction in patients with early type 2 diabetes mellitus. *Int J Cardiol*. (2007) 122:e36–8. doi: 10.1016/j.ijcard.2007.07.057

38. Quilliot D, Alla F, Böhme P, Bruntz JF, Hammadi M, Dousset B, et al. Myocardial collagen turnover in normotensive obese patients: relation to insulin resistance. *Int J Obes*. (2005) 29:1321–8. doi: 10.1038/sj.ijo.0803022

39. Wang X, McLennan SV, Allen TJ, Tsoutsman T, Semsarian C, Twigg SM. Adverse effects of high glucose and free fatty acid on cardiomyocytes are mediated by connective tissue growth factor. *Am J Physiol-Cell Physiol*. (2009) 297:C1490–500. doi: 10.1152/ajpcell.00049.2009

40. Rodríguez-Calvo R, Girona J, Rodríguez M, Samino S, Barroso E, De Gonzalo-Calvo D, et al. Fatty acid binding protein 4 (FABP4) as a potential biomarker reflecting myocardial lipid storage in type 2 diabetes. *Metabolism*. (2019) 96:12–21. doi: 10.1016/j.metabol.2019.04.007

41. Akbal E, Özbek M, Güneş F, Akyürek Ö, Üreten K, Delibaşı T. Serum heart type fatty acid binding protein levels in metabolic syndrome. *Endocrine*. (2009) 36:433–7. doi: 10.1007/s12020-009-9243-6

42. Howarth FC, Shamsi NA, Qaydi MA, Mazrouei MA, Qureshi A, Chandranath SI, et al. Effects of brain natriuretic peptide on contraction and intracellular ca 2+ in ventricular myocytes from the streptozotocin-induced diabetic rat. *Ann N Y Acad Sci*. (2006) 1084:155–65. doi: 10.1196/annals.1372.007

43. Jensen J, Schou M, Kistorp C, Faber J, Hansen TW, Jensen MT, et al. MR-proANP and incident cardiovascular disease in patients with type 2 diabetes with and

without heart failure with preserved ejection fraction. *Cardiovasc Diabetol*. (2020) 19:180. doi: 10.1186/s12933-020-01155-9

44. Malachias MVB, Wijkman MO, Bertoluci MC. NT-proBNP as a predictor of death and cardiovascular events in patients with type 2 diabetes. *Diabetol Metab Syndr*. (2022) 14:64. doi: 10.1186/s13098-022-00837-6

45. Neves JS, Baptista R, Azevedo De Pape E, Rodrigues Pereira M, Paulos R, Pinheiro Dos Santos J, et al. Recommendations for the use of natriuretic peptides for early diagnosis of heart disease in patients with diabetes: a consensus report by SPEDM, SPC, NEDM-SPMI and APMGF. *Rev Port Cardiol*. (2025) 44:57–67. doi: 10.1016/j.repc.2024.07.010

46. Yang H, Feng AY, Lin SD, Yu LC, Lin XF, Yan XQ, et al. Fibroblast growth factor-21 ameliorates diabetic cardiomyopathy via AMPK-mediated antioxidation and lipid-lowering effects in the heart. *Clin Sci (London England: 1979)*. (2017) 131:1421–36. doi: 10.1038/s41419-018-0307-5

47. Yang H, Feng A, Lin S, Yu L, Lin X, Yan X, et al. Fibroblast growth factor-21 prevents diabetic cardiomyopathy via AMPK-mediated antioxidation and lipid-lowering effects in the heart. *Cell Death Dis*. (2008) 9:227. doi: 10.1038/s41419-018-0307-5

48. Sørensen MH, Bojer AS, Jørgensen NR, Broadbent DA, Plein S, Madsen PL, et al. Fibroblast growth factor-23 is associated with imaging markers of diabetic cardiomyopathy and anti-diabetic therapeutics. *Cardiovasc Diabetol*. (2020) 19:158. doi: 10.1186/s12933-020-01135-z

49. Rijzewijk LJ, Diamant M, Bax JJ, Hammer S, Romijn JA, de Roos A, et al. Myocardial steatosis is an independent predictor of diastolic dysfunction in type 2 diabetes mellitus. *J Am Coll Cardiol*. (2008) 52:1793–9. doi: 10.1016/j.jacc.2008.07.062

50. Hilvo M, Vasile VC, Donato LJ, Hurme R, Laaksonen R. Ceramides and ceramide scores: clinical applications for cardiometabolic risk stratification. *Front Endocrinol*. (2020) 11:570628. doi: 10.3389/fendo.2020.570628

51. Lai S, Fu X, Yang S, Zhang S, Lin Q, Zhang M, et al. G protein-coupled receptor kinase-2: A potential biomarker for early diabetic cardiomyopathy. *J Diabetes*. (2020) 12:247–58. doi: 10.1111/1753-0407.12991

52. Zhang YL, Wei JR. 3-Nitrotyrosine, a biomarker for cardiomyocyte apoptosis induced by diabetic cardiomyopathy in a rat model. *Mol Med Rep*. (2013) 8:767–72. doi: 10.3892/mmr.2013.1644

53. Jakubiak GK, Cieślar G, Stanek A. Nitrotyrosine, nitrated lipoproteins, and cardiovascular dysfunction in patients with type 2 diabetes: what do we know and what remains to be explained? *Antioxidants*. (2022) 11:856. doi: 10.3390/antiox11050856

54. Su N, Zhang XH, Wang Y, Lu KN, Cao MF. Value of noncoding RNAs in the early diagnosis of diabetic cardiomyopathy. *J Shandong First Med Univ Shandong Acad Med Sci*. (2024) 45:637–40 (in Chinese).

55. Widyantoro B, Emoto N, Nakayama K, Anggrahini DW, Adiarto S, Iwasa N, et al. Endothelial cell–derived endothelin-1 promotes cardiac fibrosis in diabetic hearts through stimulation of endothelial-to-mesenchymal transition. *Circulation*. (2010) 121:2407–18. doi: 10.1161/CIRCULATIONAHA.110.938217

56. Guo Q, Zhu Q, Zhang T, Qu Q, Cheang I, Liao S, et al. Integrated bioinformatic analysis reveals immune molecular markers and potential drugs for diabetic cardiomyopathy. *Front Endocrinol*. (2022) 13:933635. doi: 10.3389/fendo.2022.933635

57. Boersma HE, Van Waateringe RP, van der Klauw MM, Graaff R, Paterson AD, Smit AJ, et al. Skin autofluorescence predicts new cardiovascular disease and mortality in people with type 2 diabetes. *BMC Endocr Disord*. (2021) 21:14. doi: 10.1186/s12902-020-00676-4

58. Yoshioka K. Skin autofluorescence is associated with high-sensitive cardiac troponin T, a circulating cardiac biomarker, in Japanese patients with diabetes: a cross-sectional study. *Diabetes Vasc Dis Res*. (2018) 15:559–66. doi: 10.1177/1479164118785314

59. Johnson R, Nxele X, Cour M, Sangweni N, Jooste T, Hadebe N, et al. Identification of potential biomarkers for predicting the early onset of diabetic cardiomyopathy in a mouse model. *Sci Rep*. (2020) 10:12352. doi: 10.1038/s41598-020-69254-x

60. Aryal B, Price NL, Suarez Y, Fernández-Hernando C. ANGPTL4 in metabolic and cardiovascular disease. *Trends Mol Med*. (2019) 25:723–34. doi: 10.1016/j.molmed.2019.05.010

61. De Gonzalo-Calvo D, van der Meer RW, Rijzewijk LJ, Smit JWA, Revuelta-Lopez E, Nasarre L, et al. Serum microRNA-1 and microRNA-133a levels reflect myocardial steatosis in uncomplicated type 2 diabetes. *Sci Rep*. (2017) 7:47. doi: 10.1038/s41598-017-00070-6

62. Tao L, Huang X, Xu M, Qin Z, Zhang F, Hua F, et al. Value of circulating miRNA-21 in the diagnosis of subclinical diabetic cardiomyopathy. *Mol Cell Endocrinol*. (2020) 518:110944. doi: 10.1016/j.mce.2020.110944

63. Guo Y, Zou J, Xu X, Zhou H, Sun X, Wu L, et al. Short-chain fatty acids combined with intronic DNA methylation of HIF3A: potential predictors for diabetic cardiomyopathy. *Clin Nutr*. (2021) 40:3708–17. doi: 10.1016/j.clnu.2021.04.007

64. Ban CR, Twigg SM, Franjic B, Brooks BA, Celermajer D, Yue DK, et al. Serum MMP-7 is increased in diabetic renal disease and diabetic diastolic dysfunction. *Diabetes Res Clin Pract*. (2010) 87:335–41. doi: 10.1016/j.diabres.2010.01.004

65. Abdelrahman AH, Salama II, Salama SI, Elmosalami DM, Ibrahim MH, Hassan EM, et al. Role of some serum biomarkers in the early detection of diabetic cardiomyopathy. *Future Sci OA*. (2021) 7:FSO682. doi: 10.2144/fsoa-2020-0184

66. Alonso N, Lupón J, Barallat J, de Antonio M, Domingo M, Zamora E, et al. Impact of diabetes on the predictive value of heart failure biomarkers. *Cardiovasc Diabetol*. (2016) 15:151. doi: 10.1186/s12933-016-0470-x

67. Pandey A, Vaduganathan M, Patel KV, Ayers C, Ballantyne CM, Kosiborod MN, et al. Biomarker-based risk prediction of incident heart failure in pre-diabetes and diabetes. *JACC Heart Fail*. (2021) 9:215–23. doi: 10.1016/j.jchf.2020.10.013

68. Flores-Ramírez R, Azpiri-López JR, González-González JG, Ordaz-Farías A, González-Carrillo LE, Carrizales-Sepúlveda EF, et al. Global longitudinal strain as a biomarker in diabetic cardiomyopathy. A comparative study with gal-3 in patients with preserved ejection fraction. *Arch Cardiol México*. (2017) 87:278–85. doi: 10.1016/j.acmx.2016.06.002

69. Rørth R, Jørgensen PG, Andersen HU, Christoffersen C, Gøtze JP, Køber L, et al. Cardiovascular prognostic value of echocardiography and N-terminal pro B-type natriuretic peptide in type 1 diabetes: the Thousand & 1 study. *Eur J Endocrinol*. (2015) 172:603–12. doi: 10.1530/EJE-19-1015

70. Zhao Y, Tang K, Tianbao X, Wang J, Yang J, Li D. Increased serum lysyl oxidase-like 2 levels correlate with the degree of left atrial fibrosis in patients with atrial fibrillation. *Biosci Rep*. (2017) 37:BSR20171332. doi: 10.1042/BSR20171332

71. Dai L, Xie Y, Zhang W, Zhong X, Wang M, Jiang H, et al. Weighted gene co-expression network analysis identifies ANGPTL4 as a key regulator in diabetic cardiomyopathy via FAK/SIRT3/ROS pathway in cardiomyocyte. *Front Endocrinol*. (2021) 12:705154. doi: 10.3389/fendo.2021.705154

72. Ponikowski P, Voors AA, Anker SD, Bueno H, Cleland JGF, Coats AJS, et al. ESC Guidelines for the diagnosis and treatment of acute and chronic heart failure: The Task Force for the diagnosis and treatment of acute and chronic heart failure of the European Society of Cardiology (ESC)Developed with the special contribution of the Heart Failure Association (HFA) of the ESC. *Eur Heart J*. (2016) 37:2129–200. doi: 10.1002/ejhf.592

frontiers | Frontiers in Endocrinology

TYPE Original Research
PUBLISHED 26 August 2025
DOI 10.3389/fendo.2025.1653927

OPEN ACCESS

EDITED BY
Ramoji Kosuru,
Versiti Blood Research Institute, United States

REVIEWED BY
Angelica Cersosimo,
University of Brescia, Italy
Mate Hajdu,
University of Pécs, Hungary
Narainrit Karuna,
Chiang Mai University, Thailand

*CORRESPONDENCE
Jin Gao
1101158649@qq.com

†These authors have contributed equally to this work

RECEIVED 25 June 2025
ACCEPTED 01 August 2025
PUBLISHED 26 August 2025

CITATION
Peng X, Huo H, Zhao Z, Cai Q, Tian J, Yang D, Song Y, Huang Y, Li Z and Gao J (2025) Impact of glucose metabolism on myocardial fibrosis and inflammation in hypertrophic cardiomyopathy: a cardiac MR study. *Front. Endocrinol.* 16:1653927. doi: 10.3389/fendo.2025.1653927

Impact of glucose metabolism on myocardial fibrosis and inflammation in hypertrophic cardiomyopathy: a cardiac MR study

Xin Peng[1,2†], Huaibi Huo[2†], Zhengkai Zhao[1], Qiuyi Cai[1], Jiangyu Tian[1], Dandan Yang[1], Yao Song[3], Yuheng Huang[4], Zhuoan Li[5] and Jin Gao[1*]

[1]Department of Radiology, The Third People's Hospital of Chengdu, Chengdu, China, [2]Department of Radiology, The First Hospital of China Medical University, Shenyang, China, [3]Department of Radiology, The Fourth Affiliated Hospital of Liaoning University of Traditional Chinese Medicine, Shenyang, China, [4]Department of Radiology and Imaging Sciences, Indiana University School of Medicine, Indianapolis, IN, United States, [5]Weldon school of Biomedical Engineering, Purdue University, West Lafayette, IN, United States

Diabetes mellitus increases the risk of adverse cardiovascular outcomes in hypertrophic cardiomyopathy (HCM) patients. This retrospective study aimed to evaluate myocardial microstructural alterations, particularly fibrosis and subclinical inflammation, in HCM patients across glycemic statuses using multiparametric cardiac magnetic resonance (CMR). Additionally, it explored the correlation between myocardial fibrosis and hemoglobin A1c (HbA1c) levels. 108 HCM patients were stratified by HbA1c levels into non-diabetic (n=38), prediabetic (n=40), and diabetic (n=30) subgroups, along with 30 healthy controls. All participants underwent 3.0-T CMR examination. Compared to non-diabetic HCM patients, prediabetic and diabetic HCM patients exhibited progressively higher mean T1 values and extracellular volume fractions (ECV) ($p < 0.001$). Similar trends were observed in hypertrophic myocardial regions, with diabetes patients showing pronounced fibrosis. Mean ECV exhibited a strong positive correlation with HbA1c levels ($r = 0.634$, $p < 0.001$). In the fully adjusted model, both T1 values and ECV demonstrated significant associations with HbA1c levels. Subclinical myocardial inflammation, as evidenced by elevated T1 and T2 values, was observed in prediabetic and diabetic patients but not in non-diabetic patients. Progression of myocardial fibrosis in HCM is linked to elevated HbA1c, especially in hypertrophied regions, even in prediabetic individuals. Subclinical myocardial inflammation was observed in HCM with glucose metabolism abnormalities. These findings underscore the importance of early glycemic control and the integration of CMR-based tissue characterization into HCM management strategies.

KEYWORDS

hypertrophic cardiomyopathy, HbA1c, cardiac magnetic resonance, myocardial fibrosis, subclinical myocardial inflammation

Introduction

Hypertrophic cardiomyopathy (HCM) is the most common inherited primary cardiomyopathy, with a prevalence of approximately 0.2% in the general population (1, 2). The pathophysiological characteristic of HCM include myocardial fibrosis, myocardial hypertrophy, and cardiac dysfunction, which substantially increase the risks of heart failure, arrhythmias, and sudden cardiac death (3, 4).

Emerging evidence indicates that hyperglycemia may stimulate the proliferation of cardiac fibroblasts and the deposition of myocardial extracellular matrix *in vitro*, thereby inducing myocardial fibrosis (5). Clinical observations have demonstrated a graded increase in myocardial fibrosis severity across three distinct patient groups: non-diabetic, pre-diabetic, and diabetic individuals (6). Particularly in HCM, diabetes mellitus appears to exacerbate myocardial fibrosis, leading to further deterioration of cardiac function (7–11). However, the specific impact of varying degrees of glucose metabolism abnormalities on myocardial microstructure in HCM remains unclear. Additionally, it is uncertain whether subclinical myocardial changes are already present in prediabetic HCM patients and whether these changes worsen with the progression of glucose metabolism abnormalities.

Cardiac magnetic resonance (CMR) imaging is considered the gold standard for assessing cardiac structure and function (12). T1 mapping and extracellular volume fraction (ECV) evaluate diffuse myocardial fibrosis, while T2 mapping detects myocardial edema and inflammation (13, 14). Therefore, multiparametric-CMR, with its high sensitivity and specificity, is capable of identifying early changes in myocardial microstructure.

Given this background, the present study aims to systematically compare myocardial microstructural differences among non-diabetic, prediabetic, and diabetic HCM patients using multiparametric CMR. Furthermore, we explore the relationship between glycated hemoglobin A1c (HbA1c) levels and myocardial fibrosis.

Methods

Ethical approval

This study was approved by the Chengdu Third People's Hospital Ethics Review Board (Ethics number: 2025-S-124). All procedures were performed in accordance with the principles of the Declaration of Helsinki. Due to its retrospective design, informed consent from participants was waived.

Study population

This retrospective study consecutively included 108 HCM patients who were evaluated with CMR imaging at Chengdu Third People's Hospital from June 2020 to July 2024. Based on glucose metabolism status, the HCM patients were divided into three subgroups: Non-diabetic HCM group (n = 38): HbA1c level < 5.7%, prediabetic HCM group (n = 40): 5.7% ≤ HbA1c level < 6.4%, and diabetic HCM group (n = 30): HbA1c level ≥ 6.5% (15). Inclusion criteria for HCM diagnosis were defined as non-dilated left ventricular hypertrophy [left ventricular maximum wall thickness (LVMWT) ≥ 15 mm or LVMWT ≥ 13 mm with a positive family history] identified on CMR (16). Exclusion criteria included: (1) concomitant uncontrolled hypertension; (2) infiltrative cardiomyopathy; (3) persistent atrial fibrillation; (4) congenital heart diseases; (5) history of myocardial infarction or significant coronary artery stenosis (≥50%); (6) poor-quality CMR images or other factors interfering with measurements (Figure 1). A control group (n=30) was selected from a pre-existing database (17, 18), matched by age and sex to the HCM cohort. The control group served primarily as a reference for non-diabetic HCM patients, allowing us to identify myocardial tissue changes associated with HCM independent of metabolic abnormalities. The control group consisted of participants with no history of cardiovascular or metabolic diseases, as confirmed by clinical assessment and medical history.

CMR imaging protocol

All participants underwent 3.0-T CMR (Magnetom Skyra, Siemens Healthcare, Erlangen, Germany) examination, following a standardized protocol that included cine imaging, pre- and post-contrast T1 mapping, T2 mapping, and late gadolinium enhancement (LGE) sequences. Cine imaging: electrocardiogram gated steady-state free precession sequences with three long-axis planes and sequential short-axis slices from the base to the apex of the left ventricle. And the typical imaging parameters were as follows: field of view (FOV) = 340×340 mm^2; slice thickness = 6 mm; flip angle = 52°; time of repetition (TR) = 3.3 ms and time of echo (TE): 1.43 ms. T1 mapping: Modified Look-Locker inversion recovery (MOLLI) sequence was used to acquire short-axis slices at the basal, mid, and apical levels, with additional two- and four-chamber views for apical HCM patients. Images were obtained before and 10–20 minutes after intravenous administration of 0.15 mmol/kg gadolinium-based contrast (gadovist, Bayer Healthcare Pharmaceuticals). The MOLLI acquisition before contrast agent administration followed the 5(3)3 protocol during a breath hold. MOLLI images acquired after contrast agent administration followed the 4(1)3(1)2 protocol during a breath hold (19, 20). And the typical imaging parameters were as follows: FOV = 340×340 mm^2; slice thickness = 8 mm; 7/8 phase partial Fourier acquisition; flip angle = 35°; TR = 354.77 ms and TE = 1.15 ms. T2 mapping: Balanced steady-state free precession (bSSFP) sequence with T2 preparation (21). And the following imaging parameters: FOV = 340×340 mm^2; slice thickness = 8 mm; 6/8 phase partial Fourier acquisition; flip angle = 12°; TR = 242.95 ms and TE = 1.49 ms. LGE imaging: Phase-sensitive inversion recovery (PSIR) sequences were acquired 10 minutes after contrast injection to evaluate myocardial fibrosis (22). Imaging was performed in four-chamber, two-chamber, and short-axis views. The inversion time was individually adjusted to null the myocardium signal.

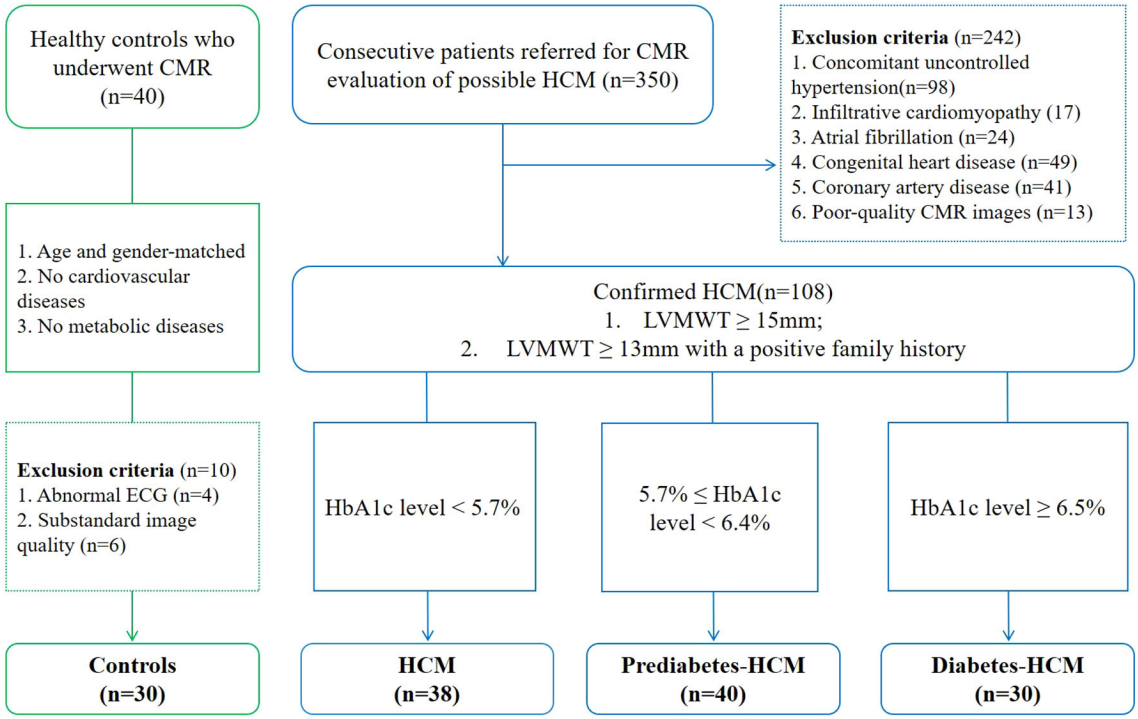

FIGURE 1
Subject flowchart. The flowchart shows the involvement of patients and controls. *CMR*, cardiac magnetic resonance; *ECG*, electrocardiogram; *HCM*, hypertrophic cardiomyopathy.

CMR data analysis

Two independent radiologists (X.P. with >6 years of experience and J.G. with >15 years of experience) analyzed sequentially numbered CMR data in a blinded manner using Medis Suite MR software (QMass and QStrain, Leiden, The Netherlands).

The endocardial and epicardial borders of the left ventricle were manually delineated on cine images to quantify left ventricular mass, volume, and ejection fraction. LVMWT was defined as the greatest linear dimension at any site within the LV myocardium. Global longitudinal strain (GLS), global radial strain (GRS), and global circumferential strain (GCS) in LV were assessed using QStrain. Strain parameters were expressed as negative (shortening) or positive (thickening) values, reflecting deformation in longitudinal, radial, or circumferential directions.

The LV myocardial T1 values and ECV were quantified using the American Heart Association 16-segment model, with measurements averaged from the basal, mid, and apical slices. Hematocrit level, obtained from venous blood samples collected within 24 hours of CMR examination, was used to calculate individual ECV (23). We further analyzed the T1 values and ECV of hypertrophic and remote myocardial regions. ΔT1 and ΔECV were calculated as the differences between the T1 and ECV values of hypertrophic and remote regions. The ΔT1 ratio was defined as the ratio of ΔT1 to the mean T1 values of remote normal regions, and the ΔECV ratio was defined as the ratio of ΔECV to the ECV of remote normal regions (Figure 2). And the definition of ΔT2 ratio follows a similar pattern. LGE was semiautomatically quantified by using the fullwidth half-maximum method with manual correction by using QMass (Medis Medical Imaging). Any obvious blood pool or pericardial partial volume artifacts were manually corrected.

Statistical analysis

Continuous data were expressed as mean ± standard deviation (SD) or median (interquartile range [IQR]), while categorical data were presented as counts with corresponding percentages. Normality was assessed using the Shapiro-Wilk test and homogeneity of variances verified with Levene's test. For normally distributed continuous variables, comparisons were conducted using one-way analysis of variance (ANOVA) followed by Tukey's honestly significant difference (HSD) *post hoc* test, whereas the Kruskal–Wallis rank-sum test with Dunn-Bonferroni *post hoc* correction was employed for non-normally distributed variables, while categorical variables were compared using the Chi-square or Fisher's exact test (when expected frequencies <5). The relationship between HbA1c levels and primary CMR findings was evaluated using Pearson or Spearman's rank correlation methods. Multiple linear regression models were employed to estimate associations of CMR tissue characterization metrics with HbA1c levels. Multivariable adjustment was performed using a systematic covariate selection strategy incorporating three components: (1) clinically established demographic and metabolic confounders (age, sex, and body mass index (BMI)); (2) variables showing significant associations in univariate analyses (P<0.10), including

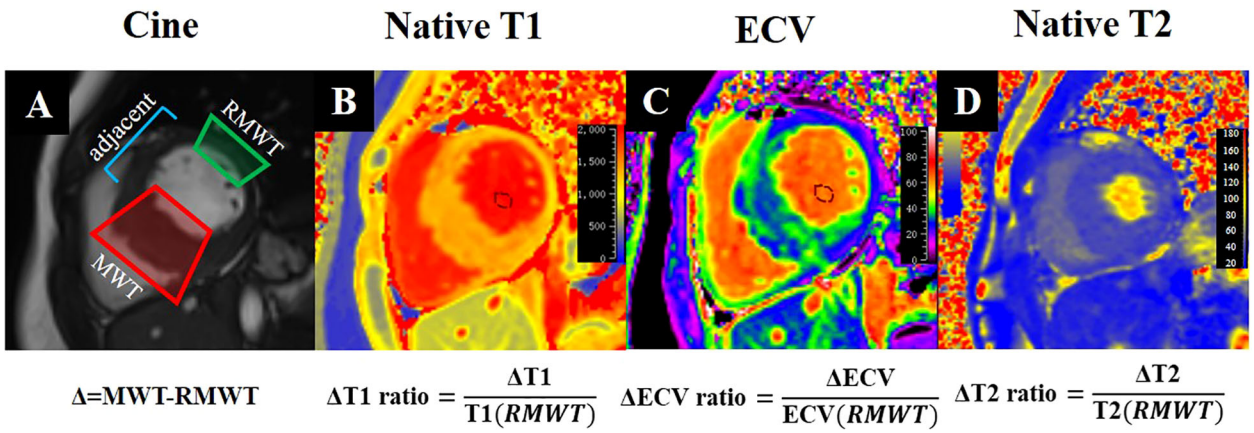

FIGURE 2
CMR tissue characterization in a 52-year-old diabetic male with interventricular septal HCM shows cine **(A)**, Native T1 **(B)**, ECV **(C)**, and Native T2 **(D)** imaging. The formulas beneath **(A)** define Δ as the difference between the MWT and RMWT regions. The formulas below **(B–D)** calculate the ΔT1, ΔECV, and ΔT2 ratios, enabling comprehensive quantitative assessment of myocardial tissue properties. *ECV*, extracellular volume; *MWT*, maximal wall thickness; *RMWT*, remote normal myocardial regions of MWT.

hypertension; and (3) HCM-specific structural parameters (left ventricular mass index, maximal wall thickness) with established prognostic relevance in disease pathophysiology. Statistical analysis was performed by using SPSS software (IBM SPSS Statistics 25.0, Armonk, New York, USA) and GraphPad Prism (version 8.0; GraphPad Software, San Diego, California, USA). All tests were two-tailed test, and a p value <0.05 was used to determine statistical significance.

Results

General characteristics and cardiac functional parameters

The baseline characteristics of the participants are summarized in Table 1. There were no significant differences in age (p=0.416), sex (p=0.372), or BMI (p=0.07) among the four groups. Similarly, no significant differences were observed in conventional cardiovascular risk factors (smoking, drinking, hypertension, and dyslipidemia) across the HCM subgroups. Demographic and clinical information were collected from medical records. Most diabetic HCM patients (80%, 24 of 30) were treated with non-insulin medications, mainly metformin (43%, 13 of 30), and only 20% (6 of 30) of the patients were treated with insulin.

The CMR findings are presented in Table 2. Compared to healthy controls, all HCM groups exhibited increased left ventricular mass index (LVMi), but no significant differences were found among the HCM subgroups. Diabetic HCM patients demonstrated significantly reduced left ventricular end-diastolic volume index (LVEDVi) and end-systolic volume index (LVESVi) compared to non-diabetic HCM patients. HCM patients exhibited significantly reduced LVGRS and LVGLS compared to healthy controls. Furthermore, as the severity of glucose metabolism abnormalities increased (from non-diabetic to prediabetic and diabetic states), there was a progressive decline in LVGRS (62.7 ± 7.5% vs. 50.2 ± 5.5% vs. 43.4 ± 6.2%, $p < 0.001$) and LVGLS (-23.2 ± 2.6% vs. -20.5 ± 3.6% vs. -18.1 ± 3.6%, $p < 0.001$) among HCM subgroups.

Myocardial tissue characterization via CMR

CMR tissue characterization results are shown in Table 3. The presence of LGE showed no significant differences among the HCM subgroups. The mean T1 values and ECV for HCM were greater than those of the healthy participants. Among the HCM subgroups, both mean T1 values and ECV increased progressively with worsening glycemic status (T1: 1223 ± 20 ms vs. 1241 ± 34 ms vs. 1263 ± 36 ms, $p < 0.001$; ECV: 28.5 ± 1.5% vs. 30.1 ± 2.4% vs. 32.1 ± 1.7%, $p < 0.001$), and a similar trend was observed in the hypertrophic myocardial regions. However, in the remote normal myocardial regions of hypertrophied segments, significant differences in T1 values and ECV were observed only between the diabetic and non-diabetic groups. Furthermore, compared to non-diabetic patients, the diabetic group demonstrated significantly higher ΔT1 ratio (0.72 ± 0.27 vs. 0.46 ± 0.22, $p < 0.001$) and ΔECV ratio (0.25 ± 0.14 vs. 0.16 ± 0.07, p < 0.001) in hypertrophic myocardial regions, while ΔT2 ratio showed no difference (Figure 3). The mean myocardial T2 values were significantly higher in prediabetic (40.0 ± 1.5 ms) and diabetic HCM patients (40.3 ± 1.8 ms) compared to healthy controls (38.9 ± 1.0 ms, $p < 0.001$), while non-diabetic HCM patients showed no significant difference.

Correlation between myocardial fibrosis and HbA1c levels

The correlation analysis demonstrated a strong positive association between mean ECV and HbA1c levels (r = 0.634, $p <$

TABLE 1 Baseline clinical characteristics.

Variables	HCM (n=38)	Prediabetes-HCM (n=40)	Diabetes-HCM (n=30)	Healthy controls (n=30)	*P* value
Age (years)	59 ± 12	58 ± 10	60 ± 9	56 ± 9	0.416
Male, n(%)	27(71.1)	21(52.5)	17(56.6)	19(63.3)	0.372
BMI (kg/m^2)	24.5 ± 3.5	25.4 ± 3.4	25.4 ± 3.5	23.4 ± 3.7	0.07
Heart rate (bpm)	68 ± 11	71 ± 14	73 ± 12	70 ± 11	0.456
Family history of HCM, n (%)	2(5.3)	1(2.5)	0(0.0)	-	0.631
Smoking, n(%)	17(44.7)	14(35.0)	11(36.6)	13(43.3)	0.789
Drinking, n(%)	13(34.2)	13(32.5)	8(26.6)	9(30.0)	0.918
Hypertension, n(%)	20(52.6)	21(52.5)	17(56.6)	0(0.0)*†‡	**<0.001**
Dyslipidemia, n(%)	10(26.3)	8(20.0)	8(26.6)	2(6.6)	0.168
HbA1c (%)	5.2 ± 0.3	6.0 ± 0.2*	7.7 ± 1.7*†	5.1 ± 0.4†‡	**<0.001**
Duration of diabetes	-	-	5.6 ± 5.8	-	-
TC (mmol/liter)	4.5 ± 1.1	4.2 ± 1.1	4.7 ± 2.2	4.5 ± 1.2	0.631
TG (mmol/liter)	2.0 ± 1.7	1.7 ± 1.1	1.7 ± 1.1	1.3 ± 0.6	0.157
LDL-C (mmol/liter)	2.6 ± 0.8	2.5 ± 0.9	2.5 ± 0.9	2.6 ± 0.7	0.901
HDL-C (mmol/liter)	1.3 ± 0.3	1.4 ± 0.4	1.3 ± 0.3	1.3 ± 0.4	0.373
Detectable hs-CRP (≥0.8 mg/L), n (%)	11(28.9)	17(42.5)	13(43.3)	10(33.3)	0.289
hs-CRP (mg/L), median (IQR)	1.9(1.2-4.1)	2.0(1.4-4.6)	4.2(2.3-7.2)	2.1(1.2-3.1)	0.126
hs-cTnT (ng/L)	16.6(8.2-23.3)	13.4(9.4-32.5)	16.2(10.8-41.7)	-	0.377
Medical therapy					
Beta-blockers, n(%)	29(76.3)	27(67.5)	24(80.0)	-	0.461
Calcium-channel blockers, n(%)	7(18.4)	10(25.0)	10(33.3)	-	0.370
ACEI/ARB, n(%)	14(36.8)	23(57.5)	17(56.7)	-	0.131
Statin, n(%)	25(65.8)	31(77.5)	21(70.0)	-	0.512
Metformin, n(%)	-	-	13(43.3)	-	-
SGLT2 inhibitor, n(%)	-	-	12(40.0)	-	-
Sulfonylurea, n(%)	-	-	4(13.3)	-	-
Acarbose, n(%)	-	-	6(20.0)	-	-
Insulin, n(%)	-	-	6(20.0)	-	-

Data are reported as mean ± SD or n (%) as appropriate.
Bold indicates *P* value <0.05. **P* <0.05 vs. HCM; †*P* <0.05 vs. Prediabetes-HCM; ‡*P* <0.05 vs. Diabetes-HCM.
BMI, Body mass index; *TC*, Total Cholesterol; *TG*, Triglycerides; *LDL-C*, Low-Density Lipoprotein Cholesterol; *HDL-C*, High-Density Lipoprotein Cholesterol; *hs-CRP*, Hypersensitive C-reactive protein; *hs-cTnT*, high-sensitivity cardiac troponin T; *ACEI/ARB*, angiotensin-converting enzyme inhibitor or angiotensin receptor blocker; *SGLT2*, sodiumdependent glucose transporters 2.

0.001). Moderate correlations were also observed between HbA1c and mean T1 values, as well as T1 values and ECV at maximal wall thickness (r= 0.535, 0.587, and 0.564 respectively, all $p < 0.001$) (Figure 4), indicating that higher HbA1c is associated with greater myocardial fibrosis.

In the fully adjusted model (adjusted for age, sex, BMI, hypertension, left ventricular mass index and maximal wall thickness), both T1 values and ECV demonstrated persistent and significant associations with HbA1c levels ($p < 0.001$) (Table 4).

Discussion

By investigating the role of CMR characterization in assessing the impact of glycemic states on myocardial microstructure in HCM patients, we demonstrated that: (a) A progressive increase in left ventricular myocardial fibrosis, as assessed by T1 values and ECV, with worsening glucose metabolism abnormalities from non-diabetic to prediabetic and diabetic states. Notably, fibrotic changes in the remote regions of hypertrophied myocardium exhibited

TABLE 2 CMR-Based cardiac function parameters.

Variables	HCM (n=38)	Prediabetes-HCM (n=40)	Diabetes-HCM (n=30)	Healthy Controls (n=30)	*P* value
LVMWT (mm)	17.7 ± 3.8	17.4 ± 3.3	17.2 ± 3.9	-	0.873
LVOT obstruction, n(%)	6(16)	14(35)	10(33)	-	0.121
LV mass (g)	118.6 ± 43.01	120.0 ± 47.4	110.98 ± 39.0	72.0 ± 15.3*†‡	**<0.001**
LV mass index (g/m^2)	68.4 ± 24.3	70.7 ± 25.8	65.0 ± 20.3	41.8 ± 6.4*†‡	**<0.001**
LVEDVi (ml/m^2)	68.2 ± 17.1	66.3 ± 15.4	57.3 ± 12.3*	66.6 ± 11.1	**0.014**
LVESVi (ml/m^2)	25.0 ± 7.5	24.5 ± 9.5	19.7 ± 5.4*†	25.2 ± 5.1‡	**0.010**
LVSVi (ml/m^2)	43.2 ± 10.9	42.0 ± 8.3	37.6 ± 8.8	41.4 ± 7.4	0.076
LVEF (%)	63.8 ± 5.5	63.9 ± 7.0	65.6 ± 5.9	62.2 ± 4.0‡	0.183
LVCOi l/(min*m^2)	2.9 ± 0.8	2.9 ± 0.8	2.7 ± 0.7	2.9 ± 0.5	0.637
LVGRS (%)	62.7 ± 7.5	50.2 ± 5.5*	43.4 ± 6.2*†	80.1 ± 6.7*†‡	**<0.001**
LVGCS (%)	-23.4 ± 3.9	-23.1 ± 4.7	-24.5 ± 4.8	-24.2 ± 2.6	0.468
LVGLS (%)	-23.2 ± 2.6	-20.5 ± 3.6*	-18.1 ± 3.6*†	-26.6 ± 1.7*†‡	**<0.001**

Data are reported as mean ± SD or n (%) as appropriate.
Bold indicates *P* value <0.05. **P* <0.05 vs. HCM; †*P* <0.05 vs. Prediabetes-HCM; ‡*P* <0.05 vs. Diabetes-HCM.
CMR, cardiac magnetic resonance; *LV*, left ventricular; *LVMWT*, LV maximal wall thickness; *LVOT*, LV outflow tract; *LVEDVi*, LV end-diastolic volume index; *LVESVi*, LV end-systolic volume index; *LVSVi*, LV stroke volume index; *LVEF*, LV ejection fraction; *LVCOi*, LV cardiac output index; *LVGRS*, LV global radial strain; *LVGCS*, LV global circumferential strain; *LVGLS*, LV global longitudinal strain.

TABLE 3 Myocardial tissue characterization with CMR.

Variables	HCM (n=38)	Prediabetes-HCM (n=40)	Diabetes-HCM (n=30)	Healthy Controls (n=30)	*P* value
Presence of LGE, n (%)	33(87)	34(85)	27(90)	-	0.822
LGE (%LV)	3.4(1.1-9.4)	5.0(1.5-18.3)	5.0(1.6-13.5)	-	0.420
LV blood T1 (ms)	1774 ± 134	1735 ± 174	1780 ± 150	1749 ± 117	0.291
RV blood T1 (ms)	1664 ± 116	1631 ± 167	1684 ± 146	1615 ± 122	0.197
T1 values-mean (ms)	1223 ± 20	1241 ± 34*	1263 ± 36*†	1187 ± 14*†‡	**<0.001**
T1 values-MWT (ms)	1240 ± 17	1268 ± 42*	1296 ± 47*†	1187 ± 14*†‡	**<0.001**
T1 values-RMWT (ms)	1186 ± 26	1197 ± 30	1210 ± 30*	1187 ± 14‡	**0.001**
ΔT1 ratio	0.463 ± 0.216	0.599 ± 0.262	0.717 ± 0.273*	-	**<0.001**
Hematocrit (%)	43.3 ± 5.0	42.2 ± 4.9	41.8 ± 5.4	42.9 ± 4.6	0.602
ECV-mean (%)	28.5 ± 1.5	30.1 ± 2.4*	32.1 ± 1.7*†	26.5 ± 2.7*†‡	**<0.001**
ECV-MWT (%)	30.7 ± 2.1	32.8 ± 3.9*	35.9 ± 3.5*†	26.5 ± 2.7*†‡	**<0.001**
ECV-RMWT (%)	26.3 ± 1.7	26.7 ± 2.1	28.8 ± 1.6*†	26.5 ± 2.7‡	**<0.001**
ΔECV ratio	0.164 ± 0.073	0.233 ± 0.191	0.248 ± 0.143*		**0.006**
T2 values-mean (ms)	39.6 ± 1.4	40.0 ± 1.5	40.3 ± 1.8	38.9 ± 1.0†‡	**0.002**
T2 values-MWT (ms)	39.8 ± 1.4	40.2 ± 1.6	40.6 ± 1.8	38.9 ± 1.0*†‡	**<0.001**
T2 values-RMWT (ms)	39.6 ± 1.3	39.9 ± 1.6	40.4 ± 1.5	38.9 ± 1.0†‡	**0.005**
ΔT2 ratio	0.006 ± 0.112	0.009 ± 0.121	0.125 ± 0.143	-	0.149

Data are reported as mean ± SD, median (IQR), or n (%) as appropriate.
Bold indicates *P* value <0.05. **P* <0.05 vs. HCM; †*P* <0.05 vs. Prediabetes-HCM; ‡*P* <0.05 vs. Diabetes-HCM.
LGE, late gadolinium enhancement; *RV*, right ventricular; *MWT*, maximal wall thickness; *RMWT*, remote normal myocardial regions of MWT; *ECV*, extracellular matrix volume fraction.

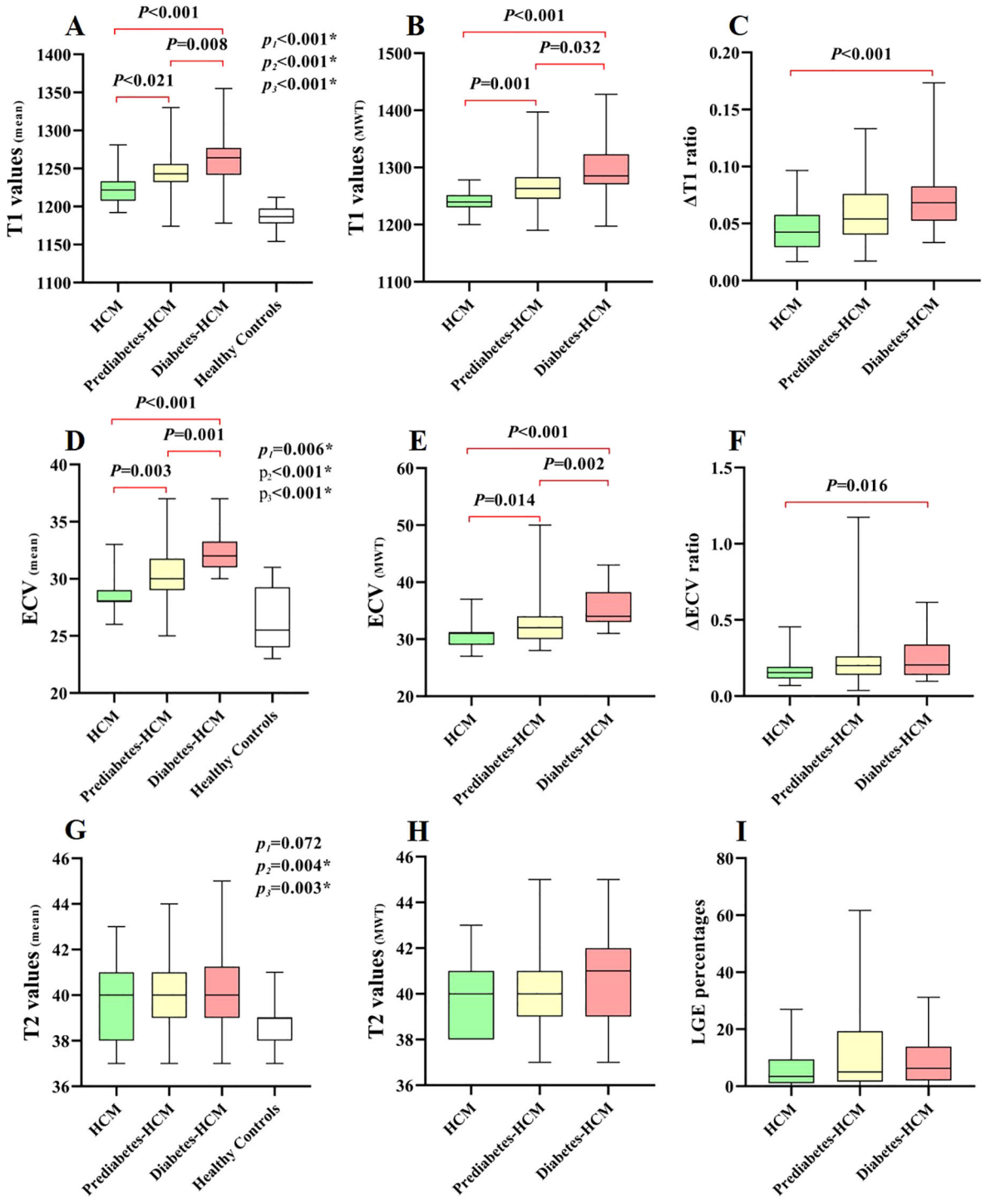

FIGURE 3
Box-whisker plots of different cardiac CMR parameters in HCM patients and healthy controls. P1, P2, and P3 denote comparisons between: 1) P1: HCM vs Healthy Controls; 2) P2: Prediabetes-HCM vs Healthy Controls; 3) P3: Diabetes-HCM vs Healthy Controls. The horizontal lines denote the 5th to 95th percentiles, the shaded boxes depict the first to third quartiles, and the central lines represent the median values. The plots demonstrate the differences in T1-related **(A–C)**, ECV-related **(D–F)**, T2-related **(G, H)** parameters, and LGE percentages **(I)** among different HCM subgroups and/or healthy controls. *LGE*, late gadolinium enhancement. * p value <0.05.

significant differences solely between diabetic and non-diabetic patients. In addition, diabetic HCM patients showed a greater fibrosis burden in hypertrophic myocardial regions compared to remote regions; (b) Subclinical myocardial inflammation, indicated by elevated T1 and T2 values, was observed in prediabetes-HCM and diabetes-HCM patients but not in non-diabetic HCM patients; (c) Glycemic abnormalities are associated with further deterioration of myocardial deformation.

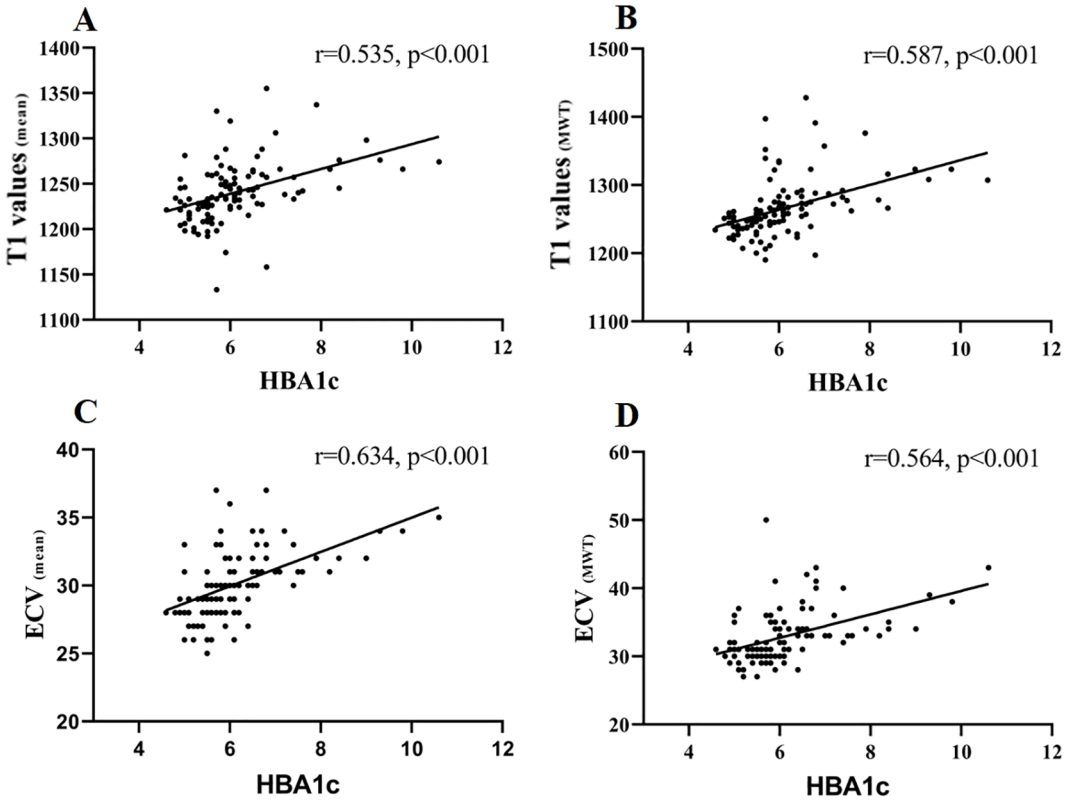

FIGURE 4
Correlation of T1 values (mean), T1 values (MWT), ECV (mean), and ECV (MWT) with HBA1c. Spearman's correlations were **(A)** T1 values (mean) and HBA1c: r = 0.535, p < 0.001; **(B)** T1 values (MWT) and HBA1c: r = 0.587, p < 0.001; **(C)** ECV (mean) and HBA1c: r = 0.634, p < 0.001; **(D)** ECV (MWT) and HBA1c: r = 0.564, p < 0.001.

Myocardial fibrosis and its correlation with HbA1c levels

Myocardial fibrosis is a hallmark pathological feature in HCM, contributing to adverse cardiovascular event (24–27). Previous research evidence has established a potential dose-response relationship between myocardial fibrosis and plasma glucose levels (6), while compelling clinical data further demonstrate that diabetes mellitus significantly exacerbates myocardial fibrosis progression in HCM patients (10, 11). Our findings corroborate previous observations, revealing a graded progression of myocardial fibrosis, as evidenced by elevated T1 values and ECV, across the spectrum from non-diabetic to prediabetic and diabetic HCM patients. Even after adjusting for multiple potential confounders, HbA1c levels remain an independent determinant of myocardial fibrosis. However, the absence of significant differences in LGE among HCM subgroups, suggests that the observed fibrotic changes might represent subtle and diffuse expansion of the extracellular matrix at an early stage, rather than irreversible myocardial focal scarring detectable by LGE (28).

Interestingly, the study appears to indicate that, compared to the non-diabetic group, diabetic group exhibited significantly elevated fibrosis not only in hypertrophied myocardial segments but also in remote regions, whereas the prediabetic group showed no notable difference in fibrosis in remote areas compared to the non-diabetic group. Furthermore, the substantial elevation of ΔT1 and ΔECV ratios in diabetic HCM patients highlights that hypertrophied myocardial regions bear a disproportionately higher burden of fibrosis. This indicates that diabetes not only amplifies fibrosis in regions already burdened by hypertrophy but also drives diffuse myocardial remodeling throughout the left ventricle in HCM. The underlying mechanisms may be attributed to hyperglycemia, which induces diffuse myocardial fibrosis in HCM patients through multiple pathways, including oxidative stress, pro-inflammatory state, growth factor secretion, neurohumoral activation, deposition of advanced glycation end-products, and activation of the renin-angiotensin-aldosterone system (29). Hyperglycemia increases reactive oxygen species, activating profibrotic signals like TGF-β and promoting fibroblast activity. AGEs accumulation further stimulates inflammation and fibrosis. RAAS activation contributes to vasoconstriction and myocardial remodeling. Together, these processes drive diffuse fibrosis, especially in hypertrophied myocardium with microvascular dysfunction (30). Additionally, hypertrophied myocardial regions in HCM exhibit more severe microvascular dysfunction and low-grade inflammation compared to remote regions (31). Hyperglycemia exacerbates endothelial dysfunction in the microvasculature (10), leading to impaired vasodilation and

TABLE 4 Associations between CMR tissue characterization metrics and HBA1c.

CMR metrics	Model 1			Model 2			Model 3		
	β (95% CI)	Standardizes *β*	*P* value	*β (95% CI)*	Standardizes *β*	*P* value	*β (95% CI)*	Standardizes *β*	*P* value
T1 values (mean)	11.673 (7.301-16.046)	0.460	**<0.001**	11.714 (7.310-16.119)	0.462	**<0.001**	11.710 (7.329-16.091)	0.461	**<0.001**
T1 values (MWT)	13.907 (8.366-19.449)	0.440	**<0.001**	13.957 (8.374-19.540)	0.441	**<0.001**	14.187 (8.625-19.750)	0.448	**<0.001**
ECV values (mean)	0.860 (0.553-1.167)	0.482	**<0.001**	0.882 (0.578-1.186)	0.494	**<0.001**	0.887 (0.581-1.193)	0.497	**<0.001**
ECV (MWT)	1.100 (0.586-1.613)	0.389	**<0.001**	1.117 (0.602-1.632)	0.395	**<0.001**	1.092 (0.582-1.602)	0.386	**<0.001**
T2 values (mean)	0.052 (-0.178-0.281)	0.044	0.655	0.049 (-0.182-0.280)	0.042	0.673	0.078 (-0.154-0.309)	0.066	0.506
T2 values (MWT)	0.128 (-0.106-0.362)	0.106	0.280	0.124 (-0.112-0.359)	0.103	0.299	0.147 (-0.089-0.384)	0.122	0.220

Results are the association of CMR tissue characterization metrics with HBA1c from linear regression model, expressed as their corresponding 95% CIs, *P* values, and standardized beta coefficients. Model 1: age, male, and BMI; Model 2: Model 1+ hypertension; Model 3: Model 2+ LVMWT, and LV mass index.

further reduction in blood perfusion, which consequently aggravates fibrosis in the hypertrophied myocardial regions.

The observed positive correlation between the severity of myocardial fibrosis, as measured by T1 values and ECV, and HbA1c levels suggests that the prediabetic stage may accelerate the progression of myocardial fibrosis in HCM patients. This association may be attributed to hyperglycemia-induced proliferation of cardiac fibroblasts and an increase in extracellular matrix production (5, 32).

Subclinical myocardial inflammation and its clinical implications

In a study of 674 HCM patients, Xu et al. demonstrated significantly elevated T2 values (33), potentially attributed to myocardial inflammatory cell infiltration and microvascular dysfunction (34, 35). In contrast, we did not observe a significant increase in T2 values in our cohort of non-diabetic HCM patients. This discrepancy may be explained by the relatively small sample size of 38 cases in our study, which could reduce statistical power and increase the likelihood of random variability and uncertainty.

However, our study revealed that prediabetic and diabetic HCM patients exhibited subclinical myocardial inflammation, as evidenced by significantly elevated T1 and T2 values compared to healthy controls. Furthermore, diabetes itself has been shown to activate myocardial inflammatory processes through mechanisms such as hyperglycemia-induced oxidative stress and cytokine release (36, 37), and the coexistence of diabetes and HCM may synergistically exacerbate myocardial inflammatory responses, potentially due to the combined effects of microvascular dysfunction in HCM and the pro-inflammatory environment induced by hyperglycemia.

Based on our findings of the additive effects of HCM and hyperglycemia on myocardial inflammation, we hypothesize that glucose metabolism abnormalities exacerbate myocardial inflammatory cell infiltration in HCM patients, leading to myocardial inflammation. This hypothesis is supported by the elevated T1 and T2 values observed in our cohort, which are indicative of tissue inflammation. However, this mechanism requires further validation through histological studies or myocardial biopsy.

Although CRP and hs-cTnT levels did not differ significantly across groups, differences in CMR parameters were observed, suggesting that CMR may be more sensitive than conventional biomarkers in detecting subtle myocardial changes associated with glycemic dysregulation at an early stage.

Impaired myocardial strain with glycemic abnormalities

Hajdu et al. (38) reported that in patients with type 1 diabetes mellitus, current HbA1c levels remained an independent predictor of impaired GLS and GCS, even after adjustment for age and hypertension. Similarly, other studies have demonstrated that diabetic patients exhibit early subclinical myocardial dysfunction, often reflected in reduced strain values, even in the absence of overt structural heart disease (39–41). Studies have shown that both HCM and diabetic patients can experience varying degrees of impaired myocardial deformation. In line with these findings, our results demonstrated a progressive decline in GRS and GLS from non-diabetic to prediabetic and diabetic HCM patients, revealing subclinical left ventricular dysfunction. The observation that strain impairment is already evident in prediabetic HCM patients further supports the hypothesis that metabolic dysregulation, particularly

glucose abnormalities, plays a critical role in exacerbating myocardial dysfunction in HCM. This decline is likely associated with increased myocardial fibrosis and inflammation (42, 43), as reported in both diabetic cardiomyopathy and advanced HCM phenotypes.

Clinical implications

This study highlights the clinical importance of glycemic assessment in HCM patients. The association between worsening glycemic status and myocardial remodeling suggests that even prediabetes may contribute to subclinical dysfunction. Early metabolic screening and multiparametric CMR can aid in risk stratification and guide timely interventions, such as lifestyle or metabolic therapy, to slow disease progression and improve outcomes.

Limitations

Our study has several limitations. First, as a retrospective single-center study with a relatively modest sample size, our analysis may have been underpowered to detect clinically relevant but subtle differences, particularly in subgroup comparisons. The inherent constraints of retrospective designs - including potential selection bias (e.g., possible overrepresentation of more severe cases at our tertiary referral center), unmeasured confounders (such as temporal variations in clinical management protocols), and incomplete medication adherence data - limit causal inference. Although no significant LGE differences were observed among glycemic subgroups, this negative finding may reflect limited statistical power for subgroup analyses rather than true biological equivalence, especially given the potential influence of glucose-lowering agents (e.g., GLP-1 receptor agonists or SGLT2 inhibitors) on myocardial remodeling that was not fully accounted for. Second, the presence of subclinical myocardial inflammation was inferred from T1 and T2 mapping rather than being confirmed by myocardial biopsy. Third, we only performed CMR assessments at a single time point, precluding the evaluation of dynamic changes in myocardial microstructure. Therefore, the findings should be interpreted with caution. Future studies should address these limitations by enrolling larger, multicenter cohorts with adequate statistical power, incorporating longitudinal imaging, and specifically evaluating the impact of glycemic abnormalities and metabolic therapies on myocardial tissue remodeling in HCM patients.

Conclusion

In summary, this study underscores the critical impact of glycemic abnormalities on myocardial microstructure in HCM patients, as revealed by tissue-characteristic CMR. Myocardial fibrosis progression is strongly associated with elevated HbA1c levels, particularly in hypertrophied regions, even in prediabetic individuals. Additionally, subclinical myocardial inflammation was evident in prediabetic and diabetic HCM patients. Our findings emphasize the role of early glycemic control in mitigating myocardial fibrosis and support the use of CMR-based tissue characterization in HCM management.

Data availability statement

The raw data supporting the conclusions of this article will be made available by the authors, without undue reservation.

Ethics statement

The studies involving humans were approved by the Chengdu Third People's Hospital Ethics Review Board (Ethics number: 2025-S-124). The studies were conducted in accordance with the local legislation and institutional requirements. The ethics committee/institutional review board waived the requirement of written informed consent for participation from the participants or the participants' legal guardians/next of kin because of the retrospective design of the studies.

Author contributions

XP: Conceptualization, Data curation, Writing – review & editing, Formal analysis, Methodology, Writing – original draft. HH: Conceptualization, Validation, Writing – original draft, Writing – review & editing. ZZ: Investigation, Methodology, Writing – original draft. QC: Investigation, Methodology, Writing – original draft. JT: Investigation, Methodology, Writing – original draft. DY: Investigation, Methodology, Writing – original draft. YS: Formal analysis, Writing – original draft. YH: Formal analysis, Writing – original draft. ZL: Formal analysis, Writing – original draft. JG: Conceptualization, Data curation, Supervision, Writing – review & editing.

Funding

The author(s) declare that financial support was received for the research and/or publication of this article. The authors state that this work has not received any funding.Author contributions XP, HH and JG contributed to the study design. XP, ZZ, QC, JT and DY contributed to patient collection and clinical data acquisition in patients. XP, ZZ, and JG contributed to CMR date acquisition in patients. YS, YH, and ZL contributed to statistical analysis. XP, HH and JG analyzed and interpreted the CMR data, and together contributed to writing manuscript and critical revision. All authors read and approved the final manuscript.

Acknowledgments

The authors would like to extend their gratitude and acknowledgements to all study participants.

Conflict of interest

The authors declare that the research was conducted in the absence of any commercial or financial relationships that could be construed as a potential conflict of interest.

Generative AI statement

The author(s) declare that no Generative AI was used in the creation of this manuscript.

Any alternative text (alt text) provided alongside figures in this article has been generated by Frontiers with the support of artificial intelligence and reasonable efforts have been made to ensure accuracy, including review by the authors wherever possible. If you identify any issues, please contact us.

Publisher's note

References

1. Liu J, Zhao S, Yu S, Wu G, Wang D, Liu L, et al. Patterns of replacement fibrosis in hypertrophic cardiomyopathy. *Radiology*. (2022) 302:298–306. doi: 10.1148/radiol.2021210914

2. Semsarian C, Ingles J, Maron MS, Maron BJ. New perspectives on the prevalence of hypertrophic cardiomyopathy. *J Am Coll Cardiol*. (2015) 65:1249–54. doi: 10.1016/j.jacc.2015.01.019

3. Shimada YJ, Raita Y, Liang LW, Maurer MS, Hasegawa K, Fifer MA, et al. Prediction of major adverse cardiovascular events in patients with hypertrophic cardiomyopathy using proteomics profiling. *Circ: Genomic Precis Med*. (2022) 15:e003546. doi: 10.1161/CIRCGEN.121.003546

4. Fahmy AS, Rowin EJ, Jaafar N, Chan RH, Rodriguez J, Nakamori S, et al. Radiomics of late gadolinium enhancement reveals prognostic value of myocardial scar heterogeneity in hypertrophic cardiomyopathy. *JACC: Cardiovasc Imaging*. (2024) 17:16–27. doi: 10.1016/j.jcmg.2023.05.003

5. Neumann S, Huse K, Semrau R, Diegeler A, Gebhardt R, Buniatian GH, et al. Aldosterone and D -glucose stimulate the proliferation of human cardiac myofibroblasts. *In vitro Hypertension*. (2002) 39:756–60. doi: 10.1161/hy0302.105295

6. Khan MA, Yang EY, Nguyen DT, Nabi F, Hinojosa J, Jabel M, et al. Examining the relationship and prognostic implication of diabetic status and extracellular matrix expansion by cardiac magnetic resonance. *Circ: Cardiovasc Imaging*. (2020) 13:e011000. doi: 10.1161/CIRCIMAGING.120.011000

7. Lee H-J, Kim H-K, Kim B-S, Han K-D, Rhee T-M, Park J-B, et al. Impact of diabetes mellitus on the outcomes of subjects with hypertrophic cardiomyopathy: a nationwide cohort study. *Diabetes Res Clin Pract*. (2022) 186:109838. doi: 10.1016/j.diabres.2022.109838

8. Wang S, Zhang K, He M, Guo H, Cui H, Wang S, et al. Effect of type 2 diabetes on cardiac arrhythmias in patients with obstructive hypertrophic cardiomyopathy. *Diabetes Metab Syndr: Clin Res Rev*. (2024) 18:102992. doi: 10.1016/j.dsx.2024.102992

9. Wasserstrum Y, Barriales-Villa R, Fernández-Fernández X, Adler Y, Lotan D, Peled Y, et al. The impact of diabetes mellitus on the clinical phenotype of hypertrophic cardiomyopathy. *Eur Heart J*. (2019) 40:1671–7. doi: 10.1093/eurheartj/ehy625

10. Jex N, Chowdhary A, Thirunavukarasu S, Procter H, Sengupta A, Natarajan P, et al. Coexistent diabetes is associated with the presence of adverse phenotypic features in patients with hypertrophic cardiomyopathy. *Diabetes Care*. (2022) 45:1852–62. doi: 10.2337/dc22-0083

11. Yu S-Q, Shi K, Li Y, Wang J, Gao Y, Shi R, et al. The impact of diabetes mellitus on cardiac function assessed by magnetic resonance imaging in patients with hypertrophic cardiomyopathy. *Cardiovasc Diabetol*. (2024) 23:293. doi: 10.1186/s12933-024-02384-y

12. Rajiah PS, François CJ, Leiner T. Cardiac MRI: state of the art. *Radiology*. (2023) 307:e223008. doi: 10.1148/radiol.223008

13. Russo V, Lovato L, Ligabue G. Cardiac MRI: technical basis. *Radiol Med*. (2020) 125:1040–55. doi: 10.1007/s11547-020-01282-z

14. Ferreira VM, Schulz-Menger J, Holmvang G, Kramer CM, Carbone I, Sechtem U, et al. Cardiovascular magnetic resonance in nonischemic myocardial inflammation. *J Am Coll Cardiol*. (2018) 72:3158–76. doi: 10.1016/j.jacc.2018.09.072

15. American Diabetes Association Professional Practice Committee, ElSayed NA, McCoy RG, Aleppo G, Balapattabi K, Beverly EA, et al. 2. Diagnosis and classification of diabetes: standards of care in diabetes—2025. *Diabetes Care*. (2025) 48:S27–49. doi: 10.2337/dc25-s002

16. Ommen SR, Ho CY, Asif IM, Balaji S, Burke MA, Day SM, et al. 2024 AHA/ACC/AMSSM/HRS/PACES/SCMR guideline for the management of hypertrophic cardiomyopathy: a report of the american heart association/american college of cardiology joint committee on clinical practice guidelines. *Circulation*. (2024) 149:e1239–311. doi: 10.1161/CIR.0000000000001250

17. Huo H, Dai X, Li S, Zheng Y, Zhou J, Song Y, et al. Diagnostic accuracy of cardiac magnetic resonance tissue tracking technology for differentiating between acute and chronic myocardial infarction. *Quant Imaging Med Surg*. (2021) 11:3070–81. doi: 10.21037/qims-20-1109

18. Peng X, Ding H, Huo H, Zheng Y, Zhou J, Li H, et al. Cardiac MRI -based assessment of myocardial injury in asymptomatic people living with human immunodeficiency virus: correlation with nadir CD4 count. *Magnetic Resonance Imaging*. (2023) 58:1815–23. doi: 10.1002/jmri.28699

19. Lu M, Zhao S, Yin G, Jiang S, Zhao T, Chen X, et al. T1 mapping for detection of left ventricular myocardial fibrosis in hypertrophic cardiomyopathy: a preliminary study. *Eur J Radiol*. (2013) 82:e225–31. doi: 10.1016/j.ejrad.2012.12.014

20. Kellman P, Wilson JR, Xue H, Bandettini WP, Shanbhag SM, Druey KM, et al. Extracellular volume fraction mapping in the myocardium, part 2: initial clinical experience. *J Cardiovasc Magn Reson*. (2012) 14:61. doi: 10.1186/1532-429X-14-64

21. Roller F, Harth S, Schneider C, Krombach G. T1, T2 mapping and extracellular volume fraction (ECV): application, value and further perspectives in myocardial inflammation and cardiomyopathies. *RöFo - Fortschr auf Geb Röntgenstrahlen bildgeb Verfahr*. (2015) 187:760–70. doi: 10.1055/s-0034-1399546

22. Kramer CM, Barkhausen J, Bucciarelli-Ducci C, Flamm SD, Kim RJ, Nagel E. Standardized cardiovascular magnetic resonance imaging (CMR) protocols: 2020 update. *J Cardiovasc Magn Reson*. (2020) 22:17. doi: 10.1186/s12968-020-00607-1

23. Ugander M, Oki AJ, Hsu L-Y, Kellman P, Greiser A, Aletras AH, et al. Extracellular volume imaging by magnetic resonance imaging provides insights into overt and sub-clinical myocardial pathology. *Eur Heart J*. (2012) 33:1268–78. doi: 10.1093/eurheartj/ehr481

24. Freitas P, Ferreira AM, Arteaga-Fernández E, De Oliveira Antunes M, Mesquita J, Abecasis J, et al. The amount of late gadolinium enhancement outperforms current guideline-recommended criteria in the identification of patients with hypertrophic cardiomyopathy at risk of sudden cardiac death. *J Cardiovasc Magn Reson*. (2019) 21:50. doi: 10.1186/s12968-019-0561-4

25. Weng Z, Yao J, Chan RH, He J, Yang X, Zhou Y, et al. Prognostic value of LGE-CMR in HCM. *JACC: Cardiovasc Imaging*. (2016) 9:1392–402. doi: 10.1016/j.jcmg.2016.02.031

26. Bruder O, Wagner A, Jensen CJ, Schneider S, Ong P, Kispert E-M, et al. Myocardial scar visualized by cardiovascular magnetic resonance imaging predicts major adverse events in patients with hypertrophic cardiomyopathy. *J Am Coll Cardiol*. (2010) 56:875–87. doi: 10.1016/j.jacc.2010.05.007

27. Chan RH, Maron BJ, Olivotto I, Pencina MJ, Assenza GE, Haas T, et al. Prognostic value of quantitative contrast-enhanced cardiovascular magnetic resonance for the evaluation of sudden death risk in patients with hypertrophic cardiomyopathy. *Circulation*. (2014) 130:484–95. doi: 10.1161/CIRCULATIONAHA.113.007094

28. Xu J, Zhuang B, Sirajuddin A, Li S, Huang J, Yin G, et al. MRI T1 mapping in hypertrophic cardiomyopathy: evaluation in patients without late gadolinium enhancement and hemodynamic obstruction. *Radiology*. (2020) 294:275–86. doi: 10.1148/radiol.2019190651

29. Salvador DB, Gamba MR, Gonzalez-Jaramillo N, Gonzalez-Jaramillo V, Raguindin PFN, Minder B, et al. Diabetes and myocardial fibrosis. *Jacc: Cardiovasc Imaging*. (2022) 15:796–808. doi: 10.1016/j.jcmg.2021.12.008

30. Salvatore T, Pafundi PC, Galiero R, Albanese G, Di Martino A, Caturano A, et al. The diabetic cardiomyopathy: the contributing pathophysiological mechanisms. *Front Med*. (2021) 8:695792. doi: 10.3389/fmed.2021.695792

31. Vanmali A, Alhumaid W, White JA. Cardiovascular magnetic resonance-based tissue characterization in patients with hypertrophic cardiomyopathy. *Can J Cardiol*. (2024) 40:887–98. doi: 10.1016/j.cjca.2024.02.029

32. Wong TC, Piehler KM, Kang IA, Kadakkal A, Kellman P, Schwartzman DS, et al. Myocardial extracellular volume fraction quantified by cardiovascular magnetic resonance is increased in diabetes and associated with mortality and incident heart failure admission. *Eur Heart J*. (2014) 35:657–64. doi: 10.1093/eurheartj/eht193

33. Xu Z, Wang J, Cheng W, Wan K, Li W, Pu L, et al. Incremental significance of myocardial oedema for prognosis in hypertrophic cardiomyopathy. *Eur Heart J Cardiovasc Imaging*. (2023) 24:876–84. doi: 10.1093/ehjci/jead065

34. Gong J, Shi B, Yang P, Khan A, Xiong T, Li Z. Unveiling immune infiltration characterizing genes in hypertrophic cardiomyopathy through transcriptomics and bioinformatics. *J Inflammation Res*. (2024) 17:3079–92. doi: 10.2147/JIR.S454446

35. Pelliccia F, Cecchi F, Olivotto I, Camici P. Microvascular dysfunction in hypertrophic cardiomyopathy. *J Clin Med*. (2022) 11:6560. doi: 10.3390/jcm11216560

36. Diamant M, Lamb HJ, Smit JWA, De Roos A, Heine RJ. Diabetic cardiomyopathy in uncomplicated type 2 diabetes is associated with the metabolic syndrome and systemic inflammation. *Diabetologia*. (2005) 48:1669–70. doi: 10.1007/s00125-005-1821-4

37. Ritchie RH, Abel ED. Basic mechanisms of diabetic heart disease. *Circ Res*. (2020) 126:1501–25. doi: 10.1161/CIRCRESAHA.120.315913

38. Hajdu M, Knutsen MO, Vértes V, Vorobcsuk-Varga N, Molnár G, Wittmann I, et al. Quality of glycemic control has significant impact on myocardial mechanics in type 1 diabetes mellitus. *Sci Rep*. (2022) 12:20180. doi: 10.1038/s41598-022-24619-2

39. Chen X, Pan J, Shu J, Zhang X, Ye L, Chen L, et al. Prognostic value of regional strain by cardiovascular magnetic resonance feature tracking in hypertrophic cardiomyopathy. *Quant Imaging Med Surg*. (2022) 12:627–41. doi: 10.21037/qims-21-42

40. Yang L, Zhang L, Cao S, Gao C, Xu H, Song T, et al. Advanced myocardial characterization in hypertrophic cardiomyopathy: feasibility of CMR-based feature tracking strain analysis in a case-control study. *Eur Radiol*. (2020) 30:6118–28. doi: 10.1007/s00330-020-06922-6

41. Fonseca CG, Dissanayake AM, Doughty RN, Whalley GA, Gamble GD, Cowan BR, et al. Three-dimensional assessment of left ventricular systolic strain in patients with type 2 diabetes mellitus, diastolic dysfunction, and normal ejection fraction. *Am J Cardiol*. (2004) 94:1391–5. doi: 10.1016/j.amjcard.2004.07.143

42. Almaas VM, Haugaa KH, Strøm EH, Scott H, Smith H-J, Dahl CP, et al. Noninvasive assessment of myocardial fibrosis in patients with obstructive hypertrophic cardiomyopathy. *Heart*. (2014) 100:631–8. doi: 10.1136/heartjnl-2013-304923

43. Neisius U, Myerson L, Fahmy AS, Nakamori S, El-Rewaidy H, Joshi G, et al. Cardiovascular magnetic resonance feature tracking strain analysis for discrimination between hypertensive heart disease and hypertrophic cardiomyopathy. *PloS One*. (2019) 14:e0221061. doi: 10.1371/journal.pone.0221061

frontiers | Frontiers in Endocrinology

TYPE Original Research
PUBLISHED 02 October 2025
DOI 10.3389/fendo.2025.1635282

OPEN ACCESS

EDITED BY
Ramoji Kosuru,
Versiti Blood Research Institute, United States

REVIEWED BY
Priyanka Choudhury,
Medical College of Wisconsin, United States
Venkata Kiran Kumar Mandlem,
University of Texas at Tyler, United States

*CORRESPONDENCE
Qing-Wu Wu
qingwu30568153@126.com

RECEIVED 28 May 2025
ACCEPTED 17 September 2025
PUBLISHED 02 October 2025

CITATION
Wu Q-W, He Y-H, Li P-H, Gu S-L, Song R, Zhang D-Y and Zhu Y-F (2025) Exploring the link between visceral fat and cardiovascular disease in type 2 diabetes: evidence from ct measurements. *Front. Endocrinol.* 16:1635282. doi: 10.3389/fendo.2025.1635282

Exploring the link between visceral fat and cardiovascular disease in type 2 diabetes: evidence from ct measurements

Qing-Wu Wu[1*], Yu-Hua He[1], Pei-Heng Li[1], Shi-Li Gu[1], Ran Song[1], Dong-Ying Zhang[1] and Yun-Feng Zhu[2]

[1]Department of Radiology, The First Affiliated Hospital of Xinxiang Medical University, Weihui, Xinxiang, Henan, China, [2]Department of Endocrinology, The First Affiliated Hospital of Xinxiang Medical University, Weihui, Xinxiang, Henan, China

Background: Visceral fat is a well-established risk factor for cardiovascular disease (CVD) in patients with type 2 diabetes (T2DM). While visceral fat is recognized as a risk factor for CVD in T2DM patients, precise quantification of this relationship using direct CT measurements requires further validation in large populations. This study seeks to examine the cross-sectional association between VFA, as measured by CT, and prevalent CVD in T2DM patients, with the aim of informing risk management strategies in this group.

Methods: This cross-sectional study analyzed data from 3,173 T2DM patients who underwent health screenings at Xinxiang First Affiliated Hospital between January 2020 and January 2025. CVD was defined as self-reported physician-diagnosed coronary artery disease, angina pectoris, stroke, congestive heart failure, or myocardial infarction, with verification through follow-up interviews when needed. CVD served as the dependent variable, while VFA, measured by CT, was the independent variable. VFA was categorized into quartiles. The association between VFA and CVD was assessed using univariate and multivariate analyses, smooth curve fitting with generalized additive models, and subgroup analyses.

Results: The prevalence of CVD increased progressively across VFA quartiles in T2DM patients. After adjusting for confounders, VFA remained independently associated with prevalent CVD (OR = 1.43, 95% CI: 1.12 – 1.65, $P < 0.001$). Patients in the highest VFA quartile (Q4) had a 2.04-fold higher liver fat content compared to those in the lowest quartile (Q1) (95% CI: 1.56 – 2.94, $P < 0.001$). Subgroup analyses confirmed that this association was consistent across different populations (interaction $P > 0.05$).

Conclusion: VFA is independently associated with prevalent CVD in T2DM patients. Future research should focus on the link between abdominal fat accumulation and CVD in this population.

KEYWORDS

visceral fat area, type 2 diabetes, cardiovascular disease, physical examination data, quantitative computed tomography

Introduction

Type 2 diabetes (T2DM) is becoming increasingly prevalent worldwide, with projections indicating that cases may rise to 1.31 billion by 2050 (1). China has one of the highest numbers of diabetes patients (2). T2DM is strongly linked to various cardiovascular diseases (CVD), and those with T2DM face a significantly higher risk of developing CVD, presenting a serious challenge to global healthcare systems (3). Recent studies underscore the importance of fat distribution, especially visceral fat, in the development of CVD in T2DM patients (4). Research has shown that visceral fat has a greater impact on metabolic health than subcutaneous fat. Excess visceral fat is associated with insulin resistance, dyslipidemia, and chronic inflammation, all of which are key risk factors for CVD (5, 6). Therefore, understanding the link between visceral fat and CVD in T2DM patients is vital for identifying high-risk individuals early and developing effective prevention strategies, which could significantly improve the quality of life for these patients.

Visceral fat area (VFA) has emerged as a significant marker of cardiovascular risk in T2DM patients (7, 8). Research indicates that visceral fat is metabolically active, releasing pro-inflammatory cytokines, adipokines, and free fatty acids into the portal circulation, which worsens insulin resistance and accelerates atherosclerosis (9–11). Unlike subcutaneous fat, which mainly stores energy, visceral fat contributes to disruptions in glucose and lipid metabolism, further increasing the risk of CVD in T2DM patients (12–14). Previous epidemiological and clinical studies, including large-scale imaging studies, have established the association between visceral adiposity and CVD in T2DM patients. However, many of these studies relied on indirect measures such as the visceral fat index, a composite measure that may be imprecise due to individual differences (15–17). Moreover, the visceral fat index may not be appropriate for Asian populations because of significant variations in fat distribution across ethnic groups (18). Other studies have used dual bioelectrical impedance analysis to estimate VFA (19–21), but this method lacks precision and cannot accurately distinguish between subcutaneous fat and VFA (22). In contrast, VFA measurement via chest CT images overcomes these limitations, providing a more precise assessment (23).

While the association between visceral adiposity and CVD in T2DM patients has been established, most evidence is based on indirect measurements or smaller study populations. This study aims to provide precise quantification of the VFA-CVD relationship using direct CT measurements in a large Chinese T2DM population. The objective is to assess the potential of VFA as a predictive biomarker for cardiovascular risk, which could inform more targeted interventions and ultimately improve cardiovascular outcomes in this high-risk population.

Materials and methods

Subjects and the inclusion criteria

This study protocol was approved by the Ethics Committee of Xinxiang First Affiliated Hospital (approval number: EC-025-374). The requirement for individual informed consent was waived by the Ethics Committee due to the retrospective design and strict anonymization of all patient data, in accordance with the Declaration of Helsinki and the Council for International Organizations of Medical Sciences (CIOMS) International Ethical Guidelines for Biomedical Research Involving Human Subjects. All data collection and processing strictly adhered to institutional data protection protocols, with researchers having access only to de-identified data. This study was conducted and reported following the Strengthening the Reporting of Observational Studies in Epidemiology (STROBE) guidelines. All research personnel completed medical ethics training and signed confidentiality agreements.

A retrospective analysis was performed on the medical records of adult T2DM patients who underwent health examinations at Xinxiang First Affiliated Hospital between January 2020 and January 2025. The inclusion criteria were: (1) T2DM patients who had a low-dose chest CT scan assessing VFA; (2) aged 20 to 80 years; and (3) complete demographic and questionnaire data. Exclusion criteria were patients with a historical or current diagnosis of any cancer, severe liver or kidney disease, thyroid disease, recent significant weight fluctuations (≥5%), pregnancy or breastfeeding, mental disturbance, or extreme values in examination results.

Initially, 6,671 T2DM patients were enrolled. After applying the exclusion criteria, 3,173 patients were retained for analysis, with 865 excluded. Among the retained patients, 923 (29.1%) reported a history of physician-diagnosed CVD (verified through our quality control procedures) and 2,250 (70.9%) reported no history of CVD. General demographic information, medical history, and medication history were collected through face-to-face interviews conducted by trained researchers. A detailed flowchart of the case selection process is shown in Figure 1.

Definitions of variables

The independent variable was VFA in T2DM, measured by quantitative CT (QCT). VFA was defined as the intraperitoneal fatty area enclosed by the peritoneal wall or fascia transversalis muscle at the level of the L2/3 intervertebral space and the umbilicus, measured in square centimeters (cm^2). CVD served as the dependent variable in this study. CVD was defined as a composite endpoint including any of the following physician-diagnosed conditions: coronary artery disease, angina pectoris, stroke, congestive heart failure, or myocardial infarction. CVD diagnosis was determined based on patient self-report of previous physician diagnosis obtained through standardized face-to-face interviews using a structured medical questionnaire. During the interview, trained researchers specifically asked each T2DM patient: 'Has a doctor or healthcare professional ever diagnosed you with any of the following cardiovascular conditions: (1) coronary artery disease, (2) angina pectoris, (3) stroke, (4) congestive heart failure, or (5) myocardial infarction?' A positive response to any of these five conditions was classified as having CVD. To ensure data quality and accuracy, any discrepancies or missing information regarding

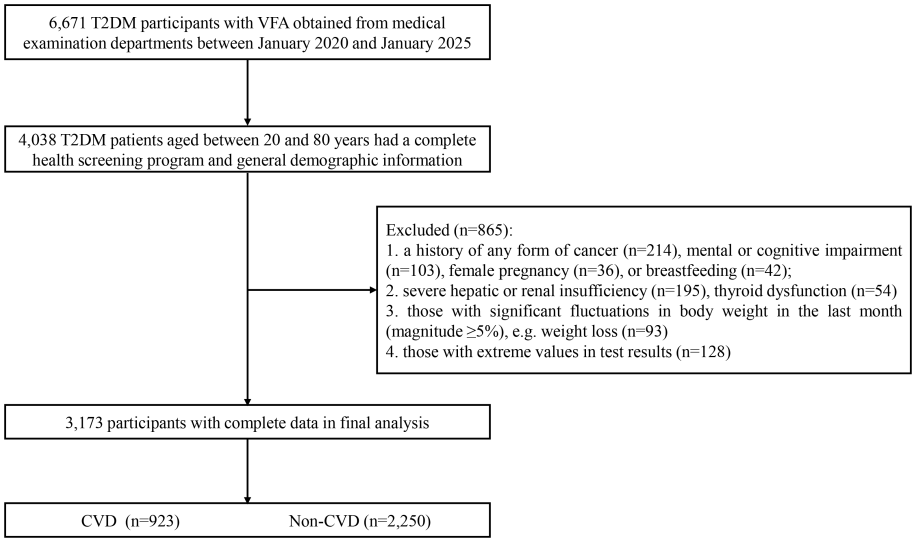

FIGURE 1
Flowchart of participants selection.

CVD history were systematically reconfirmed with participants through additional in-person interviews or telephone follow-up. These physician-diagnosed cardiovascular disease histories were classified according to the International Statistical Classification of Diseases and Related Health Problems, 10th edition (ICD-10), using the following specific codes: coronary artery disease (I20-I25.9), angina pectoris (I20.0-I20.9), congestive heart failure (I50.0, I50.1, I50.9), myocardial infarction (I21-I23), and stroke (I60-I69) (24). All analyses were based on verified CVD status as defined above, with quality control measures implemented to ensure data accuracy.

The diagnosis of T2DM followed the American Diabetes Association criteria (25): a previous physician diagnosis of diabetes, current treatment with hypoglycemic medications, fasting plasma glucose (FPG) ≥ 7.0 mmol/L, glycosylated hemoglobin (HbA1c) level ≥ 6.5%, 2-hour oral glucose tolerance test (OGTT) blood glucose ≥ 11.1 mmol/L, or use of insulin or oral hypoglycemic agents.

Body mass index (BMI) was calculated as weight (kg)/height^2 (m^2) and categorized according to Chinese standards (26): normal weight (< 24 kg/m^2), overweight (≥ 24 kg/m^2, < 28 kg/m^2), and obese (≥ 28 kg/m^2).

Hypertension was defined as having two consecutive measurements of systolic blood pressure (SBP) ≥ 140 mmHg or diastolic blood pressure (DBP) ≥ 90 mmHg, self-reported hypertension, use of antihypertensive drugs, or current antihypertensive therapy (27).

Estimated glomerular filtration rate (eGFR) was calculated using the formula: eGFR = 175 * serum creatinine^ (-1.154) * age^ (-0.203) * 0.742 (if female) * 1.212 (if black) (28). eGFR is expressed in mL/min/1.73 m^2, with serum creatinine in mg/dL and age in years.

Current smoking was defined as self-reported smoking by the participant. Current alcohol consumption was defined as the intake of at least one alcoholic beverage per week in the 12 months preceding the health screening.

All T2DM patients were divided into quartiles based on VFA levels: Q1 (33.30–172.00 cm^2), Q2 (172.10–219.90 cm^2), Q3 (220.00–271.90 cm^2), and Q4 (272.10–497.90 cm^2).

Laboratory measurements

All researchers underwent standardized training to ensure objectivity and accuracy. Before the examination, they collected basic information from participants using a standardized questionnaire. This included a history of cardiovascular disease, liver and kidney disease, various cancers, and the use of diabetes, hypertension, and lipid-lowering medications, as well as recent weight changes. After completing the questionnaires, the data was organized, summarized, and verified. Any discrepancies or missing information, particularly regarding cardiovascular disease history, were systematically reconfirmed with participants through additional in-person interviews or telephone follow-up to ensure data accuracy and completeness.

Height was measured using a stadiometer, and weight was recorded with a weighing scale. Fasting venous blood samples were collected from all participants at 8 a.m. after a 12-hour fast. These samples were analyzed for creatinine (Cre), blood urea nitrogen (BUN), total cholesterol (TC), low-density lipoprotein cholesterol (LDL-C), triglycerides (TG), high-density lipoprotein cholesterol (HDL-C), FBG, and HbA1c. FBG was measured using an Olympus® AU 5800 fully automated biochemistry analyzer (Beckman Coulter Inc., Brea, CA, USA). Other biochemical parameters were measured following standard laboratory protocols. Blood pressure (SBP and DBP) was measured using an electronic sphygmomanometer (OMRON U30, Omron

Corporation, Kyoto, Japan). Measurements were taken on the right arm of each T2DM patient, positioned semi-flexed at heart level.

VFA measurement

VFA was measured using low-dose chest CT scan data, a routine examination for assessing pulmonary lesions during health check-ups. The scan range included the L3 vertebra, minimizing unnecessary radiation exposure. All participants were scanned using the same 64-detector row CT scanner with standardized parameters: slice thickness 5.0 mm, tube voltage 120 kVp, tube current 100–150 mAs (auto-adjusted based on patient habitus), reconstruction matrix 512×512, calibrated weekly with a phantom (Mindways, Austin, TX, USA) to ensure consistent data quality. After scanning, a trained radiologist measured VFA using the QCT Pro 6.1 supplemental tissue measurement application from Mindways Software. This software performs QCT measurements on two standardized anatomical levels: (1) L2/3 intervertebral space, identified using sagittal reformatted images; (2) umbilicus level, verified by external anatomical landmarks and coronal reformats based on chest CT scan data. The application automatically segmented adipose tissue using standardized Hounsfield unit thresholds (-190 to -30 HU) and calculated the VFA in these slices. The final VFA value represents the average of measurements from both anatomical levels. To minimize measurement errors, care was taken to avoid artifacts from lumbar internal fixation, intestinal gas, or high-density contents. As illustrated in Figure 2. This measurement technique has been validated in the Chinese population (29). Further details on the measurement process can be found in previous studies (30, 31).

To ensure measurement reliability, intra-observer reproducibility was assessed by repeating measurements on 300 randomly selected cases (10% of total sample) after a 4-week interval, achieving an intraclass correlation coefficient (ICC) of 0.96 (95% CI: 0.94-0.98).

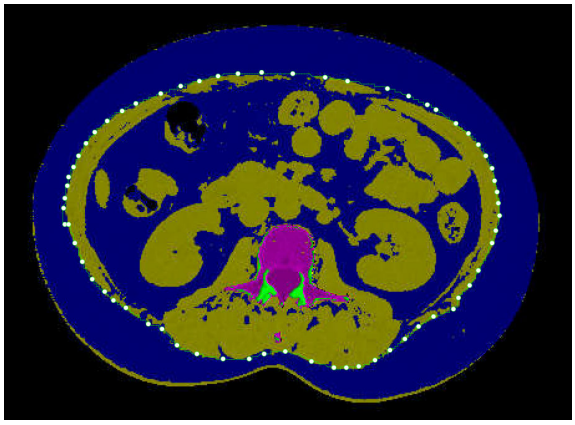

FIGURE 2
Abdominal quantitative computed tomography (QCT) image demonstrates abdominal fat distribution. The dark blue area represents non-adipose tissue and background, yellow regions indicate subcutaneous and visceral fat, and the magenta area represents specific visceral structures. The white dotted line delineates the boundary between subcutaneous and visceral fat compartments.

Statistical analysis

All statistical analyses were conducted using R version 4.2.0 (R Foundation) and EmpowerStats (http://www.empowerstats.com, X&Y Solutions, Inc., Boston, MA). All tests were two-tailed, with a significance level set at $P < 0.05$.

Normality tests were performed on all datasets to assess continuous variables. Normally distributed continuous variables were reported as mean ± standard deviation, and group differences were evaluated using t-tests or rank-sum tests. Categorical variables were presented as frequencies and percentages, with comparisons made using chi-square tests.

Univariate analysis was used to evaluate the impact of various variables on CVD. Subsequently, multivariate logistic regression was conducted to assess the relationship between VFA and CVD, adjusting for covariates including sex, age, ethnicity, hypertensive medication, diabetes medication, lipid-lowering drugs, current smoking, current alcohol consumption, hypertension, BMI, BUN, creatinine, eGFR, LDL-C, TG, and HDL-C. Covariates with a variance inflation factor (VIF) >10 were excluded. Four models were developed in this study: a crude model with no adjustments, Model I adjust for demographic variables (sex, age, and ethnicity), Model II adjusting for demographic factors along with hypertensive drugs, diabetes drugs, lipid-lowering drugs, current smoking, alcohol consumption, hypertension, and BMI, and Model III adjusting for all previously mentioned confounders. The results from Model III were used for subsequent analyses. VFA was categorized into quartiles, with the lowest quartile serving as the reference group, to assess the relationship between VFA and CVD. A generalized additive model (GAM) with smooth curve fitting was employed to explore the dose-response relationship between VFA and CVD. Finally, stratified analyses and interaction tests based on Model III were performed to determine whether the relationship between VFA and CVD was consistent across different subgroups.

Results

Baseline details about T2DM

This study included 3,173 T2DM participants, comprising 2,254 men and 919 women. Participants were divided into four groups based on visceral fat area (VFA) quartiles: Q1 (33.30–172.00 cm^2, n = 793), Q2 (172.10–219.90 cm^2, n = 793), Q3 (220.00–271.90 cm^2, n = 792), and Q4 (272.10–497.90 cm^2, n = 795). As shown in Figure 3, the prevalence of CVD increased progressively across the VFA quartiles. Compared to the Q1 group, participants in the Q4 group (highest VFA) were more likely to be male, have a higher BMI, smoke and drink, have hypertension, use antihypertensive drugs, and have higher levels of Cre, TC, LDL-C, TG, FBG, and

CVD prevalence (all $P < 0.05$). They also had lower HDL-C levels ($P < 0.05$). There were no significant differences in other variables (all $P > 0.05$), as shown in Table 1.

Univariate analysis

Univariate logistic regression analysis was used to evaluate the impact of traditional variables on CVD and to select covariates for subsequent multivariate analysis. As shown in Table 2, male sex, older age, higher BMI, current smoking, current drinking, hypertension, eGFR, LDL-C, and TG were identified as risk factors for CVD (all $P < 0.05$). In contrast, the use of hypertensive drugs, diabetic drugs, lipid-lowering drugs, TC, and HDL-C levels were protective factors against CVD (all $P < 0.05$). Ethnic group, creatinine (Cre), and BUN did not show significant correlations (all $P > 0.05$).

Associations between VFA and CVD of T2DM according to the different models

Multivariate regression analysis was conducted to account for confounding variables, and four models were developed. As shown in Table 3, the crude model, which did not adjust for any covariates, revealed a positive correlation between VFA and CVD (OR = 1.01, 95% CI: 1.00 - 1.02, $P < 0.001$). After adjusting for demographic variables such as sex, age, and ethnic group (Model I), a positive correlation between VFA and CVD was confirmed (OR = 1.02, 95% CI: 1.01– 1.06, $P < 0.001$). In Model II and Model III, VFA remained independently associated with an increased risk of CVD (OR = 1.43, 95% CI: 1.12 – 1.65, $P < 0.001$ in Model III). Specifically, for each unit increase in VFA, the odds of having prevalent CVD were 1.43 times higher. Additionally, when the VFA was divided into quartiles, after adjusting for confounding variables, the odds of having prevalent CVD in the Q4 group was 2.04 times higher than in the Q1 group ($P < 0.001$). Moreover, the association between VFA and CVD risk in T2DM patients was further examined through GAM smoothing curve fitting, which indicated a linear association (P-nonlinearity > 0.05). Each 10 cm^2 increase in VFA was associated with an odds ratio of 1.43 (95% CI: 1.12–1.65) for CVD risk (Figure 4).

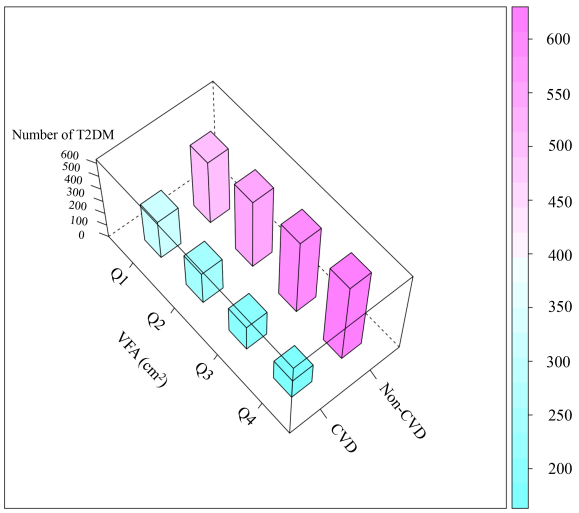

FIGURE 3
The total height of each quartile column of the 3D histogram of CVD incidence by quartile of VFA represents the total number of people in that group. VFA, visceral fat area; CVD, cardiovascular disease.

Subgroup analysis

As illustrated in Figure 5, the subgroup analyses revealed consistent findings. No significant interactions were observed when stratified by sex (female/male), ethnic group (non-Han/Han), age (<60 years/≥60 years), BMI (<24 kg/m^2/≥24, <28 kg/m^2/≥28 kg/m^2), current smoking (yes/no), current drinking (yes/no), hypertension (yes/no), use of antihypertensive drugs (yes/no), diabetic drugs (yes/no), or lipid-lowering drugs (yes/no) (P for interaction > 0.05).

Discussion

This cross-sectional analysis, conducted over six years of VFA data collection from health screening participants, demonstrated a positive association between VFA and prevalent CVD, even after adjusting for confounding variables. This relationship remained consistent across various subgroups, including sex, ethnic group, age, BMI, smoking status, drinking status, hypertension, and the use of antihypertensive, diabetic, and lipid-lowering drugs. This study provides important validation of the VFA-CVD relationship using precise QCT measurements in a large Chinese T2DM population. Our findings complement existing evidence by demonstrating this association through direct imaging-based quantification rather than indirect measures. These findings will aid primary care physicians in assessing CVD risk based on VFA and offer valuable guidance for the prevention and management of CVD in T2DM patients.

Our findings are consistent with several landmark studies that have established the relationship between visceral adiposity and CVD. Previous research using indirect measures has demonstrated this association, and our study extends these findings by providing precise quantification through direct CT measurements. Previous studies have shown that central obesity is a common feature of insulin resistance and its associated CVD (32–34). China has one of the highest prevalence rates of central obesity and T2DM (35–37). VFA is a key feature of central obesity (37). Excessive visceral fat accumulation can lead to the secretion of large amounts of inflammatory cytokines, resulting in low-grade inflammation, insulin resistance, and ultimately, the development of CVD (38). Moreover, inflamed adipocytes significantly reduce the production and secretion of adiponectin, impairing its role in protecting pancreatic β-cells from lipotoxicity and enhancing insulin sensitivity (39). While earlier research has suggested that VFA is

10.3389/fendo.2025.1635282

TABLE 1 Baseline characteristics of T2DM.

Variables	Q1 (33.30-172.00)	Q2 (172.10-219.90)	Q3 (220.00-271.90)	Q4 (272.10-497.90)	*P*-value
N	793	793	792	795	
Sex, n (%)					<0.001
Female	518 (65.32)	271 (34.17)	90 (11.36)	40 (5.03)	
Male	275 (34.68)	522 (65.83)	702 (88.64)	755 (94.97)	
Ethnic group, n (%)					0.638
Non-han	70 (8.83)	68 (8.58)	66 (8.33)	57 (7.17)	
Han	723 (91.17)	725 (91.42)	726 (91.67)	738 (92.83)	
Age, years	61.11 ± 11.62	61.05 ± 11.93	60.49 ± 11.70	60.30 ± 11.43	0.110
<60	382 (48.17)	400 (50.44)	413 (52.15)	430 (54.09)	
>=60	411 (51.83)	393 (49.56)	379 (47.85)	365 (45.91)	
BMI, kg/m^2	23.10 ± 2.38	24.74 ± 2.46	25.80 ± 2.62	27.61 ± 3.24	<0.001
<24	561 (70.74)	345 (43.51)	197 (24.87)	112 (14.09)	
>=24, <28	199 (25.09)	371 (46.78)	448 (56.57)	325 (40.88)	
>=28	33 (4.16)	77 (9.71)	147 (18.56)	358 (45.03)	
Current smoking, n (%)					<0.001
No	759 (95.71)	768 (96.85)	736 (92.93)	730 (91.82)	
Yes	34 (4.29)	25 (3.15)	56 (7.07)	65 (8.18)	
Current drinking, n (%)					<0.001
No	761 (95.96)	742 (93.57)	725 (91.54)	714 (89.81)	
Yes	32 (4.04)	51 (6.43)	67 (8.46)	81 (10.19)	
Hypertension, n (%)					<0.001
No	498 (62.80)	489 (61.66)	436 (55.05)	396 (49.81)	
Yes	295 (37.20)	304 (38.34)	356 (44.95)	399 (50.19)	
Hypertensive drugs, n (%)					<0.001
No	580 (73.14)	564 (71.12)	517 (65.28)	488 (61.38)	
Yes	213 (26.86)	229 (28.88)	275 (34.72)	307 (38.62)	
Diabetes drugs, n (%)					0.416
No	753 (94.96)	760 (95.84)	763 (96.34)	754 (94.84)	
Yes	40 (5.04)	33 (4.16)	29 (3.66)	41 (5.16)	
Lipid-lowering drugs, n (%)					0.678
No	777 (97.98)	773 (97.48)	770 (97.22)	779 (97.99)	
Yes	16 (2.02)	20 (2.52)	22 (2.78)	16 (2.01)	
Cre, μmol/L	63.51 ± 19.43	68.98 ± 17.10	73.19 ± 19.55	75.26 ± 44.13	<0.001
BUN, mmol/L	5.07 ± 2.36	5.19 ± 2.25	5.31 ± 2.48	5.17 ± 2.42	0.252
eGFR, mL/min/1.73m^2	97.19 ± 23.70	96.74 ± 22.11	97.81 ± 25.08	98.30 ± 25.01	0.584
TC, mmol/L	4.70 ± 1.15	4.75 ± 1.23	4.81 ± 1.23	4.82 ± 1.20	0.040
LDL-C, mmol/L	2.70 ± 0.92	2.72 ± 0.95	2.76 ± 0.94	2.89 ± 0.85	0.038

(Continued)

10.3389/fendo.2025.1635282

TABLE 1 Continued

Variables	Q1 (33.30-172.00)	Q2 (172.10-219.90)	Q3 (220.00-271.90)	Q4 (272.10-497.90)	*P*-value
Lipid-lowering drugs, n (%)					0.678
TG, mmol/L	1.65 ± 1.19	2.22 ± 2.22	2.47 ± 2.34	2.61 ± 2.26	<0.001
HDL-C, mmol/L	1.35 ± 0.34	1.20 ± 0.26	1.14 ± 0.26	1.12 ± 0.24	<0.001
FBG, mmol/L	7.07 ± 2.35	7.70 ± 2.41	7.62 ± 2.17	7.74 ± 2.23	<0.001
HbA1c, %	6.06 ± 2.78	6.13 ± 2.96	6.17 ± 2.82	6.08 ± 3.01	0.865
VFA, cm^2	132.72 ± 29.71	196.75 ± 13.89	245.27 ± 14.76	320.49 ± 41.26	<0.001
CVD, n (%)					<0.001
No	630 (79.45)	591 (74.53)	538 (67.93)	491 (61.76)	
Yes	163 (20.55)	202 (25.47)	254 (32.07)	304 (38.24)	

BMI, body mass index; Cre, Creatinine; BUN, blood urea nitrogen; eGFR, estimated glomerular filtration rate; TC, total cholesterol; LDL-C, low-density lipoprotein cholesterol; TG, triglycerides; HDL-C, high-density lipoprotein cholesterol; FBG, fasting blood glucose; HbA1c, Glycosylated hemoglobin; VFA, visceral fat area; CVD, cardiovascular disease.

TABLE 2 Univariate logistic regression analyses for CVD.

Variables	Statistics	OR (95%CI)	*P*-value
Sex, n (%)			
Female	919 (28.96)	Reference	
Male	2,254 (71.04)	1.19 (1.00, 1.42)	0.045
Ethnic group, n (%)			
Non-han	261 (8.23)	Reference	
Han	2,912 (91.77)	1.26 (0.94, 1.69)	0.121
Age, years			
<60	1,625 (51.21)	Reference	
>=60	1,548 (48.79)	1.31 (1.12, 1.52)	<0.001
BMI, kg/m^2			
<24	1,215 (38.29)	Reference	
>=24, <28	1,343 (42.33)	1.46 (1.22, 1.74)	<0.001
>=28	615 (19.38)	1.90 (1.54, 2.35)	<0.001
Current smoking, n (%)			
No	2,993 (94.33)	Reference	
Yes	180 (5.67)	1.81 (1.33, 2.46)	<0.001
Current drinking, n (%)			
No	2,942 (92.72)	Reference	
Yes	231 (7.28)	1.78 (1.36, 2.35)	<0.001
Hypertension, n (%)			
No	1,819 (57.33)	Reference	
Yes	1,354 (42.67)	1.76 (1.51, 2.05)	<0.001
Hypertensive drugs, n (%)			
No	2,149 (67.73)	Reference	
Yes	1,024 (32.27)	-1.98 (-2.32, -1.69)	<0.001
Diabetic drugs, n (%)			
No	3,030 (95.49)	Reference	
Yes	143 (4.51)	-1.56 (-2.20, -1.10)	0.012
Lipid-lowering drugs, n (%)			
No	3,099 (97.67)	Reference	
Yes	74 (2.33)	-1.68 (-2.70, -1.05)	0.030
Cre, μmol/L	70.24 ± 27.75	1.00 (1.00, 1.01)	0.812
BUN, mmol/L	5.18 ± 2.38	1.01 (0.98, 1.04)	0.644
eGFR, mL/min/1.73m^2	97.51 ± 24.00	1.00 (1.00, 1.01)	0.008
TC, mmol/L	4.77 ± 1.20	0.98 (0.92, 1.05)	0.598
LDL-C, mmol/L	2.72 ± 0.92	0.97 (0.89, 1.05)	0.024
TG, mmol/L	2.24 ± 2.09	1.04 (1.00, 1.08)	0.026
HDL-C, mmol/L	1.20 ± 0.29	-0.78 (-1.02, -0.60)	0.072
VFA, cm^2	223.86 ± 73.92	1.00 (1.00, 1.01)	<0.001

BMI, body mass index; Cre, Creatinine; BUN, blood urea nitrogen; eGFR, estimated glomerular filtration rate; TC, total cholesterol; LDL-C, low-density lipoprotein cholesterol; TG, triglycerides; HDL-C, high-density lipoprotein cholesterol; FBG, fasting blood glucose; HbA1c, Glycosylated hemoglobin; VFA, visceral fat area; CVD, cardiovascular disease; OR, odd ratio.

one of the most valuable predictors of CVD in T2DM patients (20, 21, 40), the precise relationship between accurately measured VFA and CVD risk remains unclear. A recent multicenter study found that even T2DM patients with visceral obesity, but normal BMI have a significantly increased risk of developing atherosclerotic CVD (4). These findings highlight the importance of assessing VFA in T2DM patients. Therefore, we believe that precise VFA measurement should be prioritized over other indicators when

TABLE 3 Multivariate regression analysis for prevalent CVD.

Variables	Crude model	Adjust I model	Adjust II model	Adjust III model
	OR (95%CI) *P*-value	OR (95%CI) *P*-value	OR (95%CI) *P*-value	OR (95%CI) *P*-value
VFA	1.01 (1.00, 1.02) <0.001	1.02 (1.01, 1.06) <0.001	1.21 (1.03, 1.36) <0.001	1.43 (1.12, 1.65) <0.001
VFA quartile				
Q1	Reference	Reference	Reference	Reference
Q2	1.62 (1.04, 1.67) 0.020	1.41 (1.10, 1.80) 0.006	1.31 (1.02, 1.70) 0.037	1.20 (1.00, 1.69) 0.045
Q3	1.82 (1.45, 2.29) <0.001	2.07 (1.60, 2.67) <0.001	1.98 (1.34, 2.35) <0.001	1.76 (1.32, 2.35) <0.001
Q4	2.39 (1.91, 2.99) <0.001	2.75 (2.13, 3.57) <0.001	2.18 (1.60, 2.97) <0.001	2.04 (1.56, 2.94) <0.001
P for trend	<0.001	<0.001	<0.001	<0.001

Non-adjusted model adjusts for: None.
Adjust I model adjust for: sex, age, and ethnic group.
Adjust II model adjust for: sex, age, ethnic group, hypertensive drugs, diabetic drugs, lipid-lowering drugs, current smoking, current drinking, hypertension, BMI.
Adjust III model adjust for: sex, age, ethnic group, hypertensive drugs, diabetic drugs, lipid-lowering drugs, current smoking, current drinking, hypertension, BMI, BUN, Cr, eGFR, LDL-C, TG, HDL-C. VFA, visceral fat area; CVD, cardiovascular disease; OR, odd ratio.

evaluating CVD risk in T2DM patients. In this study, we used low-dose chest CT to measure VFA, with data derived from chest CT scans originally performed for lung cancer screening in T2DM patients. This approach ensures accurate VFA measurement while minimizing additional radiation exposure from repeated scans.

Building on this foundation, our study assessed the relationship between VFA and CVD risk by analyzing health examination data from T2DM patients. We observed that CVD incidence increased progressively with higher VFA levels. Even after adjusting for confounding factors, VFA remained independently and positively associated with prevalent CVD across multiple regression models. Importantly, this relationship remained robust across various subgroup analyses, consistent with previous findings using VFA measured by dual bioelectrical impedance analysis, which also suggested that VFA could be a risk marker for CVD in T2DM patients (20, 21, 41). Visceral adipose tissue, primarily located in the mesentery and omentum, drains directly into the liver through the portal circulation. Compared to subcutaneous adipocytes, visceral adipocytes are more metabolically active, more sensitive to lipolysis, and more resistant to insulin (12). Additionally, increased VFA promotes the secretion of plasminogen activator inhibitor-1 (PAI-1), leading to a hypercoagulable state, thereby raising the risk of atherosclerosis and coronary heart disease (42, 43). A prospective study of 97 hemodialysis patients reported that VFA is an independent predictor of CVD and all-cause mortality in this population (44). Another study involving 15,350 adult hypertensive participants found that visceral fat accumulation and prolonged exposure to high levels of visceral fat are significant risk factors for CVD (45). These findings underscore the robustness of VFA as a predictor of CVD events across various populations.

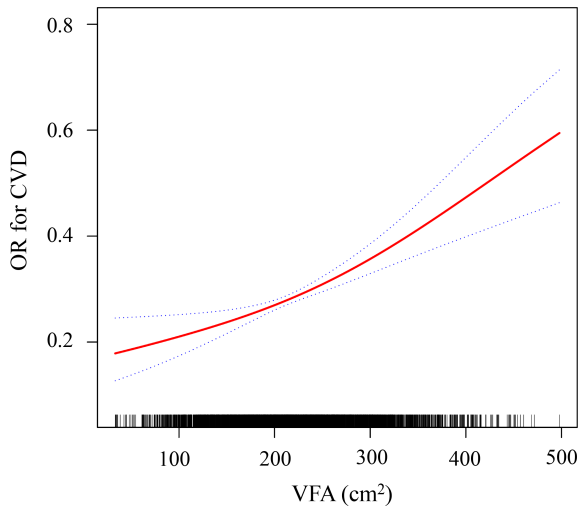

FIGURE 4
Generalized additive model (GAM) smoothing curve showing the linear dose–response association between VFA and CVD risk in T2DM (P_nonlinearity > 0.05). The red solid line represents the estimated probability, and the shaded area represents the 95% CI. All covariates were adjusted in this model. All covariates, including ex, age, ethnic group, hypertensive drugs, diabetic drugs, lipid-lowering drugs, current smoking, current drinking, hypertension, BMI, BUN, Cr, eGFR, LDL-C, TG, HDL-C were adjusted in this model. VFA, visceral fat area; CVD, cardiovascular disease; OR, odd ratio.

However, a recent longitudinal study based on the Chinese adult population identified a nonlinear relationship between the Chinese Visceral Adiposity Index (CVAI) and coronary heart disease risk, with a stronger association in men than in women (16). Unlike our study, this research used CVAI as the dependent variable, which includes waist circumference, BMI, triglycerides, HDL-C, and age (46). Although CVAI may better estimate visceral fat content in Chinese individuals, we believe the study may not have sufficiently accounted for confounding factors, potentially explaining the discrepancy with our findings. Additionally, a recent prospective study of 704 adult T2DM patients reported that perirenal fat thickness is an independent predictor of 10-year CVD risk in T2DM patients (47). This suggests that future research should explore the relationship between various visceral fat deposits and CVD in T2DM patients, allowing for the development of more precise prevention strategies to reduce CVD risk.

10.3389/fendo.2025.1635282

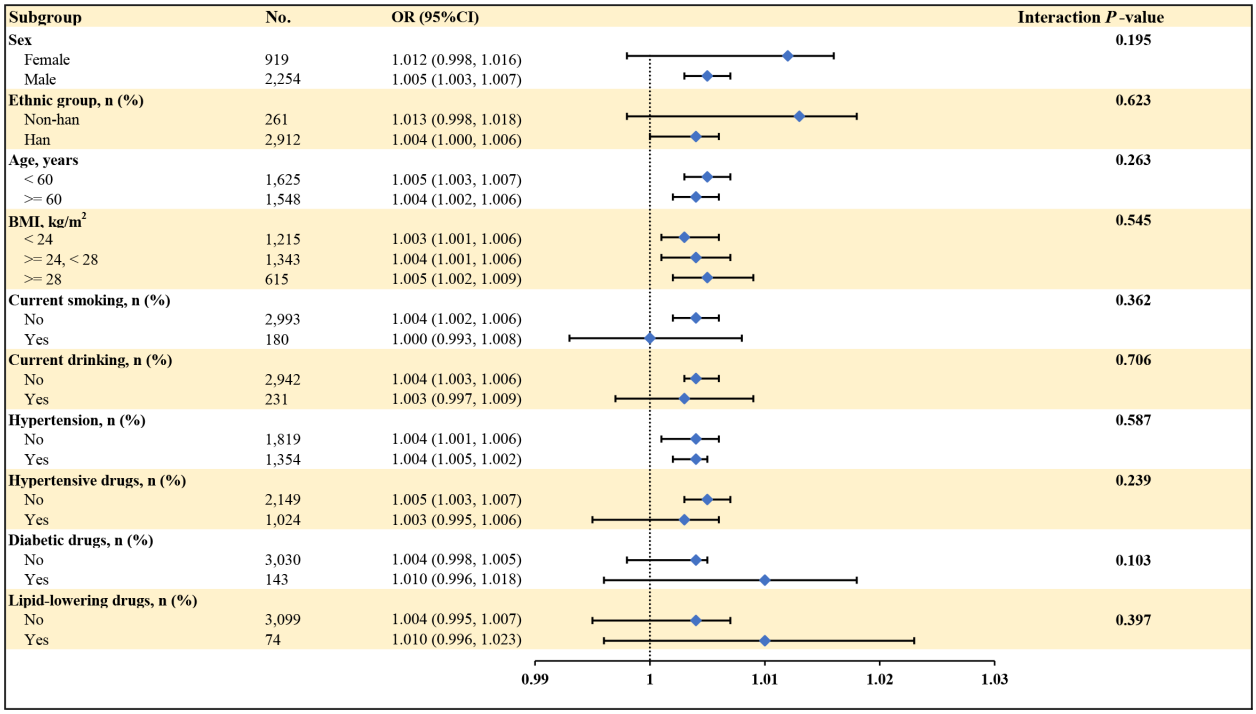

FIGURE 5
The association between VFA and the risk of CVD in T2DM according to different subgroups. Adjusted for all covariates except for this subgroup of variables. BMI, body mass index. VFA, visceral fat area; CVD, cardiovascular disease; OR, odd ratio.

Limitations and strengths

The key strengths of this study include: First, VFA was measured using QCT, enabling precise measurements based on lung cancer screening CT data without additional radiation exposure. Second, rigorous statistical methods were employed, offering robust support for the adjusted logistic regression analyses. However, the study has important limitations. Most importantly, the cross-sectional design of this study prevents establishment of causal relationships between VFA and CVD. Our findings demonstrate statistical association only and cannot determine whether VFA accumulation leads to CVD development, whether underlying CVD contributes to visceral fat accumulation, or whether both are consequences of common underlying pathophysiological processes. The temporal sequence between VFA changes and CVD development cannot be determined from our data. Therefore, our results should be interpreted as evidence of cross-sectional association rather than causation, and longitudinal studies are needed to establish any potential causal relationships. Additionally, the health screening program's constraints limit the collection of certain covariates, such as inflammatory markers (e.g., hs-CRP). Finally, the study was conducted at a single health screening center in China, which may limit the generalizability of the findings to other populations. What's more, while our study provides precise quantification of the established VFA-CVD relationship, it should be acknowledged that this represents a validation and methodological refinement of existing knowledge rather than a novel discovery of previously unknown associations. Last, regarding CVD ascertainment, while our study relied on patient self-report of physician diagnoses, we implemented quality control measures including systematic verification of discrepancies or missing information through follow-up interviews. This approach, commonly used in large epidemiological studies, provides a balance between feasibility and accuracy. However, the lack of direct access to medical records means that some degree of recall bias or misclassification cannot be completely excluded, though our verification procedures likely minimized such errors.

Conclusion

Our study validates and precisely quantifies the independent positive association between VFA and increased CVD risk in T2DM patients, confirming previous observations through direct imaging measurements, with this relationship remaining robust across various subgroups. These findings suggest that VFA could serve as a clinical marker for CVD risk in T2DM patients, emphasizing the importance of monitoring VFA changes as part of CVD prevention strategies. Future prospective longitudinal studies should focus on fat accumulation around different abdominal organs in T2DM patients and assess whether changes in fat deposits predict CVD development. Such investigations could be crucial for enhancing the quality of life for T2DM patients.

Data availability statement

The original contributions presented in the study are included in the article/supplementary material, further inquiries can be directed to the corresponding author/s.

Ethics statement

The studies involving humans were approved by The research protocol received ethics approval from the Ethics Committee at The First Affiliated Hospital of Xinxiang Medical University, in conformity with the Declaration of Helsinki guidelines (Approval Code: EC-025-374). The studies were conducted in accordance with the local legislation and institutional requirements. The ethics committee/institutional review board waived the requirement of written informed consent for participation from the participants or the participants' legal guardians/next of kin because This is a retrospective study that does not involve any personal information of patients; therefore, informed consent is not required, as approved by the ethics committee.

Author contributions

Q-WW: Writing – review & editing, Writing – original draft, Software, Conceptualization, Investigation. Y-HH: Methodology, Data curation, Supervision, Conceptualization, Writing – review & editing, Writing – original draft. P-HL: Project administration, Formal analysis, Validation, Visualization, Writing – review & editing, Writing – original draft. S-LG: Supervision, Writing – original draft, Writing – review & editing, Project administration, Validation, Methodology. RS: Formal analysis, Writing – original draft, Funding acquisition, Resources, Writing – review & editing, Project administration. D-YZ: Visualization, Project administration, Resources, Validation, Writing – review & editing, Writing – original draft. Y-FZ: Writing – original draft, Formal analysis, Validation, Methodology, Project administration, Writing – review & editing, Supervision.

Funding

The authors declare that no financial support was received for the research, and/or publication of this article.

Acknowledgments

We thank all the medical staff of the First Affiliated Hospital of Xinxiang Medical University for their support of this study.

Conflict of interest

The authors declare that the research was conducted in the absence of any commercial or financial relationships that could be construed as a potential conflict of interest.

Generative AI statement

The author(s) declare that no Generative AI was used in the creation of this manuscript.

Any alternative text (alt text) provided alongside figures in this article has been generated by Frontiers with the support of artificial intelligence and reasonable efforts have been made to ensure accuracy, including review by the authors wherever possible. If you identify any issues, please contact us.

Publisher's note

References

1. Ong KL, Stafford LK, McLaughlin SA, Boyko EJ, Vollset SE, Smith AE, et al. Global, regional, and national burden of diabetes from 1990 to 2021, with projections of prevalence to 2050: a systematic analysis for the Global Burden of Disease Study 2021. *Lancet (London England)*. (2023) 402:203–34. doi: 10.1016/S0140-6736(23)01352-2

2. Sun H, Saeedi P, Karuranga S, Pinkepank M, Ogurtsova K, Duncan BB, et al. Mbanya JC et al: IDF Diabetes Atlas: Global, regional and country-level diabetes prevalence estimates for 2021 and projections for 2045. *Diabetes Res Clin Pract*. (2022) 183:109119. doi: 10.1016/j.diabres.2021.109119

3. Piché ME, Tchernof A, Després JP. Obesity phenotypes, diabetes, and cardiovascular diseases. *Circ Res*. (2020) 126:1477–500. doi: 10.1161/CIRCRESAHA.120.316101

4. Zheng J, Hu Y, Xu H, Lei Y, Zhang J, Zheng Q, et al. Guo Q et al: Normal-weight visceral obesity promotes a higher 10-year atherosclerotic cardiovascular disease risk in patients with type 2 diabetes mellitus-a multicenter study in China. *Cardiovasc Diabetol*. (2023) 22:137. doi: 10.1186/s12933-023-01876-7

5. Kishida K, Funahashi T, Matsuzawa Y, Shimomura I. Visceral adiposity as a target for the management of the metabolic syndrome. *Ann Med*. (2012) 44:233–41. doi: 10.3109/07853890.2011.564202

6. Neeland IJ, Poirier P, Després JP. Cardiovascular and metabolic heterogeneity of obesity: clinical challenges and implications for management. *Circulation*. (2018) 137:1391–406. doi: 10.1161/CIRCULATIONAHA.117.029617

7. Xu K, Zheng Q, Shao J, Yang L, Dai Y, Zhang J, et al. Cheng J et al: Sex differences in the association between visceral adipose tissue and atherosclerosis in type 2 diabetes patients with normal bodyweight: A study in a Chinese population. *J Diabetes Invest*. (2023) 14:92–101. doi: 10.1111/jdi.13913

8. Zhao L, Zhou X, Chen Y, Dong Q, Zheng Q, Wang Y, et al. Xu F et al: Association of visceral fat area or BMI with arterial stiffness in ideal cardiovascular health metrics among T2DM patients. *J Diabetes*. (2024) 16:e13463. doi: 10.1111/1753-0407.13463

9. Piché ME, Poirier P, Lemieux I, Després JP. Overview of epidemiology and contribution of obesity and body fat distribution to cardiovascular disease: an update. *Prog Cardiovasc Dis*. (2018) 61:103–13. doi: 10.1016/j.pcad.2018.06.004

10. Liu J, Fox CS, Hickson DA, May WD, Hairston KG, Carr JJ, et al. Impact of abdominal visceral and subcutaneous adipose tissue on cardiometabolic risk factors: the Jackson Heart Study. *J Clin Endocrinol Metab*. (2010) 95:5419–26. doi: 10.1210/jc.2010-1378

11. Virtue S, Vidal-Puig A. Adipose tissue expandability, lipotoxicity and the Metabolic Syndrome–an allostatic perspective. *Biochim Biophys Acta*. (2010) 1801:338–49. doi: 10.1016/j.bbalip.2009.12.006

12. Ibrahim MM. Subcutaneous and visceral adipose tissue: structural and functional differences. *Obes reviews: an Off J Int Assoc Study Obes*. (2010) 11:11–8. doi: 10.1111/j.1467-789X.2009.00623.x

13. Bonen A, Tandon NN, Glatz JF, Luiken JJ, Heigenhauser GJ. The fatty acid transporter FAT/CD36 is upregulated in subcutaneous and visceral adipose tissues in human obesity and type 2 diabetes. *Int J Obes (2005)*. (2006) 30:877–83. doi: 10.1038/sj.ijo.0803212

14. Carobbio S, Pellegrinelli V, Vidal-Puig A. Adipose tissue function and expandability as determinants of lipotoxicity and the metabolic syndrome. *Adv Exp Med Biol*. (2017) 960:161–96. doi: 10.1007/978-3-319-48382-5_7

15. Ren Y, Cheng L, Qie R, Han M, Kong L, Yan W, et al. Dose-response association of Chinese visceral adiposity index with comorbidity of hypertension and diabetes mellitus among elderly people. *Front Endocrinol*. (2023) 14:1187381. doi: 10.3389/fendo.2023.1187381

16. Xie Y, Zhang Y, Qin P, Ping Z, Wang C, Peng X, et al. Wang L et al: The association between Chinese Visceral Adipose Index and coronary heart disease: A cohort study in China. *Nutrition metabolism Cardiovasc diseases: NMCD*. (2022) 32:550–9. doi: 10.1016/j.numecd.2021.10.020

17. Yu J, Yi Q, Chen G, Hou L, Liu Q, Xu Y, et al. The visceral adiposity index and risk of type 2 diabetes mellitus in China: A national cohort analysis. *Diabetes/metabolism Res Rev*. (2022) 38:e3507. doi: 10.1002/dmrr.3507

18. Lear SA, Humphries KH, Kohli S, Chockalingam A, Frohlich JJ, Birmingham CL. Visceral adipose tissue accumulation differs according to ethnic background: results of the Multicultural Community Health Assessment Trial (M-CHAT). *Am J Clin Nutr*. (2007) 86:353–9. doi: 10.1093/ajcn/86.2.353

19. Omura-Ohata Y, Son C, Makino H, Koezuka R, Tochiya M, Tamanaha T, et al. Efficacy of visceral fat estimation by dual bioelectrical impedance analysis in detecting cardiovascular risk factors in patients with type 2 diabetes. *Cardiovasc Diabetol*. (2019) 18:137. doi: 10.1186/s12933-019-0941-y

20. Xu L, Song P, Xu J, Zhang H, Yu C, Guan Q, et al. Viscus fat area contributes to the Framingham 10-year general cardiovascular disease risk in patients with type 2 diabetes mellitus. *Life Sci*. (2019) 220:69–75. doi: 10.1016/j.lfs.2019.01.036

21. Qiu Y, Deng X, Sha Y, Wu X, Zhang P, Chen K, et al. Yuan G et al: Visceral Fat Area, Not Subcutaneous Fat Area, is Associated with Cardiac Hemodynamics in Type 2 Diabetes. *Diabetes Metab syndrome obesity: Targets Ther*. (2020) 13:4413–22. doi: 10.2147/DMSO.S284420

22. Shuster A, Patlas M, Pinthus JH, Mourtzakis M. The clinical importance of visceral adiposity: a critical review of methods for visceral adipose tissue analysis. *Br J Radiol*. (2012) 85:1–10. doi: 10.1259/bjr/38447238

23. Lee SJ, Liu J, Yao J, Kanarek A, Summers RM, Pickhardt PJ. Fully automated segmentation and quantification of visceral and subcutaneous fat at abdominal CT: application to a longitudinal adult screening cohort. *Br J Radiol*. (2018) 91:20170968. doi: 10.1259/bjr.20170968

24. Dang K, Wang X, Hu J, Zhang Y, Cheng L, Qi X, et al. The association between triglyceride-glucose index and its combination with obesity indicators and cardiovascular disease: NHANES 2003-2018. *Cardiovasc Diabetol*. (2024) 23:8. doi: 10.1186/s12933-023-02115-9

25. ElSayed NA, Aleppo G, Aroda VR, Bannuru RR, Brown FM, Bruemmer D, et al. Johnson EL et al: Erratum. *2. Classification diagnosis diabetes: Standards Care Diabetes-2023. Diabetes Care*. (2023) 46:S19–40. doi: 10.2337/dc23-S002

26. Zhou BF. Predictive values of body mass index and waist circumference for risk factors of certain related diseases in Chinese adults–study on optimal cut-off points of body mass index and waist circumference in Chinese adults. *Biomed Environ sciences: BES*. (2002) 15:83–96.

27. Zhang M, Shi Y, Zhou B, Huang Z, Zhao Z, Li C, et al. Li X et al: Prevalence, awareness, treatment, and control of hypertension in China, 2004-18: findings from six rounds of a national survey. *BMJ (Clinical Res ed)*. (2023) 380:e071952. doi: 10.1136/bmj-2022-071952

28. Levey AS, Coresh J, Greene T, Stevens LA, Zhang YL, Hendriksen S, et al. Using standardized serum creatinine values in the modification of diet in renal disease study equation for estimating glomerular filtration rate. *Ann Internal Med*. (2006) 145:247–54. doi: 10.7326/0003-4819-145-4-200608150-00004

29. Zeng Q, Wang L, Dong S, Zha X, Ran L, Li Y, et al. Lu Y et al: CT-derived abdominal adiposity: Distributions and better predictive ability than BMI in a nationwide study of 59,429 adults in China. *Metabolism: Clin Exp*. (2021) 115:154456. doi: 10.1016/j.metabol.2020.154456

30. Huo L, Li K, Deng W, Wang L, Xu L, Shaw JE, et al. Optimal cut-points of visceral adipose tissue areas for cardiometabolic risk factors in a Chinese population: a cross-sectional study. *Diabetic medicine: J Br Diabetic Assoc*. (2019) 36:1268–75. doi: 10.1111/dme.14060

31. Wang L, Wang W, Xu L, Cheng X, Ma Y, Liu D, et al. Relation of visceral and subcutaneous adipose tissue to bone mineral density in chinese women. *Int J Endocrinol*. (2013) 2013:378632. doi: 10.1155/2013/378632

32. Stefan N. Causes, consequences, and treatment of metabolically unhealthy fat distribution. *Lancet Diabetes Endocrinol*. (2020) 8:616–27. doi: 10.1016/S2213-8587(20)30110-8

33. Zhang S, Huang Y, Li J, Wang X, Wang X, Zhang M, et al. Increased visceral fat area to skeletal muscle mass ratio is positively associated with the risk of cardiometabolic diseases in a Chinese natural population: A cross-sectional study. *Diabetes/metabolism Res Rev*. (2023) 39:e3597. doi: 10.1002/dmrr.3597

34. Lee SR, Heo JH, Jo SL, Kim G, Kim SJ, Yoo HJ, et al. Baek IJ et al: Progesterone receptor membrane component 1 reduces cardiac steatosis and lipotoxicity via activation of fatty acid oxidation and mitochondrial respiration. *Sci Rep*. (2021) 11:8781. doi: 10.1038/s41598-021-88251-2

35. Ramachandran A, Chamukuttan S, Shetty SA, Arun N, Susairaj P. Obesity in Asia–is it different from rest of the world. *Diabetes/metabolism Res Rev*. (2012) 28 Suppl 2:47–51. doi: 10.1002/dmrr.2353

36. Barba C, Cavalli-Sforza T, Cutter J, Darnton-Hill I, Deurenberg P, Deurenberg-Yap M, et al. Appropriate body-mass index for Asian populations and its implications for policy and intervention strategies. *Lancet (London England)*. (2004) 363:157–63. doi: 10.1016/S0140-6736(03)15268-3

37. Mu L, Liu J, Zhou G, Wu C, Chen B, Lu Y, et al. Nasir K et al: Obesity Prevalence and Risks Among Chinese Adults: Findings From the China PEACE Million Persons Project, 2014-2018. *Circ Cardiovasc Qual outcomes*. (2021) 14:e007292. doi: 10.1161/CIRCOUTCOMES.120.007292

38. Marcelin G, Silveira ALM, Martins LB, Ferreira AV, Clément K. Deciphering the cellular interplays underlying obesity-induced adipose tissue fibrosis. *J Clin Invest*. (2019) 129:4032–40. doi: 10.1172/JCI129192

39. Straub LG, Scherer PE. Metabolic messengers: adiponectin. *Nat Metab*. (2019) 1:334–9. doi: 10.1038/s42255-019-0041-z

40. Qiao T, Luo T, Pei H, Yimingniyazi B, Aili D, Aimudula A, et al. Association between abdominal obesity indices and risk of cardiovascular events in Chinese populations with type 2 diabetes: a prospective cohort study. *Cardiovasc Diabetol*. (2022) 21:225. doi: 10.1186/s12933-022-01670-x

41. Mao J, Gan S, Gong S, Zhou Q, Yu F, Zhou H, et al. Visceral fat area is more strongly associated with arterial stiffness than abdominal subcutaneous fat area in Chinese patients with type 2 diabetes. *Diabetol Metab syndrome*. (2024) 16:123. doi: 10.1186/s13098-024-01356-2

42. Harris MM, Stevens J, Thomas N, Schreiner P, Folsom AR. Associations of fat distribution and obesity with hypertension in a bi-ethnic population: the ARIC study. *Atheroscl Risk Communities Study. Obes Res*. (2000) 8:516–24. doi: 10.1038/oby.2000.64

43. Bouchi R, Takeuchi T, Akihisa M, Ohara N, Nakano Y, Nishitani R, et al. Minami I et al: High visceral fat with low subcutaneous fat accumulation as a determinant of atherosclerosis in patients with type 2 diabetes. *Cardiovasc Diabetol*. (2015) 14:136. doi: 10.1186/s12933-015-0302-4

44. Xiong Y, Yu Y, Jiang H, Yang Q, Liao R, Wang L, et al. Visceral fat area is a better predictor than coronary artery calcification score for cardiovascular outcomes and all-cause death in patients on hemodialysis. *J Renal nutrition: Off J Council Renal Nutr Natl Kidney Foundation*. (2021) 31:306–12. doi: 10.1053/j.jrn.2020.08.009

45. Wu Y, Xu W, Guo L, Li W, Zhang L, Gao L, et al. Association of the time course of Chinese visceral adiposity index accumulation with cardiovascular events in patients with hypertension. *Lipids Health Dis*. (2023) 22:90. doi: 10.1186/s12944-023-01852-w

46. Xia MF, Chen Y, Lin HD, Ma H, Li XM, Aleteng Q, et al. Pan BS et al: A indicator of visceral adipose dysfunction to evaluate metabolic health in adult Chinese. *Sci Rep*. (2016) 6:38214. doi: 10.1038/srep38214

47. Wang W, Lv FY, Tu M, Guo XL. Perirenal fat thickness contributes to the estimated 10-year risk of cardiovascular disease and atherosclerotic cardiovascular disease in type 2 diabetes mellitus. *Front Endocrinol*. (2024) 15:1434333. doi: 10.3389/fendo.2024.1434333

frontiers | Frontiers in Endocrinology

TYPE Original Research
PUBLISHED 29 October 2025
DOI 10.3389/fendo.2025.1693820

OPEN ACCESS

EDITED BY
Ramoji Kosuru,
Versiti Blood Research Institute, United States

REVIEWED BY
Lexun Wang,
Guangdong Pharmaceutical University, China
Shimaa K. Saber,
Mansoura University, Egypt

*CORRESPONDENCE
Qiu Chen
chenqiu1005@cdutcm.edu.cn

†PRESENT ADDRESS
Chan Zhu,
Key Laboratory of Birth Defects and Related Diseases of Women and Children, Chengdu, Sichuan, China

RECEIVED 27 August 2025
ACCEPTED 06 October 2025
PUBLISHED 29 October 2025

CITATION
Wang Y, Zhou Q, Li C, Chenmou X, Zhu C and Chen Q (2025) Construction and evaluation of a combined model of NAA/STZ-induced type 2 diabetes with carotid balloon injury in SD rats.
Front. Endocrinol. 16:1693820.
doi: 10.3389/fendo.2025.1693820

Construction and evaluation of a combined model of NAA/STZ-induced type 2 diabetes with carotid balloon injury in SD rats

Yanmei Wang[1,2], Qian Zhou[2], Chengshan Li[3], Xiaojing Chenmou[3], Chan Zhu[2,4†] and Qiu Chen[2*]

[1]Clinical Teaching and Research Department, Ya'an Polytechnic College, Ya'an, Sichuan, China, [2]Department of Endocrinology, Hospital of Chengdu University of Traditional Chinese Medicine, Chengdu, Sichuan, China, [3]Internal Medicine Department II, Ya'an Polytechnic College Affiliated Hospital, Ya'an, Sichuan, China, [4]Department of Traditional Chinese Medicine, West China Second University Hospital, Sichuan University, Chengdu, Sichuan, China

Purpose: Diabetic macroangiopathy is a leading cause of disability and mortality in type 2 diabetes mellitus (T2DM) patients, but existing animal models have limitations such as complex genetic manipulation or long induction cycles. This study constructed and evaluated a combined model of nicotinamide (NAA)/streptozotocin (STZ)-induced T2DM and carotid balloon injury in Sprague–Dawley (SD) rats.

Methods: Sixty male SD rats were divided into four groups: control, VBI (only vascular balloon injury), T2DM (only NAA/STZ-induced T2DM), and T2DM+VBI (combined model) groups. T2DM was induced via NAA (110 mg/kg) followed by STZ (65 mg/kg); VBI was performed via a percutaneous transluminal coronary angioplasty (PTCA) balloon catheter. Over 6 weeks, metabolic indicators [intake, excretion, body weight, and random blood glucose (RBG)] were monitored; carotid tissues were collected at 2, 4, and 6 weeks post-VBI for HE staining and immunohistochemistry (α-SMA, F4/80, and MMP-9); and blood cell counts and plasma biochemistry were analyzed.

Results: The T2DM induction success rate was 90% (no mortality); the postoperative mortality rate was 14.3% in the T2DM+VBI group (vs. 7% in the VBI group). The T2DM and T2DM+VBI groups presented typical diabetic symptoms and persistent hyperglycemia. Histologically, only the VBI and T2DM+VBI groups exhibited time-dependent neointimal proliferation, with T2DM+VBI exhibiting a larger neointimal area, a greater proliferation index, more severe luminal stenosis (2-week hyperplasia comparable to VBI 6 weeks) and increased F4/80-positive macrophages/MMP-9 (poor plaque stability). No major organ abnormalities (except T2DM hepatic steatosis) or intergroup blood parameter differences were found.

Conclusion: This combined model has stable hyperglycemia, obvious neointimal hyperplasia, rapid modeling and a high success rate (optimal observation window: 2–4 weeks post-VBI). It recapitulates diabetic macroangiopathy pathology and is suitable for investigating therapeutic efficacy and related molecular/cellular mechanisms.

KEYWORDS

type 2 diabetes mellitus (T2DM), vascular balloon injury (VBI), neointimal hyperplasia, diabetic macroangiopathy, nicotinamide (NAA), streptozotocin (STZ)

1 Introduction

Diabetic macroangiopathy is an atherosclerosis-related complication of long-term hyperglycemia, commonly affecting medium-sized arteries such as the coronary, cerebral basilar, carotid, renal, and lower limb arteries. In patients with type 2 diabetes, macroangiopathy is more prevalent and constitutes a major cause of disability and mortality (1–3). Hyperglycemia-induced oxidative stress and endothelial dysfunction promote the expression of adhesion molecules, chemokines, and other proinflammatory mediators, leading to extensive macrophage infiltration and the migration and proliferation of vascular smooth muscle cells. High glucose levels trigger glycosylation and the synthesis of oxidized low-density lipoprotein, further promoting foam cell formation in plaques, inducing smooth muscle apoptosis, and inhibiting collagen synthesis—all of which increase the risk of subsequent plaque rupture. Additionally, high glucose activates platelets and reduces the levels of endogenous platelet inhibitors, thereby promoting thrombosis (4, 5). Thus, diabetes is a well-recognized risk factor for atherosclerotic diseases, and cardiovascular events due to plaque rupture are significantly more common in diabetic patients, which is attributed to more extensive vascular involvement and diffuse atherosclerotic lesions (6).

The mechanisms underlying the progression from hyperglycemia to arterial inflammatory injury involve genetic, epigenetic, and cellular signaling pathways. Notably, oxidative stress and inflammation interact as key drivers (7). Reconstruction of this process requires a representative animal model. Rodents are widely used in biological and preclinical research because of their practical and economic advantages. However, mice lack cholesteryl ester transfer protein, leading to a distinct lipoprotein distribution compared with that of humans; this reduces circulating cholesteryl ester levels, protecting against atherosclerosis (8). Thus, generating atherosclerotic plaques in mice requires genetic manipulation, often involving crossbreeding with diabetic gene-deficient mice to model diabetic macroangiopathy—limiting large-scale application (9). A high-fat diet combined with streptozotocin (STZ) is commonly used to induce such models in rats, but this approach suffers from a long induction period, expensive feed, poor palatability, inadequate intimal hyperplasia, and failure to replicate atherosclerotic lesions optimally (10).

With the widespread implementation of percutaneous interventional therapy, clinical observations have shown that atherosclerotic plaque formation not only occurs naturally but also develops following arterial endotheliectomy, balloon angioplasty, and stent implantation (11). Subsequent animal studies demonstrated that balloon inflation and rotation can lead to complete denudation of vascular monolayer endothelial cells and that invasive neointima formation at the injury site follows a time-dependent pattern—this accelerates the spontaneous progression of atherosclerosis. Against this backdrop, the carotid balloon injury model was developed; rats are typically the preferred animal model, primarily because of their favorable size-related advantages (12). Vascular balloon injury (VBI) offers high reproducibility, controllable injury severity and length, simplicity, low postoperative mortality, and short modeling time, making it widely used in atherosclerosis research (13).

Nicotinamide (NAA) combined with STZ induction, first proposed by Masiello P et al. in 1998, was used to construct nonobese type 2 diabetes models in rats (14) and has since been extended to mice. It is widely used in studies of diabetes pathogenesis and complications and in preclinical drug screening (15, 16). Owing to the cytotoxicity of STZ to pancreatic β-cells and the global cytoprotective effect of NAA, this model leverages the contradictory effects of STZ on β-cells: early intervention with NAA can preserve a certain proportion of residual pancreatic β-cells, enabling them to release insulin under glucose stimulation (16, 17). While insulin resistance is lacking, it mimics pancreatic β-cell dysfunction in type 2 diabetes.

In this study, we constructed a combined model of NAA/STZ-induced type 2 diabetes with carotid balloon injury in Sprague–Dawley (SD) rats, monitored changes in metabolic indicators and the degree of arterial intimal thickening after modeling, and compared it with models of diabetes alone or balloon injury alone. A relatively comprehensive evaluation of this model has been performed.

2 Materials and methods

2.1 Material

Nicotinamide (NAA) and streptozotocin (STZ) were purchased from Sigma–Aldrich (St. Louis, MO, USA). Sodium citrate buffer (1 mol/L, pH 4.5, sterile) was obtained from Solarbio (Beijing, China). The primary antibodies used included rabbit anti-F4/80 (AR0279, Shenda Bio, China), rabbit anti-α-SMA (α-smooth muscle actin, 19245, CST, USA), and rabbit anti-MMP-9 (anti-matrix metalloproteinase-9, A11147, ABclonal, USA) antibodies. HRP-conjugated secondary antibodies were obtained from ZSGB-Bio (Beijing, China), and DAB dye was purchased from Dako (Denmark).

2.2 Animals

SD rats were purchased from Dashuo Experimental Animal Co., Ltd. (License No. SCXK 2020-30, Chengdu, China) and housed in an SPF environment with a 12 h light/dark cycle, 3–4 rats per cage, controlled temperature (23 ± 2 °C), and humidity (50–60%). All protocols were approved by the Experimental Animal Ethics Committee of the Affiliated Hospital of Chengdu University of Traditional Chinese Medicine (2021SDL-005).

2.3 Induction of type 2 diabetes in SD rats via the combination of NAA and STZ

SD rats were fasted overnight. After being weighed, they were intraperitoneally injected with 5% (w/v) NAA working solution at

110 mg/kg, followed by 1% (w/v) STZ working solution at 65 mg/kg 15 minutes later (14, 18). Random blood glucose (RBG) was measured 3 and 7 days post-modeling; values ≥ 16.7 mmol/L indicated successful induction (19, 20).

2.4 Establishment of a macroangiopathy model via carotid balloon injury

The rats were anesthetized with an intraperitoneal injection of 1% (w/v) pentobarbital sodium (40 mg/kg). After neck disinfection, a midline cervical incision was made, and the subcutaneous tissues and glands were bluntly dissected to expose the left sternocleidomastoid muscle. The common, external, and internal carotid arteries were identified, and silk thread was tied to temporarily occlude blood flow. A pressure pump was connected to a percutaneous transluminal coronary angioplasty (PTCA) balloon catheter to test airtightness, which was then evacuated to negative pressure for use. A "V"-shaped incision parallel to the vessel long axis was made 3 mm from the external carotid bifurcation. The balloon was advanced from the incision to the proximal common carotid artery, the common carotid occlusion was released, and the balloon was advanced 1–2 cm further. The pump was pressurized to 3–4 ATMs (with slight friction felt during rotation/retraction), and the balloon was withdrawn to the incision while rotating. This inflation–retraction cycle was repeated twice. After the third withdrawal, the balloon was deflated and removed, and then the external carotid proximal to the incision was ligated. The internal carotid occlusion was released to restore blood flow, confirmed by visible pulsation (12). The incision was sutured, and heparin (100 IU/kg) was injected intraperitoneally for anticoagulation. The rats were housed individually until recovery and then were grouped with other postoperative littermates. All balloon injuries were performed by the same surgeon.

2.5 Experimental design

2.5.1 Grouping and treatment

After 7 days of acclimation, 60 male SD rats (180–200 g) were randomly divided into normal and diabetic groups. The diabetes group received NAA followed by STZ; the normal group received 0.9% saline (1 mL/rat) and sodium citrate buffer (2 mL/rat) via intraperitoneal injection. After 1 week, diabetic rats (meeting the blood glucose criteria) were randomized to the T2DM+VBI (undergoing carotid balloon injury) or T2DM (diabetes control) groups; normal rats were randomized to the VBI (carotid balloon injury) or control (normal control) groups (Figure 1).

2.5.2 Feeding protocol

The rats were fed standard rodent chow with ad libitum access to food and water. Daily water intake (mL/rat·d) was recorded. Cage bedding (corncob) was weighed before and after replacement to estimate daily excretion (g/rat·d). The remaining feed was weighed weekly, and fresh feed (1500 g) was provided to calculate the average daily food intake (g/rat·d). Five rats per group were weighed weekly, and tail vein RBG was measured.

At 2 and 4 weeks post-VBI, 3 rats per group were euthanized with 3% pentobarbital sodium, and the left common carotid artery was collected for histological staining. At 6 weeks post-VBI, the remaining rats were euthanized; abdominal aorta blood was

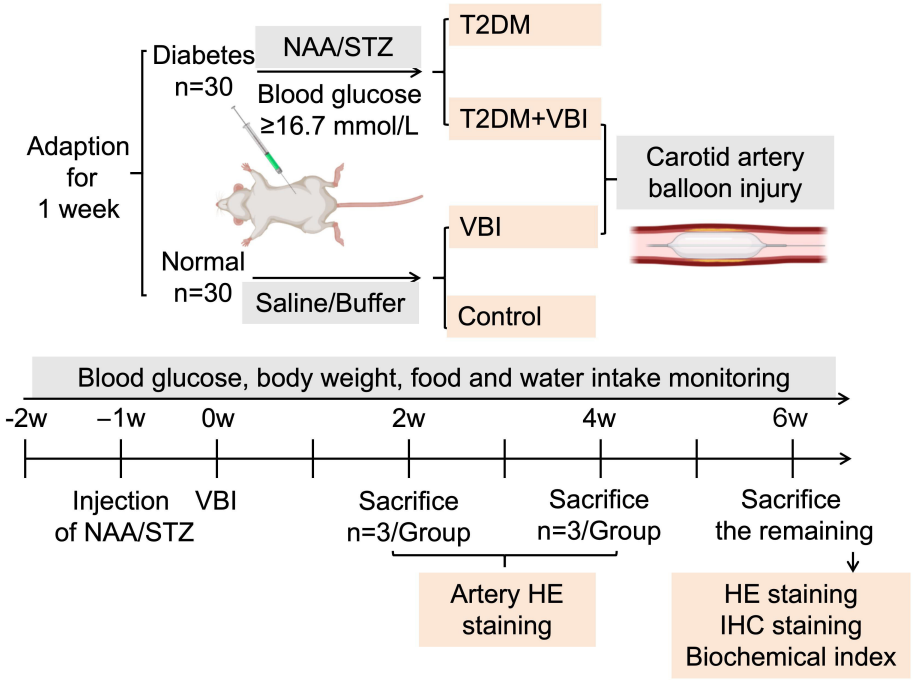

FIGURE 1
Experimental grouping and protocol. VBI, vascular balloon injury; T2DM, type 2 diabetes mellitus; NAA, nicotinamide; STZ, streptozotocin.

collected for biochemical analysis, and the left common carotid artery and major organs were harvested for histological and immunohistochemical staining (Figure 1).

2.6 HE staining

Carotid arteries and organs were fixed in 4% (w/v) paraformaldehyde for ≥24 h, embedded in paraffin, and sectioned (4 μm). Hematoxylin and eosin (HE) staining was performed according to standard protocols. The sections were imaged via an automatic inverted fluorescence microscope (IX83, Olympus, Japan), and morphometric analysis was conducted with ImageJ (Fiji for Mac OS X, NIH, USA). Lumen, internal elastic lamina (IEL), and external elastic lamina (EEL) areas were measured by a blinded observer.

2.7 Immunohistochemical staining

Four-micrometer paraffin sections of injured arteries were deparaffinized, rehydrated, subjected to antigen retrieval, blocked, and then incubated overnight at 4 °C with the following primary antibodies: rabbit anti-F4/80 (1:100), anti-α-SMA (1:100), anti-MMP-9 (1:100), and anti-TNF-α (1:50). The sections were labeled with HRP-conjugated secondary antibodies and visualized with DAB. Images were captured via a microscope, and positive areas were quantified via ImageJ by a double-blinded investigator.

2.8 Statistical analysis

The data were analyzed via SPSS Statistics 26.0 (IBM, USA) and are expressed as the means ± standard deviations (SDs). Normality was tested via the Shapiro–Wilk test; nonparametric tests were used for nonnormal data. For comparisons between two groups, an unpaired t test was used; Welch's correction was applied when variances were unequal. For comparisons among multiple independent groups, one-way ANOVA with Tukey's *post hoc* test was employed; in cases of unequal variances, Brown–Forsythe/Welch ANOVA with Dunnett's T3 test was used instead. To compare the mean differences between groups with multifactorial interactions, two-way ANOVA was performed; if the sphericity assumption was violated, Geisser–Greenhouse correction was adopted, and Tukey's test was used for pairwise comparisons between groups. A value of $P < 0.05$ was considered statistically significant.

3 Results

3.1 General conditions and metabolic indicators

The rats in the control group generally maintained good health: they appeared lively and robust, with clean, glossy fur, and no spontaneous deaths occurred during the feeding period. In the VBI group, the rats exhibited mild lethargy on the second day after carotid balloon injury surgery but were not different from normal rats for the remainder of the observation period. Only one rat in this group died from anesthesia prior to model establishment, resulting in a mortality rate of 7%. For the rats subjected to diabetes induction (via STZ combined with NAA injection), no deaths occurred within one week post-injection. Among the 30 rats, 27 met the predefined blood glucose criteria, yielding a diabetes model success rate of 90%. Subsequently, 14 adult diabetic rats were randomly selected and subjected to carotid balloon injury surgery (assigned to the T2DM +VBI group). One rat died intraoperatively, and another died during postoperative resuscitation, leading to a mortality rate of 14.3%. The remaining 13 diabetic rats were allocated to the T2DM group. No deaths occurred in either the T2DM+VBI group or the T2DM group during the subsequent feeding period.

As shown in Figure 2A and Supplementary Table 1, the control and VBI groups had similar food intakes (~25 g/rat·d). The T2DM and T2DM+VBI groups presented significantly increased intake postmodeling: T2DM remained at ~50 g/rat·d, whereas T2DM+VBI intake decreased slightly 1 week post-injury and then approached T2DM levels. Since food intake was recorded only once per week, this measurement could reflect only the overall trend and did not allow for the calculation of significant differences.

Water intake was similar in the VBI and control groups (~50 mL/rat·d, not significant; Figure 2B). The T2DM and T2DM+VBI groups presented significantly increased water intake postmodeling ($P < 0.001$ vs. Control). T2DM intake remained >150 mL/rat·d, whereas T2DM+VBI intake decreased postinjury and then rose slowly but remained higher than Control and lower than T2DM intake ($P < 0.01$ vs. Control and $P < 0.05$ vs. T2DM at all post-VBI time points, Figure 2B and Supplementary Table 2).

The VBI and control cages were clean with formed feces; the T2DM and T2DM+VBI cages were dirty with loose stools. The weight increase of the cushion material determined by weighing the cage boxes was similar between the VBI and control groups (Figure 2C). The excretion of the T2DM and T2DM+VBI groups increased significantly post-modeling ($P < 0.01$ vs. Control). T2DM +VBI excretion decreased postinjury and then approached T2DM levels, with significant differences at 1, 2, 4, and 5 weeks post-VBI ($P < 0.05$, Supplementary Table 3).

Body weight increased in all groups over the observation period (Figure 2D). Specifically, the body weight of the VBI group was significantly lower than that of the control group only at 1 week post-injury ($P < 0.01$). The body weight of the T2DM group was lower than that of the control group at week 1 and weeks 3–6 ($P < 0.05$). In the T2DM+VBI group, the body weight was lower than that in the control group starting at 2 weeks post-VBI ($P < 0.05$); this group showed a consistent trend of change with the T2DM group, with statistical significance observed only at week 6 ($P < 0.05$, Supplementary Table 4).

The random blood glucose levels of the control and VBI groups were essentially identical, with both remaining stable at baseline levels throughout the entire experimental period; no significant

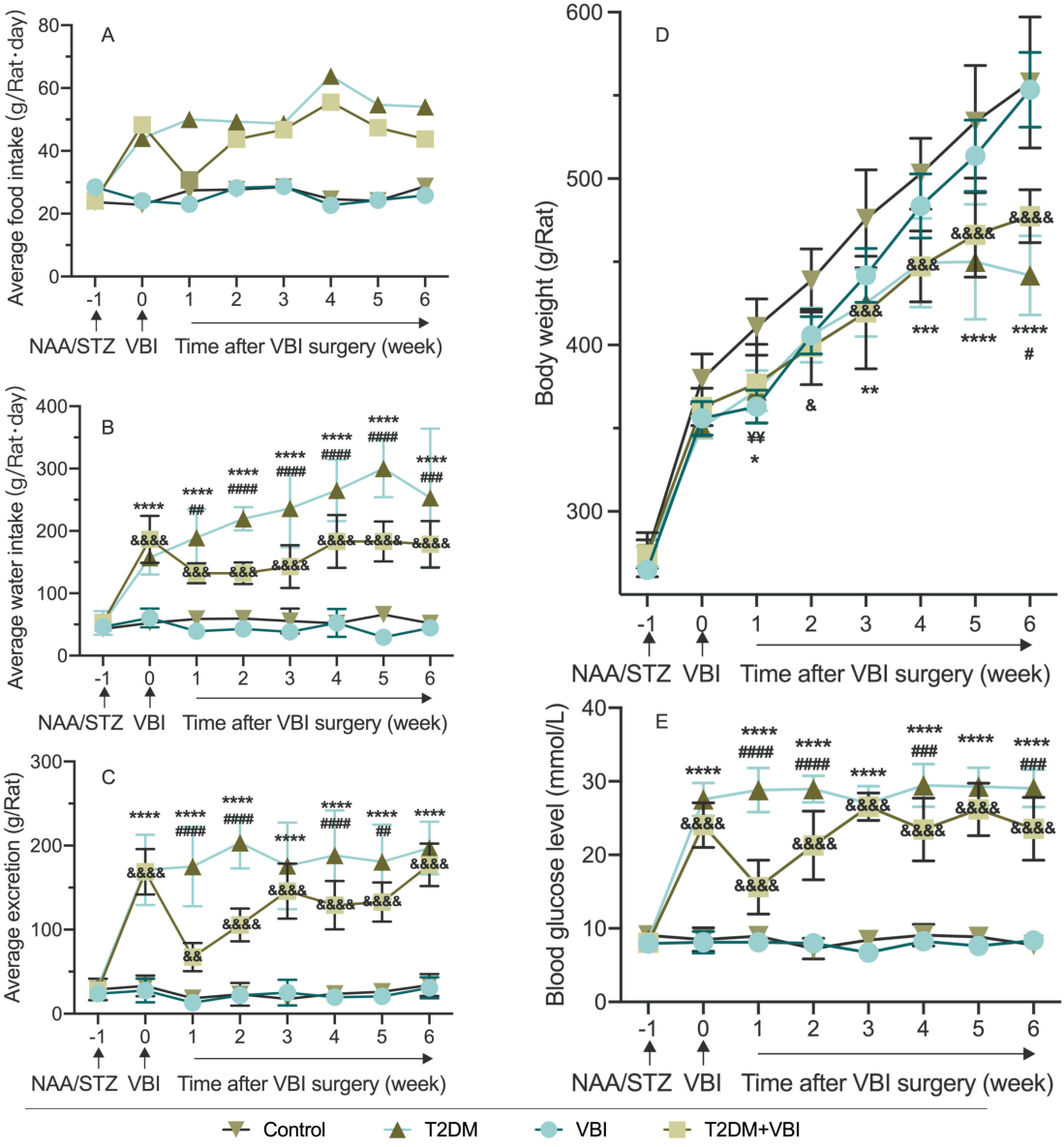

FIGURE 2
Comparison of average food intake. **(A)**, Water intake **(B)**, excretion **(C)**, body weight **(D)**, and random blood glucose **(E)** in rats after modeling. VBI, vascular balloon injury; T2DM, type 2 diabetes mellitus; NAA, nicotinamide; STZ, streptozotocin. Two-way ANOVA was performed for statistical comparison, and Geisser–Greenhouse correction was adopted if the sphericity assumption was violated: *: Comparison between the T2DM group and the control group (*P < 0.05; **P < 0.01; ***P < 0.001; ****P < 0.0001). & Comparison between the T2DM+VBI group and the control group (&P < 0.05; &&P < 0.01; &&&P < 0.001; &&&&P < 0.0001); ¥: Comparison between the VBI group and the control group (¥¥P < 0.01); #: Comparison between the T2DM+VBI group and the T2DM group (#P < 0.05; ##P < 0.01; ###P < 0.001; ####P < 0.0001).

differences were observed between these two groups (Figure 2E). Following modeling with STZ combined with NAA, the RBG levels of the rats in the T2DM and T2DM+VBI groups increased significantly. Compared with the control group, both groups presented statistically significant differences in blood glucose at all time points after diabetes induction (P < 0.001). For the T2DM group, blood glucose levels remained above 25 mmol/L and exhibited no significant fluctuations over time. After balloon injury surgery, the RGB level of the T2DM+VBI group decreased to 15.62 ± 3.66 mmol/L; although it gradually increased again, it remained slightly lower than that of the T2DM group (P < 0.05 at 1–2, 4, and 6 weeks post-VBI, Supplementary Table 5).

3.2 Comparison of carotid artery histomorphology

At 2, 4, and 6 weeks after vascular injury, samples were harvested from the left common carotid artery of the rats in each group for histological examination. Owing to varying degrees of

10.3389/fendo.2025.1693820

vascular lumen compression during paraffin embedding, which led to a reduced lumen deformation area, the measured lumen area was only used for calculating the intimal proliferation area and was not subjected to statistical analysis. In addition, no obvious intimal proliferation was observed in sections from rats in the normal control group or diabetes group; the monolayer vascular endothelium was closely attached to the internal elastic membrane, making it impossible to accurately distinguish the boundary between the two. Therefore, the intimal area and its related calculations were only performed for the VBI group and T2DM+VBI group. Two weeks after balloon injury, the carotid intima began to proliferate to varying degrees. In the presence of diabetes, the proliferation area increased with increasing injury time (Figure 3A). When the two groups were compared, intimal proliferation was more pronounced in diabetic rats after balloon injury; by 6 weeks post-injury, the vascular intima in most cases had thickened to a degree that nearly occluded the lumen and disrupted blood flow. Quantitative analysis revealed that at 2, 4, and 6 weeks post-injury, the neointimal area (IEL area–lumen area) in the T2DM+VBI group was significantly larger than that in the VBI group ($P<0.01$, Figure 3B). Similarly, statistical analysis of the proliferation index (neointimal area/media area) and stenosis

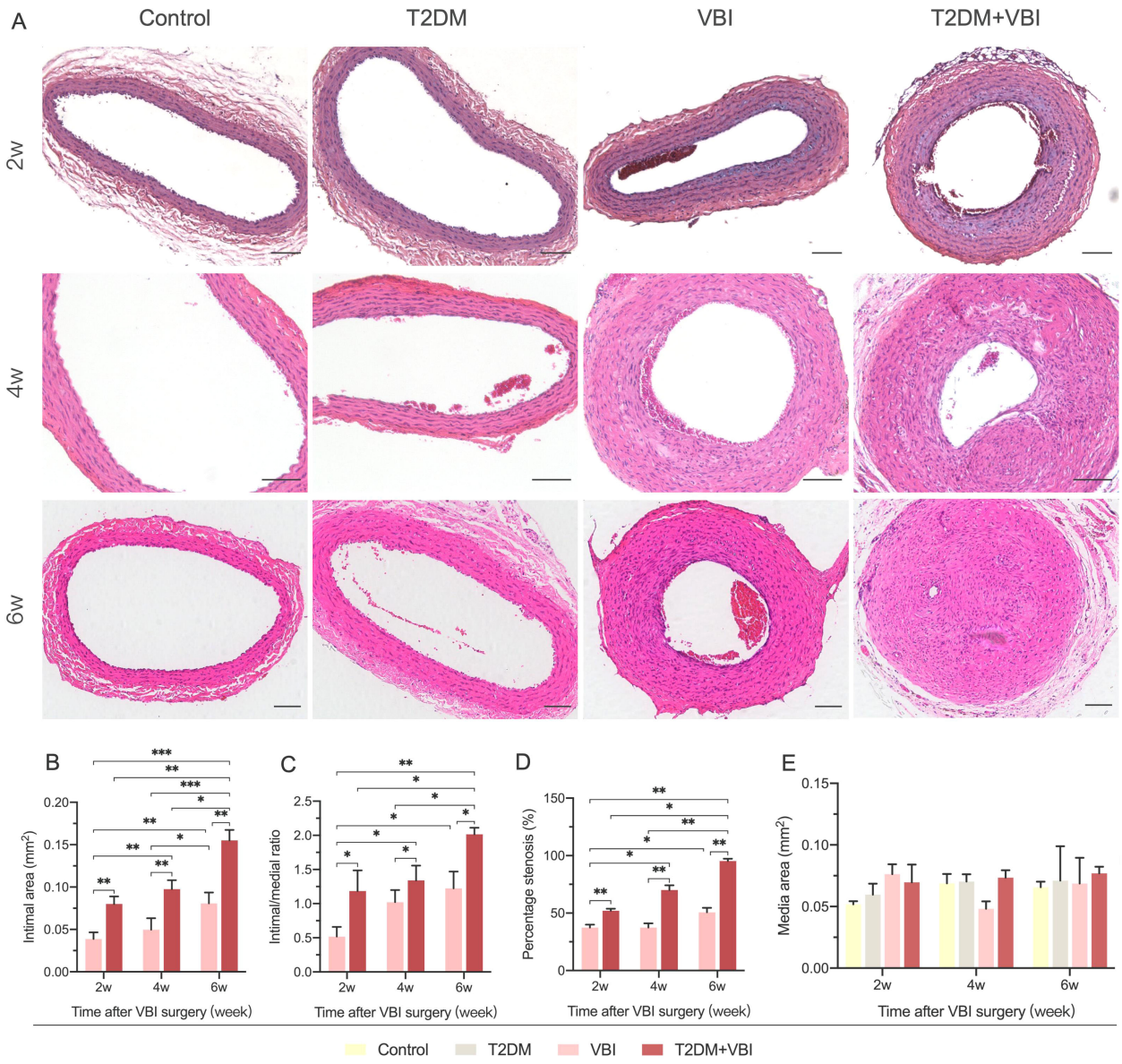

FIGURE 3
Comparison of carotid artery histomorphology (HE Staining) after balloon injury. **(A)** Representative HE-stained images of the carotid artery at 2, 4, and 6 weeks post-balloon injury in each group. **(B)** Comparison of the neointimal area at different time points after surgery among the groups. **(C)** Comparison of the arterial proliferation index at different time points after surgery among the groups. **(D)** Comparison of the percentage of carotid artery stenosis at different time points after surgery among the groups. **(E)** Comparison of the arterial media area at different time points after surgery among the groups. VBI, vascular balloon injury; T2DM, type 2 diabetes mellitus. Scale bar = 100 μm. Two-way ANOVA was performed for statistical comparison, and Geisser–Greenhouse correction was adopted if the sphericity assumption was violated, *P < 0.05; **P < 0.01; ***P < 0.001.

percentage [1 – (lumen area/IEL area)] (21, 22) revealed that both parameters were significantly greater in the T2DM+VBI group than in the VBI group, with statistically significant differences at each time point (P<0.01, Figures 3C, D). Notably, at 2 weeks post-injury, the neointimal area, proliferation index, and stenosis percentage in the T2DM+VBI group were comparable to those in the VBI group at 6 weeks post-injury, with no statistically significant differences (2w T2DM+VBI group vs. 6w VBI group: neointimal area=0.080 ± 0.009 mm^2 vs. 0.081 ± 0.013 mm^2, P = 0.9983; proliferation index=1.19 ± 0.30 vs. 1.22 ± 0.25, P = 0.9247; stenosis percentage=52.10 ± 1.68% vs. 50.63 ± 3.93%, P = 0.9995). In addition, there was no statistically significant difference in the arterial media area (EEL area – IEL area) among the different sampling time points (Figure 3E).

3.3 Immunohistochemical analysis of neointima

To further analyze and compare the compositional and structural changes in proliferating vascular endothelial cells, immunohistochemical staining was performed for the classical vascular smooth muscle cell molecular marker α-SMA and the macrophage-specific marker F4/80 in carotid artery tissues obtained from the rats in each group at 6 weeks post-injury. As shown in Figure 4A, in the control and T2DM groups, the arterial wall was smooth, the internal elastic lamina remained intact, and endothelial cells uniformly covered the IEL surface. The cells in the arterial media were arranged neatly, with abundant α-SMA expression detected between the internal and external elastic laminae. F4/80-positive cells were only scattered in an extremely sparse distribution. In the VBI group, despite significant thickening of the vascular intima, the spindle-shaped cells within the intima were relatively uniformly arranged and clustered on the luminal side. In contrast, the T2DM+VBI group presented unclear cellular structure and markedly disorganized arrangement in the thickened intima. Notably, both the VBI and T2DM+VBI groups presented prominent α-SMA expression in the proliferative intimal region, indicating that neointimal formation is driven primarily by the migration and proliferation of vascular smooth muscle cells. Quantitative analysis revealed no statistically significant difference in the proportion of the α-SMA-positive stained area within the

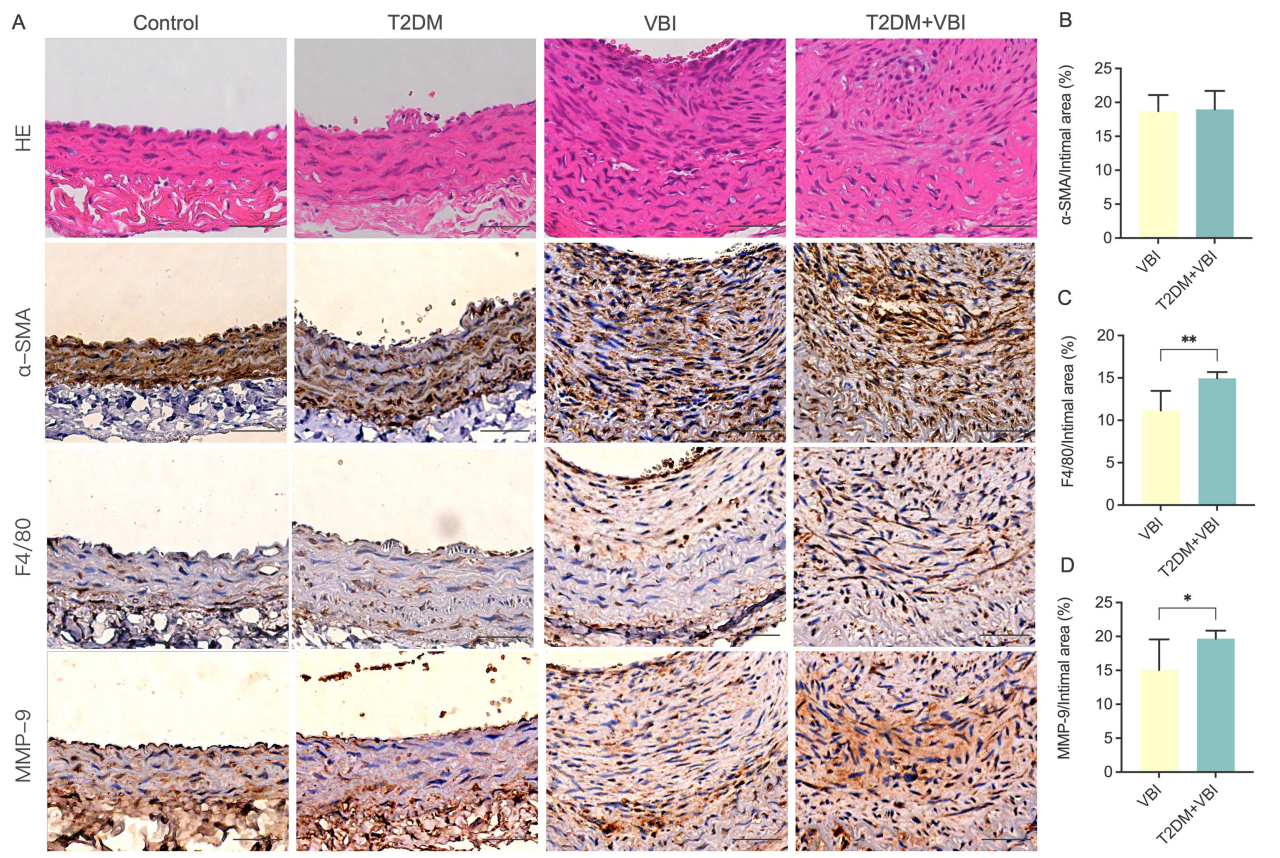

FIGURE 4
Comparison of carotid artery histopathological and immunohistochemical staining at 6 weeks post-balloon injury. **(A)** Representative images of immunohistochemical staining of the carotid artery in each group. **(B)** Ratio of the α-SMA-positive area to the neointimal area. **(C)** Ratio of the F4/80-positive area to the neointimal area. **(D)** Ratio of the MMP-9-positive area to the neointimal area. VBI, vascular balloon injury; T2DM, type 2 diabetes mellitus; α-SMA, α-smooth muscle actin; F4/80, macrophage marker; MMP, matrix metalloproteinases. Scale bar = 50 μm. Unpaired t tests were used for statistical comparisons, and Welch's correction was applied when variances were unequal, *P < 0.05, **P < 0.01.

neointima between the two groups (VBI group vs. T2DM+VBI group: 18.71 ± 2.376% vs. 18.98 ± 2.710%, P = 0.7577; Figures 4A, B). In F4/80-stained sections, the number of F4/80-positive cells in the proliferative intimal region was significantly greater in the T2DM+VBI group than in the VBI group (VBI group vs. T2DM +VBI group: 11.17 ± 2.297% vs. 14.97 ± 0.7204%, P = 0.0125), suggesting enhanced macrophage infiltration and more severe inflammatory responses (Figures 4A, C). Additionally, when the samples were stained with antibodies against matrix metalloproteinase-9 (MMP-9), extensive positive staining was also observed in the T2DM+VBI group. Compared with that in the VBI group, the proportion of MMP-9-positive stained area in the neointima in the VBI group was significantly different (VBI group vs. T2DM+VBI group: 15.07 ± 4.491% vs. 19.68 ± 1.183%, P = 0.0049; Figures 4A, D).

3.4 HE Staining of major organs

As shown in Figure 5, no significant histomorphological abnormalities were observed in hematoxylin–eosin (HE)-stained sections of the heart, lungs, spleen, or kidneys across all treatment groups; specifically, no pathological changes (e.g., cell degeneration, necrosis, or inflammatory cell infiltration) were detected. In HE-stained liver sections from the T2DM group, marked hepatocellular swelling with steatosis was observed, and some hepatocytes exhibited reticular fragmentation or even ballooning degeneration. Concurrently, numerous vacuoles (resulting from lipid droplet dissolution) were noted. In contrast, the T2DM+VBI group exhibited relatively mild hepatocellular injury, with only scattered, loosely arranged, and edematous hepatocytes (indicated by arrows); the overall cellular arrangement was comparable to that of the VBI group and the control group.

3.5 Whole blood cell and plasma biochemical analyses

Analysis of whole blood cell parameters in the rats across all the groups revealed the following: after STZ combined with NAA, the red blood cell (RBC) and white blood cell (WBC) counts in the T2DM and T2DM+VBI groups decreased to varying extents

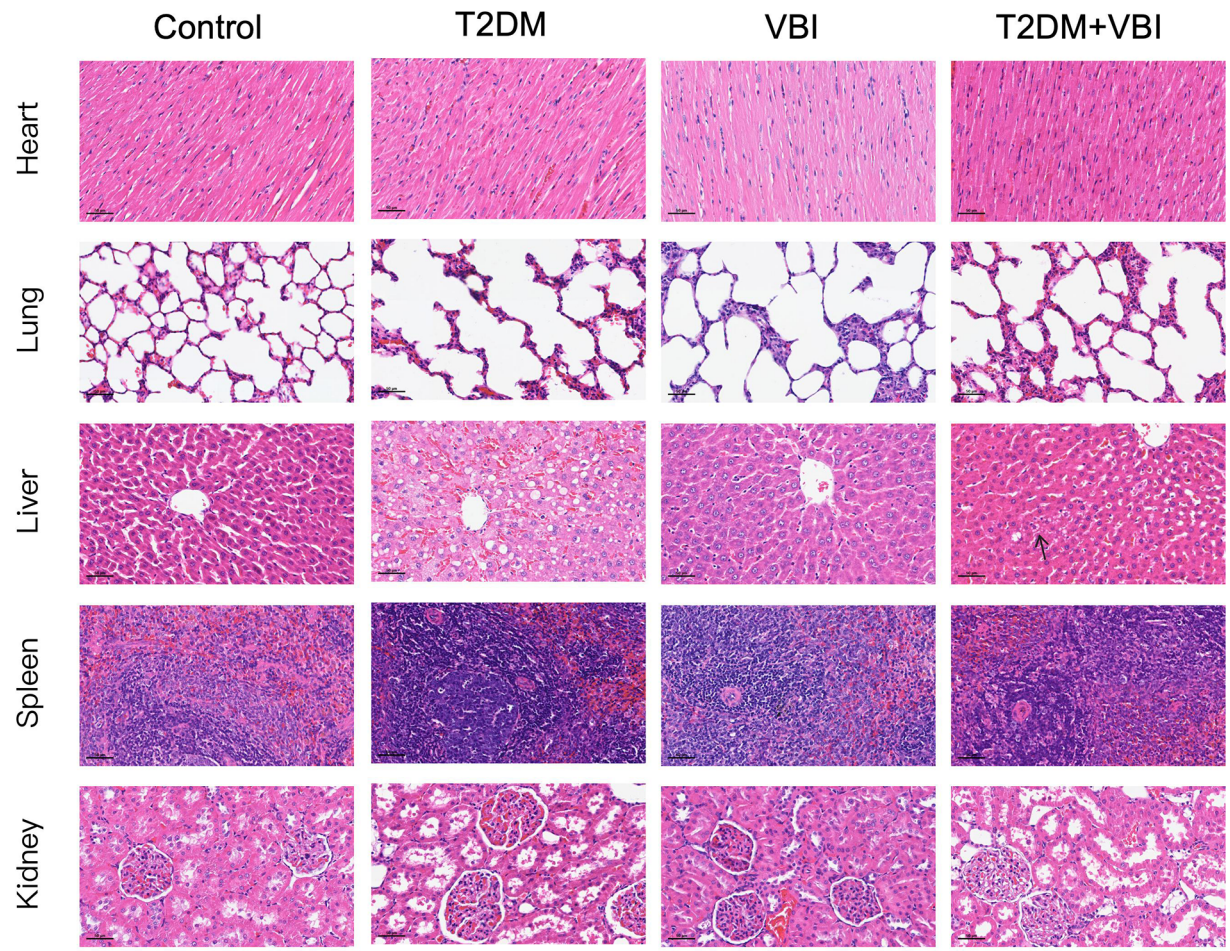

FIGURE 5
HE-stained sections of major organs from each group at 6 weeks post-VBI. VBI, vascular balloon injury; T2DM, type 2 diabetes mellitus. Scale bar = 50 μm.

compared with those in the control group and the VBI group; however, these differences did not reach statistical significance. No significant intergroup differences were observed in hemoglobin (HGB) or platelet (PLT) levels (Figures 6A–D).

Liver and kidney function analyses: Rats in the T2DM group presented significant increases in plasma aspartate transaminase (AST) levels, along with slight increases in plasma creatinine (Cr) and urea nitrogen (UN) levels. Nevertheless, these changes were not statistically significant compared with those of the other groups. Additionally, liver and kidney function parameters in the T2DM +VBI group were comparable to those in the control group, with no significant differences detected (Figures 6E–I).

Lipid metabolism: At 6 weeks post-modeling, the VBI group presented slight decreases in plasma total cholesterol (TC) and low-density lipoprotein (LDL) levels, although these reductions were not statistically significant. Moreover, the plasma lipid and lipoprotein levels in the T2DM and T2DM+VBI groups were comparable to those in the control group, with no significant intergroup differences observed (Figures 6J, K).

4 Discussion

Previous studies have applied arterial balloon injury intervention to STZ-induced diabetic animal models to investigate its therapeutic efficacy and underlying mechanisms; however, a comprehensive evaluation of this combined model is lacking (23–25). In the present study, we successfully established a combined model of NAA/STZ-induced type 2 diabetes mellitus and carotid balloon injury (T2DM+VBI model) in SD rats. On the basis of this model, we conducted a relatively comprehensive investigation to compare time-dependent arterial intimal thickening and postinjury changes in metabolic indicators between the T2DM+VBI group and two control groups: the T2DM group (SD rats with NAA/STZ-induced T2DM but no VBI) and the VBI group (SD rats with VBI but no T2DM). This work lays a foundation for the subsequent promotion and application of this combined model in studies exploring drug efficacy and potential mechanisms.

For diabetes induction, we used a combination of NAA at 110 mg/kg and STZ at 65 mg/kg. Although the initially proposed doses of these two agents are 230 mg/kg and 65 mg/kg, respectively (14), the NAA dose was reduced in practice to weaken its protective effect (NAA exhibits a 100% protective effect against STZ-induced pancreatic β-cell damage at adequate doses); this adjustment was intended to improve the diabetes induction rate. Additionally, the key to the combined use of NAA and STZ lies in standardizing the dosage, administration route, and timing across all experimental animals, which ensures the comparability of metabolic data between groups.

Streptozotocin (STZ) is widely utilized in chemically induced diabetes models. Owing to its structural similarity to glucose, STZ acts as a glucose analog and is selectively taken up by pancreatic β-cells via glucose transporter-2 (GLUT2), a membrane protein abundantly expressed on the β-cell surface. Upon entering β-cells, the nitrosoamide moiety of STZ exerts genotoxic and cytotoxic effects by attacking genomic DNA and inducing alkylation. This STZ-mediated DNA damage triggers excessive activation of poly-ADP-ribose-polymerase-1 (PARP-1), an enzyme that utilizes nicotinamide adenine dinucleotide (NAD+) as a substrate to catalyze poly-ADP-ribosylation. Sustained PARP-1 overactivation depletes intracellular NAD+ and adenosine triphosphate (ATP), ultimately resulting in β-cell necrosis (16). The sirtuin (SIRT) family of enzymes also relies on NAD+ as a cosubstrate to catalyze the deacylation of lysine residues on target proteins, generating NAA and 2-O-acetyl-ADP-ribose as byproducts (26). Among SIRTs, SIRT1 plays a pivotal role in cellular defense against oxidative stress and in modulating insulin sensitivity and β-cell function in the context of the pathophysiological network of nonalcoholic fatty liver disease and T2DM (17). Notably, both the PARP-1 and SIRT enzymes share NAD+ as a critical substrate and produce endogenous NAA as a common product; thus, their activities can be inhibited by exogenous NAA (17, 18, 26). Leveraging this NAA-induced suppression, the combination of STZ and NAA achieves two key objectives for T2DM modeling: downregulating PARP-1 activation to preserve residual β-cells and inhibiting SIRT1 to mimic insulin resistance. As a model of nonobese T2DM, the STZ + NAA system has distinct advantages for diabetes research: it maintains stable moderate hyperglycemia without requiring exogenous insulin for animal survival, retains partial glucose-stimulated insulin secretion capacity, and responds to sulfonylureas. These features make it highly suitable for evaluating the biochemical and pharmacological effects of potential antidiabetic agents in a model that mirrors key characteristics of human T2DM (16).

For the evaluation of diabetes model success, we adopted an RBG threshold of ≥ 16.7 mmol/L as the criterion, which was determined on the basis of two considerations. First, rats exhibited reduced food intake postballoon injury, and fasting blood glucose monitoring (which requires food restriction) further increased animal mortality. Thus, random blood glucose monitoring was used, and consistency was maintained throughout the feeding period. Second, blood glucose measurement in rats is frequently accompanied by stress, and the baseline RBG of normal rats fluctuates approximately 9 mmol/L, approaching the clinical diagnostic threshold of 11.1 mmol/L for random blood glucose in patients with diabetes mellitus. Furthermore, our preliminary experiments (data not shown) revealed that rats with RBG levels between 11.1 and 16.7 mmol/L tended to spontaneously revert to normoglycemia during the diabetic feeding period. These factors collectively justified the use of an RBG level of 16.7 mmol/L as a criterion for successful diabetes induction. On the basis of the aforementioned induction protocol and criteria, this study achieved a high diabetes induction rate (90%) and a low mortality rate (0%) during the diabetes modeling phase.

For carotid balloon injury modeling, we employed a 1.5 × 12 mm PTCA balloon dilation catheter. Compared with traditional Fogarty balloon thrombectomy catheters, PTCA balloons are more cost-effective and readily accessible to our research team. Historically, the rat carotid artery balloon injury model was primarily established via Fogarty balloon embolectomy

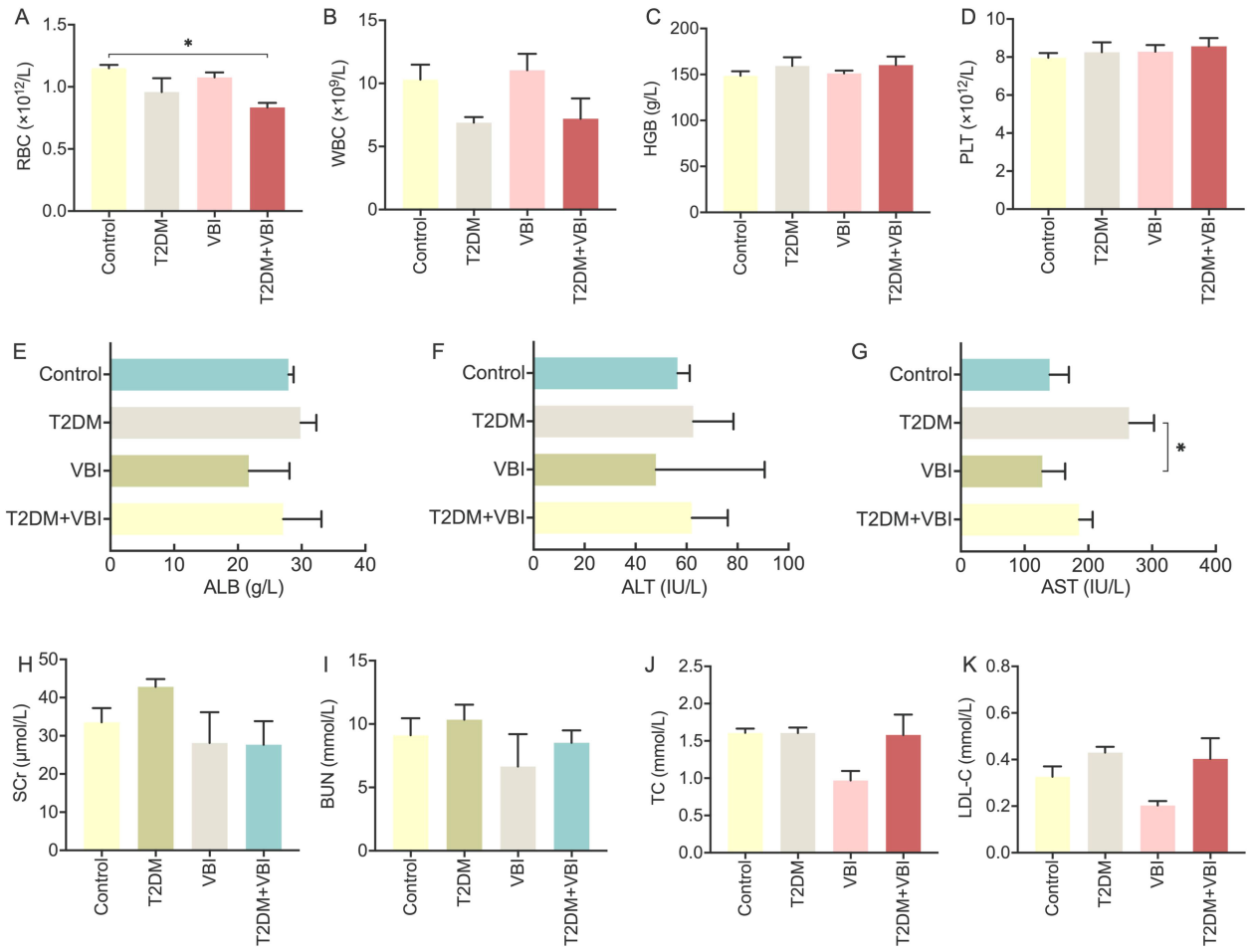

FIGURE 6
Analysis and comparison of whole blood cell and plasma biochemical parameters in diabetic rats at 6 weeks post-VBI. **(A)** RBC: red blood cell count analysis; **(B)** WBC: total white blood cell count analysis; **(C)** HGB: hemoglobin quantitative analysis; **(D)** PLT: platelet count analysis; **(E)** ALB: plasma albumin measurement; **(F)** ALT: alanine aminotransferase assay; **(G)** AST: aspartate aminotransferase assay; **(H)** SCr: plasma creatinine measurement; **(I)** BUN: plasma urea nitrogen determination; **(J)** TC: plasma total cholesterol concentration; **(K)** LDL-C: plasma low-density lipoprotein cholesterol measurement. VBI, vascular balloon injury; T2DM, type 2 diabetes mellitus. One-way ANOVA with Tukey's *post hoc* test and Brown–Forsythe/Welch ANOVA with Dunnett's T3 test were used for statistical comparison, *P < 0.05.

catheters, as early PTCA balloons were generally too large to be applied in small animal models (12, 27). Notably, the two types of balloons differ significantly in their design and functional characteristics. The Fogarty balloon exhibits high compliance, expanding both radially (along the vessel diameter) and longitudinally (along the vessel length) upon inflation, which makes it suitable for surgical thrombectomy (27, 28). In contrast, PTCA balloons—originally developed for coronary artery interventions—possess slight compliance and can maintain their inflated size even as pressure increases, and when paired with a pressure pump, they enable precise and controlled dilation (27, 29). Considering that previous studies have confirmed that Fogarty balloons and PTCA balloons induce comparable levels of arterial wall damage (27, 30), PTCA balloons are now feasible for carotid angioplasty in rats owing to advancements in catheter technology—particularly in size, specifications, and materials (29). Even among personnel with extensive experience in arterial balloon injury procedures, the mortality rate remained higher in the diabetic group than in the nondiabetic group (14.3% vs. 7%). This difference may be attributed to increased platelet aggregation and thrombotic risk, which are driven by elevated oxidative stress levels and activated proinflammatory mediator levels in diabetic animals (31). Given the above considerations, it is necessary to appropriately increase the intragroup sample size during actual experiments, with adjustments on the basis of pre-experimental data regarding diabetes induction rates and animal mortality.

Throughout the entire feeding period, we continuously monitored and systematically recorded changes in diabetes-related metabolic indicators in the rats across all the groups. Considering that urine monitoring via metabolic cages may disrupt rats' daily activities and is not sustainable, we adopted a cage weighing method to estimate excretion. Although this method yields data with lower precision than metabolic cages do, it offers a clear advantage over qualitative observation by enabling quantitative estimation of excretion (32). Observations revealed that rats in the nondiabetic groups—regardless of whether they

received carotid balloon injury—exhibited no significant fluctuations in food intake, water intake, excretion, or blood glucose levels, with consistent trends in body weight gain. These findings indicate that carotid balloon injury has no significant effect on the daily activities or basic metabolic homeostasis of nondiabetic rats. In contrast, rats with NAA/STZ-induced T2DM presented typical diabetic symptoms (polydipsia, polyphagia, and polyuria) within one week of modeling, accompanied by a significant elevation in blood glucose levels. For the T2DM group, the aforementioned indicators (food intake, water intake, excretion, and blood glucose) remained consistently high, with only occasional minor fluctuations. In the T2DM+VBI group, the rats exhibited a one-week decrease in food intake, water intake, and excretion after balloon injury surgery; although their blood glucose levels also decreased significantly during this period, they remained significantly higher than those in the control group. These indicators (intake, excretion, and blood glucose) subsequently gradually increased; however, while they did not reach the levels observed in the T2DM group, they were still significantly higher than those in the control group. Notably, starting from the second week post-VBI, the blood glucose levels of the T2DM+VBI group remained above the threshold for successful diabetes induction. In terms of body weight, the T2DM+VBI group and T2DM-only group presented similar trends: both groups presented significantly lower body weights than the control group did, with this significant difference first observed around the third week after diabetes induction (corresponding to the second week after balloon injury). These results validated the efficacy of the NAA/STZ-induced T2DM model: in addition to displaying typical diabetic symptoms, the diabetic rats maintained a sustained increase in blood glucose levels. After balloon injury, the metabolic indicators of diabetic rats were partially affected, but their blood glucose levels still met the criteria for a stable diabetic model, and they continued to exhibit prominent diabetic symptoms. Additionally, because metabolic indicators in the T2DM+VBI group remained consistently lower than those in the T2DM-only group postballoon injury, we hypothesize that this may be related to the transient reduction in food intake caused by surgical stress. This reduction may allow pancreatic islet cells adequate rest for partial functional recovery, thereby moderately mitigating metabolic abnormalities (33).

To assess the impact of diabetic model on intimal hyperplasia severity at the balloon injury site, we harvested the common carotid arteries of the rats in each group at 2, 4, and 6 weeks after vascular injury for histological analysis. The results revealed no proliferative lesions in carotid artery sections from the rats in the normal control group or the T2DM group. The arterial walls were smooth, the internal elastic membrane was intact, and no luminal stenosis was observed. In rats subjected to carotid balloon injury, varying degrees of proliferative lesions were evident 2 weeks post-surgery, and the proliferative area gradually expanded as the postinjury period increased. At each test time point, the degree of carotid intimal proliferation and luminal stenosis was significantly greater in diabetic rats than in those subjected to balloon injury only. By 6 weeks after balloon injury, the vascular intima in most diabetic rats had thickened to nearly occlude the lumen and disrupt blood flow. This result confirmed that the diabetic milieu can accelerate the development of intimal proliferative lesions after endothelial injury. Notably, the carotid intimal proliferation data in the T2DM+VBI group at 2 weeks post-injury were comparable to those in the VBI group at 6 weeks, which also indicates that carotid artery injury in the context of diabetes can further shorten the modeling time and that 2–4 weeks after balloon injury is the appropriate modeling period.

For subsequent immunohistochemical analyses, we stained vascular tissues harvested at 6 weeks post-injury for the vascular smooth muscle cell marker α-SMA and the macrophage marker F4/80. The results confirmed that, regardless of the presence or absence of diabetes, the primary cellular components of the proliferative intima were macrophages and vascular smooth muscle cells. Notably, the proliferation and infiltration of these two cell types were more prominent in diabetic rats than in control rats. In addition, α-SMA staining in the VBI group revealed aggregation and bundling of spindle-shaped cells on the luminal side of the endothelium, a finding considered indicative of fibrous cap formation and a hallmark of stable plaques. In contrast, the T2DM+VBI group presented unclear cellular structure and significantly disorganized arrangement within the thickened intima. For further investigation, we stained the neointima with MMP-9, a representative marker of plaque rupture and remodeling, and observed a larger area of positive expression in the T2DM+VBI group, indicating that in the diabetic milieu, the proliferative intima undergoes more severe inflammatory damage, and the lesions exhibit relatively poor stability. Notably, the homolog of F4/80 in human tissues serves as a highly specific marker for eosinophils and is undetectable in monocytes or macrophages (34). Thus, when researchers aim at cross-species comparisons, CD68 is a more appropriate choice, as this marker is consistently expressed across humans, mice, and rats (35, 36). Although CD68 is not as specific as F4/80 (34, 37), it still provides a better bridge for translational relevance between rodent and human studies. The failure to combine the detection of CD68 and F4/80 during the initial experimental design is a limitation of our study.

Six weeks after balloon injury, histological examinations were performed on the major organs of the rats in each group. In HE-stained liver sections, hepatocytes in the T2DM group presented significant fatty degeneration and ballooning changes, whereas only scattered, loosely arranged, and edematous cells were observed in the T2DM+VBI group. No obvious abnormalities were found in other organs across all groups. Additionally, comparative analyses of whole blood cell count and plasma biochemical parameters revealed no statistically significant differences between the groups. Even in the absence of significant differences in hematological, biochemical, and histological assessments, these results hold substantial value for validating the translational relevance of the combined model. Specifically, they confirm that the model avoids inducing acute, severe organ injury—including overt hepatic/renal dysfunction and severe dyslipidemia. This is critical because such severe pathological states are not characteristic of early-stage T2DM-associated complications in humans; instead, they introduce confounding variables that overwhelm the specific metabolic-related effects of

T2DM itself on vascular injury. Notably, nonsignificant differences do not equate to "no biological effect": mildly elevated ALT/AST levels paired with histological evidence of mild steatosis would mirror early-stage T2DM-related liver dysfunction, and nonsignificant BUN/SCr differences do not exclude early DN. Integrating advanced functional assessments (e.g., GFR) and histological evaluations (e.g., PAS staining for kidneys, oil red O staining for liver) would enhance the model's ability to recapitulate the full spectrum of T2DM-associated pathologies (17, 18). On the basis of the current dataset, the combined model successfully maintains organ function within the range of subclinical dysfunction during the early stages of T2DM and vascular injury.

5 Conclusion

In this study, we successfully established an SD rat model of NAA/STZ-induced type 2 diabetes combined with carotid artery balloon injury and proposed that 2–4 weeks after balloon injury constitutes a relatively appropriate time window for model establishment. Consistent with the metabolic profiles of rats with simple diabetes, this model displays persistently elevated blood glucose levels and distinct diabetic symptoms from 2 weeks post-injury onward. Compared with those in rats subjected to balloon injury alone, the injured intima in the diabetic environment shows accelerated proliferation, with more severe intimal hyperplasia and lumen stenosis, more prominent inflammatory cell infiltration and proliferation, and poor stability of the proliferative intima. Overall, this model offers advantages such as significant intimal hyperplasia, short modeling duration, stable blood glucose levels, high modeling success rate, and low cost. It can be applied to future research on potential drug effects and their mechanisms.

Data availability statement

The original contributions presented in the study are included in the article/Supplementary Material. Further inquiries can be directed to the corresponding author.

Ethics statement

The animal study was approved by Experimental Animal Ethics Committee of the Affiliated Hospital of Chengdu University of Traditional Chinese Medicine. The study was conducted in accordance with the local legislation and institutional requirements.

Author contributions

YW: Conceptualization, Data curation, Formal Analysis, Writing – original draft. QZ: Writing – review & editing, Formal Analysis, Visualization. CL: Writing – review & editing, Software, Validation. XC: Investigation, Writing – review & editing, Validation. CZ: Investigation, Project administration, Visualization, Writing – review & editing. QC: Funding acquisition, Resources, Supervision, Writing – review & editing.

Funding

The author(s) declare financial support was received for the research and/or publication of this article. 2022 Institutional Research Project of Ya'an Polytechnic College (No. yzyzk202208); 2023 Institutional Research Innovation Team Construction Project of Ya'an Polytechnic College (No. yzykytd202301); 2023 Noncommunicable Chronic Diseases-National Science and Technology Major Project (No. 2023ZD0509400); 2024 Science and Technology Plan Project of Sichuan Province (Key Research and Development Project, No. 2024YFFK0300).

Conflict of interest

The authors declare that the research was conducted in the absence of any commercial or financial relationships that could be construed as a potential conflict of interest.

Generative AI statement

The author(s) declare that no Generative AI was used in the creation of this manuscript.

Any alternative text (alt text) provided alongside figures in this article has been generated by Frontiers with the support of artificial intelligence and reasonable efforts have been made to ensure accuracy, including review by the authors wherever possible. If you identify any issues, please contact us.

Publisher's note

Supplementary material

The Supplementary Material for this article can be found online at: https://www.frontiersin.org/articles/10.3389/fendo.2025.1693820/full#supplementary-material

References

1. Bragg F, Holmes MV, Iona A, Guo Y, Du H, Chen Y, et al. Association between diabetes and cause-specific mortality in rural and urban areas of China. *JAMA*. (2017) 317:280–9. doi: 10.1001/jama.2016.19720

2. Zhang X, Ran X, Xu Z, Cheng Z, Shen F, Yu Y, et al. Epidemiological characteristics of lower extremity arterial disease in Chinese diabetes patients at high risk: a prospective, multicenter, cross-sectional study. *J Diabetes Complicat*. (2018) 32:150–6. doi: 10.1016/j.jdiacomp.2017.10.003

3. Einarson TR, Acs A, Ludwig C, Panton UH. Prevalence of cardiovascular disease in type 2 diabetes: a systematic literature review of scientific evidence from across the world in 2007-2017. *Cardiovasc Diabetol*. (2018) 17:83. doi: 10.1186/s12933-018-0728-6

4. Rendra E, Riabov V, Mossel DM, Sevastyanova T, Harmsen MC, Kzhyshkowska J. Reactive oxygen species (ROS) in macrophage activation and function in diabetes. *Immunobiol*. (2019) 224:242–53. doi: 10.1016/j.imbio.2018.11.010

5. Beckman JA, Creager MA, Libby P. Diabetes and atherosclerosis: epidemiology, pathophysiology, and management. *JAMA*. (2002) 287:2570–81. doi: 10.1001/jama.287.19.2570

6. Gargiulo S, Gramanzini M, Mancini M. Molecular imaging of vulnerable atherosclerotic plaques in animal models. *Int J Mol Sci*. (2016) 17:1–44. doi: 10.3390/ijms17091511

7. Leon BM, Maddox TM. Diabetes and cardiovascular disease: Epidemiology, biological mechanisms, treatment recommendations and future research. *World J Diabetes*. (2015) 6:1246–58. doi: 10.4239/wjd.v6.i13.1246

8. Oppi S, Luscher TF, Stein S. Mouse models for atherosclerosis research-which is my line? *Front Cardiovasc Med*. (2019) 6:46. doi: 10.3389/fcvm.2019.00046

9. Choi JSY, de Haan JB, Sharma A. Animal models of diabetes-associated vascular diseases: an update on available models and experimental analysis. *Br J Pharmacol*. (2021) 179:748–69. doi: 10.1111/bph.15591

10. Azemi AK, Mokhtar SS, Hou LJ, Sharif SET, Rasool AHG. Model for type 2 diabetes exhibits changes in vascular function and structure due to vascular oxidative stress and inflammation. *Biotech Histochem*. (2021) 96:498–506. doi: 10.1080/10520295.2020.1823480

11. Simsekyilmaz S, Liehn EA, Militaru C, Vogt F. Progress in interventional cardiology: challenges for the future. *Thromb Haemost*. (2015) 113:464–72. doi: 10.1160/th14-07-0599

12. Tulis D. Rat carotid artery balloon injury model. *Methods Mol Med*. (2007) 139:1–30. doi: 10.1007/978-1-59745-571-8_1

13. Jeremy J, Thomas A. Animal models for studying neointima formation. *Curr Vasc Pharmacol*. (2010) 8:198–219. doi: 10.2174/157016110790887027

14. Masiello P, Broca C, Gross R, Roye M, Manteghetti M, Hillaire-Buys D, et al. Experimental NIDDM: development of a new model in adult rats administered streptozotocin and nicotinamide. *Diabetes*. (1998) 47:224–9. doi: 10.2337/diab.47.2.224

15. Liu M, Wang R, Hoi MPM, Wang Y, Wang S, Li G, et al. Nano-based drug delivery systems for managing diabetes: recent advances and future prospects. *Int J Nanomed*. (2025) 20:6221–52. doi: 10.2147/ijn.S508875

16. Rais N, Ved A, Ahmad R, Parveen K, Gautam GK, Bari DG, et al. Model of streptozotocin-nicotinamide induced type 2 diabetes: a comparative review. *Curr Diabetes Rev*. (2022) 18:e171121198001. doi: 10.2174/1573399818666211117123358

17. Zhang CY, Zhu XJ, Sun WD, Bi SZ, Lai SY, An L, et al. Nicotinamide N-methyltransferase in non-alcoholic fatty liver disease: Mechanistic insights and emerging therapeutic strategies. *Arch Biochem Biophys*. (2025) 772:110558. doi: 10.1016/j.abb.2025.110558

18. Yan LJ. The nicotinamide/streptozotocin rodent model of type 2 diabetes: renal pathophysiology and redox imbalance features. *Biomol*. (2022) 12:1–16. doi: 10.3390/biom12091225

19. He J, Yuan G, Zhang J, Guo X. Approach to creating early diabetic peripheral neuropathy rat model. *J Peking Univ Health Sci*. (2019) 51:1150–4. doi: 10.19723/j.issn.1671-167X.2019.06.030

20. Yu WJ, Yang M, He CX, Jin YJ, Li Z, Li P, et al. Construction of a rat model of Alzheimer disease combined with type 2 diabetes mellitus and preliminary evaluation of its pathological changes. *Chin J Pathophysiol*. (2022) 38:10. doi: 10.3969/j.issn.1000-4718.2022.11.005

21. Polyak B, Medved M, Lazareva N, Steele L, Friedman G. Magnetic nanoparticle-mediated targeting of cell therapy reduces in-stent stenosis in injured arteries. *ACS Nano*. (2016) 10:9559–69. doi: 10.1021/acsnano.6b04912

22. Zhang R, Liu R, Liu C, Pan L, Qi Y, Cheng J, et al. A pH/ROS dual-responsive and targeting nanotherapy for vascular inflammatory diseases. *Biomater*. (2020) 230:119605. doi: 10.1016/j.biomaterials.2019.119605

23. Wang L, Zhang D, Zhan W, Zeng Z, Yin J, Wang K, et al. Chinese medicine Fufang Zhenzhu Tiaozhi capsule ameliorates coronary atherosclerosis in diabetes mellitus-related coronary heart disease minipigs. *BioMed Pharmacother*. (2022) 156:113831. doi: 10.1016/j.biopha.2022.113831

24. Lin CM, Wang BW, Fang WJ, Pan CM, Shyu KG, Hou SW. Catalpol ameliorates neointimal hyperplasia in diabetic rats. *Planta Med*. (2019) 85:406–11. doi: 10.1055/a-0818-3689

25. Zhang YQ, Tian F, Zhou Y, Chen YD, Li B, Ma Q, et al. Nicorandil attenuates carotid intimal hyperplasia after balloon catheter injury in diabetic rats. *Cardiovasc Diabetol*. (2016) 15:1–16. doi: 10.1186/s12933-016-0377-6

26. Fan L, Cacicedo JM, Ido Y. Impaired nicotinamide adenine dinucleotide (NAD (+)) metabolism in diabetes and diabetic tissues: Implications for nicotinamide-related compound treatment. *J Diabetes Investig*. (2020) 11:1403–19. doi: 10.1111/jdi.13303

27. Doornekamp FN, Borst C, Haudenschild CC, Post MJ. Fogarty and percutaneous transluminal coronary angioplasty balloon injury induce comparable damage to the arterial wall but lead to different healing responses. *J Vasc Surg*. (1996) 24:843–50. doi: 10.1016/s0741-5214(96)70021-6

28. Ákos B, Dóra P, Fanni Éva S, Edit D. Post-thromboembolectomy pseudoaneurysms affecting below-the-knee arteries and their management strategies: A literature review. *J Clin Med*. (2025) 14:1–9. doi: 10.3390/jcm14072176

29. Amstutz C, Behr J, Krebs S, Haeberlin A, Vogel R, Zurbuchen A, et al. Design of percutaneous transluminal coronary angioplasty balloon catheters. *BioMed Eng Online*. (2023) 22:1–23. doi: 10.1186/s12938-023-01155-2

30. Zhou YP, Huang L, Li AM, Song Y, Jin J, Cui B. Comparison of two types of balloon catheter to establish rat carotid injury model. *Med J West China*. (2007) 19:3. doi: 10.3969/j.issn.1672-3511.2007.03.005

31. Khosravi M, Poursaleh A, Ghasempour G, Farhad S, Najafi M. The effects of oxidative stress on the development of atherosclerosis. *Biol Chem*. (2019) 400:711–32. doi: 10.1515/hsz-2018-0397

32. Gao TT, Sun TQ, Liu XX, Ren YL, Qiu YF, Wang J, et al. Study on the amount of corncob bedding in IVC system of SPF rats and mice. *Lab Anim Sci*. (2022) 39:59-64. doi: 10.3969/j.issn.1006-6179.2022.02.010

33. Hammer SS, Vieira CP, McFarland D, Sandler M, Levitsky Y, Dorweiler TF, et al. Fasting and fasting-mimicking treatment activate SIRT1/LXRalpha and alleviate diabetes-induced systemic and microvascular dysfunction. *Diabetologia*. (2021) 64:1674–89. doi: 10.1007/s00125-021-05431-5

34. Hamann J, Koning N, Pouwels W, Ulfman LH, van Eijk M, Stacey M, et al. EMR1, the human homolog of F4/80, is an eosinophil-specific receptor. *Eur J Immunol*. (2007) 37:2797–802. doi: 10.1002/eji.200737553

35. Wang S, Chen Y, Hong W, Li B, Zhou Y, Ran P. Chronic exposure to biomass ambient particulate matter triggers alveolar macrophage polarization and activation in the rat lung. *J Cell Mol Med*. (2022) 26:1156–68. doi: 10.1111/jcmm.17169

36. Tang J, Zhou Z, Wang G, Tu H, Cui X, Jia J, et al. Induction and characterization of oral submucous fibrosis model with different pathological stages in rats and mice. *Sci Rep*. (2025) 15:31128. doi: 10.1038/s41598-025-16715-w

37. Ferenbach D, Hughes J. Macrophages and dendritic cells: what is the difference? *Kidney Int*. (2008) 74:5–7. doi: 10.1038/ki.2008.189

frontiers | Frontiers in Endocrinology

TYPE Review
PUBLISHED 04 December 2025
DOI 10.3389/fendo.2025.1696344

OPEN ACCESS

EDITED BY
Ramoji Kosuru,
Versiti Blood Research Institute, United States

REVIEWED BY
Nawfal Hasan Siam,
Independent University, Bangladesh
Venkata Kiran Kumar Mandlem,
University of Texas at Tyler, United States

*CORRESPONDENCE
Yunpeng Jin
8013013@zju.edu.cn

RECEIVED 31 August 2025
REVISED 14 November 2025
ACCEPTED 17 November 2025
PUBLISHED 04 December 2025

CITATION
Deng S, Tayefi F and Jin Y (2025) Metabolic-stress-induced mitochondrial calcium dysregulation: a central hub in diabetic cardiomyopathy pathogenesis and treatment. *Front. Endocrinol.* 16:1696344.
doi: 10.3389/fendo.2025.1696344

Metabolic-stress-induced mitochondrial calcium dysregulation: a central hub in diabetic cardiomyopathy pathogenesis and treatment

Siqi Deng, Fatemeh Tayefi and Yunpeng Jin*

Department of Cardiology, The Fourth Affiliated Hospital of School of Medicine, and International School of Medicine, International Institutes of Medicine, Zhejiang University, Yiwu, Zhejiang, China

Diabetic cardiomyopathy (DCM), as a devastating complication of diabetes mellitus (DM), arises from a complex interplay between systemic metabolic derangements and myocardial vulnerability. While hyperglycemia, lipotoxicity, and insulin resistance are established drivers of cardiac dysfunction, the precise mechanisms linking these metabolic insults to cardiac dysfunction remain elusive. Recent evidence suggests that the dysregulation of mitochondrial calcium homeostasis plays a critical role in integrating diabetic metabolic stress and cardiomyocyte fate. This review synthesizes recent advances in understanding how mitochondrial calcium mishandling—encompassing impaired uptake, excessive release, and buffering failure—orchestrates the pathological triad of bioenergetic deficit, oxidative stress, and cell death in DCM. We delve into the molecular mechanisms underpinning this dysregulation, highlighting its interplay with the diabetic metabolic milieu. Furthermore, we critically evaluate novel therapeutic strategies targeting mitochondrial calcium fluxes, including the inhibition of the mitochondrial calcium uniporter (MCU), the activation of the mitochondrial $Na^+/Ca^{2+}/Li^+$ exchanger (NCLX), and the modulation of the mitochondrial permeability transition pore (mPTP), discussing their clinical translation potential and existing challenges. By reframing DCM through the lens of mitochondrial calcium homeostasis, this review not only synthesizes current knowledge but also provides a critical comparison of emerging therapeutic strategies and evaluates the formidable challenges in their clinical translation, thereby bridging the gap between endocrine metabolism and cardiac pathophysiology and offering nuanced perspectives for biomarker discovery and stage-specific interventions.

KEYWORDS

diabetic cardiomyopathy, mitochondrial calcium, calcium homeostasis, mitochondrial dysfunction, heart failure, therapeutic targets

Highlights

- Mitochondrial calcium (Ca^{2+}) imbalance is a core mechanism linking systemic metabolic stress to cardiac dysfunction in diabetes.
- Diabetic conditions (hyperglycemia, advanced glycation end products (AGEs), and oxidative stress) directly impair the molecular machinery of mitochondrial calcium uptake (MCU) and release (mPTP, NCLX).
- Mitochondrial calcium imbalance triggers a vicious cycle of energy crisis, oxidative damage, and cardiomyocyte death, culminating in heart failure.
- Therapeutic strategies targeting mitochondrial calcium fluxes (e.g., cardiac-specific MCU inhibitors, NCLX activators) show promise in preclinical models.
- Translating these strategies to the clinic requires stage-specific approaches and reliable biomarkers of mitochondrial function.

1 Introduction

1.1 Background

Diabetic cardiomyopathy (DCM), a pathophysiological condition induced by diabetes mellitus (DM), is a significant contributor to heart failure (HF) (1). Leading global health organizations, including the World Health Organization (WHO), the American Heart Association (AHA), and the International Diabetes Federation (IDF), have identified DCM as a predominant cause of mortality in patients with diabetes (2–4).

Recent population-based studies report that 12–17% of patients with type 2 diabetes (T2D) are diagnosed with DCM, while systematic cardiac phenotyping reveals subclinical cardiac dysfunction in over 50% of these patients (5, 6). Prospective cohort data indicate that 29% of asymptomatic T2D patients progress to overt DCM within 5 years, primarily driven by metabolic stress and microvascular injury (7). The trajectory involves progressive myocardial fibrosis and inflammation, ultimately culminating in HF (8). Notably, DCM is associated with a 75% higher risk of cardiovascular mortality than non-diabetic HF, after adjustment for comorbidities (9). The persistent and significant contribution of diabetic cardiomyopathy to the global burden of cardiovascular mortality has been further emphasized in recent large-scale epidemiological studies (10).

The global burden of DCM has mirrored the diabetes pandemic, with age-standardized prevalence rising by 7.9% annually between 2017 and 2022. This increase strongly correlates with regional T2D growth rates (ρ=0.91, $p<0.001$) (11). More recent estimates from the Global Burden of Disease Study underscore the escalating burden, highlighting the urgent need for targeted interventions (12). Mechanistic drivers (e.g., mitochondrial dysfunction, lipotoxicity) remain therapeutic targets; however, no disease-modifying therapies currently exist (13, 14). Ongoing research continues to delineate the intricate mechanisms, including mitochondrial calcium dysregulation, that underpin the progression from diabetes to heart failure (15). This therapeutic gap is further emphasized in contemporary reviews, which call for a deeper understanding of the fundamental pathophysiological processes, such as mitochondrial quality control and ion homeostasis (16).

Mitochondrial calcium (Ca^{2+}) imbalance is a key pathophysiological link between diabetic metabolic derangements and myocardial dysfunction. Given the multitude of Ca^{2+}-handling proteins that regulate the Ca^{2+} transients in cardiomyocytes, DCM has been shown to disrupt these proteins through altered expression, function, or both (17). Mitochondria buffer cytosolic Ca^{2+} concentrations, thereby playing a central role in cardiac excitation-contraction coupling (ECC) (18, 19). Impairment of this mitochondrial function compromises cardiac contractility and contributes to cardiac dysfunction (18). In diabetic mice, studies have demonstrated impaired cardiac mitochondrial function associated with ultrastructural defects (20). Conversely, under pathological conditions—such as ischemia, infarction, and pressure overload—cellular stress induces excessive cytosolic Ca^{2+} accumulation, leading to mitochondrial Ca^{2+} overload. This overload increases reactive oxygen species (ROS) generation, disrupts mitochondrial membrane potential ($\Delta\Psi$), and promotes opening of the mitochondrial permeability transition pore (mPTP), accompanied by ATP depletion (21, 22). Collectively, these events trigger cardiomyocyte death and progressive cardiac dysfunction. Therefore, maintaining the mitochondrial Ca^{2+} homeostasis is essential for cardiomyocyte survival and functional integrity. Reflecting this, mitochondrial calcium homeostasis is increasingly recognized as a central integrator of metabolic stress and cardiac dysfunction in diabetes, bridging systemic derangements to myocardial injury (23).

This review summarizes recent advances in mitochondrial Ca^{2+}homeostasis, emphasizing its critical role in cardiac Ca^{2+} regulation. It also outlines emerging therapeutic strategies targeting mitochondrial Ca^{2+} pathways for DCM treatment and prevention.

Abbreviations: AHA, American Heart Association; AAV9, Adeno-Associated Virus serotype 9; AGEs, Advanced Glycation End products; AMPK, AMP-activated Protein Kinase; ATP, Adenosine Triphosphate; Bax, BCL2-Associated X protein; β-HB, β-Hydroxybutyrate; Ca^{2+}, Calcium; Casp3, Caspase 3; CypD, Cyclophilin D; Cyt c, Cytochrome c; DCM, Diabetic Cardiomyopathy; DM, Diabetes Mellitus; $\Delta\Psi m$, Mitochondrial Membrane Potential; EC_{50}, Half-Maximal Effective Concentration; EMRE, Essential MCU Regulator; ETC, Electron Transport Chain; FBXL4, F-Box and Leucine-Rich Repeat Protein 4; F-ATP synthase, FoF1-ATP Synthase; HF, Heart Failure; H+/Ca^{2+} exchanger, Proton/Calcium Exchanger; IC_{50}, Half-Maximal Inhibitory Concentration; IDH3, Isocitrate Dehydrogenase 3; IMM, Inner Mitochondrial Membrane; JPH2, Junctophilin-2; MCU, Mitochondrial Calcium Uniporter; MCUR1, Mitochondrial Calcium Uniporter Regulator 1; MICU1/2/3, Mitochondrial Calcium Uptake protein 1/2/3; mNCX, Mitochondrial Na^+/Ca^{2+} Exchanger; mPTP, Mitochondrial Permeability Transition Pore; Na^+/Ca^{2+} exchanger (NCX), Sodium/Calcium Exchanger; NCLX, Mitochondrial $Na^+/Ca^{2+}/Li^+$ Exchanger; RIRR, ROS-Induced ROS Release; ROS, Reactive Oxygen Species; Ru265, MCU inhibitor compound; RyR, Ryanodine Receptor; T2D/T2DM, Type 2 Diabetes (Mellitus); $\Delta\Psi m$, Mitochondrial Membrane Potential.

2 Mitochondrial calcium homeostasis: basics and regulatory mechanisms

2.1 Mechanisms of mitochondrial calcium uptake and release

In general, the physiological concentration of mitochondrial Ca^{2+} is tightly regulated by two major operative regulatory systems that either release Ca^{2+} into the cytosol or take up Ca^{2+} from the cytosol. Voltage-dependent anion channel 1 (VDAC1), located on the outer mitochondrial membrane, acts as the first gatekeeper of Ca^{2+} entering mitochondria (24). Initially, Ca^{2+} accumulates in the mitochondrial intermembrane space (IMS), and then, it enters the mitochondrial matrix through the mitochondrial Ca^{2+} uniporter (MCU). By interacting with various regulatory proteins, such as calcium uptake proteins (MICUs), the MCU forms a functional complex that precisely controls the uptake of Ca^{2+} into the matrix. Conversely, Ca^{2+} stored in the matrix can be transported back to IMS through Na^+/Ca^{2+} (NCX) or H^+/Ca^{2+}exchangers (25), as well as by mPTP opening when the cell is under stress (26, 27). Although Ca^{2+} uptake and release appear to be two independent processes, some studies indicate that an interlink may exist between them. For example, mitochondrial Ca^{2+} uptake may affect the initiation and activation of the releasing system, particularly mPTP opening during stress (28–30). In addition to these conventional regulatory apparatuses, newly identified proteins are being discovered that contribute to mitochondrial Ca^{2+} homeostasis and cardiac mitochondrial function. One such example is valosin-containing protein (VCP), an AAA+ ATPase that has been recently implicated in the regulation of both mitochondrial calcium uptake (by modulating MCU complex stability) and mPTP opening under stress conditions (31).

2.1.1 Mitochondrial calcium uptake

Mitochondria possess a low-affinity, high-capacity calcium ion uptake system, primarily mediated by the MCU (32). MCU is present in almost all cell types and functions as a highly selective calcium channel responsible for Ca^{2+} uptake in mitochondria (33). There are two transmembrane domains located in the inner mitochondrial membrane (IMM), with both the N-terminal and C-terminal domains facing the mitochondrial matrix. The N-terminal domain (NTD) is believed to regulate Ca^{2+} uptake rate (34). Although studies on the molecular nature of the MCU complex began in the 1970s, MCU itself was not identified and confirmed as an essential component of the MCU until 2011 (35–37). Since then, the structure of the MCU has been elucidated in various species, including fungi, C. elegans, zebrafish, and humans (33). The transmembrane and NTD structures are conserved across species, highlighting their essential role in mitochondrial Ca^{2+} homeostasis. Over the years of effort, the core components of the MCU complex (MCU, EMRE, MICU1, MICU2) and associated regulatory factors (such as MCUR1 and MICU3) have been identified. Cryo-electron microscopy technology has specifically elucidated the structure of the MCU-EMRE core channel, offering a molecular foundation for comprehending its functional mechanisms. The identification of MICU1 and MICU2 as gatekeepers that prevent Ca^{2+} uptake under resting conditions represented a breakthrough in understanding the regulation of the uniporter (38). Wang, Y., and his team further elucidated the molecular basis of the MICU1/2 gating role using cryo-electron microscopy (39).

2.1.1.1 Cytosolic low-calcium state ($[Ca^{2+}]$- < 1–3 μM)

Biological systems feature exquisitely designed molecular switches. The response of MICU1/2 to calcium ions is not a binary "on/off" switch but rather the result of graded conformational changes. At calcium concentrations below 1 μM, MICU1/2 stably blocks the channel; between 1 and 3 μM, it partially opens; and at approximately 3 μM, the channel becomes fully open (enabling efficient calcium uptake). Thus, activation occurs over a concentration range rather than at a single threshold. The MICU1/MICU2 heterodimer (or, in some cases, MICU1 homodimers) interacts via its positively charged domain with negatively charged regions near the entrance of the MCU-EMRE pore. This physical blocking effect significantly reduces the MCU channel's affinity for Ca^{2+} (manifested as an increased Kd), effectively closing the channel and preventing leakage of low-level Ca^{2+} into the mitochondria under resting conditions. This regulation is crucial for maintaining matrix ion homeostasis and energy efficiency.

2.1.1.2 Cytosolic elevated-calcium state ($[Ca^{2+}]$- > 10 μM)

When cytosolic (or intermembrane space) $[Ca^{2+}]$ levels rise, Ca^{2+} binds to the EF-hand domains of MICU1 and MICU2. Ca^{2+} binding induces a significant conformational change in MICU1, weakening or abolishing the physical blockade of the MCU pore by the MICU1/MICU2 complex. As a result, the channel "gate" opens, significantly enhancing the MCU channel's affinity for Ca^{2+}. This allows efficient and rapid Ca^{2+} uptake into the mitochondrial matrix, supporting cellular processes such as energy production and signal transduction.

2.1.2 Mitochondrial calcium release

The mechanisms of mitochondrial calcium release are primarily categorized into the following three types:

2.1.2.1 mPTP

The mPTP is a non-selective, high-conductance channel in the inner mitochondrial membrane. Its sustained opening is a catastrophic event, fundamentally altering mitochondrial homeostasis. While it can lead to the release of Ca^{2+} and other small molecules, its primary pathological role is to cause the irreversible collapse of the $\Delta\Psi m$, uncoupling oxidative phosphorylation and leading to ATP depletion. Furthermore, osmotic imbalance causes mitochondrial swelling and rupture of the outer membrane, releasing pro-apoptotic factors like cytochrome c, thereby initiating cell death pathways (26, 27, 40). Transient opening leads to the release of calcium ions and small molecules. The molecular composition of mPTP has been a subject

of significant recent controversy. The classical model previously described the mPTP as comprising three components: adenine nucleotide translocase (ANT—located in the inner membrane), the voltage-dependent anion channel (VDAC—located in the outer membrane), and cyclophilin D (CypD—a matrix protein, regulatory subunit). CypD binding to ANT promotes pore opening (41). However, recent studies propose a revised model: compelling recent evidence strongly points towards the F_0F_1-ATP synthase—specifically its dimers, oligomers, or the c-subunit ring—possibly forming the core pore channel. Genetic knockout experiments have shown that the absence of ANT or VDAC does not completely prevent mPTP opening (42), whereas experimental targeting of F-ATP synthase effectively modulates the mPTP (43).

2.1.2.2 Mitochondrial Na^+/Ca^{2+} exchanger

Under specific conditions (e.g., decreased cytosolic Ca^{2+} levels, reduced ΔΨm), mitochondria can also release calcium via the sodium-calcium exchanger (38). This exchanger represents the primary "physiological" pathway for mitochondrial calcium efflux. It utilizes the Na^+ electrochemical gradient across the inner membrane (positive outside, negative inside, and high cytosolic Na^+ concentration) to actively exchange matrix Ca^{2+} for cytosolic Na^+ at a stoichiometry of 3 Na^+: 1 Ca^{2+}. The primary physiological pathway for mitochondrial Ca^{2+} efflux is mediated by the mitochondrial Na^+/Ca^{2+} exchanger (mNCX), whose molecular identity is the $Na^+/Ca^{2+}/Li^+$ exchanger (NCLX), encoded by the SLC8B1 gene (44).

2.1.2.3 Rapid mode release

In response to brief, high-frequency cytosolic Ca^{2+} pulses, mitochondria exhibit an extremely rapid calcium release (and uptake), far exceeding the rate mediated by mNCX. This release is independent of the mPTP, and while its molecular identity remains an area of active investigation, it represents a distinct mode of mitochondrial Ca^{2+} flux (22).

2.2 Mitochondrial Ca^{2+} buffering

Mitochondrial Ca^{2+} buffering mechanisms (such as calcium phosphate precipitation) are key processes for maintaining matrix calcium homeostasis. They temporarily sequester excess Ca^{2+} in the form of chemical precipitation, thereby preventing cellular damage caused by calcium overload.

Regulatory factors, such as the phosphate transporter (PiC), are part of this process. Kwong, J. Q., and colleagues, using a cardiac-specific model of PiC knockout mice (cPiC-KO), demonstrated the following pathway:

PiC deficiency → Reduced mitochondrial phosphate (Pi) uptake → Inhibition of calcium phosphate precipitation formation → Mitigation of respiratory chain damage caused by calcium overload → →Maintenance of ATP synthesis.

Furthermore, cPiC-KO mice exhibited a 60% reduction in myocardial infarct size and improved cardiac function (LVEF improved by 35%) following ischemia-reperfusion (I/R) injury (45).

It has been reported that the mitochondrial calcium buffering mechanism can prevent mPTP opening triggered by calcium oscillations, such as those occurring during systole in cardiomyocytes (46).

2.3 Core functions of mitochondrial calcium signaling

Mitochondrial Ca^{2+} signaling orchestrates cellular homeostasis through three cardinal mechanisms: optimization of bioenergetic output via TCA cycle and oxidative phosphorylation (OXPHOS) regulation, bidirectional modulation of ROS homeostasis, and regulation of cell death pathways via the mPTP. Precise spatiotemporal control of this signaling axis is indispensable for physiological function; its dysregulation precipitates metabolic insufficiency, oxidative injury, or apoptotic cell death.

2.3.1 Regulation of energy metabolism

Calcium influx into the mitochondrial matrix serves as a critical activator of rate-limiting dehydrogenases within the tricarboxylic acid (TCA) cycle. Specifically, Ca^{2+} directly stimulates:

Pyruvate dehydrogenase complex (PDH), relieving inhibitory constraints to accelerate pyruvate decarboxylation to acetyl-CoA (47); isocitrate dehydrogenase (IDH3) (48); and α-ketoglutarate dehydrogenase complex (OGDH) (49).

This concerted activation markedly elevates NADH and $FADH_2$ production. These electron carriers subsequently fuel the electron transport chain (ETC), augmenting the proton gradient (Δψm) across the inner mitochondrial membrane. The resulting hyperpolarization potentiates ATP synthase activity, substantially enhancing OXPHOS efficiency (47). Critically, mitochondrial Ca^{2+} uptake through the MCU provides a rapid transduction mechanism that synchronizes mitochondrial energy production with cytosolic Ca^{2+} transients evoked by physiological stimuli (e.g., hormonal signaling or excitation-contraction coupling). This enables real-time matching of mitochondrial ATP production with cellular energy demand (49).

2.3.2 Bidirectional control of ROS

Mitochondrial Ca^{2+} exerts context-dependent effects on redox balance. At physiological concentrations, Ca^{2+} attenuates ROS generation through dual mechanisms: (i) enhanced ATP synthesis mitigates ETC over-reduction, limiting electron leakage; and (ii) activation of the NRF2 antioxidant pathway upregulates mitochondrial ROS-scavenging systems, including manganese superoxide dismutase (MnSOD) and peroxiredoxin 3 (Prx3) (50). Conversely, pathological Ca^{2+} overload induces oxidative stress via (i) structural impairment of ETC complexes (notably Complex I), exacerbating electron escape; (ii) mPTP induction culminating in Δψm dissipation and catastrophic ROS release (51); (iii) context-dependent activation of pro-oxidant enzymes (e.g., glycerol-3-phosphate dehydrogenase) (52); and (iv) suppression of endogenous antioxidant capacity (53).

2.3.3 Apoptotic regulation via mPTP

Matrix Ca^{2+} accumulation serves as an essential trigger for mPTP opening, with co-factors (elevated ROS, diminished Δψm) synergistically lowering its activation threshold. Pore induction initiates a lethal cascade: mitochondrial swelling and irreversible Δψm collapse terminate OXPHOS, while efflux of pro-apoptotic factors (cytochrome *c*, apoptosis-inducing factor) activates caspase-dependent apoptosis (40). Key regulatory components include CypD, whose Ca^{2+}-facilitated binding to the ATP synthase c-ring promotes pore formation (54), and modulatory proteins adenine nucleotide translocator (ANT) and phosphate carrier (PiC) that fine-tune mPTP sensitivity (55). The susceptibility to mPTP-mediated cell death is profoundly influenced by the systemic metabolic milieu. AMPK is a crucial integrator of energy and oxidative stress, critically regulates cardiac tolerance to ischemia/reperfusion injury, and its dysregulation in diabetes exacerbates mPTP-dependent cell death (56).

3 Mitochondrial calcium homeostasis dysregulation in DCM

3.1 Mitochondrial Ca^{2+} dysregulation phenomena observed in both preclinical and clinical studies of DCM include specific manifestations and consequences resulting from mitochondrial Ca^{2+} overload or impaired uptake

3.1.1 Core dysregulation phenomena (preclinical and clinical evidence)

Reduced Mitochondrial Ca^{2+} Uptake Studies have demonstrated the following: In preclinical models of DCM, such as models (db/db mice, STZ rats), exhibit decreased baseline mitochondrial Ca^{2+} content in cardiomyocytes and significantly attenuated mitochondrial Ca^{2+} elevation following β-adrenergic stimulation (17, 57).

Conversely, evidence from human DCM comes from myocardial biopsies of T2DM patients, which reveal reduced MCU protein expression and impaired mitochondrial Ca^{2+} buffering capacity (58). This phenomenon is attributed to direct hyperglycemic impairment: high glucose reduces the myocardial mitochondrial Ca^{2+} uptake rate, correlating with impaired MCU function (57). Transcriptional downregulation: Boudina et al. demonstrated that decreased PGC-1α expression in diabetic myocardium leads to reduced transcription of mitochondrial calcium transporters (including MCU and MICU1) (59). Oxidative damage: Ye, G. et al. proved that persistent ROS generation oxidatively modifies MCU channel subunits, diminishing their activity (30).

Increased release of mitochondrial Ca^{2+} and heightened sensitivity of mPTP are observed.

Experimental evidence demonstrates that in db/db mouse cardiac mitochondria, significantly less Ca^{2+} load is required to induce mPTP opening. Calcium retention capacity (CRC) is decreased. Inhibition of the mNCX improves calcium homeostasis (60). In isolated mitochondria: Mitochondria incubated under high glucose conditions exhibit increased susceptibility to mPTP opening (61). Mechanisms underlying elevated mPTP sensitivity: Upregulation of mNCX: Hyperglycemia activates protein kinase C (PKC) and Rho-associated kinase (ROCK), leading to increased expression and activity of mNCX (62). ROS/RNS-mediated modification of CypD: Accumulation of ROS (particularly H_2O_2 generated from superoxide dismutation) and lipid peroxidation products (e.g., 4-HNE) directly modify CypD, significantly lowering the threshold for mPTP opening (61). Increased intracellular $[Na^+]$: Inhibition of Na^+/K^+-ATPase by advanced glycation end products (AGEs) in late stages elevates intracellular $[Na^+]$. This promotes mNCX-mediated Ca^{2+} efflux from mitochondria (63).

3.1.1.1 Decoupling of cytosolic-mitochondrial calcium transients

Reported findings: Confocal imaging (64) (STZ rat cardiomyocytes): Cytosolic Ca^{2+} transients exhibit reduced amplitude and delayed recovery. Mitochondrial Ca^{2+} responses display a more pronounced lag relative to cytosolic signals. Electron microscopy (65) (human diabetic myocardium): Reduced sarcoplasmic reticulum (SR)-mitochondria contact sites are observed. Mechanisms underlying this decoupling include Sarcoplasmic Reticulum (SR) Dysfunction: Hyperglycemia suppresses SERCA2a (66) activity via oxidative modifications and O-GlcNAcylation modifications. Hyperglycemia increases RyR leak due to pathological hyperphosphorylation by PKA/PKC (67). Structural Disruption: Decreased Junctophilin-2 (JPH2) expression in diabetic myocardium increases the coupling distance between SR and mitochondria and impairs the efficiency of microdomain Ca^{2+} transfer (68).

3.1.2 Pathological consequences of mitochondrial Ca^{2+} overload or impaired uptake

The dysregulation of mitochondrial Ca^{2+} homeostasis, whether it manifests as insufficiency, local overload, or signaling decoupling, sets in motion a cascade of pathological events that drive the progression of DCM. As summarized in Table 1, these consequences are multifaceted and interlinked.

Insufficient mitochondrial Ca^{2+} uptake, driven by persistent hyperglycemia and insulin resistance, creates a profound energy crisis. The lack of Ca^{2+}-mediated activation of TCA cycle dehydrogenases leads to reduced $NADH/FADH_2$ production and, consequently, impaired ATP synthesis (69, 70). This bioenergetic deficit directly compromises cardiac contractility (71). Furthermore, this metabolic stagnation promotes a reliance on fatty acid oxidation while suppressing glucose utilization, exacerbating lipotoxic accumulation within the myocardium. Clinically, this manifests initially as early diastolic dysfunction, which progressively deteriorates into overt systolic failure.

Local mitochondrial Ca^{2+} overload, often triggered by acute stressors like ischemia or sympathetic excitation in the diabetic heart, initiates a destructive cycle. The overload induces a massive

TABLE 1 Presents the pathological consequences of mitochondrial Ca^{2+} overload or impaired uptake.

Disorder type	Trigger conditions	Core consequences	Disease phenotypes	References
Insufficient Ca^{2+}	Persistent hyperglycemia /Insulin resistance	Energy Crisis:↓TCA cycle enzyme activity →↓ATP synthesis →↓Contractility Metabolic Stagnation:↑Fatty acid oxidation + ↓Glucose utilization →Lipotoxic Accumulation	Early Diastolic Dysfunction →Systolic Dysfunction Deterioration	(57–59, 69–71)
Local Ca^{2+} Overload	Stress(e.g.,Ischemia,Sympathetic Excitation)	Oxidative Stress Burst:↑mPTP Opening + ↑ROS→Membrane Lipid/ Protein Damage Cell Death: Apoptosis(Cyt c Release) & Necrosis(ATP Depletion)	Myocardial Cell Loss→Fibrosis→Cardiac Chamber Enlargement	(21, 22, 51, 60, 61, 72–75)
Ca^{2+} Signal Decoupling	SR Dysfunction + Structural Damage	Electromechanical Desynchrony: Delayed Cytosolic Ca^{2+} Clearance →Diastolic Dysfunction Worsening Energy Supply Lag: Mitochondria Fail to Respond to Metabolic Demands	Arrhythmia Risk↑ + Exercise Tolerance ↓	(64–68, 76–78)
Inflammatory Activation	mtDNA Release (via mPTP) + ROS Burst + Metabolic Danger Signals	• Inflammasome Activation (e.g., NLRP3) • Pro-inflammatory Cytokine Release (e.g., IL-1β, IL-18) • Immune Cell Infiltration	Myocardial Inflammation → Amplification of Injury & Fibrosis	(40, 73, 75)
Impaired Mitophagy	Loss of Ca^{2+}-mediated Activation Signals + Oxidative Damage to Mitophagy Proteins	• Accumulation of Damaged Mitochondria • Aggravated ROS Production & Energy Deficit • Failed Quality Control	Accelerated Cardiomyocyte Senescence & Death	(20, 79)
Mitochondrial Dynamics Imbalance	Ca^{2+}-dependent Activation of Fission Proteins (e.g., Drp1) + Reduced Fusion	• Excessive Mitochondrial Fission • Fragmented Mitochondrial Network • Compromised Metabolic Flexibility	Energetic Inefficiency & Increased Susceptibility to Apoptosis	(20, 80)
Sustained ER Stress	Disrupted ER-Mitochondria Ca^{2+} Crosstalk + Unfolded Protein Load	• Activation of UPR Pathways (PERK, IRE1α, ATF6) • Exacerbated Insulin Resistance & Apoptosis • Worsening of Ca^{2+} Handling Defects	Aggravated Contractile Dysfunction & Cell Loss	(79)
Microvascular Dysfunction	Endothelial Cell Mitochondrial Ca^{2+} Dysregulation + AGE/ROS insult	• Reduced NO Bioavailability • Increased Endothelial Permeability & Inflammation • Impaired Vasodilation	Myocardial Ischemia & Perfusion-Contraction Mismatch	(63, 73)

*Ca^{2+}, Calcium; ATP, Adenosine Triphosphate; ROS, Reactive Oxygen Species; Cyt c, Cytochrome c; SR, Sarcoplasmic Reticulum; mtDNA, Mitochondrial DNA; IL, Interleukin; mPTP, Mitochondrial Permeability Transition Pore; UPR, Unfolded Protein Response; AGEs, Advanced Glycation End Products; NO, Nitric Oxide.

burst of ROS and sensitizes the mPTP, leading to irreversible opening. This results in oxidative damage to lipids and proteins and the release of pro-apoptotic factors like cytochrome c, triggering both apoptotic and necrotic cell death (74, 75). The ensuing loss of cardiomyocytes is replaced by fibrotic tissue, leading to cardiac chamber enlargement and progressive remodeling.

3.1.2.1 Ca^{2+} Signal decoupling between cytosolic and mitochondrial compartments

DCM severely compromises the efficient transfer of calcium from the sarcoplasmic reticulum (SR) to the mitochondria, which is crucial for matching energy production to demand. This decoupling of Ca^{2+} signals arises from a combination of SR dysfunction and structural damage. Hyperglycemia suppresses SERCA2a activity through oxidative and O-GlcNAcylation modifications, impairing SR Ca^{2+} reuptake and delaying cytosolic Ca^{2+} clearance (66). Concurrently, it promotes pathological hyperphosphorylation of the ryanodine receptor (RyR) by PKA/PKC, increasing its leakiness (67). The downregulation of Junctophilin-2 (JPH2) in the diabetic myocardium increases the physical distance between the SR and mitochondria (68). This combination of functional and structural defects results in electromechanical desynchrony, manifesting as delayed cytosolic Ca^{2+} transients and worsened diastolic dysfunction. Additionally, mitochondria do not detect or respond to cytosolic Ca^{2+} signals, resulting in an energy supply lag that cannot accommodate abrupt metabolic demands, thereby diminishing exercise tolerance and elevating the risk of arrhythmias.

3.1.2.2 Inflammatory activation

Mitochondrial Ca^{2+} dysregulation is a potent trigger of sterile inflammation in DCM. Pathological mPTP opening and ROS bursts can cause the release of mitochondrial DNA (mtDNA) and other damage-associated molecular patterns (DAMPs) into the cytosol. These molecules serve as strong danger signals that activate the inflammasome, especially the NLRP3 inflammasome. This, in turn, catalyzes the maturation and release of potent pro-inflammatory cytokines such as IL-1β and IL-18 and promotes immune cell infiltration into the myocardium. This chronic, low-grade inflammatory activation amplifies initial injury, promotes fibrotic remodeling, and creates a vicious cycle that further deteriorates cardiac function.

3.1.2.3 Impaired mitophagy

The selective removal of damaged mitochondria, known as mitophagy, is essential for maintaining a healthy mitochondrial network. This process is often Ca^{2+}-dependent. In DCM, the loss of proper Ca^{2+}-mediated activation signals, combined with oxidative

damage to key mitophagy proteins (e.g., PINK1/Parkin), impairs mitophagic flux. The resulting accumulation of damaged mitochondria becomes a persistent source of ROS and contributes to the energy deficit. This failure in mitochondrial quality control accelerates cardiomyocyte senescence and death, as the cell is unable to clear its dysfunctional power plants.

3.1.2.4 Mitochondrial dynamics imbalance

Mitochondria exist in a dynamic equilibrium of fission and fusion. Ca^{2+} is a key regulator of this process. In DCM, pathological matrix Ca^{2+} levels promote the activation of fission proteins like Drp1, while fusion processes (mediated by proteins like Mitofusin 2) are often suppressed. This condition leads to a mitochondrial dynamics imbalance skewed towards excessive fission. The result is a fragmented mitochondrial network characterized by small, punctate organelles that are bioenergetically inefficient and more susceptible to apoptosis. This loss of metabolic flexibility and interconnectivity further deepens the energetic crisis in the failing diabetic heart.

3.1.2.5 Sustained ER stress

The endoplasmic reticulum (ER) and mitochondria are physically and functionally connected at mitochondria-associated membranes (MAMs), where they exchange Ca^{2+}. Disruption of this ER-mitochondria Ca^{2+} crosstalk in DCM, often due to the structural and functional defects mentioned earlier, leads to sustained ER stress. The accumulation of unfolded proteins in the ER activates the unfolded protein response (UPR) pathways (PERK, IRE1α, ATF6). Chronic UPR activation exacerbates insulin resistance, promotes apoptosis, and further worsens cellular Ca^{2+} handling defects, creating a feed-forward loop of cellular injury and aggravated contractile dysfunction.

3.1.2.6 Microvascular dysfunction

The impact of mitochondrial Ca^{2+} dysregulation extends beyond cardiomyocytes to cardiac endothelial cells. In these cells, similar dysregulation, compounded by insults from AGEs and ROS, contributes to microvascular dysfunction. This manifests as reduced nitric oxide (NO) bioavailability, increased endothelial permeability, inflammation, and impaired vasodilation. The resulting compromise in coronary microcirculation leads to myocardial ischemia and a perfusion-contraction mismatch, further starving cardiomyocytes of oxygen and nutrients and exacerbating the core pathology of DCM.

3.2 Key pathways/mechanisms underlying mitochondrial calcium dysregulation in DCM

3.2.1 Energy metabolism impairment

McCormack, J.G., and colleagues demonstrated the reduction in activity of the Ca^{2+}-dependent dehydrogenase OGDH (69). Inhibited mitochondrial Ca^{2+} uptake obstructs the TCA cycle (70). This leads to decreased ATP production and consequent reduction in myocardial contractility (71).

3.2.1.1 Exacerbated oxidative stress

Ca^{2+} overload induces excessive ROS generation (72), causing oxidative damage to mitochondrial proteins, lipids, and DNA (73). This establishes a vicious cycle of mitochondrial dysfunction and progressive oxidative injury (81). Mitochondrial calcium dysregulation exacerbates oxidative stress in diabetic cardiomyopathy through converging mechanisms, with the core pathways summarized in Figure 1.

3.2.1.2 Pathological mPTP opening

Ca^{2+} overload serves as the primary trigger for mPTP opening (74). Sustained opening results in mitochondrial swelling and rupture, cytochrome c release, and activation of cardiomyocyte apoptosis and necrosis (75). And myocyte loss and cardiac fibrosis. Pathological opening of the mPTP triggers a lethal cascade in myocardial cells, with the resultant pathological outcomes depicted in Figure 2.

3.2.1.3 Abnormal calcium signaling

The interplay between cytosolic and mitochondrial Ca^{2+} handling is crucial. Dysregulation of SERCA2a, as occurs in DCM, delays cytosolic Ca^{2+} clearance during diastole, contributing to diastolic dysfunction. This persistent elevation in cytosolic Ca^{2+} can, in turn, lead to passive, pathological loading of mitochondria, especially if the MCU complex is dysregulated. Recent studies higdemonstrate that in DCM, the coexistence of reduced MCU expression and impaired SERCA2a function leads to a mishandling of Ca both compartments, severely compromising excitation-contraction coupling and overall cardiac performance (76–78, 82).

3.3 Pathological interconnections with diabetic metabolic dysregulation

Scholars summarize four major injury axes in diabetes: glucotoxicity, lipotoxicity, oxidative stress, and insulin resistance. Through crosstalk, they collectively suppress the calcium homeostasis network (83).

In greater detail:

Glucotoxicity: Suarez and his team discovered that high glucose activates PKCβ, which phosphorylates the MCU subunit (MiCu1) at Ser^{57}, inhibiting calcium uptake capacity (↓40%), leading to cardiomyocyte energy metabolism disorders (84).

Advanced Glycation End Products (AGEs): Bidasee, K. R., and his team found that AGEs, via RAGE activation, inhibit SERCA activity, resulting in passive mitochondrial Ca^{2+} overload (85).

Oxidative Stress: In the pathogenic mechanisms of diabetes, oxidative stress has a significant influence. Seifer, D. R., and his team discovered that the PERK-ATF4 axis downregulates MICU1 expression, causing dysregulated mitochondrial calcium uptake (79). High glucose-induced ROS activates PKCδ to phosphorylate CypD at Ser^{191}, lowering the mPTP opening threshold ($\Delta\Psi m$ collapse accelerated 3-fold) (86).

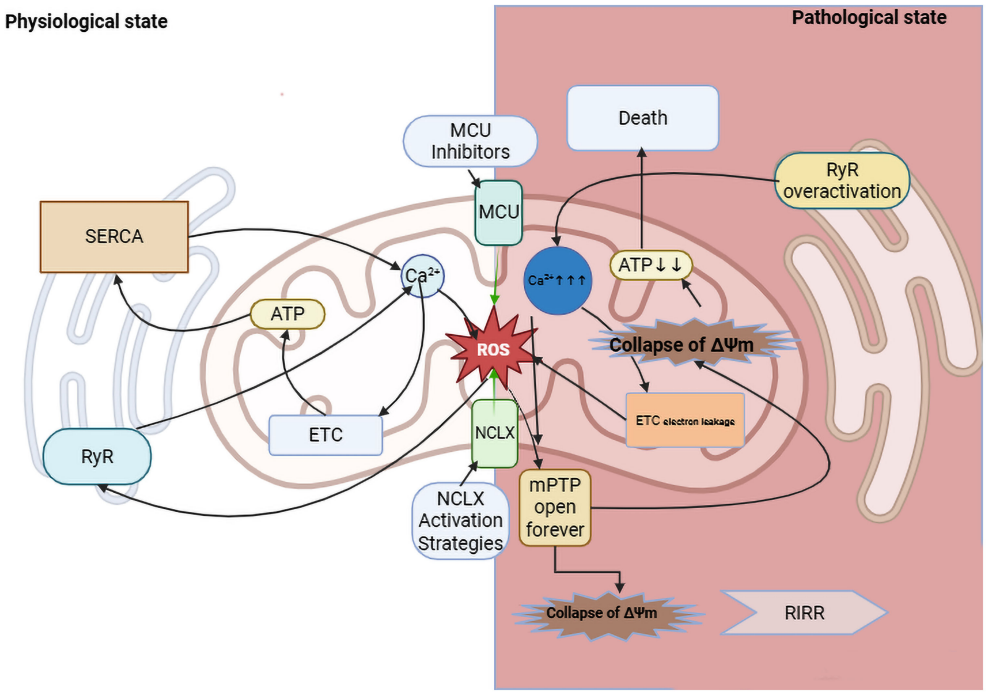

FIGURE 1
Mechanisms of oxidative stress exacerbation by mitochondrial Ca^{2+} dysregulation in DCM. Ca^{2+}, ROS, and ATP engage in a close, dynamic, and bidirectional interplay at both mitochondrial and cellular levels, forming a core pathological network in DCM. Under diabetic conditions, they form a vicious cycle, particularly characterized by Ca^{2+} overload triggering ROS production, which further disrupts Ca^{2+} homeostasis and energy metabolism. Mitochondria serve as the primary site of convergence for these factors. Their internal dynamics—such as mPTP opening and changes in ΔΨm—combined with the unique ROS-induced ROS release (RIRR) mechanism, enable rapid amplification of minor perturbations, ultimately leading to a drastic switch in cellular fate. Potential therapeutic strategies to break this cycle are highlighted: (1) Inhibition of the Mitochondrial Calcium Uniporter (MCU) to reduce pathological Ca^{2+} influx; (2) Activation of the mitochondrial $Na^+/Ca^{2+}/Li^+$ Exchanger (NCLX) to enhance Ca^{2+} efflux. MCU, Mitochondrial Calcium Uniporter; NCLX, Mitochondrial $Na^+/Ca^{2+}/Li^+$ Exchanger; mPTP, Mitochondrial Permeability Transition Pore; ETC, Electron Transport Chain; SERCA, Sarco/Endoplasmic Reticulum Ca2+-ATPase; ROS, Reactive Oxygen Species; RIRR, ROS-Induced ROSRelease.

Lipotoxicity and Insulin Resistance: Anderson, E. J., and their team discovered that abnormal fatty acid metabolism inhibits NCLX activity (87).

Collectively, these diabetic injury axes converge on the molecular machinery of mitochondrial Ca^{2+} homeostasis, making it a final common pathway translating systemic metabolic insults into overt cardiac disease.

3.4 Clinical translation: diagnostic and therapeutic implications

The dysregulation of mitochondrial Ca^{2+} homeostasis identified in DCM presents significant opportunities for advancing clinical management. Critically, specific dysregulation patterns—such as reduced MCU expression in myocardial biopsies from T2DM patients (58) and heightened mPTP sensitivity in preclinical models (60, 61)—may serve as novel stratification biomarkers. These could identify high-risk individuals progressing from subclinical cardiac dysfunction to overt heart failure, a transition observed in ~29% of asymptomatic T2DM patients within 5 years (7).

However, current clinical tools (e.g., echocardiography, serum BNP) lack the sensitivity to evaluate mitochondrial Ca^{2+} handling directly. Emerging noninvasive techniques—such as hyperpolarized ^{13}C-MRI probing calcium-associated metabolic disturbances (88) or mitochondria-targeted PET tracers—hold promise for bridging this gap. It is very important to test these methods against histological gold standards, such as MCU protein quantification in biopsies. Building upon these emerging imaging techniques, a multi-modal biomarker approach is crucial for the early detection, risk stratification, and therapeutic monitoring of DCM. Table 2 summarizes a range of possible biomarkers based on mitochondrial calcium dysregulation. It compares their detection methods, benefits, and how ready they are for use in clinical settings. The "Translational Readiness Level" (TRL) is scored on a 1–9 scale, where 1–3 indicates basic research, 4–6 indicates clinical assay development/validation, and 7–9 indicates routine clinical application.

Therapeutically, the identification of such biomarkers would enable stage-specific interventions. For instance, patients with predominant MCU downregulation and bioenergetic deficit (e.g., early-stage DCM) might benefit from strategies to augment mitochondrial Ca^{2+}uptake. In contrast, those with evidence of heightened mPTP sensitivity or impaired NCLX function (e.g., advanced DCM) could be prioritized for trials with mPTP inhibitors or NCLX activators, respectively. The development of

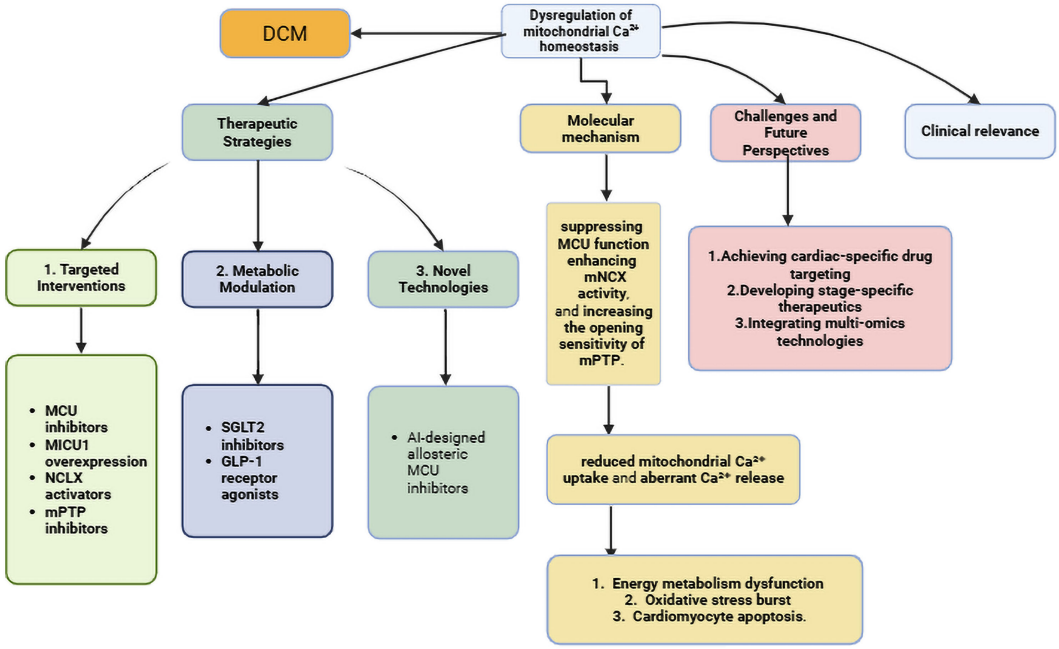

FIGURE 2
Pathological consequences of mPTP opening in DCM. Ca^{2+} directly binds to CypD and induces its conformational change; the Ca^{2+}-CypD complex targets the F-ATP synthase (involving the F-ATP synthase pore-forming hypothesis), leading to mPTP opening and triggering a pathological cascade reaction. Ca^{2+}, Calcium; Cyp D, Cyclophilin D; Mptp, Mitochondrial Permeability Transition Pore; ROS, Reactive Oxygen Species.

these biomarkers is therefore not merely diagnostic but foundational to a precision medicine approach for DCM.

Therapeutically, stage-specific interventions are warranted:

Early-stage DCM (compensatory phase): Augmenting mitochondrial Ca^{2+}uptake [e.g., via AMP-activated Protein Kinase AMPKγ1/PGC-1α axis activation (91)] may correct bioenergetic insufficiency.

Advanced DCM (decompensated phase): Inhibiting mPTP opening (e.g., CypD-targeted agents) or enhancing Ca^{2+} efflux [e.g., NCLX activators (92)] could attenuate cardiomyocyte loss.

TABLE 2 Potential diagnostic biomarkers of mitochondrial calcium dysregulation in diabetic cardiomyopathy.

Category	Target/Marker	Detection method	Key advantages	Translational readiness level (TRL)	Challenges
Tissue	MCU ↓	Biopsy + WB/IHC	Direct pathological readout.	3-4 (Requires invasive procedure)	Invasive
	mPTP sensitivity ↑	Isolated mitochondria assay	Functional, prognostic	3 (Ex vivo validation in human tissue)	Fresh tissue needed.
	NCLX ↓	Biopsy + flux assay	Efflux pathway target	2-3 (Preclinical evidence)	Not standardized
Imaging	TCA-linked metabolism	Hyperpolarized ^{13}C-MRI	Non-invasive, real-time	5-6 (Early-phase clinical trials)	High cost, complex
	ΔΨm	PET tracers	Global mitochondrial health	4-5 (Tracer development & preclinical validation)	Limited human validation
	SR-Mitochondria coupling	Super-resolution microscopy	Structural defect detection	2 (Preclinical technology)	Research-only
Blood	ccf-mtDNA	qPCR/ddPCR	Liquid biopsy, serial use	5 (Assay established; clinical correlation ongoing)	Low disease specificity (89, 90)
	MICU1/MCU (plasma)	ELISA (hypothetical)	Minimally invasive	1-2 (Hypothetical/early research)	Unclear tissue correlation

*TRL, Translational Readiness Level; WB, Western Blot; IHC, Immunohistochemistry; CRC, Calcium Retention Capacity; ccf-mtDNA, Circulating Cell-free Mitochondrial DNA; q/ddPCR, Quantitative/Digital Droplet PCR; NGS, Next-Generation Sequencing; ELISA, Enzyme-Linked ImmunosorbentAssay.

Clinical trials should prioritize agents with cardioselectivity [e.g., MCU-i4 (93)] to minimize off-target effects.

4 Therapeutic strategies targeting mitochondrial calcium homeostasis

Table 3 summarizes recent advances in the pharmacological modulation of mitochondrial Ca^{2+} flux. Key strategies include direct MCU inhibition, MICU1 modulation, NCLX activation, mPTP inhibition, targeting, and mitochondrial antioxidants with distinct efficacy and safety profiles.

4.1 MitoQ: mitochondria-targeted antioxidant

4.1.1 Inhibiting mitochondrial Ca^{2+} overload/ restoring physiological uptake

4.1.1.1 MCU inhibitors

Research on MCU inhibitors has yielded progress while also revealing temporary limitations. Xie, Y., and colleagues discovered that the novel inhibitor Ru265 (IC_{50}=28 nM) mitigated calcium overload post-myocardial infarction (mitochondrial $[Ca^{2+}]$ ↓62%), but >5 mg/kg dosing caused a 40% decline in murine exercise endurance (94). Although not tested in a pure DCM model, the cardiac-specific MCU inhibitor MCU-i4 shows promise in ischemia-reperfusion injury models, a common comorbidity in patients with diabetes. It reduced infarct size by 35% without detectable hepatorenal toxicity (93). Researchers are still looking into the translational potential of MCU inhibition. Recent studies have further elucidated the role of MCU in cardiac physiology and disease, confirming its inhibition as a potent strategy to protect against calcium overload injury in various models, including ischemia-reperfusion (102). A particularly promising development is the emergence of novel, tissue-specific MCU inhibitors designed to minimize systemic side effects, as highlighted in recent preclinical assessments (103). However, the critical challenge remains in achieving a therapeutic window that mitigates pathology without compromising physiological energy production, especially in the chronic setting of DCM.

4.1.1.2 MICU 1/2 functional regulation

Researchers targeting MICU1/2 functional regulation have achieved significant progress. MICU1 overexpression improved mitochondrial function in diabetic cardiomyopathy (ATP ↑50%) by stabilizing cristae structure—an effect distinct from MCU regulation (95). Conversely, Tomar, D., and team found that whole-body MICU1 knockout exacerbated sepsis-induced cardiac dysfunction, while cardiac-specific overexpression required precise dose control (*>2-fold expression induced contractile suppression*) (92).

4.1.1.3 NCLX activation strategies

Research on NCLX activation strategies has become a prominent focus. Luongo, T. S., and colleagues showed that AAV9-NCLX therapy increased the rate at which calcium leaves the mitochondria by 70% and the left ventricular ejection fraction (LVEF) by 25% (P<0.01) in heart failure models (96). Concurrently, studies revealed that the compound NCLX-273 (EC_{50}=0.15 μM)

TABLE 3 Pharmacological strategies targeting mitochondrial calcium homeostasis in cardiac and non-cardiac models.

Target/Compound	Potency (μM)	Model ♥/◆	Key outcome & safety*	Ref.
MCU inhibitor				
Ru265	0.028	♥ MI	Mito-$[Ca^{2+}]$ ↓62%; exercise ↓40%	(94)
MCU-i4	0.5	♥ I/R	Infarct ↓35%; no hepato-renal tox.	(93)
MICU1-OE (AAV9)	—	♥ DCM	ATP ↑50%; >2× OE depresses contract.	(95)
NCLX activator				
AAV9-NCLX	—	♥ HF	LVEF ↑25%; efflux ↑70%	(96)
NCLX-273	0.15	◆ kidney	Renal protection; cardiac data NA	(97)
mPTP inhibitor				
TRO40303	—	♥ STEMI	Infarct ↓18%; nephrotoxicity ↑2.4×	(98)
Sanglifehrin A	—	♥ PO	Fibrosis ↓40%; F <5% oral	(99)
Mitochondrial antioxidant				
MitoTEMPO	—	♥ DCM	ROS ↓65%; E/e′ ↓28%	(100)
MitoQ	—	◆ ageing	Mitophagy ↓40% → cardiac damage	(101)

*♥ cardiac; ◆ non-cardiac.
MCU, Mitochondrial Calcium Uniporter; MI, Myocardial Infarction; Ca^{2+}, Calcium; I/R, Ischemia/Reperfusion; MICU1, Mitochondrial Calcium Uptake 1; AAV9, Adeno-Associated Virus serotype 9; NCLX, Na+/Ca2+/Li+ Exchanger (Mitochondrial); HF, Heart Failure; LVEF, Left Ventricular Ejection Fraction; mPTP, Mitochondrial Permeability Transition Pore; CsA, Cyclosporine A; STEMI, ST-Elevation Myocardial Infarction; ROS, Reactive Oxygen Species; E/e′, Ratio of early mitral inflow velocity to early diastolic mitral annular velocity; PINK1, PTEN Induced Kinase 1; Parkin, Parkin RBR E3 Ubiquitin Protein Ligase; MitoTEMPO, a mitochondria-targeted antioxidant specifically designed to reduce oxidative stress within mitochondria.

selectively activates renal tubular NCLX, mitigating acute kidney injury while exhibiting significantly reduced cardiotoxicity compared to CGP-37157 (97).

4.1.1.3 Inhibition of mPTP opening

Research has revealed the therapeutic potential of mPTP inhibitors, though limitations persist. Atar, D., and team demonstrated that the CsA analog TRO40303 reduced infarct size by 18% (*P=0.03*) in diabetic STEMI patients yet failed to improve long-term LVEF and resulted in a 2.4-fold increase in nephrotoxicity incidence (98). Complementarily, Karch, J.'s group found Sanglifehrin A attenuated myocardial fibrosis by 40%, but its <5% oral bioavailability necessitates nano-carrier delivery systems (99).

4.1.1.4 Mitochondrial-targeted antioxidant therapy

Researchers targeting mitochondrial antioxidants have mitigated Ca^{2+}-induced ROS damage with nuanced outcomes. Dare, A. J., and team demonstrated that MitoTEMPO (1.5 mg/kg) reduced mitochondrial ROS by 65% and improved diastolic function (E/e' ↓28%) in diabetic hearts, yet failed to reverse fibrosis (100). Zielonka, J.'s group uncovered a paradoxical effect: chronic MitoQ administration suppressed mitophagy (PINK1/Parkin pathway ↓40%), accelerating myocardial damage in aging models (101).

4.1.1.5 Counteracting mitochondrial metabolic dysregulation

Current hypoglycemic/lipid-modulating drugs demonstrate potential indirect protective effects on mitochondrial Ca^{2+} homeostasis. Lopaschuk, G. D.'s team demonstrated that empagliflozin reduces mitochondrial calcium overload risk by elevating ketone body β-HB (calcium transient amplitude ↓25%) (104). Pugazhenthi, S.'s group indicated that liraglutide activates PKA, thereby enhancing MCU closure threshold (*calcium overload threshold ↑3-fold*) (105). Foretz, M., and colleagues found that metformin inhibits the MCU complex via AMPK (calcium uptake ↓30%), while potentially exacerbating energy crises in heart failure patients (106).

4.2 Emerging next-generation therapeutic strategies

Zaha, V. G., and their team discovered that AAV9-mediated AMPKγ1 overexpression enhances PGC-1α activity, improving calcium handling in DCM (calcium transient decay accelerated by 40%) (91). Rocha, A. G., and their team discovered that delivering a Mitofusin 2 (MFN2) agonist using the mitochondria-targeted peptide SS-31 restores mitochondrial fusion in diabetic cardiomyopathy (fission/fusion ratio decreased by 60%), resulting in a doubled mPTP opening threshold (80).

Comparative analysis of mitochondrial calcium-targeting strategies reveals distinct advantages and limitations. MCU inhibition (e.g., MCU-i4) effectively prevents calcium overload but risks impairing physiological energy production, creating a therapeutic window challenge. In contrast, NCLX activation enhances calcium efflux without compromising uptake, offering a more physiological approach, but it faces specificity hurdles. The translation of these strategies from preclinical models to clinical practice faces several barriers: (1) species differences in calcium handling proteins, (2) the dynamic nature of the diabetic metabolic milieu that alters drug responses, and (3) the heterogeneity of DCM progression stages requiring personalized approaches. Notably, while MCU inhibitors show promise in acute injury models, NCLX activators may be better suited for chronic DCM management where calcium efflux capacity is progressively impaired.

4.2.1 Comparative analysis of mitochondrial calcium-targeting therapeutic strategies

While the array of therapeutic strategies targeting mitochondrial calcium is expanding, a critical and comparative evaluation reveals distinct advantages, limitations, and potential synergies.

4.2.1.1 MCU inhibition vs. NCLX activation

This represents a fundamental philosophical dichotomy in therapeutic approach. MCU inhibition (e.g., with MCU-i4) is primarily a preventive strategy, aiming to block the entry point of calcium during pathological overload, as seen in ischemia-reperfusion injury. Its main strength is that it works well in emergency situations. However, its major limitation is the "therapeutic window" challenge; since MCU is essential for physiological energy production, excessive or chronic inhibition risks exacerbating the bioenergetic deficit that characterizes DCM. In contrast, NCLX activation is a corrective or facilitative strategy. It does not interfere with physiological uptake but enhances the clearance of excess calcium, thereby breaking the cycle of overload. This makes it theoretically more suitable for chronic conditions like DCM, where efflux mechanisms are progressively impaired. The translational hurdle for NCLX activators lies in achieving tissue and context specificity to avoid systemic disturbances in calcium signaling.

4.2.1.2 Stage-specific considerations

The choice of strategy may be critically dependent on the stage of DCM. In early-stage DCM, characterized by impaired calcium uptake and bioenergetic deficit, strategies to augment physiological uptake (e.g., via AMPK/PGC-1α activation) or stabilize the MCU complex might be beneficial. Conversely, in advanced DCM, where calcium overload and mPTP sensitization dominate, MCU inhibitors, NCLX activators, or mPTP blockers would be more logical choices. This underscores the necessity of precision medicine and reliable biomarkers to stratify patients.

4.2.1.3 Combination therapies

Given the complexity of DCM, multitarget approaches may be required. For instance, a combination of a mild MCU modulator (to

prevent severe overload) with an NCLX activator (to promote efflux) and a mitochondrial antioxidant (to reduce ROS-triggered mPTP opening) could offer synergistic benefits, potentially at lower, safer doses of each agent. However, the combination also increases the risk of unforeseen off-target effects and necessitates sophisticated pharmacokinetic studies.

5 Challenges and future directions

The translation of mitochondrial calcium homeostasis as a therapeutic target from compelling preclinical data to clinical reality for DCM patients is fraught with challenges. This section delineates the principal barriers and outlines promising avenues for future research.

5.1 The specificity and safety hurdle of pharmacological intervention

A primary concern in targeting mitochondrial calcium fluxes is achieving therapeutic efficacy without disrupting physiological function. MCU inhibitors exemplify this "double-edged sword" effect. While they potently prevent pathological calcium overload, their chronic use risks exacerbating the pre-existing bioenergetic deficit that characterizes DCM by blunting the calcium signals essential for stimulating ATP production (107, 108). Furthermore, systemic inhibition of a ubiquitous protein like MCU may incur off-target effects in other high-energy-demand tissues, such as skeletal muscle and neurons. Therefore, the development of cardiac-targeted delivery systems (e.g., using cardiotropic viral vectors or nanoparticle carriers) or conditionally activatable prodrugs (designed to be active only in the pathological microenvironment, e.g., during excessive ROS or Ca^{2+} levels) is a critical future direction (93, 107).

5.2 Heterogeneity in mitochondrial calcium dysregulation across different stages of DCM

DCM is a progressive disease, and the nature of mitochondrial calcium dysregulation evolves with its stages. In the early compensatory phase, the primary defect is often impaired mitochondrial Ca^{2+} uptake due to downregulation of the MCU complex and PGC-1α. This condition leads to a bioenergetic deficit but not overt overload. The heart may try to make up for it in other ways. However, as the disease advances to the decompensated phase, chronic metabolic stress and cellular damage predispose the myocardium to pathological Ca^{2+} overload. This process is characterized by increased susceptibility to mPTP opening, exacerbated by oxidative stress and the dysregulation of efflux pathways like NCLX. Wu, S., and their team gave us important information by demonstrating stage-specific regulatory mechanisms, such as FBXL4-mediated degradation of MCU in the decompensated phase, which fundamentally alters the mitochondrial calcium handling phenotype (109, 110). This heterogeneity necessitates stage-specific therapeutic interventions.

5.3 Bridging the translational gap: from animal models to human DCM

A significant barrier to clinical progress is the limited predictive value of current preclinical models. Rodent models of diabetes (e.g., db/db mice, STZ rats) capture certain metabolic features but fail to fully recapitulate the chronic, multi-factorial nature of human DCM, which develops over decades amidst complex genetic backgrounds and comorbidities.

Key limitations include:

- Species Differences: The expression, regulation, and relative importance of proteins like MCU and NCLX can differ between rodents and humans.
- Model Uniformity vs. Patient Heterogeneity: Genetically uniform animal models do not reflect the vast heterogeneity of human DCM, leading to over-optimistic drug efficacy that fails in diverse clinical populations.
- The Dynamic Diabetic Milieu: Preclinical testing often occurs in a stable metabolic state, unlike the fluctuating glucose, insulin, and adipokine levels in patients, which can profoundly alter drug responses.
- To bridge this gap, future research must prioritize:
- Human-Relevant Models: Utilizing induced pluripotent stem cell-derived cardiomyocytes (iPSC-CMs) from diabetic patients with and without cardiomyopathy.
- Comorbidity-Incorporated Designs: Testing drug efficacy in models that combine diabetes with other common comorbidities like hypertension or aging.
- Biomarker-Driven Stratification: The discovery and validation of non-invasive biomarkers (as proposed in Table 2) are paramount for identifying responsive patient subpopulations in clinical trials.

5.4 The rationale for multitarget combination therapies

Given the complex, interconnected pathology of DCM, simultaneously targeting multiple nodes in the mitochondrial calcium network may yield synergistic benefits. Hamilton, S., and colleagues provided a proof-of-concept, demonstrating that dual inhibition of the inositol trisphosphate receptor (IP3R) and MCU was more effective in modulating mitochondrial Ca^{2+} uptake in heart failure than either approach alone (111). Logical combinations for DCM could include a mild MCU modulator (to prevent severe overload) with an NCLX activator (to enhance clearance) and a mitochondrial antioxidant (to reduce ROS-mediated mPTP sensitization). However, such strategies require sophisticated pharmacokinetic and safety studies to avoid unforeseen off-target effects.

5.5 Harnessing novel technologies for mechanistic insight and drug discovery

Cutting-edge technologies stand poised to transform the future of DCM research and therapy development:

- Single-Cell and Spatial Omics: Technologies like scRNA-seq are already illuminating the cellular heterogeneity of the failing heart, identifying distinct cardiomyocyte subpopulations with unique calcium handling gene expression profiles (112). This makes it possible to find new cell-specific targets and biomarkers.
- Advanced Imaging: Real-time mitochondrial calcium monitoring with improved genetically encoded indicators (e.g., mtGCaMP) and hyperpolarized ^{13}C-MRI, which can probe calcium-related metabolic fluxes, offer non-invasive windows into mitochondrial function *in vivo* (88, 113).
- Artificial Intelligence (AI): AI-driven drug design is breaking new ground in targeting complex proteins, like the MCU complex (114). AI-designed allosteric inhibitors have demonstrated effectiveness in alleviating mitochondrial calcium overload in heart failure models (115), and quantum machine learning is currently facilitating the precise prediction of drug-channel interactions (116).

6 Conclusions

Mitochondrial calcium homeostasis has emerged from the periphery to claim its position as a central integrator in the pathogenesis of diabetic cardiomyopathy. It functions as a critical signaling nexus, translating the systemic metabolic insults of diabetes—hyperglycemia, lipotoxicity, oxidative stress, and insulin resistance—into the cardinal features of myocardial dysfunction: bioenergetic deficit, oxidative injury, and cardiomyocyte loss. The diabetic environment directly attacks the molecular machinery that controls mitochondrial calcium. This causes problems with uptake through the MCU complex, sensitized efflux through the mPTP, and dysregulated extrusion through NCLX.

The therapeutic landscape is evolving to target this hub, but our analysis reveals that the choice of strategy is not trivial. The fundamental dichotomy between MCU inhibition (a preventive strategy against overload) and NCLX activation (a corrective strategy to enhance efflux) represents a critical trade-off between preventing toxicity and maintaining physiological energy production. The optimal choice varies depending on the stage of DCM and the predominant nature of the calcium handling defect in a particular patient.

Therefore, the path forward must be guided by precision medicine. Success will depend on our ability to leverage emerging technologies—from single-cell omics and AI to advanced imaging—to develop reliable biomarkers for patient stratification and to design cardioselective therapies that are effective within the complex, dynamic metabolic context of diabetes. Ultimately, safeguarding the mitochondrial calcium gateway may be the key to protecting the diabetic heart and altering the devastating cardiovascular destiny of millions of patients worldwide.

Author contributions

SD: Writing – original draft. FT: Writing – original draft. YJ: Writing – original draft.

Funding

The author(s) declare that no financial support was received for the research, and/or publication of this article.

Conflict of interest

The authors declare that the research was conducted in the absence of any commercial or financial relationships that could be construed as a potential conflict of interest.

Generative AI statement

The author(s) declare that Generative AI was used in the creation of this manuscript. Generative AI tools were used to assist with language translation and text editing; all content has been verified by the authors.

Any alternative text (alt text) provided alongside figures in this article has been generated by Frontiers with the support of artificial intelligence and reasonable efforts have been made to ensure accuracy, including review by the authors wherever possible. If you identify any issues, please contact us.

Publisher's note

References

1. Dillmann WH. Diabetic cardiomyopathy. *Circ Res*. (2019) 124:1160–2. doi: 10.1161/CIRCRESAHA.118.314665

2. World Health Organization. *Global Report on Diabetes*. Geneva, Switzerland: World Health Organization (2016).

3. American Diabetes Association. *Diabetes and Cardiovascular Disease*. Arlington: American Diabetes Association (2019).

4. International Diabetes Federation. *IDF Diabetes Atlas*. *10th ed*. Brussels: International Diabetes Federation (2021).

5. Paolillo S, Marsico F, Prastaro M, Dellegrottaglie S, Esposito L, Marciano C, et al. Diabetic cardiomyopathy: definition, diagnosis, and therapeutic implications. *Heart Failure Clinics*. (2019) 15:341–7. doi: 10.1016/j.hfc.2019.02.003

6. Lu Y, Zhang H, Teng D, Liu L, Chen L, Wang Y, et al. Prevalence and prognosis of subclinical diabetic cardiomyopathy: a prospective cohort study using cardiac MRI. *JACC: Cardiovasc Imaging*. (2022) 15:1462–74. doi: 10.1016/j.jcmg.2022.02.016

7. Jensen MT, Søgaard P, Andersen HU, Bech J, Hansen TF, Jørgensen PG, et al. Progression of diabetic cardiomyopathy in type 1 diabetes: the FinnDiane study. *Diabetes Care*. (2021) 44:2050–6. doi: 10.2337/dc21-0092

8. Jia G, Hill MA, Sowers JR. Diabetic cardiomyopathy: an update of mechanisms contributing to this clinical entity. *Circ Res*. (2018) 122:624–38. doi: 10.1161/CIRCRESAHA.117.311586

9. Seferović PM, Petrie MC, Filippatos GS, Anker SD, Rosano G, Bauersachs J, et al. Type 2 diabetes mellitus and heart failure: a position statement from the Heart Failure Association of the European Society of Cardiology. *Eur J Heart Failure*. (2018) 20:853–72. doi: 10.1002/ejhf.1170

10. Chen D, Sindone A, Huang MLH, Peter K, Jenkins AJ. Diabetic cardiomyopathy: insights into pathophysiology, diagnosis and clinical management. *J Mol Cell Cardiol*. (2025) 206:55–69. doi: 10.1016/j.yjmcc.2025.06.013

11. Roth GA, Mensah GA, Johnson CO, Addolorato G, Ammirati E, Baddour LM, et al. Global burden of cardiovascular diseases and risk factors, 1990–2019: update from the GBD 2019 study. *J Am Coll Cardiol*. (2020) 76:2982–3021. doi: 10.1016/j.jacc.2020.11.010

12. Roth GA, Mensah GA, Johnson CO, Addolorato G, Ammirati E, Baddour LM, et al. Global burden of cardiovascular diseases and risk factors, 1990–2022: update from the GBD 2022 study. *J Am Coll Cardiol*. (2024) 83:2619–76. doi: 10.1016/j.jacc.2024.03.543

13. Murarka S, Movahed MR. Diabetic cardiomyopathy. *J Cardiac Failure*. (2020) 26:291–303. doi: 10.1016/j.cardfail.2019.12.017

14. Tan Y, Zhang Z, Zheng C, Wintergerst KA, Keller BB, Cai L. Mechanisms of diabetic cardiomyopathy and potential therapeutic strategies: preclinical and clinical evidence. *Nat Rev Cardiol*. (2020) 17:585–607. doi: 10.1038/s41569-020-0339-2

15. Mann C, Braunwald E, Zelniker TA. Diabetic cardiomyopathy revisited: The interplay between diabetes and heart failure. *Int J Cardiol*. (2025) 438:133554. doi: 10.1016/j.ijcard.2025.133554

16. Tan Y, et al. Diabetic cardiomyopathy: from molecular mechanisms to therapeutic strategies. *J Mol Cell Biol*. (2023) 15:mjad041. doi: 10.1093/jmcb/mjad041

17. Santulli G, Xie W, Reiken SR, Marks AR. Mitochondrial calcium overload is a key determinant in heart failure. *Proc Natl Acad Sci United States America*. (2015) 112:11389–94. doi: 10.1073/pnas.1513047112

18. Dorn GW 2nd, Kitsis RN. The mitochondrial dynamism–mitophagy–cell death interactome in heart failure. *Circ Res*. (2020) 127:1051–3. doi: 10.1161/CIRCRESAHA.120.317777

19. Kim JC, Son MJ, Woo SH. Regulation of cardiac calcium by mechanotransduction: role of mitochondria. *Arch Biochem Biophysics*. (2018) 659:33–41. doi: 10.1016/j.abb.2018.09.021

20. Vásquez-Trincado C, García-Carvajal I, Pennanen C, Parra V, Hill JA, Rothermel BA, et al. Mitochondrial dynamics, mitophagy, and cardiovascular disease. *J Physiol*. (2016) 594:509–25. doi: 10.1113/JP271301

21. Griffiths EJ, Balaska D, Cheng WHY. The ups and downs of mitochondrial calcium signalling in the heart. *Biochim Biophys Acta*. (2010) 1797:856–64. doi: 10.1016/j.bbabio.2010.04.004

22. Finkel T, Menazza S, Holmström KM, Parks RJ, Liu J, Sun J, et al. The ins and outs of mitochondrial calcium. *Circ Res*. (2015) 116:1810–9. doi: 10.1161/CIRCRESAHA.116.305484

23. Choudhury P, Kosuru R, Cai Y. Editorial: The complex phenotype of diabetic cardiomyopathy: clinical indicators and novel treatment targets. *Front Endocrinol*. (2024) 15:1497352. doi: 10.3389/fendo.2024.1497352

24. Camara AKS, Zhou Y, Wen PC, Tajkhorshid E, Kwok WM. Mitochondrial VDAC1: a key gatekeeper as potential therapeutic target. *Front Physiol*. (2017) 8:460. doi: 10.3389/fphys.2017.00460

25. Pathak T, Trebak M. Mitochondrial Ca^{2+} signaling. *Pharmacol Ther*. (2018) 192:112–23. doi: 10.1016/j.pharmthera.2018.07.003

26. Molnár MJ, Kovács GG. Mitochondrial diseases. *Handb Clin Neurol*. (2017) 145:147–55. doi: 10.1016/B978-0-12-802395-2.00010-9

27. Zhou B, Tian R. Mitochondrial dysfunction in the pathophysiology of heart failure. *J Clin Invest*. (2018) 128:3716–26. doi: 10.1172/JCI120849

28. Demaurex N, Rosselin M. Redox control of mitochondrial calcium uptake. *Mol Cell*. (2017) 65:961–2. doi: 10.1016/j.molcel.2017.03.010

29. Samanta K, Mirams GR, Parekh AB. Sequential forward and reverse transport of the Na^+/Ca^{2+} exchanger generates Ca^{2+} oscillations within mitochondria. *Nat Commun*. (2018) 9:156. doi: 10.1038/s41467-017-02638-2

30. Feno S, Butera G, Vecellio Reane D, Rizzuto R, Raffaello A. Crosstalk between calcium and ROS in pathophysiological conditions. *Oxid Med Cell Longevity*. (2019) 2019:9324018. doi: 10.1155/2019/9324018

31. Stoll S, Xi J, Ma B, Leimena C, Behringer EJ, Qin G, et al. The valosin-containing protein protects the heart against pathological Ca^{2+} overload by modulating Ca^{2+} uptake proteins. *Toxicological Sci*. (2019) 168:450–67. doi: 10.1093/toxsci/kfz009

32. Rizzuto R, De Stefani D, Raffaello A, Mammucari C. Mitochondria as sensors and regulators of calcium signalling. *Nat Rev Mol Cell Biol*. (2012) 13:566–78. doi: 10.1038/nrm3412

33. Liu JC. Is the MCU indispensable for normal heart function? *J Mol Cell Cardiol*. (2020) 143:175–83. doi: 10.1016/j.yjmcc.2020.04.034

34. Lee SK, Shanmughapriya S, Mok MCY, Dong Z, Tomar D, Carvalho E, et al. Structural insights into mitochondrial calcium uniporter regulation by divalent cations. *Cell Chem Biol*. (2016) 23:1157–69. doi: 10.1016/j.chembiol.2016.07.012

35. Baughman JM, Perocchi F, Girgis HS, Plovanich M, Belcher-Timme CA, Sancak Y, et al. Integrative genomics identifies MCU as an essential component of the mitochondrial calcium uniporter. *Nature*. (2011) 476:341–5. doi: 10.1038/nature10234

36. De Stefani D, Raffaello A, Teardo E, Szabo I, Rizzuto R. A forty-kilodalton protein of the inner membrane is the mitochondrial calcium uniporter. *Nature*. (2011) 476:336–40. doi: 10.1038/nature10230

37. Marchi S, Pinton P. The mitochondrial calcium uniporter complex: molecular components, structure and physiopathological implications. *J Physiol*. (2014) 592:829–39. doi: 10.1113/jphysiol.2013.268235

38. Wang Y, Nguyen NX, She J, Zeng W, Yang Y, Bai XC, et al. Structural mechanism of EMRE-dependent gating of the human mitochondrial calcium uniporter. *Cell*. (2019) 177:1252–1261.e7. doi: 10.1016/j.cell.2019.03.050

39. Fan C, Fan M, Orlando BJ, Fastman NM, Zhang J, Xu Y, et al. Structural basis of the MICU1-MICU2 heterodimer interface in MCU regulation. *Nature*. (2020) 585:641–6. doi: 10.1038/s41586-020-2679-9

40. Bernardi P, Rasola A, Forte M, Lippe G. The mitochondrial permeability transition pore: channel formation by F-ATP synthase, integration in signal transduction, and role in pathophysiology. *Physiol Rev*. (2015) 95:1111–55. doi: 10.1152/physrev.00001.2015

41. Baines CP, Kaiser RA, Sheiko T, Craigen WJ, Molkentin JD. Voltage-dependent anion channels are dispensable for mitochondrial-dependent cell death. *Nat Cell Biol*. (2007) 9:550–5. doi: 10.1038/ncb1575

42. Wu Y, Rasmussen TP, Koval OM, Joiner MLA, Hall DD, Chen B, et al. The mitochondrial uniporter controls fight or flight heart rate increases. *Nat Commun*. (2015) 6:6081. doi: 10.1038/ncomms7081

43. Mnatsakanyan N, Llaguno MC, Yang Y, Yan J, Weber J , Sigworth FJ, et al. A mitochondrial megachannel resides in monomeric F_1F_O ATP synthase. *Proc Natl Acad Sci United States America*. (2019) 116:19963–8. doi: 10.1073/pnas.1904776116

44. Palty R, Silverman WF, Hershfinkel M, Caporale T, Sensi SL, Parnis J, et al. NCLX is an essential component of mitochondrial Na^+/Ca^{2+} exchange. *Cell Metab*. (2010) 12:54–62. doi: 10.1016/j.cmet.2010.05.011

45. Kwong JQ, Huo J, Bround MJ, Boyer JG, Schwan J, Oydanich M, et al. The mitochondrial phosphate carrier modulates cardiac metabolism and protects against ischemia-reperfusion injury. *Nat Metab*. (2021) 3:1382–96. doi: 10.1038/s42255-021-00468-7

46. Boyman L, Kekenes-Huskey PM, Lederer WJ, Marsh JD, Chatham JC, Lindert S, et al. Mitochondrial calcium buffering contributes to the maintenance of basal cardiac function. *Circ Res*. (2019) 124:664–78. doi: 10.1161/CIRCRESAHA.118.313444

47. Glancy B, Balaban RS. Role of mitochondrial Ca^{2+} in the regulation of cellular energetics. *Biochemistry*. (2012) 51:2959–73. doi: 10.1021/bi2018909

48. Spinelli JB, Haigis MC. The multifaceted contributions of mitochondria to cellular metabolism. *Nat Cell Biol*. (2018) 20:745–54. doi: 10.1038/s41556-018-0124-1

49. Nemani N, Shanmughapriya S, Madesh M. Molecular regulation of MCU: implications in physiology and disease. *Cell Calcium*. (2020) 87:102186. doi: 10.1016/j.ceca.2020.102186

50. Zorov DB, Juhaszova M, Sollott SJ. Mitochondrial reactive oxygen species (ROS) and ROS-induced ROS release. *Physiol Rev*. (2014) 94:909–50. doi: 10.1152/physrev.00026.2013

51. Görlach A, Bertram K, Hudecova S, Krizanova O. Calcium and ROS: a mutual interplay. *Redox Biol*. (2015) 6:260–71. doi: 10.1016/j.redox.2015.08.010

52. Mráček T, Drahota Z, Houštěk J. The function and the role of the mitochondrial glycerol-3-phosphate dehydrogenase in mammalian tissues. *Biochim Biophys Acta*. (2013) 1827:401–10. doi: 10.1016/j.bbabio.2012.11.014

53. Angelova PR, Abramov AY. Role of mitochondrial ROS in the brain: from physiology to neurodegeneration. *FEBS Lett.* (2018) 592:692–702. doi: 10.1002/1873-3468.12964

54. Baines CP, Kaiser RA, Purcell NH, Blair NS, Osinska H, Hambleton MA, et al. Loss of cyclophilin D reveals a critical role for mitochondrial permeability transition in cell death. *Nature*. (2005) 434:658–62. doi: 10.1038/nature03434

55. Bonora M, Morganti C, Morciano G, Pedriali G, Lebiedzinska-Arciszewska M , Aquila G, et al. Mitochondrial permeability transition involves dissociation of F_1F_O ATP synthase dimers and C-ring conformation. *EMBO Rep.* (2017) 18:1077–89. doi: 10.15252/embr.201643602

56. Kandula N, Kumar S, Mandlem VKK, Siddabathuni A, Singh S, Kosuru R. Role of AMPK in myocardial ischemia-reperfusion injury-induced cell death in the presence and absence of diabetes. *Oxid Med Cell Longevity*. (2022) 2022:7346699. doi: 10.1155/2022/7346699

57. Lu Z, Jiang YP, Xu WH, Ballou LM, Cohen IS, Lin RZ. Hyperglycemia acutely decreases mitochondrial Ca^{2+} uptake in cardiac myocytes. *Cardiovasc Diabetol.* (2018) 17:151. doi: 10.1186/s12933-018-0795-8

58. Marques MD, Santos C, Costa T, Ferreira J, Oliveira M, Silva R, et al. Diabetes and cardiac fibrosis: a tissue-based post-mortem analysis with real-world data. *J Clin Endocrinol Metab.* (2022) 107:e2776–84. doi: 10.1210/clinem/dgac234

59. Karamanlidis G, Bautista-Hernandez V, Feneley M, Garcia-Menendez L, Margulies KB, Tian R, et al. Defective DNA replication impairs mitochondrial biogenesis in human failing hearts. *Circ Res.* (2013) 112:673–8. doi: 10.1161/CIRCRESAHA.111.300374

60. Liu T, Takimoto E, Dimaano VL, DeMazumder D, Kettlewell S, Smith G, et al. Inhibiting mitochondrial Na^+/Ca^{2+} exchange prevents sudden death in a Guinea pig model of heart failure. *Circ Res.* (2014) 115:44–54. doi: 10.1161/CIRCRESAHA.115.303062

61. Thandavarayan RA, Giridharan VV, Sari FR, Arumugam S, Pitchaimani V, Karuppagounder V, et al. Dominant-negative p38α mitogen-activated protein kinase prevents cardiac apoptosis and remodeling after streptozotocin-induced diabetes mellitus. *Am J Physiology-Heart Circulatory Physiol.* (2015) 309:H911–9. doi: 10.1152/ajpheart.00282.2015

62. Shi K, Wang F, Xia T, Wang X, Sun D, Jiang L, et al. PKCβII-activated NOX4-derived reactive oxygen species in cardiomyocytes induces mitochondrial damage and apoptosis during hyperglycemia. *Free Radical Biol Med.* (2020) 146:234–47. doi: 10.1016/j.freeradbiomed.2019.11.007

63. Pal PB, Roy SG, Chattopadhyay S, Bandyopadhyay A, Basu S, Pal P, et al. Glycated albumin suppresses myocardial contraction by antagonizing SERCA2a and impairing mitochondrial function. *Biochem Pharmacol.* (2022) 195:114862. doi: 10.1016/j.bcp.2021.114862

64. Zhang L, Cannell MB, Kim SJ, Watson PA, Roderick HL, Bootman MD. Altered calcium homeostasis in the cardiac myocytes of dystrophin-deficient mdx mice. *Cardiovasc Res.* (2010) 87:63–73. doi: 10.1093/cvr/cvq021

65. Frustaci A, Kajstura J, Chimenti C, Jakoniuk I, Leri A, Maseri A, et al. Myocardial cell death in human diabetes. *Circ Res.* (2000) 87:1123–32. doi: 10.1161/01.RES.87.12.1123

66. Kho C, Lee A, Jeong D, Oh JG, Chaanine AH, Kizana E, et al. SUMO1-dependent modulation of SERCA2a in heart failure. *Nature*. (2022) 582:79–84. doi: 10.1038/s41586-022-04712-2

67. Santulli G, Pagano G, Sardu C, Xie W, Reiken S, D'Ascia SL, et al. Calcium release channel RyR2 regulates insulin release and glucose homeostasis. *J Clin Invest.* (2015) 125:1968–78. doi: 10.1172/JCI79273

68. Seidlmayer LK, Gomez-Garcia MR, Blatter LA, Pavlov E, Dedkova EN. Inorganic polyphosphate is a potent activator of the mitochondrial permeability transition pore in cardiac myocytes. *J Gen Physiol.* (2012) 139:321–31. doi: 10.1085/jgp.201210788

69. Ritchie RH, Abel ED. Basic mechanisms of diabetic heart disease. *Circ Res.* (2020) 126:1501–25. doi: 10.1161/CIRCRESAHA.120.315913

70. Garbincius JF, Elrod JW. Mitochondrial calcium exchange in physiology and disease. *Physiol Rev.* (2022) 102:893–992. doi: 10.1152/physrev.00041.2020

71. Brown DA, Perry JB, Allen ME, Sabbah HN, Stroud DM, Das S, et al. Mitochondrial function as a therapeutic target in heart failure. *Nat Rev Cardiol.* (2019) 16:33–44. doi: 10.1038/s41569-018-0079-8

72. Schofield JH, Schafer ZT. Mitochondrial reactive oxygen species and mitophagy: A complex and nuanced relationship. *Antioxidants Redox Signaling.* (2021) 34:517–30. doi: 10.1089/ars.2020.8058

73. Sies H, Jones DP. Reactive oxygen species (ROS) as pleiotropic physiological signalling agents. *Nat Rev Mol Cell Biol.* (2020) 21:363–83. doi: 10.1038/s41580-020-0230-3

74. Bernardi P, Di Lisa F. The mitochondrial permeability transition pore: molecular nature and role as a target in cardioprotection. *J Mol Cell Cardiol.* (2015) 78:100–6. doi: 10.1016/j.yjmcc.2014.09.023

75. Halestrap AP, Richardson AP. The mitochondrial permeability transition: a current perspective on its identity and role in ischemia/reperfusion injury. *J Mol Cell Cardiol.* (2015) 78:129–41. doi: 10.1016/j.yjmcc.2014.08.018

76. Liu T, Yang N, Sidor A, O'Rourke B, O'Rourke J, Sadoshima J, et al. Mitochondrial dysfunction in diabetic cardiomyopathy: The role of mitochondrial Ca2+. *Circ Res.* (2020) 126:1533–50. doi: 10.1161/CIRCRESAHA.119.315432

77. Lu X, Ginsburg KS, Kettlewell S, Bossuyt J, Smith GL, Bers DM. Measuring local gradients of intramitochondrial $[Ca^{2+}]$ in cardiac myocytes during sarcoplasmic reticulum Ca^{2+} release. *Circ Res.* (2013) 112:424–31. doi: 10.1161/CIRCRESAHA.111.300501

78. Drago I, De Stefani D, Rizzuto R, Pozzan T. Mitochondrial Ca^{2+} uptake contributes to buffering cytosolic Ca^{2+} peaks in cardiomyocytes. *Proc Natl Acad Sci United States America*. (2012) 109:12986–91. doi: 10.1073/pnas.1210718109

79. Seifer DR, Ly LD, Han X, Nassif NT, Johnson P, Ho P, et al. Endoplasmic reticulum stress activates PERK-ATF4 to induce mitophagy in diabetic hearts. *Cardiovasc Res.* (2021) 117:2367–82. doi: 10.1093/cvr/cvaa271

80. Rocha AG, Franco A, Krezel AM, Rumsey JM, Alberti JM, Knight WC, et al. MFN2 agonists reverse mitochondrial fragmentation in diabetic cardiomyopathy. *J Clin Invest.* (2022) 132:e162357. doi: 10.1172/JCI162357

81. Indo HP, Yen HC, Nakanishi I, Matsumoto KI, Tamura M, Nagano Y, et al. A mitochondrial superoxide theory for oxidative stress diseases and aging. *J Clin Biochem Nutr.* (2015) 56:1–7. doi: 10.3164/jcbn.14-42

82. Gómez J, Santiago D, Martínez L, Rodríguez P. Cardiomyocyte dysfunction in diabetic cardiomyopathy is mediated by mitochondrial calcium uniporter (MCU) and sodium/calcium/lithium exchanger (NCLX) imbalance. *Diabetes*. (2020) 69:1192–205. doi: 10.2337/db19-0999

83. Rrown DA, Griendling KK. Metabolic regulation of calcium signaling in cardiomyocytes: Implications for diabetic cardiomyopathy. *Circ Res.* (2022) 131:182–203. doi: 10.1161/CIRCRESAHA.122.320448

84. Suarez J, Hu Y, Makino A, Fricovsky E, Wang H, Dillmann WH. Alterations in mitochondrial Ca^{2+} handling in cardiac myocytes from diabetic db/db mice. *Diabetes*. (2013) 62:2921–30. doi: 10.2337/db12-1653

85. Eric JR, Bidasee KR, Uhl K, Zhang Y, Shao CH, Patel K, et al. Advanced glycation end products (AGEs) and receptor for AGEs (RAGE) in patients with diabetic cardiomyopathy. *Diabetes*. (2019) 68. doi: 10.2337/db19-175-LB

86. Javadov S, Jang S, Agostini B. Mitochondrial permeability transition pore opening as an endpoint to initiate cell death and as a putative target for cardioprotection. *Cell Physiol Biochem*. (2014) 33:1363–81. doi: 10.1159/000358697

87. Hamilton S, Terentyeva R, Kim TY, Bronk P, Clements RT, Choi BR, et al. Combined inhibition of IP3R and MCU modulates mitochondrial Ca2+ uptake in heart failure. *J Am Coll Cardiol.* (2021) 77:195. doi: 10.1016/S0735-1097(21)01319-1

88. Rider OJ, Apps A, Miller JJJ, Lau JYC, Lewis AJM, Peterzan MA, et al. Non-invasive *in vivo* assessment of cardiac metabolism in the healthy and diabetic human heart using hyperpolarized ^{13}C MRI. *Circ Res*. (2020) 126:725–36. doi: 10.1161/CIRCRESAHA.119.316260

89. Li H, Yao W, Liu Z. Circulating mitochondrial DNA as a potential biomarker for cardiac injury. *Crit Care*. (2020) 24:259. doi: 10.1186/s13054-020-02974-8

90. Bredy C, Ministeri M, Kempny A, Alonso-Gonzalez R, Swan L, Uebing A, et al. Mitochondrial dysfunction and cardiovascular disease: role of non-coding RNAs and liquid biopsy. *J Am Heart Assoc.* (2022) 11:e026711. doi: 10.1161/JAHA.122.026711

91. Zaha VG, Young LH. AMPK activation: a therapeutic target for type 2 diabetes? *Diabetes Metab J.* (2021) 45:516–28. doi: 10.4093/dmj.2021.0197

92. Tomar D, Thomas M, Garbincius JF, Kolmetzky DW, Salik O, Jadiya P, et al. MICU1 protects against sepsis-induced myocardial dysfunction by preventing calpain-mediated RyR2 degradation. *Cell Death Dis.* (2021) 12:899. doi: 10.1038/s41419-021-04194-6

93. Feng J, Zhu M, Schaub MC, Gehrig P, Roschitzki B, Lucchinetti E, et al. MCU-i4: a novel mitochondrial calcium uniporter inhibitor with cardioprotective effects. *Br J Pharmacol.* (2021) 178:2956–71. doi: 10.1111/bph.15487

94. Xie Y, Li J, Kang R, Tang D. Mitochondrial calcium uniporter inhibitor Ru265 improves cardiac function in mice with acute myocardial infarction. *J Am Heart Assoc.* (2023) 12:e029123. doi: 10.1161/JAHA.122.029123

95. Zhang H, Wang P, Bisetto S, Yoon Y, Chen Q, Sheu SS, et al. MICU1 regulates mitochondrial cristae structure and function independent of the mitochondrial calcium uniporter. *Circ Res.* (2023) 132:999–1015. doi: 10.1161/CIRCRESAHA.122.321994

96. Luongo TS, Lambert JP, Gross P, Nwokedi M, Lombardi AA, Shanmughapriya S, et al. Enhanced NCLX-dependent mitochondrial calcium efflux attenuates pathological remodeling in heart failure. *JACC: Basic to Trans Sci.* (2020) 5:786–98. doi: 10.1016/j.jacbts.2020.06.008

97. Nita II, Hershfinkel M, Sekler I. Mitochondrial NCLX prevents calcium overload and necrosis in the renal tubules. *Kidney Int.* (2022) 101:990–1005. doi: 10.1016/j.kint.2021.12.034

98. Atar D, Arheden H, Berdeaux A, Bonnet JL, Carlsson M, Clemmensen P, et al. TRO40303 for myocardial protection in diabetic patients with STEMI: a *post hoc* analysis of the MITOCARE trial. *Cardiovasc Diabetol.* (2021) 20:132. doi: 10.1186/s12933-021-01326-2

99. Karch J, Bround MJ, Khalil H, Sargent MA, Latchman N, Terada N, et al. Inhibition of mitochondrial permeability transition by sanglifehrin A alleviates necrosis and fibrosis in pressure overload cardiomyopathy. *Nat Commun.* (2022) 13:4241. doi: 10.1038/s41467-022-31942-9

100. Dare AJ, Logan A, Prime TA, Rogatti S, Goddard M, Bolton EM, et al. The mitochondria-targeted anti-oxidant MitoTEMPO improves cardiac function in diabetic cardiomyopathy. *JACC: Basic to Trans Sci.* (2021) 6:900–14. doi: 10.1016/j.jacbts.2021.09.005

101. Zielonka J, Joseph J, Sikora A, Kalyanaraman B. Mitochondria-targeted triphenylphosphonium-based compounds: syntheses, mechanisms of action, and therapeutic and diagnostic applications. *Chem Rev*. (2017) 117:10043–120. doi: 10.1021/acs.chemrev.7b00042

102. Rajesh M, Mukhopadhyay P, Bátkai S, Patel V, Saito K, Matsumoto S, et al. Cannabidiol attenuates cardiac dysfunction, oxidative stress, fibrosis, and inflammatory and cell death signaling pathways in diabetic cardiomyopathy. *J Am Coll Cardiol*. (2010) 56:2115–25. doi: 10.1016/j.jacc.2010.07.033

103. García-Rivas G, Lozano O, Bernal-Ramírez J, Silva-Platas C, Salazar-Ramírez F, Méndez-Fernández A, et al. Cannabidiol prevents heart failure dysfunction and remodeling through preservation of mitochondrial function and calcium handling. *JACC. Basic to Trans Sci*. (2025) 10:800–21. doi: 10.1016/j.jacbts.2024.12.009

104. Lopaschuk GD, Verma S. Mechanisms of cardiovascular benefits of SGLT2 inhibitors. *Circ Res*. (2020) 126:1586–602. doi: 10.1161/CIRCRESAHA.120.316949

105. Pugazhenthi S, Qin L, Reddy PH. GLP-1 receptor agonists improve mitochondrial calcium handling in diabetic hearts. *Cell Metab*. (2023) 35:316–31. doi: 10.1016/j.cmet.2022.12.011

106. Foretz M, Guigas B, Viollet B. Metformin as a mitochondrial modulator in heart disease. *Nat Metab*. (2021) 3:1590–3. doi: 10.1038/s42255-021-00488-3

107. Luongo TS, Lambert JP, Yuan A, Zhang X, Gross P, Song J, et al. The mitochondrial calcium uniporter matches energetic supply with cardiac workload during stress and modulates permeability transition. *Cell Rep*. (2015) 12:23–34. doi: 10.1016/j.celrep.2015.06.017

108. Kwong JQ, Huo J, Bround MJ, Boyer JG, Schwanekamp JA, Ghazal S, et al. The mitochondrial calcium uniporter selectively matches metabolic output to acute contractile stress in the heart. *Cell Rep*. (2017) 21:3189–203. doi: 10.1016/j.celrep.2017.10.035

109. Wu S, Lu Q, Wang Q, Ding Y, Ma Z, Mao X, et al. Heterogeneity of mitochondrial calcium handling in cardiac cells during heart failure progression. *Circ Res*. (2020) 126:e32–47. doi: 10.1161/CIRCRESAHA.119.315334

110. Murphy E, Ardehali H, Balaban RS, DiLisa F, Dorn GW, Kitsis RN, et al. Mitochondrial function, biology, and role in disease: a scientific statement from the American Heart Association. *Circ Res*. (2022) 130:1827–47. doi: 10.1161/RES.0000000000000548

111. Hamilton S, Terentyeva R, Kim TY, Bronk P, Clements RT, Choi BR, et al. Combined inhibition of IP3R and MCU modulates mitochondrial Ca^{2+} uptake in heart failure. *J Am Coll Cardiology 77(18 Supplement*. (2021) 1):195. doi: 10.1016/S0735-1097(21)01319-1

112. Litviňuková M, Talavera-López C, Maatz H, Reichart D, Worth CL, Lindberg EL, et al. Cells of the adult human heart. *Nature*. (2020) 588:466–72. doi: 10.1038/s41586-020-2797-4

113. Tarasov AI, Sargsyan A, Cai N, Wu D, Bautista-Barrufet A, Vélez P, et al. The mitochondrial Ca^{2+} uniporter MCU is essential for glucose-induced ATP increases in pancreatic β-cells. *PloS One*. (2022) 17:e0260900. doi: 10.1371/journal.pone.0260900

114. Schneider P, Walters WP, Plowright AT, Sieroka N, Listgarten J, Goodnow RA, et al. Rethinking drug design in the artificial intelligence era. *Nat Rev Drug Discov*. (2020) 19:353–64. doi: 10.1038/s41573-019-0050-3

115. Forsberg EA, De Mario A, Nogara L, Piro S, Carrer A, Giorgi C, et al. AI-guided design of an MCU allosteric inhibitor rescues mitochondrial calcium overload in heart failure. *Cell*. (2022) 185:3161–3175.e20. doi: 10.1016/j.cell.2022.07.014

116. Liu Y, Zhang Q, Wang H, Li Y, Zhao Y, Lu S. Accurate prediction of calcium channel-drug binding affinity with quantum machine learning. *Science*. (2023) 382:eadf3255. doi: 10.1126/science.adf3255

Frontiers in Endocrinology

Explores the endocrine system to find new therapies for key health issues

The second most-cited endocrinology and metabolism journal, which advances our understanding of the endocrine system. It uncovers new therapies for prevalent health issues such as obesity, diabetes, reproduction, and aging.

Discover the latest Research Topics

See more →

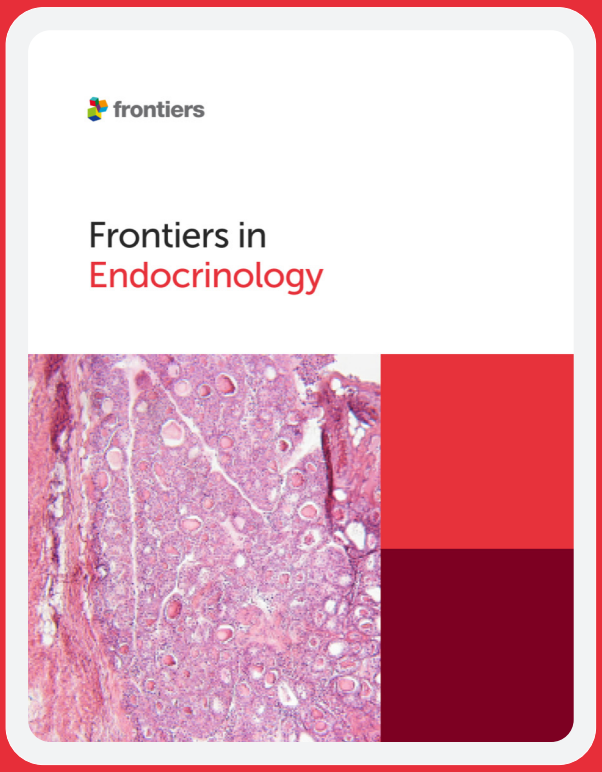

Frontiers

Avenue du Tribunal-Fédéral 34
1005 Lausanne, Switzerland
frontiersin.org

Contact us

+41 (0)21 510 17 00
frontiersin.org/about/contact